Role of Neuropilins in Zebrafish Heart Regeneration.

Vanessa Lowe

2017

Division of Medicine, University College London

A thesis submitted to University College London for the degree of Doctor of Philosophy (Ph.D.)

Declaration

I, Vanessa Lowe, confirm that the work presented in this thesis is my own. Where information has been derived from other sources, I confirm that this has been indicated in the thesis.

Acknowledgments

Firstly, I'd like to thank the British heart foundation, the research carried out in this PhD would not be possible without their generosity and funding for the studentship.

I cannot express my gratitude enough for the support and mentoring by my Supervisors. It is through their encouragement, and motivation that this PhD was the success it transpired to be.

- Professor Ian Zachary has imparted a wealth of knowledge and guidance that has helped me develop my problem solving, data interpretation and innovative thinking. He has been incredibly supportive to my studies, funding the continuation of my experiments and career advice. I thank him for welcoming me into his group, providing me with feedback on my thesis and his incredibly efficient proof reading.

- Dr. Caroline Pellet-Many designed the foundations of this brilliant project and taught me the essential lab and surgical skills I needed to carry out my studies. She has paid great attention to detail to my experiments and thesis, I thank her for her thorough approach (now termed CQC- Caroline quality control) to help me generate the best work I possibly can. I feel privileged to have been her first PhD student. Her enthusiasm for science has resonated with me and will remain a hugely positive influence on the academic path I intend to take.

I would like say a huge thank you the Cardiovascular Biology and Magnus group, past and present, not only are they great scientists, they are a pleasure to work with and I have made some wonderful friends in this lab. From Ian Evans always being on hand to help me with any issues, Laura teaching me all things ImageJ and saving the day with the vorfÜhreffekt to Jenny solving my PVA revelation; everyone in the lab has made a positive impact in my studies in one way or another, there are too many to list!

I'd also like to thank other groups within the Rayne that have made my PhD experience a unique and fun one. In particular, I'd like to thank the Pineda Torra group and

Cardiovascular Genetics, they have been generous with equipment sharing and have been very welcoming. I am now an honorary member of the watermelon and cactus club and delighted to be a part of the many social events they have arranged over the years.

I'd like to thank Prof. Nadia Mercader (CNIC, Madrid) for teaching us the cryoinjury procedure that formed the basis of this project, and her provision of probes. Additionally, Prof. Paul Riley and his lab in Oxford for the provision of essential transgenic epicardial zebrafish lines used in the study. Roisin Brid Doohan (CNIC, Madrid) and Dr. Mathilda Mommersteeg (University of Oxford) for teaching me histological techniques. Dr. Gaia Gestri for demonstrating the *in situ* hybridisation protocol. I'd like to thank Dr. Alessandro Fantin (Institute of Ophthalmology, UCL) for advice mutant fish line generation.

I would like to take the opportunity to acknowledge the UCL fish facility, they have taken care of the animals used throughout the studies, willingly provided me with stocks of their own fish and allowed me to set up a surgical area for the procedures

My friends outside of academia have been incredibly supportive and encouraging throughout the PhD. In particular, my housemates who have been understanding, considerate and reassuring throughout the writing of my thesis, apologies for being very antisocial over the festive season.

Lastly, I'd like to thank family, a special mention to my parents, I wouldn't be here without their unconditional love and support throughout my entire studies, regardless of how long I've been a student! They are the best.

Abstract

Background. Unlike adult mammals, zebrafish can regenerate their heart. Several mechanisms are essential to achieve regeneration; these include:

- the de-differentiation and proliferation of cardiomyocytes contributing to new myocardium,
- angiogenesis to provide a blood supply to the injured area
- epicardial activation, leading to the establishment of a scaffold for the proliferating cardiomyocytes, vessel supporting mural cells and cytokine secretion.

Platelet-derived growth factor (Pdgf), Vascular endothelial growth factor (Vegf), Transforming Growth Factor beta (Tgfβ) and Fibroblast growth factor (Fgf) signalling play critical roles in the zebrafish heart regeneration. Neuropilins (NRPs) are cell surface co-receptors that have been implicated in VEGF, PDGF, FGF, TGFβ signalling.

Aims. I hypothesised that neuropilins are required for the regenerative response, and investigated the role of neuropilins in zebrafish heart regeneration following cryoinjury.

Results. Zebrafish have four neuropilins isoforms, *nrp 1a, 1b, 2a* and *2b*. I found that all isoforms were upregulated in the ventricle following cardiac cryoinjury. Neuropilins were strongly expressed, at both the mRNA and protein level, by the activated epicardium and endocardium and at the injured/healthy myocardium border. Neuropilin upregulation coincides with leucocyte infiltration to the injured area, epicardial activation and initiation of neovascularisation, implicating a role of *nrps* in these processes. A *nrp1a* mutant, encoding a truncated, non-functional protein, showed a significant delay in heart regeneration in comparison to wild type fish. Furthermore, epicardial cells from *nrp1a* mutant zebrafish heart explants displayed an impaired response to activation by cryoinjury.

Conclusions. Nrp1 plays a key role in zebrafish heart regeneration, mediated through epicardial activation and migration and likely contributes to further physiological processes in other cardiac cell-types. This is the first report of an injury-induced epicardial activation phenotype caused by the disruption of a single allele in zebrafish.

Table of contents

Declaration **2**

Acknowledgments **3**

Abstract **5**

Table of contents **7**

List Of Figures **14**

List of Tables **18**

Abbreviations **19**

1 Introduction **26**

1.1 Zebrafish as a model to study cardiovascular biology **26**

1.1.1 Zebrafish Cardiogenesis **27**

1.2 Adult zebrafish cardiovascular system **37**

1.2.1 Heart structure and circulation **37**

1.2.2 Electrical properties and conduction of the zebrafish heart **40**

1.3 Use of zebrafish to study cardiac disease **42**

1.3.1 Genetic manipulation of zebrafish genome **42**

1.3.2 Cardiovascular disease models in the zebrafish **46**

1.3.3 Zebrafish myocardial infarction models **47**

1.4 Mechanisms of zebrafish heart regeneration **51**

1.4.1 Regenerative capacity of the zebrafish **51**

1.4.2 Inflammation **52**

1.4.3 Fibrosis 54
1.4.4 Cardiomyocyte proliferation 57
1.4.5 Revascularisation 62
1.4.6 Epicardial response in zebrafish heart regeneration 66
1.5 Neuropilin as a potential contributor to zebrafish cardiac regeneration 72
1.5.1 Neuropilin structure 72
1.5.2 Neuropilin 1 77
1.5.3 Neuropilin-2 80
1.5.4 Neuropilins in development 81
1.5.5 Neuropilins ligands and physiological functions 84
1.6 Hypothesis 93
1.7 Aims 94
2 Materials and Methods 95
2.1 Animals 95
2.1.1 Husbandry 95
2.1.2 Animal details 95
2.1.3 Zebrafish breeding 97
2.1.4 Cryoinjury 97
2.1.5 Fin clip 98
2.2 Tissue collection 100
2.2.1 Heart collection 100
2.2.2 RNA preservation 100
2.2.3 Protein preservation 100

2.2.4 Histology preparation 100
2.2.5 *In vitro* assay 101
2.2.6 Embryo harvest 101
2.3 PCR 101
2.3.1 Principle of PCR 101
2.3.2 Genotyping 105
2.3.3 RT-qPCR 107
2.4 Histology 112
2.4.1 Immunofluorescence 112
2.4.2 Acid Fuchsin Orange G 115
2.4.3 *In situ* hybridisation 116
2.5 Zebrafish primary *in vitro* epicardial culture 123
2.5.1 Assay 123
2.5.2 Immunofluorescence 123
2.6 Rat epicardial culture and assays 124
2.7 Western blotting 124
2.7.1 Principle of Western blotting 124
2.7.2 Lysate preparation 125
2.7.3 Western protocol 127
2.8 Statistics 128
3 Results chapter 1: Characterisation of neuropilin expression in adult zebrafish heart regeneration 130
3.1 Establishing the zebrafish cryoinjury model of cardiac damage 130

3.1.1 Heart regeneration after cryoinjury 132
3.1.2 Regeneration 132
3.1.3 Scar composition 133
3.1.4 RT-qPCR quality measurements 135
3.1.5 RT- qPCR results 139
3.1.6 *In situ* hybridisation 144
3.2 Positive control riboprobe whole mount *in situ* hybridisation 144
3.3 Neuropilin isoform probe validation using whole mount *in situ* hybridisation 145
3.4 Positive riboprobe localisation in the injured adult zebrafish heart 147
3.5 Neuropilin mRNA localisation in the injured zebrafish heart 147
3.5.1 Localisation of *nrp1a* mRNA in the regenerating zebrafish heart 149
3.5.2 Localisation of *nrp1b* mRNA in the regenerating zebrafish heart 149
3.5.3 Localisation of *nrp2a* mRNA in the regenerating zebrafish heart 150
3.5.4 Localisation of *nrp2b* mRNA in the regenerating zebrafish heart 150
3.6 Discussion 152
3.6.1 Technique validation 152
3.6.2 Nrp mRNA regulation 152
3.6.3 qPCR 155
3.6.4 *In situ* hybridisation 156
3.6.5 Summary 157
4 Results chapter 2: Cell-type specific nrp expression in zebrafish heart regeneration 158

4.1 NRP C-terminus sequence similarities 158
4.2 Neuropilin protein regulation in the cryoinjured heart 161
4.3 Neuropilin localisation in the regenerating zebrafish heart 164
4.3.1 Nrp1 expression in the endocardium 164
4.3.2 Nrp1 expression in the myocardium 171
4.3.3 Nrp1 expression in the epicardium 171
4.3.4 Nrp2 expression in the endocardium 176
4.3.5 NRP2 antibody cross-reactivity to zebrafish 177
4.3.6 Nrp2 in inflammatory cells after cardiac damage 177
4.3.7 Nrp2 expression in cardiomyocytes 179
4.3.8 Nrp2 expression in endo and epithelial –to mesenchymal transition in the zebrafish heart 181
4.4 Discussion 182
4.4.1 Nrp1 regulation 182
4.4.2 Nrp2 regulation 185
4.4.3 Summary 187
5 Results Chapter 3: Heart Regeneration in *nrp1a* mutant zebrafish 188
5.1 *nrp1a* mutant fish identification 188
5.2 *nrp1a* mutant line characterisation 189
5.3 Nrp1a expression in the *nrp1a*$^{sa1485/sa1485}$ mutant line 192
5.4 *nrp1a*$^{sa1485/sa1485}$ anatomical characterisation 192
5.5 Regenerative capacity in *nrp1a*$^{sa1485/sa1485}$ 195
5.1 Discussion 199

5.1.1 *Nrp1a* mutants are viable 199

5.1.2 Nrp1a expression downregulated in homozygous mutants 201

5.1.3 *Nrp1a* mutants have reduced survival and delayed regenerative response 201

5.5.1 Summary 202

6 Results chapter 4: Role of NRP1 in the epicardium 203

6.1 Neuropilin activity in epicardial cells 203

6.1.1 Epicardial *in vitro* assay validation 203

6.1.2 Cryoinjured heart epicardial expansion 207

6.1.3 Epicardial outgrowth is impaired in the absence of *nrp1a* 209

6.1.4 Epicardial proliferation is unaffected by Nrp1a 211

6.1.5 Rat epicardial cell *in vitro* studies 213

6.2 Discussion 217

6.2.1 Epicardial cells are cultured *in vitro* from ventricle apices 217

6.2.2 Epicardial expansion is increased in cryoinjured ventricle apices *in vitro* 218

6.2.3 Epicardial cells express Nrp1 *in vitro* 219

6.2.4 Nrp1a is required for injury-induced epicardial activation 220

6.2.5 Candidate signalling pathways mediated by NRP1 in rat epicardial cells 220

6.3 Summary 222

7 Discussion 223

7.1 Relevance and quantification of the zebrafish cryoinjury model 224

7.2 Neuropilins are upregulated after cardiac damage 226

7.3 Regeneration is delayed in Nrp1a mutant 230

7.4 Novel Nrp1 role in epicardium 233

7.5 Future directions 235

7.5.1 Neuropilin mutant lines 235

7.5.2 Role of neuropilins in specific cells types 237

7.5.3 Neuropilin signalling and function in heart regeneration 239

7.5.4 Implications for translational research 241

7.6 Conclusions 242

References 243

List Of Figures

Figure 1 Zebrafish heart morphogenesis 30

Figure 2 Proepicardium adherence to developing zebrafish heart 35

Figure 3 Adult zebrafish heart 39

Figure 4 Cardiac electrophysiological properties human, zebrafish and mouse 41

Figure 5 Gene expression manipulation techniques in the zebrafish 45

Figure 6 Myocardial infarction models in regenerative animals 50

Figure 7 Phases of cardiac regeneration in zebrafish 55

Figure 8 Cardiomyocyte nuclear content and proliferative capacity 60

Figure 9 Signalling pathways and cellular mechanisms in zebrafish heart regeneration. 65

Figure 10 Epicardial-derived cells (EPDC) in the embryonic and injured mammalian heart 67

Figure 11 Epicardial epithelial to mesenchymal transition (EMT) 71

Figure 12 Neuropilin structure 76

Figure 13 Neuropilin isoform homology 78

Figure 14 Soluble neuropilin mechanisms 79

Figure 15 NRP trafficking of VEGFR2 88

Figure 16 Cryoinjury procedure 99

Figure 17 Polymerase Chain Reaction Schematic 104

Figure 18 Sanger Sequencing 106

Figure 19 *In situ* hybridisation 117

Figure 20 *In situ* probe synthesis 119

Figure 21 pGEM®T easy vector map 119

Figure 22 Loss of GFP signal in the cryoinjury lesion 131

Figure 23 Recovery of Zebrafish heart following cryoinjury regeneration 134

Figure 24 RNA integrity of zebrafish ventricle RNA extracts 135

Figure 25 Absolute qPCR post-run analysis 136

Figure 26. nrp gene expression in the cryoinjured zebrafish heart 138

Figure 27 Regulation of genes associated with angiogenesis in the cryoinjured zebrafish heart 141

Figure 28 Gene expression of growth factors and receptors previously reported in the regenerating zebrafish heart 143

Figure 29 Positive riboprobe validation 145

Figure 30 nrp riboprobe specificity validation 146

Figure 31. Positive riboprobe mRNA detection in the injured zebrafish heart 148

Figure 32 nrp mRNA localisation in the cryoinjured zebrafish heart 151

Figure 33 NRP C-terminus amino acid sequence alignment 159

Figure 34 Nrp1 is regulated in cryoinjured zebrafish ventricle 163

Figure 35 Nrp1 colocalises with endothelium and endocardium in sham-operated hearts 164

Figure 36 Nrp1 is expressed by the activated endocardium and neovasculature during the inflammatory phase (1 dpci) 167

Figure 37 Nrp1 is expressed by the activated endocardium and neovasculature during reparative phase 168

Figure 38 Nrp1 expression in the endocardium at 7dpci 170

Figure 39 NRP1 is expressed in migrating sub-epicardial cardiomyocytes 173

Figure 40 Nrp1 is expressed by epicardial cells 174

Figure 41 nrp1a mRNA localisation is reflected by Nrp1 immunostaining 175

Figure 42 Nrp2 expression is limited in endothelium and endocardium 176

Figure 43 Inflammatory cells express Nrp2 178

Figure 44 Nrp2 localises with viable cardiomyocytes 180

Figure 45 Activated endocardium and epicardium express Nrp2 181

Figure 46 nrp1a mutant sequencing 190

Figure 47 nrp1a mRNA expression in homozygous nrp1a$^{sa1485/sa1485}$ mutants 191

Figure 48 Nrp1a protein analysis of the nrp1a homozygous mutant 193

Figure 49 Wild type and mutant fish measurements 194

Figure 50 Recovery from cryoinjury is delayed in the nrp1a mutant 196

Figure 51 Wound closure in nrp1a mutant 198

Figure 52 Epicardial outgrowth in vitro assay validation 205

Figure 53 Epicardial outgrowth immunofluorescent cytochemistry 206

Figure 54 Cryoinjury induces epicardial expansion and activation. 208

Figure 55 Epicardial migration is impaired in nrp1a mutants 210

Figure 56 Epicardial proliferation in nrp1a mutants 212

Figure 57 Rat epicardial signalling in vitro 215

Figure 58 Rat epicardial FGF signalling in vitro 216

Figure 59 Pdgf-induced cardiomyocyte migration 232

Figure 60 Nrp1a function in the epicardium 234

Figure 61 Zebrafish cardiomyocyte in vitro culture 238

Figure 62 Schematic representation of transwell migration assay 241

List of Tables

Table 1 Full-length NRP amino acid sequence similarity (%)..... 73

Table 2 nrp expression patterns in developing zebrafish embryo..... 83

Table 3 Details of zebrafish used in the study..... 96

Table 4 qPCR primer details for housekeeper and neuropilin genes..... 111

Table 5 Immunofluorescence antibody details..... 114

Table 6 Acid Fuchsin Orange G staining key..... 115

Table 7: *In situ* RNA probe details..... 120

Table 8 Western blotting antibody details..... 129

Table 9 Cellular expression of *nrps* in adult zebrafish heart..... 229

Abbreviations

aa: Amino acid

AFOG: Acid Fuschin Orange G

(AS): Anti-sense riboprobe

bp: Base pairs

bFGF: Basic fibroblast growth factor

BCIP: 5-Bromo-4-chloro-3'-indolyphosphate

BMP: Bone morphogenic protein

BSA: Bovine Serum Albumin

cmlc2: Cardiac myosin light chain 2

cDNA: Complementary DNA

CM: Cardiomyocyte

CS: Chondroitin sulfate

ct: Cycle threshold

CUB: Protein domain sharing homology with complement factor C1s/C1r, Uegf (sea urchin fibropellins) and Bone Morphogenetic Protein 1 (BMP1).

DAMPs: Danger associated molecular patterns

ddH_2O: Double distilled water

dNTP: Deoxynucleotide

ddNTP: Dideoxynucleotide

DEPC: Diethylpyrocarbonate

DIG: Digoxenin

DMEM: Dulbecco's Modified Eagle's medium

DNA: Deoxyribonucleic acid

dpci: Days post cryoinjury:

dpf: Days post fertilisation

dsDNA: Double-stranded DNA

DTA: Diphtheria toxin A

(E): Embryonic day

EC: Endothelial cells

ECM: Extracellular matrix

EMT: Epithelial to mesenchymal transition

ENU: N-ethyl-N-nitrosourea

EPDC: Epicardium-derived cells

ERK: Extracellular signal-regulated kinases

FA58C: Protein domain that shares structural similarity to the C-termini anion-binding structures of blood coagulation factors V and VIII

FGF: Fibroblast growth factor

Fgfr: FGF receptors

fli1a: Friend leukaemia integration 1a

FLK-1: Fetal Liver Kinase 1

fn: Fibronectin

Fwd: Forward

GAG: Glycosaminoglycan

GAPDH: Glyceraldehyde 3-phosphate dehydrogenase

gDNA: Genomic DNA

GFP: Green fluorescent protein

gDNA: Genomic DNA

gRNA: Guide RNA

hpf: Hours post fertilisation

HRP: Horseradish peroxidase

HSP: Heparin sulfate proteoglycan

IF: Immunofluorescence

IFNγ: Interferon gamma

Ig: Immunoglobulin

IL: Interlukin

ISH: *In situ* hybridisation

ISV: Intersegmental vessel

itgb3: Integrin β3

Kb: Kilo base pair

kDa: Kilo Dalton

KD: Knockdown

KDR: Kinase insert domain-containing receptor

LAP: Latency associated peptide

LDS: Lithium dodecyl sulfate

ltbp3: Latent transforming growth factor beta binding protein

MAB: Maleate buffer

MAM: Protein domain that shares homology to mephrin (a cell-surface glycoprotein), A5 antigen and receptor tyrosine protein phosphatase μ and κ

MAP: Mitogen-activated protein

MAPK: Mitogen-activated protein kinase

MCP: Monocyte chemoattractant protein

Mefc2b: Myocyte enhancer factor 2b

MI: Myocardial infarction

MMP: Matrix metalloproteinases

MO: Morpholino

mRNA: Messenger RNA

mmHg: Millimetres if mercury

NBT: Nitro-blue tetrazolium

NRP: Neuropilin

PAGE: Polyacrylamide gel electrophoresis

PBS: Phosphate buffer saline

PBST: Phosphate Buffer Saline Tween

PCNA: proliferative cell nuclear antigen

PCR: Polymerase chain reaction

Pdgf: Platelet derived growth factor

Pdgfrβ: Pdgf receptor β

PDVF: Polyvinylidene fluoride membrane

PECAM: Platelet and endothelial cell adhesionmolecule

PFA: Paraformalhyde

PKC: Protein kinase C

PlGF: Placental growth factor

qPCR: Quantitative PCR

RA: Retinoic acid

Raldh2: Retinoic acid synthase enzyme retinaldehyde dehydrogenase 2

RARs: Retinoic acid receptors

Rho: Ras homolog gene family

Rev: Reverse

RIN: RNA integrity

RIPA: Radioimmunoprecipitation assay

RNA: Ribonucleic acids

ROS: Reactive oxygen species

RT-qPCR: Quantitative reverse transctiption PCR

RTK: Receptor tyrosine kinases

RXR: Retinoid X receptor

(S): Sense riboprobe

Scr: Scrambled short-hairpin RNA

SEM: Standard error mean

Sema: Sempahorin

SDS: Sodium dodecyl sulfate

SH1: Src homology domain-1

Shh: Sonic hedgehog

shRNA: Short hairpin RNA

sNRP: Soluble NRP

SQTS: Short-QT syndrome

SSC: Saline-Sodium Citrate

Taq: Thermus aquaticus

Tbx(*n*): T-box transcription factor(number)

TCEP: Tris(2-carboxyethyl)phosphine

TF: Transcription factor

TGFβ: Transforming growth factor beta

TGFβRs: TGFβ receptors

TILLING: Targeting-induced local lesion

TNFα: Tumour necrosis factor alpha

Treg: Regulatory T cell

tRNA: Transfer RNA

Tβ4: Thymosin beta 4

VE-cadherin: Vascular endothelial-cadherin

VEGF: Vascular endothelial growth factor

VEGFR: VEGF receptors

VSMC: Vascular smooth muscle cell

w/v: Weight per volume
WT: Wild Type
Wt1: Wilms' tumor 1

zERG: Zebrafish ether-à-go-go-related gene

zf: Zebrafish

ZIRC: Zebrafish international resource centre

ZMP: Zebrafish mutagenesis project

Notes on nomenclature:

Zebrafish genes are written in lowercase in italics: *e.g. cmlc2*

Zebrafish proteins are written in Capitalised words: *e.g.* Cmlc2

Where an antibody targeted to a human epitope is used, the mammalian nomenclature is used: *e.g.* GAPDH

Where an antibody targeted to a zebrafish epitope is used, the zebrafish nomenclature is used: *e.g.* Raldh2

1 Introduction

Myocardial infarction (MI) is the leading cause of death worldwide (Kabir *et al*., 2007; Sidney *et al*., 2013; Unal *et al*., 2005). MI is commonly referred to as a heart attack, and results from coronary artery occlusion consequently restricting blood supply to the cardiac tissue. Insufficient blood flow causes tissue ischaemia and leads to the death of the cardiac cells in the affected area. In adult mammals, damaged cardiac tissue is replaced with a fibrotic scar that does not possess the electrical or contractile properties of the healthy cardiac tissue (Laflamme and Murry, 2011; Pfeffer and Braunwald, 1990). Scar formation increases the risk of MI recurrence, sudden cardiac death, and heart failure, amongst other accompanying complications (Bui *et al*., 2011; Gaziano, 2007). Medical interventions have increased MI patient survival rates (Bui *et al*., 2011; Hardoon *et al*., 2011; Kabir *et al*., 2007; Unal *et al*., 2005); however no cure exists to reverse the permanent damage of a patient's heart other than heart transplant. Understanding cardiac repair mechanisms could identify therapies to stimulate heart regeneration and alleviate secondary complications in MI survivors. Neonatal mammals (Porrello *et al*., 2011b; Zogbi *et al*., 2014), urodele amphibians (Oberpril.Jo and Oberpril.Jc, 1974; Rumyantsev, 1977) and zebrafish (Poss *et al*., 2002) possess the remarkable ability to fully regenerate their heart after cardiac injury as well as removing scar tissue. The zebrafish in recent years has emerged as a valuable model organism for studying cardiovascular development and regeneration, and has provided promising insights into the cellular and molecular mechanisms that orchestrate endogenous heart regeneration, as yet unachievable in humans.

1.1 Zebrafish as a model to study cardiovascular biology

The zebrafish, *Danio rerio*, is a tropical freshwater fish native to North Indian Rivers. It is approximately 3.5 – 4.5 cm in length and readily identified by its distinctive striped scales pattern. Studying zebrafish has many advantages. They are vertebrates with a high number of conserved human-related genes; thus, at least one zebrafish ortholog exists

for 71.4% of human protein encoding genes (Howe *et al*., 2013). Zebrafish embryonic development is external, fast and the transparency of the eggs and early embryos provide an optically accessible means to visualise development. Additionally, an expanding range of genetic tools is readily available to manipulate the zebrafish genome. Furthermore, the zebrafish is practically and economically advantageous, given that large numbers of animals can be kept in a relatively small space at low cost.

The extraordinary regenerative capacity of the zebrafish has attracted great scientific interest. The zebrafish can regenerate multiple organs and appendages, such as, fins (Johnson and Weston, 1995), maxillary barbel (LeClair and Topczewski, 2010), retinae (Vihtelic and Hyde, 2000), optic and spinal nerves (Becker *et al*., 1997; Bernhardt *et al*., 1996). In 2002, Kenneth Poss and colleagues discovered the zebrafish could also regenerate the heart after amputation of 20% of the ventricle. This section will describe the similarities and differences between the zebrafish and human heart and highlight the relevance for using the zebrafish as a model organism to study cardiac function and disease.

1.1.1 Zebrafish Cardiogenesis

Mechanisms governing regenerative events often recapitulate developmental processes. The heart is the first organ to fully develop and function during vertebrate embryogenesis, a process that occurs by 2 days post fertilization (dpf) in zebrafish, 12 days in mice and 35 days in humans (Stainier, 2001). Several cardiac developmental processes and cardiac structural features are conserved between all vertebrate species and thus, zebrafish has been used to model cardiac development in humans. Zebrafish have proven a valuable tool to the development community as optical clarity allows detailed imaging of developmental processes. Zebrafish embryos can survive for up to 5 days post fertilisation (dpf) with severe cardiac phenotypes because they are able to obtain oxygen by passive diffusion (Hu *et al*., 2001). This has permitted large-scale forward and reverse genetic screening and phenotypic characterisation of genes influencing cardiac development, to an advanced stage, that would otherwise be embryonic lethal in mammals. Thus, several genes orchestrating different aspects of

cardiac development in the zebrafish have been characterised, many of which parallel those implicated in mammalian cardiogenesis.

Cardiac progenitor cells can be identified in the late blastula, upon expression of transcription factor (TF) *gata5*, at 5 hours post fertilisation (hpf) in the developing zebrafish embryo (Figure 1A) (Reiter *et al*., 1999). Expression of the vertebrate early myocardial gene *nkx2.5* is targeted by *gata5* just before gastrulation in mesodermal progenitor cells (Kishimoto *et al*., 1997; Reiter *et al*., 1999). The zebrafish genome encodes two orthologs of mammalian Nkx2.5, *nkx2.5* and *nkx2.7* (Lee *et al*., 1996), that drive expression of myocardial genes such as troponin T and tropomyosin (Stainier, 2001). By 15 hpf (the 14-somite stage), two bilaterally aligned cell populations of cardiac fate form, called the cardiac primordia (or the first heart field) (Yelon *et al*., 1999) (Figure 1B). The two primordia contain future ventricular cardiomyocytes on the internal lateral side closest to the mid-line and cells destined for the atrium are on the external margin of the fields (Stainier *et al*., 1993). The ventricular and atrial cardiac progenitor cells remain distinctly separated throughout the entirety of cardiogenesis, and express chamber specific sarcomeric myosins; the ventricular cells express *my7* at an earlier stage (16hpf) and atrial progenitors express *my6* (22hpf) (Berdougo *et al*., 2003; Yelon *et al*., 1999). The two parallel populations of progenitor cells migrate towards the midline and fuse (Figure 1D). This process requires *hand2* expression and lysosphingolipids to regulate extracellular fibronectin for correct fusion(Garavito-Aguilar et al., 2010), similar to mammalian heart morphogenesis that demonstrates reliance on fibronectin deposition (George *et al*., 1997). Additionally, the second heart field (consisting of mesodermal progenitor cells intended as ventricular and smooth muscle cells of the outflow tract) merge with the migrating bilateral cardiac primordia to form the cardiac cone in a process known as asymmetric involution (Rohr *et al*., 2008) (Figure 1D). Between 24 and 28 hpf the heart cone elongates along the middle of the fish forming the primitive structure of the heart, the heart tube, and begins spontaneous peristaltic contractions (Figure 1E). *Islet1* is required for an initial phase of cardiomyocyte differentiation starting at the ventricle and terminating at the atrial

portion of the heart tube (de Pater *et al*., 2009). Following heart tube formation, the organ migrates to the left and begins to loop giving rise to two distinct compartments by 36 hpf (Figure 1F)(de Pater *et al*., 2009; Lu *et al*., 2016). Second heart field populations are added to the heart (described in 1.1.1.2), valvugenesis takes place and the proepicardium adheres (see 1.1.1.4) to give rise to a mature heart (Figure 1G).

1.1.1.1 Endocardium morphogenesis

In mammalian development, endocardial precursors give rise to the endothelial layer lining the lumen of cardiac chambers and a subpopulation create the septum and cardiac valves (Eisenberg and Markwald, 1995). The population of blastula cells (blastomeres) that give rise to zebrafish endocardium can be identified at 5 hpf at the anterior lateral plate mesoderm in close proximity to the cardiac progenitor cell population. Endocardial precursors migrate to the midline at 15 hpf (preceding heart tube formation) at the location where bilateral primordia fuse (Bussmann *et al*., 2007)(Figure 1C). Endocardial progenitor establishment at the midline is crucial for heart tube formation, and the interaction between myocardial progenitors and endocardial progenitors is critical for heart development (Holtzman *et al*., 2007). Endocardial progenitor cell migration to the midline is governed in part by a slit1/roundabout (Robo)/Vascular endothelial growth factor (VEGF) axis essential for heart tube formation (Fish *et al*., 2011; Schoenebeck *et al*., 2007).

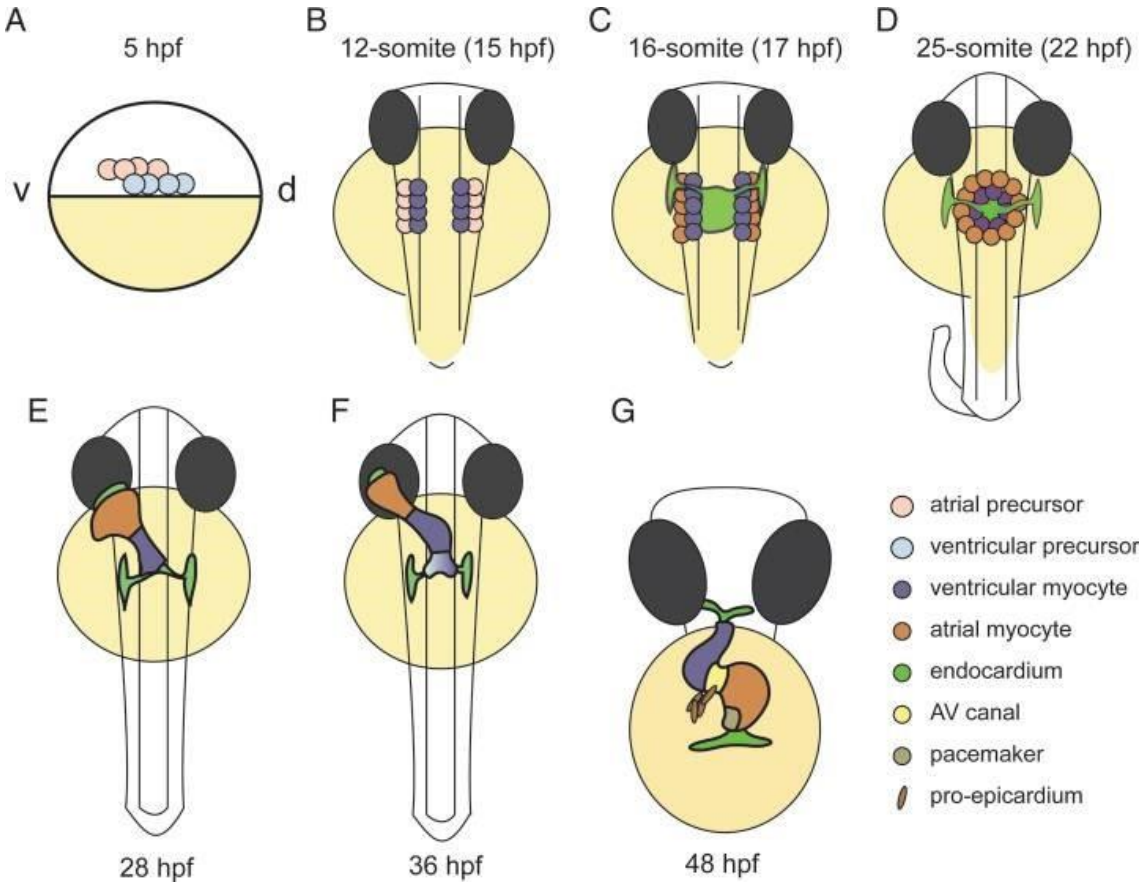

Figure 1 Zebrafish heart morphogenesis

Schematic representation of zebrafish heart development. (A) Cardiac progenitors are identified from 5 hours post fertilisation (hpf), located bilaterally in the lateral marginal zone. Atrial precursors are positioned more ventral (v) and ventricular precursors lie more dorsal (d) (B) At 15hpf cardiac primordia are bilaterally aligned at the anterior lateral plate mesoderm (ALPM) proximal to the mid-hind brain (C) Endocardial progenitors are established at the midline before the primordia that (D) migrate towards the midline and fuse to form the heart cone via asymmetrical involution, with ventricular cells at the apex and atrial cells at the wider base. (E) The heart elongates giving rise to the heart tube that begins peristaltic contractions. (F) The heart tube undergoes looping morphogenesis to form distinct atrium and ventricle compartments by 36 hpf. (G) Cardiac maturation occurs; cell populations from the second heart field increase heart size, valvugenesis takes place and proepicardium adhere to heart surface. Image modified from Bakkers (2011)

The endocardium is subject to hydrodynamic forces that stimulate endocardium maturation and morphogenesis. Mechanisms that allow the endocardium to detect different fluidic forces exerted by blood flow are largely unknown. Platelet endothelial cell adhesion molecule-1 (PECAM-1) and vascular endothelial cadherin (VE-cadherin) stimulate VEGF-independent VEGF receptor (VEGFR) 2 and VEGFR3 autophosphorylation and signalling in response to fluidic flow forces (Baeyens et al., 2016). The biological function associated with VEGF-independent VEGFR stimulation is not clearly defined, however in the zebrafish it is proposed to influence cardiac looping and cell-cell junctions (Mitchell *et al*., 2010).

1.1.1.2 Second heart field

The four-chambered mammalian heart develops from two distinct populations of cardiac progenitor cells: the first heart field develops from cells at the lateral mesodermal plate early in development and contributes to the left ventricle (*see* 1.1.1), and the second heart field derived from cells at the pharyngeal mesoderm contribute to the atria and outflow tract (Cai et al., 2003; Waldo et al., 2001). Zebrafish do not have a right atrium, rather, the simple cardiac structure of the zebrafish only contains an outflow tract, raising initial scepticism whether the zebrafish contained a second heart field during development. A second heart field has been observed in the zebrafish and contributes to development of the arterial pole, particularly the distal ventricle and outflow tract (de Pater *et al*., 2009; Hami *et al*., 2011). Homeobox transcription factor, *islet-1,* is expressed by all second heart field progenitor cells in mammals, however zebrafish do not (de Pater *et al*., 2009). Instead, cells positive for latent transforming growth factor beta (TGFβ) binding protein 3 (*ltbp3*) and *nkx2.5* expression were identified as zebrafish second heart field cardiac progenitor cells that are located at the pharyngeal mesoderm (Zhou *et al*., 2011b). The second heart field contributes cardiomyocytes for heart tube elongation at the venous pole from 28 hpf, simultaneous to cardiac looping (Figure 1E) and outflow tract endothelium (Lazic and Scott, 2011). Fibroblast growth factor (Fgf)8 signalling is required for second heart field cardiomyocyte addition at the arterial pole *via* Bmp4 signalling (Reifers *et al*., 2000;

Sorrell and Waxman, 2011). Additionally, myocyte enhancer factor 2cb (Mefc2b), sonic hedgehog (Shh) and T-box1 (Tbx1) signalling have also been described to mediate second heart field cardiomyocyte contribution to the heart (de Pater *et al*., 2009; Dyer and Kirby, 2009; Lazic and Scott, 2011; Xu *et al*., 2004), in line with mammalian second heart field signalling, supporting the existence of conserved mechanisms in higher and lower vertebrates despite the latter's overall simpler cardiac structure.

1.1.1.3 Cardiac maturation

At 48 hours post fertilisation, the zebrafish heart is fully functional and made of two defined chambers, the ventricle and atrium, however at this stage, the heart is formed by only two layers; the endocardium and the myocardium (Stainier *et al*., 1993). Outflow tract (*bulbus arteriosus*) formation, epicardial layer establishment and trabeculation of the myocardium are required to complete cardiac maturation after cardiac looping.

The myocardium expands and chambers trabeculate during cardiac maturation; trabeculae are muscular projections lined with endocardium that protrude into the cardiac chambers in a seemingly irregular manner (Gupta and Poss, 2012; Staudt *et al*., 2014). The trabeculae serve to increase chamber surface area, contribute to electrical signal conductivity and enhance contraction. Absence of trabeculae lead to cardiomyopathies, severely impaired cardiac function and potential lethality in both humans and zebrafish (Jenni *et al*., 1999; Liu *et al*., 2010). An overwhelming body of studies indicate that the endocardium strongly influences myocardial morphogenesis through a variety of signals that are observed in zebrafish and higher vertebrates (Gassmann *et al*., 1995; Kramer *et al*., 1996; Lai *et al*., 2010; Lee *et al*., 1995; Liu *et al*., 2010; Peshkovsky *et al*., 2011). Endocardium-derived FGF and neuregulin signals induce cardiomyocyte proliferation, differentiation and trabeculation of the embryonic mammalian heart (de Pater *et al*., 2009; Molina *et al*., 2009). This interaction is recapitulated in the zebrafish, where the endocardium influences cardiomyocyte maturation via Brg1 (a chromatin remodelling protein) and bone morphogenic protein (Bmp) 10 production (Samsa *et al*., 2013; Stankunas *et al*., 2008). Trabeculae fail to develop in zebrafish *cloche* mutants that lack endocardium, leading to the conclusion

that endocardial maturation precedes cardiac maturation (Stainier *et al*., 1995; Suri *et al*., 1996). Cardiomyocytes that provide the cell population for trabeculae are stimulated to proliferate by Fgf. The cardiomyocytes of the heart tube express Fgf receptors (Fgfrs) simultaneous to epicardial maturation, whereby the epicardium produces Fgf9 (*see* 1.1.1.4) (Lavine *et al*., 2005).

The zebrafish outflow tract comprises the *bulbus arteriosus* and ventral aorta and forms after 48 hpf (Grimes and Kirby, 2009). The development of the *bulbus arteriosus* remains largely uncharacterised. Humans do not have a *bulbus arteriosus*, but it is considered analogous to the arterial trunk (*conotruncus*) observed during higher vertebrate development (Brown *et al*., 2016). The *bulbus arteriosus* expresses a specific elastin extracellular matrix (ECM) protein *eln2,* ortholog of tropoelastin, that possesses mechanical properties to protect gills from fluctuating forces generated during systole (see 1.2.1).

1.1.1.4 Epicardium in heart development

The epicardium is the final layer of the heart to form; it is essential for full cardiac development and function (Manner, 1993), contributing to non-myocardial lineage resident cardiac cells and central to injury response (Kikuchi *et al*., 2011a; Manuel Gonzalez-Rosa *et al*., 2012). It begins to form at embryonic day (E) 9.75 (until E11) in the mouse, Hamburger Hamilton (HH) stage 18 in the chick, and 72 h post fertilisation (hpf) in the zebrafish (Masters and Riley, 2014). The epicardium is a heterogeneous mesothelial monolayer that forms from epicardial precursors sourced from two distinct populations of spherical cells during zebrafish development. The predominant source of epicardial precursors is the proepicardium that is located in the inner lining of the pericardial wall close to the atrioventricular canal (Serluca, 2008). Movement from the contracting heart releases epicardial precursors into the pericardial cavity that then circulate within the pericardial fluid until they eventually adhere to the myocardium (Peralta *et al*., 2013) (Figure 2). A second population of epicardial precursors arises from the cranial pericardial mesothelium and migrates as a cellular bridge to the heart and directly adheres to the myocardium (Plavicki *et al*., 2014) (Figure 2). Once adhered to

the myocardial surface, epicardial cells expand and migrate over the surface of the underlying myocardium. Epicardium establishment in the zebrafish differs to that of the mammalian heart, in that the epicardium forms during mid-gestation concomitantly with cardiac looping (Masters and Riley, 2014). After cardiac development, embryonic developmental markers (such as TBX18 and Wilm's tumor 1 (WT1)) of the epicardium are switched off and the epicardium enters a quiescent state (Chen *et al*., 2002).

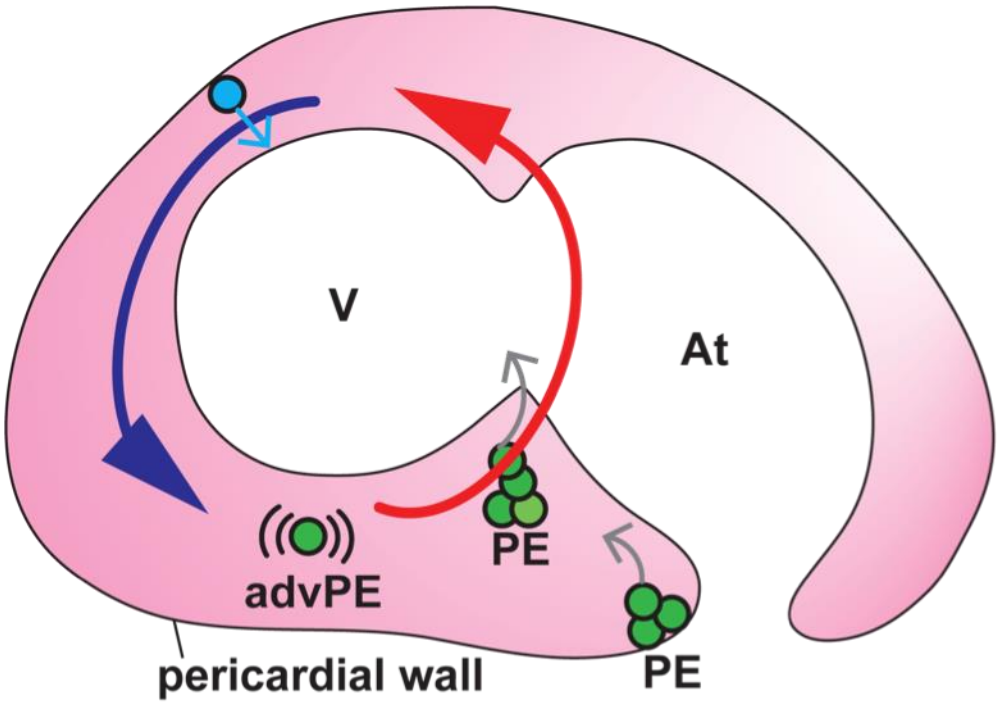

Figure 2 Proepicardium adherence to developing zebrafish heart

Diagrammatic representation of epicardial progenitor cell attachment to the developing zebrafish heart. Epicardial precursors are released (small grey arrows) from proepicardium (PE) clusters (green) in the pericardial wall and circulate as advected PE (advPE) in the pericardial fluid (pink). Directionality and velocity of advPE movement is generated by heart contractions, strong fluid forces occur at the atrioventricular boundary (red arrow) and weaker fluid force at the ventricle (V) (blue arrow). Epicardial precursors eventually contact and adhere to the ventricle surface, once attached they proliferate and populate a monolayer of cells encasing the heart to form the complete epicardium. A population of epicardial cells originates from single cells that delaminate from the pericardium mesothelium (blue circle) and are transferred to the ventricle surface (grey arrow) *via* a cellular bridge. At – atrium. Image adapted from Peralta *et al* (2014).

It is widely accepted that epicardial-derived cells (EPDCs) contribute to fibroblasts and mural vascular supporting cells, but their contribution to endothelial cells and cardiomyocytes are still under debate (Poelmann *et al*., 2002; Red-Horse *et al*., 2010). It has been shown in chicken embryos that EPDCs migrate towards the myocardium and differentiate into coronary vascular smooth muscle cells and fibroblasts (Mikawa and Gourdie, 1996). EPDCs may also be driven toward a myocardial lineage in mammalians and zebrafish by FGF/VEGF/thymosinβ4 (Tβ4) signalling (Cai *et al*., 2008; Smart *et al*., 2007; Wills *et al*., 2008; Zhou *et al*., 2008), and other studies suggest they can transdifferentiate to endothelial cells to contribute to coronary vasculature (Dettman *et al*., 1998; Perez-Pomares *et al*., 2002).

The epicardium is an important source of trophic factors that support myocardium maturation and autocrine signalling to co-ordinate its own maturation and differentiation (Cai *et al*., 2008; Katz *et al*., 2012; Zhou *et al*., 2008). Retinoic acid (RA) (also referred to as vitamin A) is abundantly produced by the epicardium. Global knock out models of the retinoic acid receptor alpha (RARα) is embryonic lethal, mutants display abnormal epicardial adherence and deformed myocardium demonstrating an essential role for epicardial-derived RA for mammalian heart development (Sucov *et al*., 1994). The epicardium and endocardium express retinaldehyde dehydrogenase 2 (RALDH2) during embryogenesis in mammals and zebrafish (D'Aniello *et al*., 2013; Niederreither *et al*., 1999). Retinoic acid signalling in the epicardium stimulates epicardium-derived production of FGFs (Lavine *et al*., 2005); and combined with cardiac fibroblasts (also derived from EPDC), provides a main source of FGF to stimulate cardiomyocyte proliferation (Merki *et al*., 2005; Nag, 1980). FGF10 enhances epicardium epithelial to mesenchymal transition (EMT), potentially *via* FGFR2 stimulation permitting migration into the myocardium and transdifferentiate to fibroblasts (Pennisi and Mikawa, 2005; Vega-Hernandez *et al*., 2011). Failure of the epicardium to undergo EMT prevents coronary vessel morphogenesis implying close association of coronary vasculature development with epicardium dynamics and signals (Tevosian *et al*., 2000).

1.1.1.5 Coronary vessel development

In mammals, coronary vasculature starts to develop approximately between E11.5 – E14.5 (Gonzalez-Iriarte *et al*., 2003; Viragh and Challice, 1981). Some vessels originate at the *sinus venosus* and expand to encase the heart towards the apex (Red-Horse *et al*., 2010), while a second population emerges from the endocardium (Tian *et al*., 2013; Wu *et al*., 2012). Coronary vasculature formation is governed by VEGF signalling that recruits existing endothelial cells to invade the subendocardial space and form vasculature; in particular, VEGF-C was identified to mediate this process (Chen *et al*., 2014; Tian *et al*., 2013). VEGF-B is associated with mediation of coronary plexus tubulogenesis once endocardial cells have been recruited (Tomanek *et al*., 2006). Lastly, some contribution to the coronary vasculature is thought to originate from the epicardium (Katz *et al*., 2012; Pennisi and Mikawa, 2005).

In the zebrafish *friend leukaemia integration 1a* (*fli1a*) positive angioblasts can be detected as early as 12 hpf and mediate vasculogenesis to form the dorsal aorta and luminal vessels by 24 hpf (Ellertsdottir *et al*., 2010; Roman *et al*., 2002). The zebrafish vasculature can be readily visualised thanks to the development of a transgenic line that expresses EGFP downstream of the *fli1a* promoter (Lawson and Weinstein, 2002) expressed in all endothelial cells (Melet *et al*., 1996; Thompson *et al*., 1998). This model has led to extensive characterisation of the zebrafish cardiovascular system, and it was described that the coronary vessel cell population primarily originates from the endocardium (Harrison *et al*., 2015). Endocardial-derived cells migrate to the subendocardial space is driven, in part, by the Cxcr4 signalling axis to give rise to coronary vessels (Harrison *et al*., 2015).

1.2 Adult zebrafish cardiovascular system

1.2.1 Heart structure and circulation

The adult zebrafish heart is approximately 1mm in length and width, and, unlike the four-chambered hearts of mammals, is made up of two chambers consisting of a single atrium and ventricle (Figure 3). The atrium is a large highly folded capacitance chamber with a thin muscular wall lined with pectinate muscle; when fully extended the atrium

can accommodate a volume larger than the ventricle (Hu *et al*., 2001). The atrium receives blood from the body *via* the *sinus venosus* (also referred to as the inflow tract) that itself receives blood from the cardinal and hepatic portal veins and contracts to fill the atrium (Figure 3). During diastole, the atrium contracts at a pressure of approximately 0.68 mmHg to direct blood through the four-leaflet atrioventricular valve into the ventricle (Figure 3) (Hu *et al*., 2001). The ventricular myocardium comprises two distinct structures: most luminal is a highly trabeculated thick muscular layer that is in contact with the endocardium, and externally, is a thin compact layer that runs perpendicular to the trabeculated layer and is connected with the epicardium. This differs to human hearts that are predominantly formed of a thick compact layer of myocardium (Sedmera *et al*., 2000). The highly trabeculated zebrafish ventricle is thought to increase surface area and contact of blood with cardiomyocytes, thus reducing dependence on coronary vasculature for nutrition and oxygen; whereas, higher vertebrates depend on coronary blood delivery to cardiomyocytes. During diastole, the ventricular pressure is approximately 0.42 mmHg allowing the blood to enter the chamber from the atrium. The ventricle then exerts a pressure of approximately 2.5mmHg during systole to direct blood through a bicuspid *bulbo*-ventricular valve into the *bulbus arteriosus* (also referred to as the outflow tract) towards the gills (Hu *et al*., 2001) (Figure 3). The *bulbus arteriosus* is a collagenous, pear-shaped appendage, rich in smooth muscle cells and connects the ventricle to the ventral aorta. It is thought to serve as a buffering chamber preventing the entry of blood under high pressure into the gills during systole, and to be comparable to the arterial trunk in higher vertebrates. The *bulbus arteriosus* is formed of three layers: an intima, media and externa layer. The intima layer is predominantly formed from smooth muscle cells, collagen and elastin fibers, the media layer is formed from helically arranged smooth muscle cells encircling the intima layer and the externa layer comprises elastic lamina. The ventral aorta has a total of 8 bifurcations that deliver blood for reoxygenation from the ventricle (*via* the *bulbus arteriosus*) to gills either side of the zebrafish (Hu *et al.,* 2001), thus, the zebrafish heart is described as a 'venous' heart that receives and pumps deoxygenated blood.

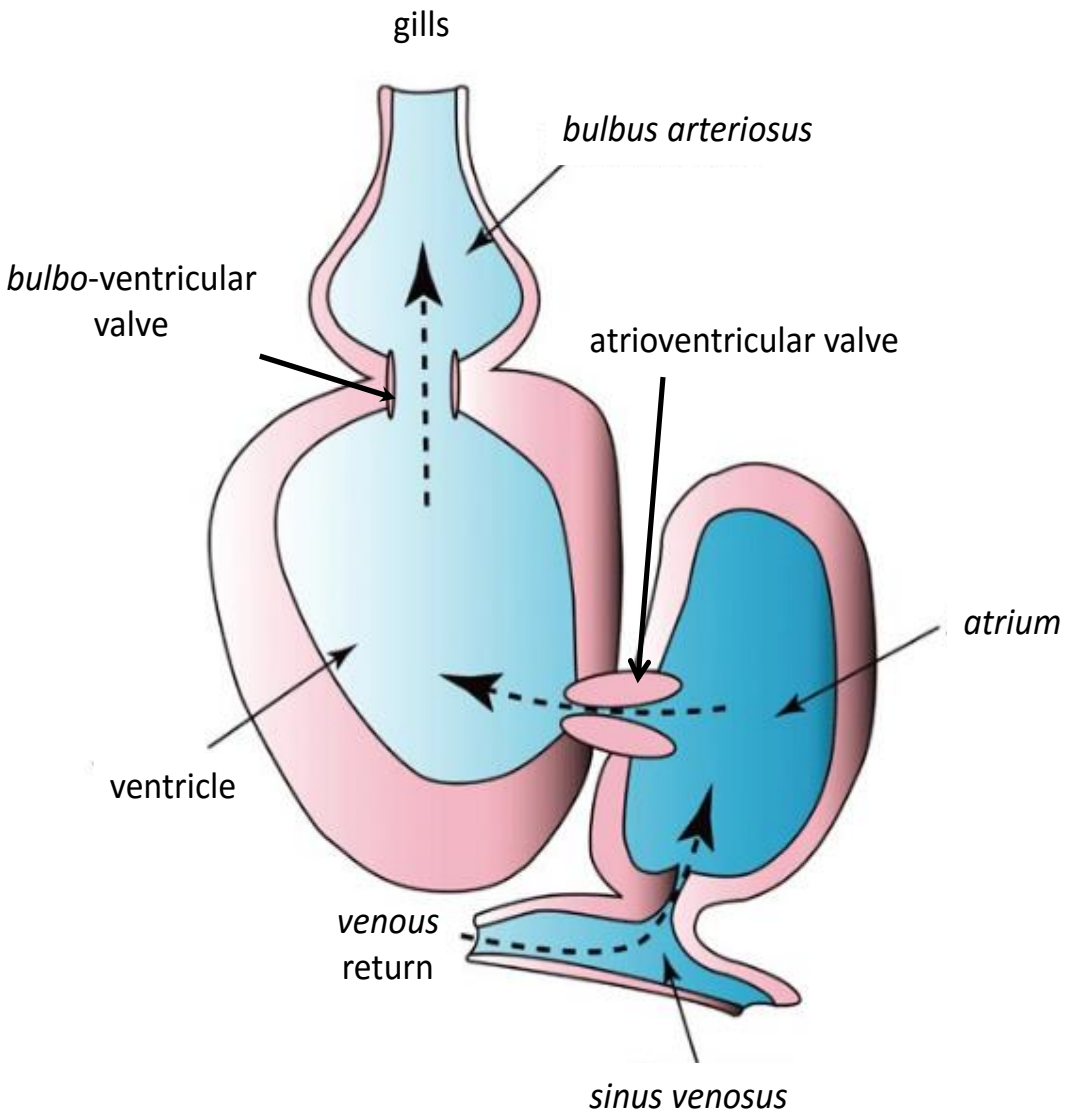

Figure 3 Adult zebrafish heart

Schematic representation of the adult zebrafish heart. Deoxygenated blood returning in veins from the body is collected in the *sinus venosus* and then fills the *atrium*. Blood is pumped into the ventricle from the *atrium via* the four-leaflet atrioventricular valve. During systole, blood exits the ventricle *via* the bicuspid *bulbo*-ventricular valve into the *bulbus arteriosus* that direct blood around the body *via* the gills for reoxygenation. Image modified from Leong *et al.* (2010)

1.2.2 Electrical properties and conduction of the zebrafish heart

The heart rate and electrophysiological properties of cardiomyocytes in the adult zebrafish heart more closely resemble that of humans than mice. The adult zebrafish heart beats at approximately 120-180 beats per minute, which is closer to the 60-100 beats per minute in humans than the rapid 600 beats per minute in mice (Milan *et al*., 2006b; Sun *et al*., 2009b). The pacemaker cell population of the zebrafish heart was identified as a group of *islet-1*, *tbx2b* positive cells arranged in a circular orientation between the *sinus venosus* and atrium interface (Tessadori *et al*., 2012) (Figure 4). The pacemaker electrophysiological properties are comparable to mammalian pacemaker cells and the location is analogous to the sinoatrial node in mammals, although the ion channels permitting electrical conductance in the pacemakers remain unknown (Poon and Brand, 2013). A delay in impulse propagation at the atrioventricular canal (termed slow conduction) has been observed to allow ventricle chamber filling from as early as 40 hpf (Chi *et al*., 2008; Milan *et al*., 2006a). This is followed by a fast conduction impulse relayed through trabeculae to achieve apex to base conduction during systole (Liu *et al*., 2010; Sedmera *et al*., 2003). Electrical impulse propagation in the zebrafish ventricle trabeculae is analogous to His-purkinje fiber conductance observed in mammals and coordinates contraction in a similar manner. Action potential amplitude and cardiomyocyte resting membrane potential are comparable between zebrafish and humans (Sedmera *et al*., 2003). Zebrafish electrocardiogram measurements display a defined P-wave, QRS-complex and T-wave and each QT interval lasts a similar amount of time as in humans (200-290 vs 300-450 ms, respectively) (Figure 4) (Milan *et al*., 2006b). Furthermore, sodium, calcium and potassium channel currents generate action potentials in a similar manner, although the ion channels that mediate the electrical conductance differ between the two species (Brette *et al*., 2008; Haverinen *et al*., 2007; Rottbauer *et al*., 2001). The cardiac electrophysiological properties of the zebrafish therefore support its use as a model to study cardiac physiology and disease.

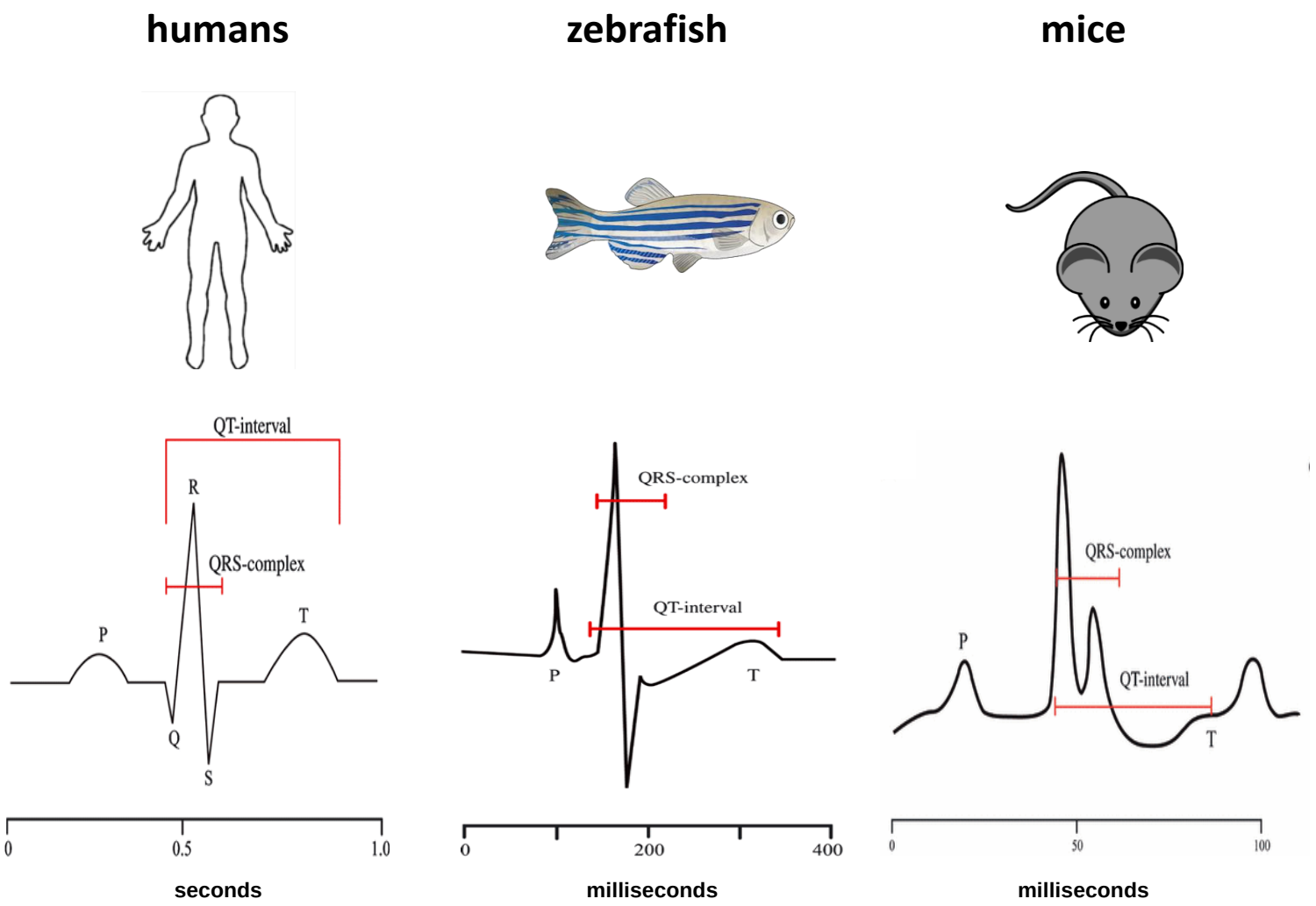

Figure 4 Cardiac electrophysiological properties human, zebrafish and mouse

Diagrammatic representative traces of electrocardiograms (ECG) from human (left), zebrafish (middle) and mice (right). The ECG of zebrafish hearts better resembles the shape and duration of one human electrical cycle (P-wave (atrial depolarization) QRS-complex (ventricular depolarization) and T wave (ventricular repolarisation)) than the ECG of mice. QT-interval encompasses the beginning of the QRS-complex to the end of the T-wave. Image modified from Leong *et al.* (2010)

1.3 Use of zebrafish to study cardiac disease

Well established techniques that allow zebrafish genome editing, and embryo optical clarity to monitor cardiac development, have paved the way for genetic screens and resulted in identification of several mutations causing phenotypes resembling human cardiomyopathies. Additionally, transgenic fluorescent reporter lines that specifically identify endothelium (Lawson and Weinstein, 2002), cardiomyocytes (Burns *et al*., 2005), epicardium (Peralta *et al*., 2013), and blood (Long *et al*., 1997) have been developed allowing visualisation of cardiovascular events. Below, I will describe the genetic manipulation techniques commonly applied to zebrafish and cardiovascular disease models currently established.

1.3.1 Genetic manipulation of zebrafish genome

Reverse genetic screening has proven a useful approach to identify candidate genes responsible for pathological phenotypes. However, genetic manipulation can be somewhat complicated in the zebrafish due to evolutionary genome duplication, thus disruption of a single allele may not present a phenotype due to redundancy and compensation of the duplicated gene (Amores *et al*., 1998; Postlethwait *et al*., 1998; Rossi *et al*., 2015). Despite the challenges, several approaches to modify the genome have been successfully applied to the zebrafish; below I describe three of the most commonly practised approaches.

1.3.1.1 Morpholinos

For several years, the use of morpholinos was the preferred method to carry out reverse genetic screening approaches in the zebrafish. Morpholino technology was introduced by Nasevicius and Ekker in 2000 who induced gene silencing *via* antisense complementarity oligonucleotides (~25mer) to disrupt target protein synthesis (Figure 5A). Morpholinos are nucleic acid analogs that contain methylenemorpholine rings in place of ribose or deoxyribose sugar in the macromolecule backbone. They can be designed to bind in close proximity to the ATG translation start site or other essential mRNA features, interfering with target gene translation or splicing to elicit target gene knockdown. Though this proved effective for studying gene functions and modelling

diseases, the technique is limited to transient gene knockdown, restricting experiments to developmental stages. Additionally, more recent observations have added a level of scepticism towards the validity of the morpholino approach. Morpholino-induced phenotypes often differ from other genetic silencing techniques of the same gene (Kok et al., 2015; Novodvorsky et al., 2015; van Impel et al., 2014), there can be widespread side effects (Eisen and Smith, 2008), and non-specific gene-targeting due to the high relative abundance of the morpholino constructs in comparison to their target is a major problem (Schulte-Merker and Stainier, 2014).

1.3.1.2 CRISPR

Clustered regularly interspaced short palindromic repeats (CRISPR) were originally identified in bacteria as a defence mechanism from bacteriophages (Barrangou *et al*., 2007). Bacteria store bacteriophage genomic sequences from a previous infection. Upon repeated infection, the bacteria generate RNA complementary to the viral genome and recruit Cas9 endonuclease to cleave viral DNA to prevent infection. CRISPR technology adapts this mechanism, using guide RNA (gRNA) that encodes a 20 base complimentary sequence to a target gene, and recruits Cas9 to the DNA to induce a blunt end double-stranded break (Figure 5B). The host molecular machinery attempts to mend the break *via* non-homologous repair that is likely to trigger random insertions and deletions of nucleotides (indels) leading to the introduction of mutations and gene disruption (Figure 5B). In zebrafish, this genome editing technique can be applied at the one cell stage during which gRNA and Cas9 (mRNA or protein) are co-microinjected into the cell, in order to induce gene disruption and produce a mutant line (Chang *et al*., 2013; Hwang *et al*., 2013). It is a highly effective genome-editing technique that achieves greater than 75% mutagenesis efficiency (Sander and Joung, 2014). This approach can also be modified to insert nucleotide sequences and generate knock-in transgenic fish lines (Bedell *et al*., 2012; Chang *et al*., 2013; Hwang *et al*., 2013).

1.3.1.3 ENU

N-ethyl-N-nitrosourea (ENU) mutagenesis is a chemical method used to induce mutations that has been widely applied in zebrafish. ENU is a highly mutagenic chemical that triggers the transfer of an ethyl group to nucleotide bases, inducing point mutations

(Coghill *et al*., 2002) and can alter 1 in every 700 bases (Davis and Justice, 1998). Spermatogenesis is targeted for mutation incorporation and male zebrafish are treated with ENU to induce anomalies randomly throughout the DNA in gametes. ENU-treated males are crossed with wild type females, and mutant founder fish are generated with random mutations in their genome (Figure 5C). Offspring (F_1) are screened for mutations using a PCR and endonuclease method termed targeting-induced local lesions in genomes (TILLING) (McCallum *et al*., 2000; Wienholds *et al*., 2002; Wienholds *et al*., 2003). Identified mutations are categorised by the function of their genetic outcome (*e.g*. nonsense mutation, loss of function, amino acid change) and F_1 fish are crossed with wild type fish to confirm transmission of the mutation in the germline (Figure 5C). The heterozygous progeny (F_2) are then incrossed and offspring are screened for phenotypes. Finally homozygous mutant fish lines can be established from the F_4 generation (Figure 5C). ENU mutant fish production and TILLING is laborious and expensive, additionally this approach does not allow targeted mutation of a specific gene, and thus this approach is more frequently carried out as part of a large-scale effort.

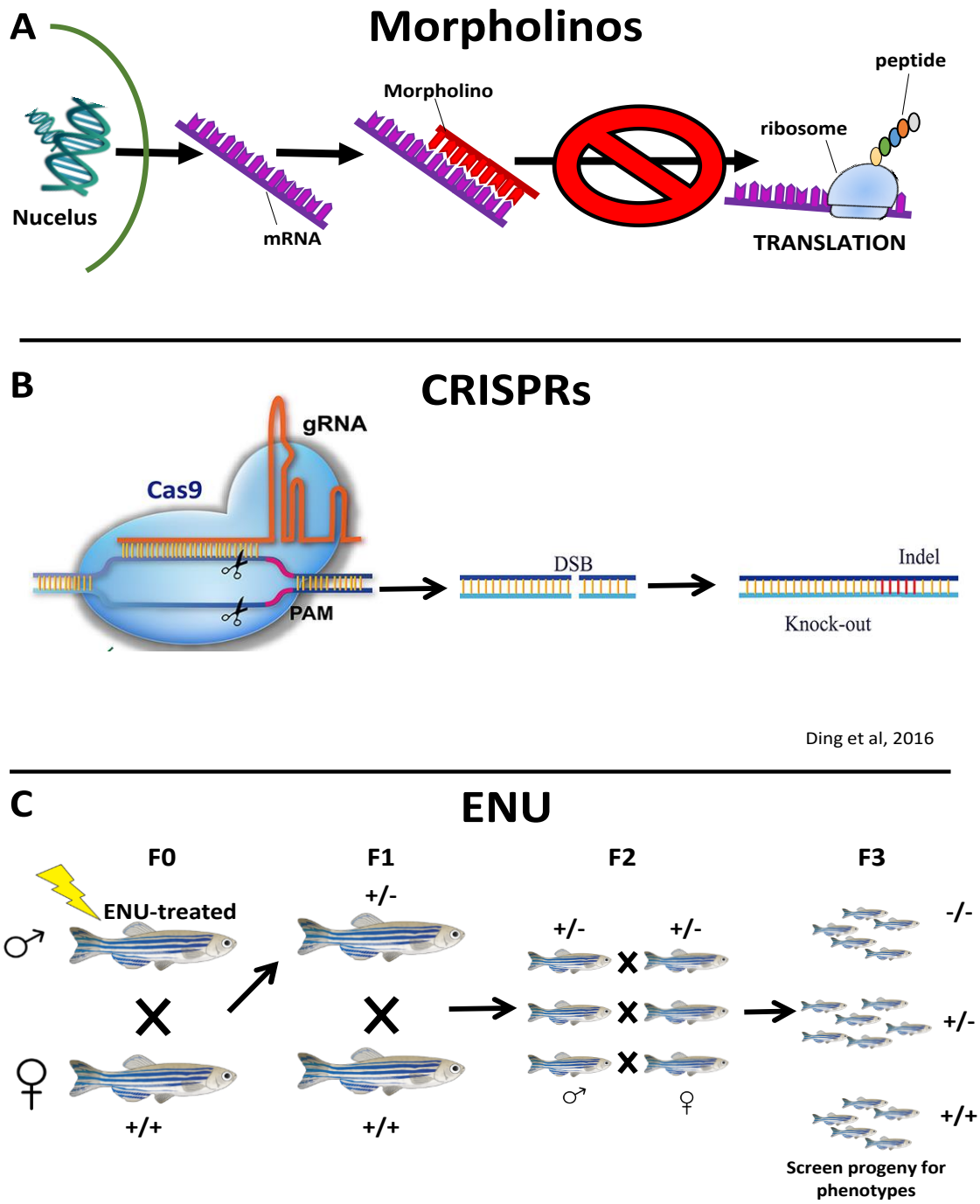

Figure 5 Gene expression manipulation techniques in the zebrafish

(A) Morpholinos (red) are anti-sense oligonucleotides analogs designed to encode the complimentary sequence to target gene mRNA (purple). When introduced to the cell, the morpholino binds to target mRNA and physically inhibits translation. **(B)** CRISPR technology utilises a customised RNA termed guide RNA (gRNA), that encodes a complimentary sequence to the target genomic DNA sequence enabling the gRNA to bind. The gRNA also encodes a Cas9 endonuclease (blue) recruitment domain that directs the Cas9 enzyme to the target sequence to induce a double strand break (DSB) ahead of the PAM (protospacer adjacent motif) sequence (pink). The cleaved DNA is repaired by non-homologous end-joining, likely resulting in the incorporation or deletion of nucleotides (indels) and the disruption of the target gene. Image modified from (Ding *et al*., 2016) **(C)** Male zebrafish are treated with the mutagenic chemical N-ethyl-N-nitrosourea (ENU) to induce mutations during spermatogenesis. The fish is crossed with WT (+/+) females and the heterozygous(+/-) progeny (F1) are crossed with wild types to confirm germline transmission to the F2 generation. F2 fish are incrossed to establish homozygous mutants in the offspring (F3).

1.3.2 Cardiovascular disease models in the zebrafish

The zebrafish heart is a simpler structure to that of higher vertebrates and may not recapitulate complications occurring in mammals and limit identification of mechanisms contributing to human cardiac diseases. Indeed, as a consequence of its anatomical features (two chambers *versus* four chambered in mammals), some human congenital heart defects involving right and left heart septation are unable to be modelled in zebrafish. However, several development mechanisms (see 1.1.1) and cardiac functions (see 1.2) are conserved between zebrafish and human hearts, supporting the use of zebrafish as a model to study cardiac disease.

Multiple mutant zebrafish lines have been developed to study human cardiovascular diseases. Arrhythmias have been modelled in zebrafish encoding ion channel mutations. For example, the *tremblor* zebrafish contains a mutation in the cardiac-specific sodium calcium exchanger, this model recapitulates ventricular fibrillation due to heightened intracellular calcium levels and irregular calcium transients (Langenbacher *et al*., 2005). Bradycardia is modelled using the *slow mo* zebrafish mutant, in which the recessive allele causes delayed heart rate due to impaired hyperpolarization-activated cation pacemaker currents (I_h) (Baker *et al*., 1997). The *reggae* (*reg*) zebrafish mutant encodes a gain-of-function mutation in the zebrafish ether-à-go-go-related gene (zERG) potassium channel and results in shortened action potentials that cause cardiac fibrillation (Hassel *et al*., 2008). The *reg* mutant closely resembles arrhythmia pathologies observed in human short-QT syndrome (SQTS) that can lead to sudden cardiac death (Schimpf *et al*., 2005).

Dilated human cardiomyopathy can be effectively modelled in the zebrafish *via tintin* gene silencing which results in the disruption of the Z-line of sarcomeres and the impairment of cardiac function (Xu *et al*., 2002). During cardiac stress due to cardiomyopathies, the hypertrophic natriuretic peptide signalling pathway is switched on in both mammals and fish. A transgenic reporter zebrafish line has been developed that expresses luciferase downstream of the natriuretic peptide promoter, this can be

used to study cardiac hypertrophy in models such as the *tintin* mutant or environmental influences that elicit hypertrophic responses (Becker *et al*., 2012).

1.3.3 Zebrafish myocardial infarction models

Several techniques have been developed to simulate cardiac damage sustained during MI in humans. They either rely on mutant or transgenic lines or physical damage by surgical means. A decade and a half ago, it was found that the zebrafish could survive the surgical removal of up to 20% of its ventricle (Poss *et al*., 2002). Initially, the zebrafish response triggers mechanisms reminiscent of those in humans after MI, including inflammation and fibrosis. However, the zebrafish can then repair the damage with new functional myocardium during a regenerative phase. The following section addresses techniques developed in zebrafish to investigate heart regeneration.

1.3.3.1 Ventricular resection

Poss and colleagues (2002) were the first to identify the regenerative capacity of the zebrafish heart using ventricular resection. In this model, approximately 20% of the ventricle is surgically removed from the adult heart using fine iridectomy scissors (Figure 6A). A clot forms immediately at the site of injury, followed by inflammation and fibrosis. The fibrotic scar is subsequently replaced by functional cardiomyocytes, completely regenerating the lost cardiac tissue within 60 days following amputation (Poss *et al*., 2002). In mammals and amphibians the scar tissue is collagen rich (Cleutjens *et al*., 1995), this is unlike the resection model in zebrafish, which results in fibrin clot formation without extensive collagen deposition within the injured area (Poss *et al.,* 2002). Furthermore, in this model, neomyogenesis predominantly produces a thick compact myocardial layer at the site of insult (Poss *et al*., 2002). The architecture of the myocardium of the uninjured zebrafish heart comprises a thin compact layer and a more prevalent trabecular layer, which suggests that resection, although achieving functional restoration, permanently alters the structural composition of the heart.

The resection model has also been investigated in neonatal mice that similarly retain regenerative capacity until 7 days post birth (Porrello *et al*., 2011b). The initial response to injury observed in mice is similar to that of zebrafish, with initial blood clotting and

inflammation followed by cardiomyocyte proliferation, resulting in minimal cardiac hypertrophy and fibrosis and leading to restoration of cardiac function within 21 days of resection (Figure 6) (Porrello *et al*., 2011b). It has since been shown that different severities of resection will determine the regenerative outcome; for example, large apical ventricular resections (>23% ventricle damage) result in incomplete regeneration and the deposition of a lasting scar in contrast to the results of 15% resection (Bryant *et al*., 2015).

1.3.3.2 Inducible genetic ablation

Inducible genetic ablation is a non-invasive procedure that causes the death of cardiomyocytes. Genetically modified zebrafish expressing inducible Cre recombinase under the control of the *cardiac myosin light chain 2* (*cmlc2*) promoter have been engineered to express the cytotoxic diphtheria toxin A *(DTA)* gene downstream of loxP sites. Tamoxifen exposure stimulates DTA production specifically in cardiomyocytes, resulting in the death of up to 60% of the cardiomyocyte population (Figure 6). Nevertheless, surviving cardiomyocytes dedifferentiate, undergo rapid proliferation and, within 30 days, complete regeneration of the cardiac tissue is achieved (Wang *et al*., 2011). This demonstrates the robust resilience of the zebrafish heart that, even after suffering a huge loss of cardiomyocytes, is able to rapidly regain full cardiac function (Wang *et al*., 2011). Despite only affecting one cardiac cell type, genetic cardiomyocyte ablation induces epicardium and endocardium activation and inflammation, similarly to other models of cardiac damage in the zebrafish. Nevertheless, the relevance of the genetic ablation technique to mammalian MI is limited because organ-wide cardiomyocyte death occurs rather than localised tissue necrosis; moreover, there is no scar formation. Genetic cardiomyocyte ablation results in reduced exercise tolerance and sudden cardiac death, mirroring some of the repercussions of heart failure, but weakly resembles mammalian MI.

1.3.3.3 Cryoinjury

Cryoinjury (also known as cryocauterisation) was developed by the group of Nadia Mercader and colleagues (2011) as an alternative model for myocardial infarction and heart regeneration in the zebrafish. A small metal filament, cooled in liquid nitrogen, is

pressed onto the exposed ventricle of the zebrafish. Subsequently, thermal shock-induced necrosis and apoptosis takes place, creating a lesion of approximately 25% of the ventricle (Figure 6). A similar injury can also be achieved by application of dry ice to the ventricle (Schnabel *et al*., 2011). The damage is extensive and spans over the endo-, myo- and epicardial layers. This model best recapitulates mammalian MI as it achieves cardiac cell death in a localised region without removal of cardiac tissue. Furthermore, the reparative process that subsequently occurs relies on the deposition of a fibrotic scar formed predominantly by a collagen-rich core and a fibrin cap. This process also resembles more closely the fibrotic response observed in humans after myocardial infarction (Chablais *et al*., 2011; Manuel Gonzalez-Rosa *et al*., 2011). The fibrotic tissue is gradually removed and replaced with proliferating cardiomyocytes to achieve complete regeneration, albeit over a longer time scale than resection, in up to 130 days (Figure 6)(Manuel Gonzalez-Rosa *et al*., 2011). Cryoinjured hearts regain reasonable cardiac function, however impaired ventricular contraction is evident due to myocardium remodelling that perturbs homogeneous contraction (Manuel Gonzalez-Rosa *et al*., 2011).

The cryoinjury procedure has been applied to the neonatal mouse (Darehzereshki *et al*., 2015). The neonatal mouse heart retains some regenerative capacity for up to 7 days post injury (see 1.3.3.1), however varying results were observed with this model. The extent of cardiac damage determines the regenerative process. Transmural damage (throughout the endo-, myo- and epicardium) results in incomplete regeneration and extensive scarring, whereas, non-transmural injury restricted to epicardial and myocardial damage, results in regeneration with scarring to a lesser extent (Figure 6)(Darehzereshki *et al*., 2015).

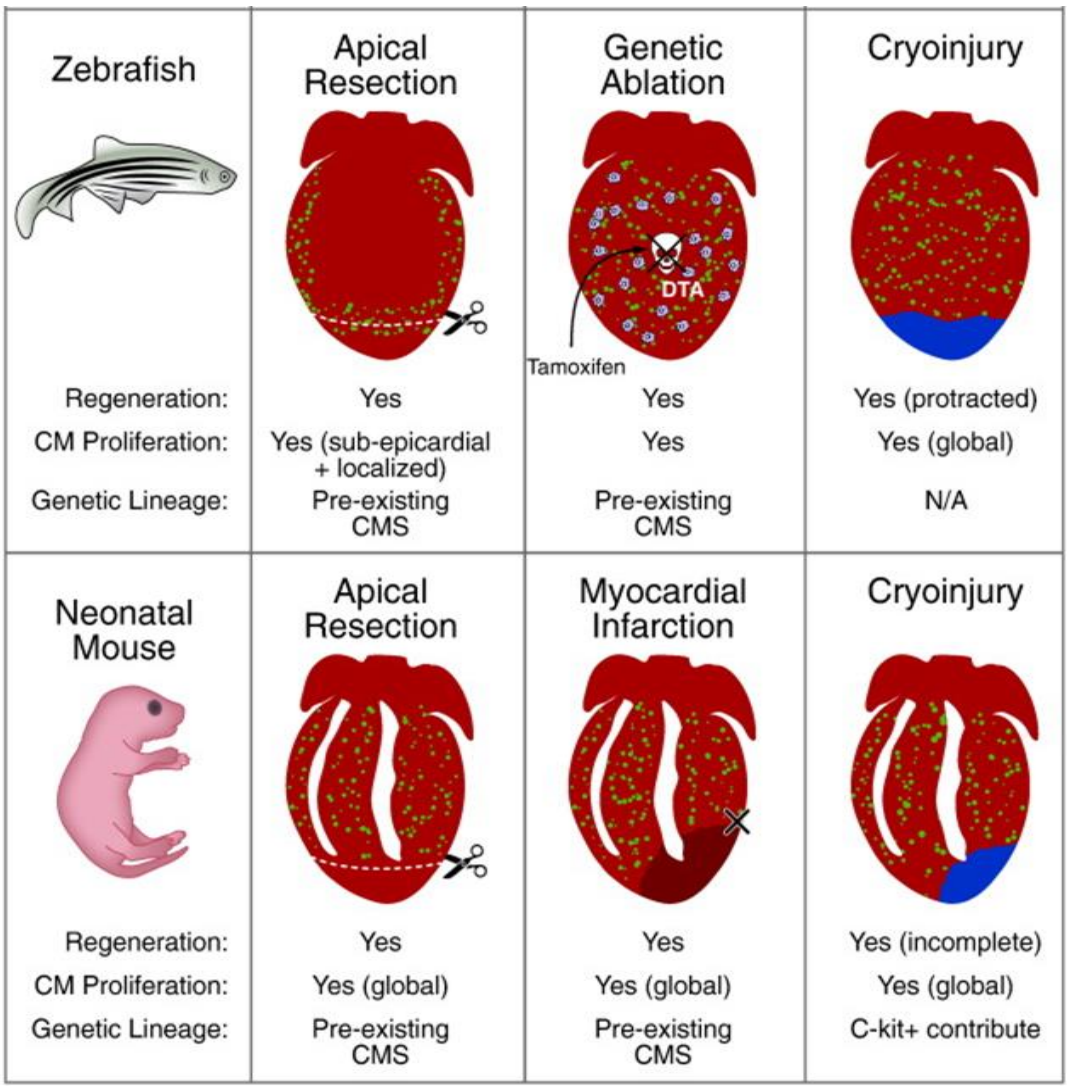

Figure 6 Myocardial infarction models in regenerative animals

Illustrative representation of the three zebrafish (upper row) and neonatal mouse (lower row) myocardial infarction models. Apical resection (also known as ventricular resection) consists of the removal of up to 20% of the ventricle. Genetic ablation involves cardiomyocyte-specific death induced by tamoxifen delivery to a transgenic fish expressing DTA under the control of Cre recombinase. Cryoinjury of the ventricle is induced by the application of a metal probe cooled in liquid nitrogen onto the exposed ventricle. Myocardial infarction can be induced in the neonatal mouse *via* ligation of a major coronary artery. Description regarding regenerative capacity, cardiomyocyte (CM) proliferation and neomyocyte origin (genetic lineage) are listed below each MI model. Image modified from (Porrello and Olson, 2014)

1.4 Mechanisms of zebrafish heart regeneration

1.4.1 Regenerative capacity of the zebrafish

Increased survival rates following MI have been achieved with improved medical interventions that allow the recovery of blood supply to the ischemic area (Kabir *et al*., 2007; Unal *et al*., 2005). However, the affected area of the heart of patients who survive MI does not regain full physiological function because of extensive fibrotic remodelling; this can result in heart failure, fatal arrhythmias amongst other secondary complications. Evidence exists supporting an endogenous ability to repair damaged cardiac tissue in humans, as observed in new-born babies who are able to recover from myocardial infarction; however this ability is lost within 6 months postnatally (Haubner et al., 2016). In contrast to zebrafish, adult mammalian hearts, once damaged, are unable to fully repair, limited cardiomyocyte proliferation takes place, and, instead of neomyogenesis, extensive collagen deposition and cardiomyocyte hypertrophy compensate for compromised cardiac function (Buja and Vela, 2008; Pasumarthi and Field, 2002; Pfeffer and Braunwald, 1990). Although the fibrotic scar prevents ventricle wall rupture, it does not possess the contractile properties of the myocardium. Furthermore, fibrotic tissue perturbs electrical conductivity that co-ordinates a synchronised heartbeat, promoting arrhythmias.

Several investigations have been initiated using the different models described in the previous section (1.3.3), in order to understand what events govern the regenerative process throughout the zebrafish life span (Itou *et al*., 2012a). Initially, inflammation (inflammatory phase) occurs in the lesion, this is followed by scar deposition (reparative phase), and finally scar tissue removal and cardiomyocyte proliferation (regenerative phase) (Figure 7) (Jopling *et al*., 2010). A genetic profile switch occurs, whereby a plethora of embryonic genes are re-expressed allowing transdifferentiation and proliferation of cells that would otherwise be quiescent.

1.4.2 Inflammation

1.4.2.1 Mammalian inflammatory phase

The death of cardiac cells following MI or cardiac insult results in the production of danger associated molecular patterns (DAMPs) and reactive oxygen species (ROS) that recruit innate immune cells to the damaged area (Timmers *et al*., 2012). Additionally, matrix metalloproteinases (MMPs) are activated, resulting in the degradation of cardiac matrix, further enhancing inflammation (Etoh *et al*., 2001; Senior *et al*., 1980; Weathington *et al*., 2006)). The initial inflammatory response lasts up to 4 days in adult mammals. It is essential for necrotic and apoptotic cell removal and central to mediating subsequent reparative events (Dobaczewski *et al*., 2010). Neutrophils and macrophages primarily infiltrate the ischemic tissue from the blood in response to inflammatory signals produced by damaged and adjacent healthy cardiomyocytes (Pfeffer and Braunwald, 1990). Macrophages secrete a cocktail of cytokines such as tumour necrosis factor alpha (TNFα), interleukin (IL)-1, IL-6, FGF and monocyte chemoattractant protein (MCP)-1 to stimulate fibroblast recruitment and proliferation and angiogenesis (Frangogiannis *et al*., 2003; Lambert *et al*., 2008).

Macrophage colony-stimulating factor (MCSF) promotes VEGF production and angiogenesis that ultimately improves cardiac function following MI and enhances cardiomyocyte preservation (Okazaki *et al*., 2007). Inflammation was reported to support cardiac function following MI in a study by Sun and colleagues (2009). In line with their findings, the inhibition of inflammation *via* the delivery of pharmacological agents, has shown deleterious consequences in mammalian MI models (Mannisi *et al*., 1987; Sun *et al*., 2009a; van Amerongen *et al*., 2007). This highlights the pivotal role of the inflammatory response following MI. Nevertheless, some conflicting results generated by other studies have shown that complete inhibition of the inflammatory response reduced infarct size and promoted cardiac healing (Oyama *et al*., 2004; Timmers *et al*., 2008), whereas other reports have shown no overall benefit of inflammation inhibition in clinical trials (Armstrong *et al*., 2007; Faxon *et al*., 2002).

Controversy remains concerning the beneficial influence of inflammation following MI. It is possible that leucocytes are associated with detrimental cardiac remodelling due

indirect activities, such as fibroblast recruitment to the lesion and the triggering of their transdifferentiation into cardiac myofibroblasts. The extent of the inflammatory response may also contribute to pathological outcomes. Acute inflammation is suggested as essential in the reparative response (Hubner *et al*., 1996); prolonged chronic inflammation can reverse these beneficial effects because it potentially promotes cardiac remodelling (Frantz *et al*., 2009). The promotion of acute inflammation following MI and the tightly regulated clearance of immune cells *via* lymphatic vessels to reduce chronic inflammation, have been proven beneficial after MI (Evans *et al*., 2013; Henri *et al*., 2016).

1.4.2.2 Zebrafish inflammatory phase

The inflammatory phase occurs from 0 to 3 days after cryoinjury of the zebrafish heart (Figure 7) (Chablais and Jazwinska, 2012). The zebrafish initiates an innate immune response whereby, infiltrating leucocytes produce pro-inflammatory cytokines, helping with the removal of cellular and matrix debris and the recruitment of fibroblast-like cells to the injury area. Several evolutionary features of innate immunity have been conserved in vertebrates (Beck and Habicht, 1991). The zebrafish genome encodes orthologs of potent pro-inflammatory cytokines that are produced following tissue injury and mediate leucocyte recruitment and inflammatory responses reminiscent of higher vertebrates (Ogryzko *et al*., 2014; Stein *et al*., 2007).

Acute inflammation is an essential step for cardiac regeneration, as it precedes and initiates the subsequent reparative phase. Huang and colleagues (2013) reported that pharmacological inhibition of inflammation with glucocorticoids perturbs phagocytic clearing of cellular debris and diminishes *vegfaa and fgfr* expression, thus reducing the revascularisation of the injured area. The anti-inflammatory treatment also attenuated cardiomyocyte proliferation, leaving a persistent scar and preventing the complete regenerative response (Huang *et al*., 2013). These observations were further supported by evidence that revealed the essential role of leukocyte-derived TGFβ signalling orchestrating the subsequent regenerative events. Indeed, inhibiting TGFβ signalling pathways during the early inflammatory phase completely inhibited cardiac regeneration (Chablais and Jazwinska, 2012). The TGFβ contribution to zebrafish heart

regeneration is dependent on activin and Smad3 signalling (see 1.5.5.5). TGFβ targets fibronectin, collagen and tenascin C synthesis, initiating inflammatory signals driving the fibrotic responses and remodelling (Chablais and Jazwinska, 2012). The resolution of the inflammation response is regulated, in part by, by hydrogen peroxide and Tβ4 signalling that inhibit pro-inflammatory interferon γ (IFNγ) and reduce inflammatory macrophage infiltration (Evans *et al*., 2013). Although initial inflammation is a prerequisite for neuronal and heart regeneration in the zebrafish (Huang *et al*., 2013; Kyritsis *et al*., 2012), it is not essential for fin regeneration (Mathew *et al*., 2007). These studies imply that acute inflammation is important for the regenerative response for both mammals and fish, but its pivotal role differs between regenerating organs.

1.4.3 Fibrosis

1.4.3.1 Adult mammals

In mammals, neutrophil apoptosis marks the resolution of the inflammation process and the initiation of the reparative (also referred to as the proliferative) phase. This phase occurs approximately 4 days following cardiac injury and continues for up to 14 days (Dobaczewski *et al*., 2010). During this phase of cardiac repair, fibroblasts are recruited to the lesion. Fibronectin and hyaluronan polysaccharide deposits produced during the inflammatory phase act as a scaffold to support cardiac structure, preventing haemorrhage and facilitating fibroblast and endothelial cell infiltration (Clark, 1988; Dobaczewski *et al*., 2006). TGFβ and platelet-derived growth factor (PDGF) produced by macrophages recruit resident cardiac fibroblasts to the injury (Yano *et al*., 2005), and induce fibroblast transdifferentiation to myofibroblasts (Brown *et al*., 1993; Dobaczewski *et al*., 2006; Serini *et al*., 1998; Ulrich *et al*., 1997). Myofibroblasts subsequently synthesise collagen deposits at the site of injury (Cleutjens *et al*., 1995). Cytokines such as basic fibroblast growth factor (bFGF) and TGFβ enhance tenascin C

production by fibroblasts at the injury border, thus facilitating myofibroblast migration, aiding delamination and cardiac tissue remodelling (Imanaka-Yoshida *et al*., 2001).

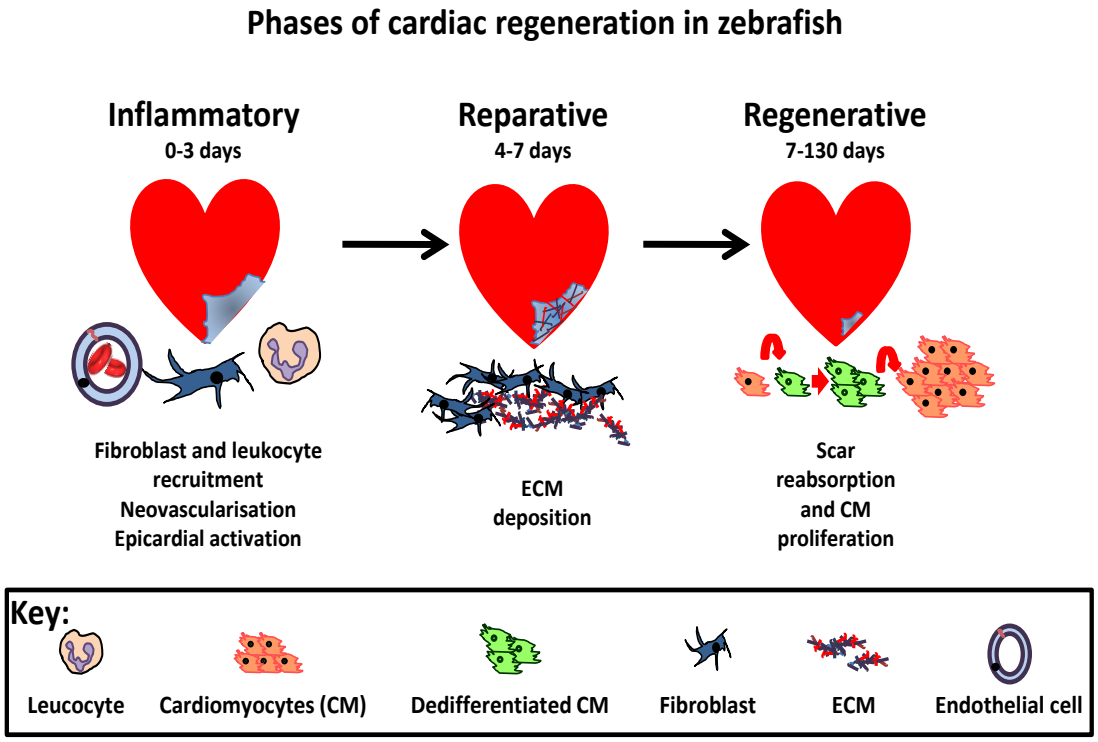

Figure 7 Phases of cardiac regeneration in zebrafish

The inflammatory phase takes place in the first three days following cryoinjury. Leucocytes infiltrate to the injured area, neovessel begin to revascularise the lesion and fibroblasts are recruited to the damaged area. Fibroblasts synthesise and secrete extracellular matrix (ECM) components during the reparative (days 4-7 post cryoinjury) phase; a collagen core and fibrin cap are produced to provide mechanical support to prevent ventricle wall rupture and scaffolding for neomyocardium. During the regenerative phase (7-130 dpci), cardiomyocytes dedifferentiate, proliferate and invade the lesion; fibrotic tissue is reabsorbed to regenerate cardiac tissue.

.

Once myofibroblasts are established at the injury site, the heart progresses towards the maturation phase of cardiac repair that lasts from 14 to 60 days post injury (Dobaczewski *et al*., 2010). Maturation involves the cross-linking of collagen extracellular matrix proteins to create a permanent and stable scaffold to provide mechanical support. Myofibroblast and vessel infiltration diminishes over time and the maturing scar becomes acellular, leaving a dense collagen scar deposit (Jennings *et al*., 1990; Lerman *et al*., 1983; Ren *et al*., 2002).

1.4.3.2 Zebrafish fibrosis

Cardiac remodelling after injury in zebrafish, similarly to mammals, is a complex process, however limited studies have focused on the fibrotic response in zebrafish heart regeneration. The reparative phase lasts from 4-7 days post injury (Figure 7) (Chablais and Jazwinska, 2012). At this stage, cellular and matrix debris within the lesion have been cleared. Tgfβ and Activin signalling induce fibronectin and collagen matrix deposition by differentiated proliferating myofibroblasts (Chablais and Jazwinska, 2012). Tgfβ type 1 receptor (Alk5/4) inhibition results in the reduction of Smad3 phosphorylation and markedly impairs the regenerative response. Tenascin C, a de-adhesive extracellular matrix protein, is implicated in cardiac remodelling at the injury border. It is essential for cardiomyocyte infiltration (Chablais and Jazwinska, 2012) which supports observations generated from adult mammalian models (Imanaka-Yoshida *et al*., 2001).

A fibrin dominant scar encases a collagen core by 7 days post cryoinjury, but the exact mechanisms, signals and cellular processes that mediate this organised scar structure remain largely unclear (Manuel Gonzalez-Rosa *et al*., 2011). The transient scar deposited in the zebrafish heart is essential for full repair; perturbation of the reparative phase with TGFβ signal inhibitors results in incomplete cardiac regeneration and gross malformation of the injured hearts due to partial ventricular rupture (Chablais and Jazwinska, 2012).

Additional fibronectin deposits are produced by the epicardium and are necessary for zebrafish heart regeneration. *Fibronectin* (*fn), fn1* and *fn1b,* expression can be observed in epicardial cells close to the injury. Concomitantly, cardiomyocytes around the injured

area express integrin β3 (itgb3). Fibronectin-itgb3 interaction is required for complete regeneration, likely through enhancing the migratory response of cardiomyocytes, as proliferation was unaffected by disruption of this pathway (Wang et al., 2013b). This is reminiscent of embryonic heart cardiac primordia fibronectin-dependent migration during heart tube formation (as described in section 1.1.1) (Garavito-Aguilar *et al*., 2010; Kupperman *et al*., 2000).

Remarkably, scar tissue is reabsorbed and replaced with new myocardium during the regenerative phase (Figure 7). The mechanisms involved in this process remain unclear. Understanding the endogenous events that trigger the removal of pathological scar tissue before maturation could help us uncover potential targets for therapies in humans.

1.4.4 Cardiomyocyte proliferation

1.4.4.1 Mammalian cardiomyocyte proliferation

The inability to replace the dead cardiomyocyte population results in the retention of fibrotic deposits within the lesion. Scar tissue does not possess any contractile properties; however, the spared myocardium must still meet cardiac demands. This ultimately causes hypertrophy of the surviving cardiomyocytes and the dilation of the ventricles, compromising heart function and leading to heart failure (Li *et al*., 1996). Mammalian cardiomyocytes become terminally differentiated shortly after birth and exhibit limited proliferative capacity thereafter (Li *et al*., 1996; Rumyantsev, 1977). Low homeostatic cardiomyocyte proliferation can be detected under basal conditions, cardiomyocyte turnover gradually declines from birth (Mollova *et al*., 2013) to approximately 0.5-1% per year in adult humans (Bergmann *et al*., 2009). Varying turnover rates are observed at different ages in other mammalian models, but mitotic cardiomyocytes consistently account for a minute percentage of the overall cardiac population (Li *et al*., 1996; Naqvi *et al*., 2014). Terminal differentiation coincides with a change in nuclear content (Li *et al*., 1998; Pasumarthi and Field, 2002). Cardiomyocytes of the neonatal mouse are mononuclear for the first 7 days after birth, then, the majority of cardiomyocytes undergo an incomplete round of cytokinesis, and remain in a

binucleated state (Figure 8). The loack of cytokinesis coincides with loss of neonatal mice regenerative capacity and upregulation of the cardiomyocyte cell cycle suppressor, *meis1* (Li *et al*., 1996; Mahmoud *et al*., 2013; Porrello *et al*., 2011a; Porrello *et al*., 2011b). In contrast, neonatal mouse cardiomyocytes have been demonstrated to retain proliferative properties up to 21 days after birth (Walsh *et al*., 2010). Despite disparities between studies, it is commonly accepted that shortly after birth, proliferative capacity diminishes. Similarly, in humans, a few months after birth, cardiomyocytes increase their DNA content and arrest in a polyploid mononuclear state (Figure 8) (Laflamme and Murry, 2011). This is associated with a loss of cardiomyocyte capacity to re-enter the cell cycle and results in the establishment of a heart described as "post-mitotic" (Mollova *et al*., 2013).

The number of cardiomyocytes in an adult mammal is predetermined and fixed postnatally; the post-mitotic human heart contains up to 9.5 billion cardiomyocytes (Mollova *et al*., 2013; Tang *et al*., 2009) of which up to a billion can be lost following MI (Murry *et al*., 2006). Post-mitotic mammalian cardiomyocytes can re-enter the cell cycle when stimulated (Engel *et al*., 2005), and following cardiac damage, approximately 3% of pre-existing cardiomyocytes on the periphery of the injury do so in a mouse model (Senyo *et al*., 2013). Nevertheless, the response is insufficient to replace damaged myocardium (Ali *et al*., 2014). Thus, other studies have made efforts to produce an alternative source of cardiomyocytes from endogenous or induced cardiac progenitor cells (Chong *et al*., 2011; Domian *et al*., 2009; Laugwitz *et al*., 2005; Smart *et al*., 2011).

In the neonatal mice models of MI *via* coronary ligation and apical resection, the primary source of neomyocytes are derived from pre-existing cardiomyocytes (Haubner *et al*., 2012). Attempts to replenish cardiac lesions by stimulating endogenous cardiomyocyte cell cycle re-entry or stem cell differentiation in adult mammals have been unsuccessful so far, but still maintain therapeutic promise (Garbern and Lee, 2013). Some studies implicate a pool of resident cardiac stem cells capable of producing a limited cardiomyocyte population, however, the consensus of these studies is that progenitor populations are insufficient to replace the huge cardiomyocyte loss that occurs following MI (Hsieh *et al*., 2007; Malliaras *et al*., 2013). One study estimated that c-kit (a receptor

tyrosine kinase) positive endogenous resident cardiac progenitor cells contribute to 0.03% or less of the total cardiomyocyte population following cardiac damage and thus questioned the physiological relevance of such a small population (Garbern and Lee, 2013; van Berlo *et al*., 2014). On the contrary, other studies reported that resident c-kit positive cells are essential for MI recovery, improve cardiac function and therefore hold therapeutic potential (Ellison *et al*., 2013; Hsieh *et al*., 2007; Loffredo *et al*., 2011; Senyo *et al*., 2013). The generation of new cardiomyocytes from a population other than pre-existing cardiomyocytes is still a hotly debated topic and an active area of research.

1.4.4.2 Zebrafish cardiomyocyte proliferation

Pre-existing cardiomyocytes are the primary source for cardiac neomyogenesis in zebrafish following cardiac injury (Gupta *et al*., 2013; Jopling *et al*., 2010; Kikuchi *et al*., 2010; Schnabel *et al*., 2011). In contrast to pathological cardiomyocyte hypertrophy occurring in the adult mammalian heart under stress, the zebrafish heart can undergo homeostatic growth to modify its size *via* cardiomyocyte proliferation throughout their lifetime (Itou *et al*., 2012a; Wills *et al*., 2008). The trigger for cardiomyocytes to re-enter the cell cycle may shed light on the proliferative capacity of adult zebrafish cardiomyocytes following cardiac damage. Cardiomyocyte mitogenic potential correlates with nuclei numbers and DNA content: neonatal mammals, urodele amphibians and teleost fish all maintain the ability to regenerate their heart, and all possess a majority of mononuclear diploid cardiomyocytes. In contrast, the adult mammalian heart is made up binucleated and polyploid cardiomyocytes. (Kikuchi and Poss, 2012). Zebrafish cardiomyocytes remain mononuclear and diploid throughout their lifespan and retain their regenerative capacity (Figure 8) (Itou *et al*., 2012a).

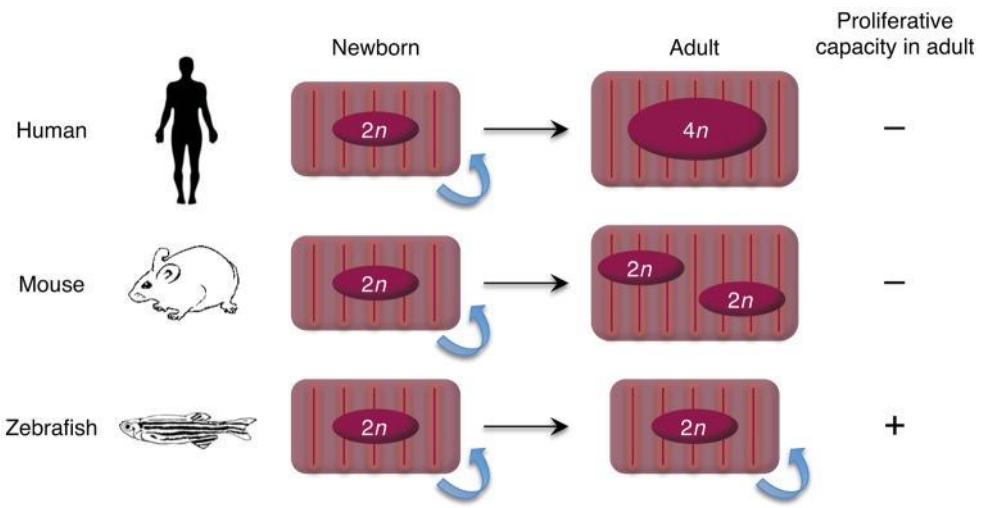

Figure 8 Cardiomyocyte nuclear content and proliferative capacity

Diagram illustrating human (upper row), mouse (middle) and zebrafish (bottom) cardiomyocytes nuclear content at birth and adulthood. Shortly after birth neonatal mammalian cardiomyocytes undergo an incomplete round of mitosis and arrest in a polyploid (human) or binucleated (mouse) state; this coincides with the time at which cardiomyocyte proliferative capacity is lost. Zebrafish cardiomyocytes remain in a mononuclear and diploid throughout their lifetime and cardiomyocytes retain proliferative potential. Blue arrows indicate regenerative capacity. Image modified from Kikuchi and Poss (2012)

Seven days after cardiac damage induced by cryoinjury, zebrafish enter the regenerative phase (Figure 7). Global cardiomyocyte proliferation is observed with increased myocardial proliferation at the injured area border and cardiomyocytes invade and replenish lost myocardium (Manuel Gonzalez-Rosa *et al*., 2011). The regenerative phase completes within 60 to 130 days (Figure 7) (Chablais and Jazwinska, 2012; Manuel Gonzalez-Rosa *et al*., 2011). Cardiomyocytes dedifferentiate and disassemble sarcomeric structures before dividing. This process is strongly associated with the expression of embryonic markers (Jopling *et al*., 2010; Kikuchi *et al*., 2010). The viable cardiomyocytes proximal to the damaged area re-express *nkx2.5* and *hand2* within 4 days of ventricular amputation (Lepilina *et al*., 2006). Further studies showed that at 7 days post-injury Fgf signalling induces *gata4* expression by subepicardial cardiomyocytes at the periphery of the injury within the compact layer. This cardiomyocyte population is thought to be the primary source of cells contributing to the regenerating neomyocardium (Kikuchi *et al*., 2010), although evidence exists for a significant contribution to new cardiac tissue by peripheral cardiomyocytes in the trabecular myocardium (Manuel Gonzalez-Rosa *et al*., 2011). NF-kappaB signalling was also demonstrated to initiate cardiomyocyte *gata5* expression upon injury (Karra *et al*., 2015). Cardiomyocytes localized at the epicardial edge of the injury proliferate extensively to provide new myocardium and migrate into the injured region leading to initial compact myocardium recovery (Gupta *et al*., 2013; Jopling *et al*., 2010). After this process, the scar is encased and the wound is described as “closed”. Subsequently the scar tissue is gradually removed and replaced with new myocardium (Gupta *et al*., 2013; Gupta and Poss, 2012; Manuel Gonzalez-Rosa *et al*., 2011).

Paracrine factors have been implicated in stimulating cardiomyocyte replication after cardiac damage in the zebrafish heart. Retinoic acid produced by the epicardium and endocardium signals to underlying healthy myocardium and is able to induce cardiomyocyte proliferation (Figure 9) (Kikuchi *et al*., 2011b). This is in contrast to the retinoic acid response observed in zebrafish during cardiac development, whereby retinoic acid was shown to restrict atrial cardiomyocyte addition from the second heart field and limit organ growth (Waxman *et al*., 2008). Leucocyte-derived TGFβ also

initiates zebrafish cardiomyocyte proliferation (Figure 9) (Chablais and Jazwinska, 2012), whereas the same signal drives pathological hypertrophy in adult mammalian hearts (Rosenkranz, 2004). It is also reported that PDGF signalling can influence the cardiomyocyte cell cycle, although it is uncertain whether this results from the secretion of mitogenic factors by PDGF-stimulated epicardium or if Pdgf can directly signal to cardiomyocytes (Kim *et al*., 2010). The epicardium also secrets Cxcl12a that signals through the cardiomyocyte receptor, Cxcr4, and induces migration and proliferation of the cells in close proximity to the lesion (Itou *et al*., 2012b).

Although the scar tissue is ultimately resorbed, extracellular matrix deposition and cardiomyocyte proliferation occur simultaneously (Kikuchi *et al*., 2010; Kikuchi and Poss, 2012). The newly generated myocardium does not recapitulate the initial architecture of the original healthy cardiac tissue, the compact layer is thicker in comparison with uninjured control hearts (Manuel Gonzalez-Rosa *et al*., 2011). Furthermore, it was reported that the regenerated myocardium presents altered contraction dynamics compared with uninjured myocardium. Despite the slight hypertrophic phenotype of the compact layer and asynchronous contraction after regeneration, cardiac function is fully restored (Manuel Gonzalez-Rosa *et al*., 2011).

1.4.5 Revascularisation

1.4.5.1 Mammalian angiogenesis

Part of the myocardium at risk is salvaged, and adverse remodelling and heart failure reduced when vascular supply to the ischemic tissue is enhanced in MI patients (Harada *et al*., 1996; Pearlman *et al*., 1995; Yanagisawa-Miwa *et al*., 1992). Although angiogenic signals are triggered early at the onset of MI, the lesion remains poorly vascularised in the mammalian heart (Dimmeler *et al*., 2005; Harrison *et al*., 2015). Hypoxia and mechanical stress induce the expression of VEGFA, a key mitogen essential for revascularisation (Heil and Schaper, 2004; Lee *et al*., 2000). VEGFA is primarily produced by hypoxic cardiomyocytes, endothelial cells and leucocytes recruited to the infarct (Berse *et al*., 1992; Taichman *et al*., 1997). Endothelial cells detect VEGFA *via* VEGFR2 (KDR), stimulating their proliferation and migration (discussed in further detail in section

1.5.5.2). The VEGFB isoform of VEGF has also been found to stimulate coronary artery growth post MI through a VEGFR1-NRP1 signalling axis in rats; however, this has not been replicated in other species (Kupatt and Hinkel, 2014; Lahteenvuo *et al*., 2009).

Despite the triggering of endogenous signalling in response to hypoxia, the blood supply to the infarcted area is insufficient; thus, stimulating revascularisation has been identified as a potential therapeutic target for the treatment of acute MI (Haider *et al*., 2009; Hao *et al*., 2007; Henry *et al*., 2003). Zangi *et al.* (2013) used modified RNA encoding VEGF in MI mice models and observed improved cardiac function in parallel with increased myocardial capillary density. The study also highlighted a previously uncharacterised epicardial response to VEGF that could also play a role in heart repair. However, attempts to increase revascularisation using VEGF, FGF or other angiogenic factors have not ameliorated cardiac dysfunction in MI patients (Haider *et al*., 2009; Henry *et al*., 2003; Losordo and Dimmeler, 2004). Although the delivery of endothelial or bone marrow-derived progenitor cells to the infarct area brings acute benefits, these effects are short-lived (Lunde *et al*., 2006; Schachinger *et al*., 2006). Additionally, VEGFA signalling, if not tightly regulated, can potentially result in the generation of leaky vessels and inhibition of vessel maturation because of interference with the PDGF pathway and mural cell recruitment (Cochain *et al*., 2013; Schwarz *et al*., 2000). One study by Hao *et al.* (2007) demonstrated that controlled VEGF and PDGF deliveries facilitated revascularisation following MI in rat and, ultimately, led to improved cardiac function

1.4.5.2 Zebrafish angiogenesis

In the injured adult zebrafish heart, new vessels are formed *via* angiogenesis (Zhao *et al*., 2014); however, until recently, the molecular mechanisms and characterisation of the revascularisation process after MI were largely undefined. Marin-Juez and colleagues (2016) reported that vessels are observed invading the cardiac lesion as early as 15 hours after cardiac damage and inhibition of the initial vascular response severely impedes the entire regenerative process. Therefore, the early-onset angiogenic response is essential for the regeneration of the zebrafish heart. Vegfaa signalling was shown to mediate early revascularisation (Figure 9) using a dominant negative Vegfaa mutant fish that presented reduced infarct vessel density, inefficient cardiomyocyte

proliferation, and permanent scar formation and failed to regenerate (Marin-Juez *et al*., 2016). Because neovascularisation precedes *vegfaa* upregulation (this occurs at 24 hour post injury); the authors hypothesised that endothelial cells responded to the local release of extracellular matrix-bound Vegfaa made available by proteolytic activity, as previously described by Ferrara *et al* (2010), but this requires further investigation.

Additionally, maturation of new coronary vessels *via* mural cell recruitment is central to the revascularisation of the cardiac lesion. Pericyte coverage maintains integrity and provides structural support for the newly formed vessels. Pdgfbb signalling is essential for endothelial cell proliferation and, upregulation of mural cell markers such as *acta2* by pericytes mediate angiogenesis following injury (Kim *et al*., 2010). The authors noted an upregulation of EMT markers such as *snail* and *twist1b* after apical resection reminiscent of arteriogenesis, which is partly regulated by FGF and PDGF signalling (Figure 9) (De Smet *et al*., 2014; Wiens *et al*., 2010). Inhibition of the Pdgfbb signalling pathway has deleterious effects on coronary vasculature formation and zebrafish heart regeneration. Whether Pdgf effects on revascularisation are mediated directly or indirectly *via* endothelial cells is unclear, but it was confirmed that Pdgf receptor β (Pdgfrβ) activity is required for vascular development in the lesion during regeneration (Figure 9) (Kim *et al*., 2010). Lepilina and colleagues (2006) demonstrated the importance of Fgf signalling for the regulation of vessel formation during zebrafish heart regeneration. Dominant negative Fgfr2 zebrafish mutants were unable to regenerate their heart after apical resection due to their inability to revascularise the injury site. These studies strongly suggest that epicardial transdifferentiation is largely regulated by Pdgf and Fgf signalling during zebrafish heart regeneration (discussed in greater detail in section 1.4.6).

.

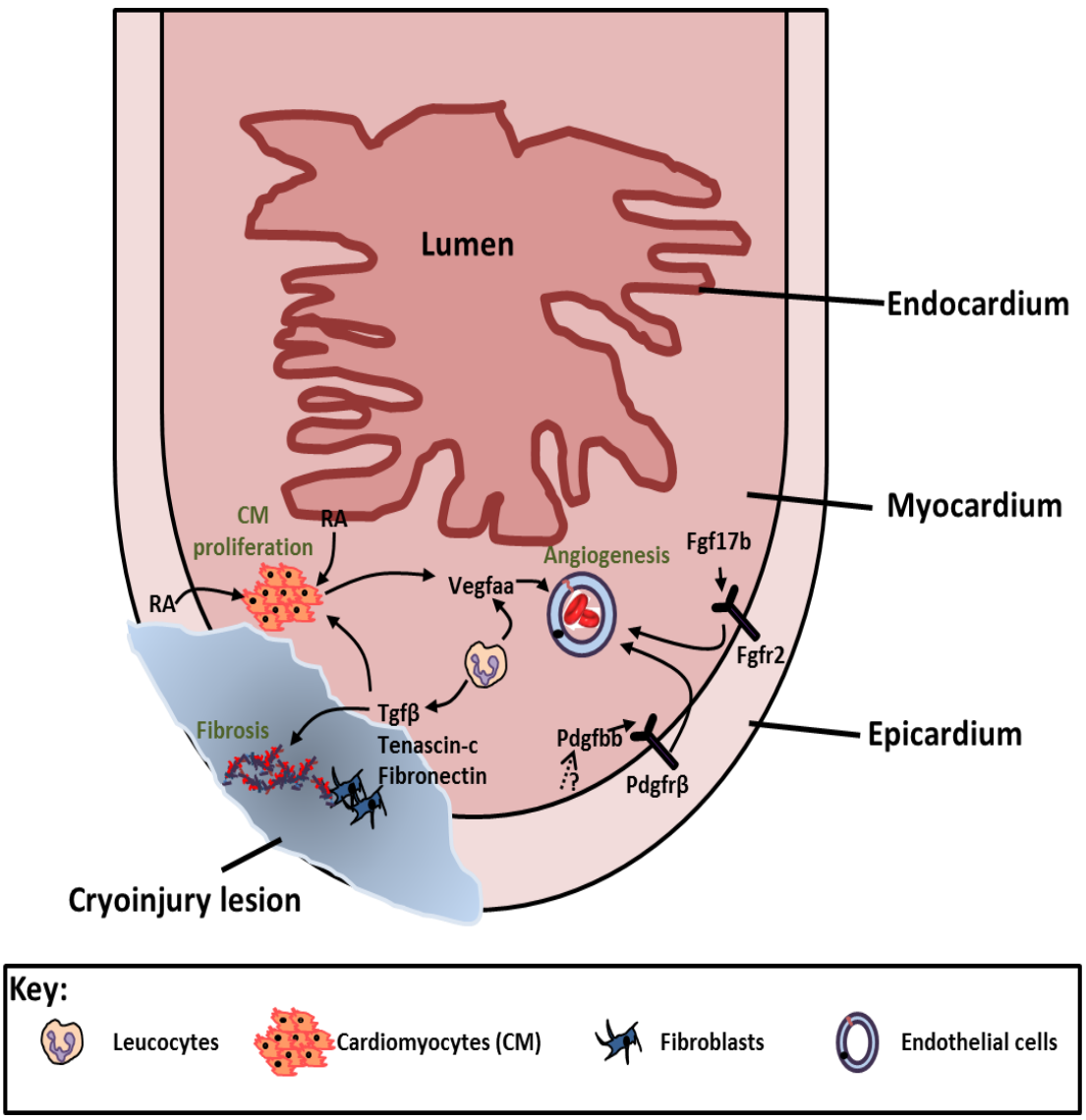

Figure 9 Signalling pathways and cellular mechanisms in zebrafish heart regeneration.

Retinoic acid (RA) produced in the epicardium and endocardium stimulate cardiomyocyte (CM) proliferation additional to Tgfβ production by fibroblasts and leucocytes. Tgfβ also coordinates fibrosis and remodelling of the lesion in conjunction with tenascin-c and fibronectin synthesised by fibroblasts. Angiogenesis is promoted by several paracrine factors, Vegfaa is produced by hypoxic cardiomyocytes. It is hypothesized that hypoxic infiltrating leucocytes and local release of ECM bound Vegfaa provide additional Vegf sources. Pdgfbb and Fgf17b (derived from cardiomyocytes) signalling through epicardial cell Pdgfrβ and Fgfr2, respectively, facilitate neovessel maturation.

1.4.6 Epicardial response in zebrafish heart regeneration

The epicardium is a mesothelial epithelial monolayer surrounding the heart. It is made of a quiescent cell population that provides basal cytokine secretion for the homeostasis of the underlying myocardium (Wills *et al*., 2008). However, following cardiac damage, the epicardium becomes "activated", proliferates and facilitates cardiac repair. This is highlighted by the expression of epicardial embryonic transcription factors; such as, *wilms tumour 1 (wt1*), *T-box 18* (*tbx18*) and *retinoic acid synthase enzyme retinaldehyde dehydrogenase 2* (*raldh2*) which are otherwise silenced shortly after cardiac maturation (Takeichi *et al*., 2013; Zhou and Pu, 2011). Injury-activated embryonic epicardial gene profile expression is conserved in adult mammals after MI (Limana *et al*., 2010; van Wijk *et al*., 2012; Zhou *et al*., 2011a), and in regenerative models such as the zebrafish and neonatal mouse (Kikuchi *et al*., 2011b; Lepilina *et al*., 2006; Manuel Gonzalez-Rosa *et al*., 2011; Porrello *et al*., 2011b). This suggests that the upregulation of epicardial developmental genes in response to cardiac damage is conserved across species.

In zebrafish, the epicardium responds to cardiac damage by proliferating extensively around the injured area (Manuel Gonzalez-Rosa *et al*., 2011; Schnabel *et al*., 2011). Organ wide epicardial activation occurs very rapidly after cardiac damage. It is evident as early as 3 hours after injury in zebrafish (Kikuchi *et al*., 2011b), within 24 hours in adult mammals (von Gise *et al*., 2011), then soon becomes restricted to the injured area. The epicardial activation is highly responsive, such that even after sham operation, *raldh2* expression is detected in the epicardium, though *wt1* and *tbx18* expression are not induced in these conditions, suggesting partial activation after sham operation (Itou *et al*., 2014). A recent study investigated the importance of the epicardium after cardiac injury using genetic ablation of the epicardial cell population, showing that hearts devoid of epicardium do not regenerate (Wang *et al*., 2015).

The role of the epicardium is central to cardiac repair and has been extensively studied. In zebrafish, it provides structural support *via* the secretion of fibronectin and thus supports myocardial proliferation and migration (Wang et al., 2013a). This is in line with the role of fibronectin during cardiogenesis when the timely migration of myocardial precursors relies on epithelial integrity (Trinh and Stainier, 2004), but contrasts with the

pathological association of ECM deposition in cardiac fibrosis following adult mammalian MI (Brooks *et al*., 2010; Knowlton *et al*., 1992; Willems *et al*., 1996).

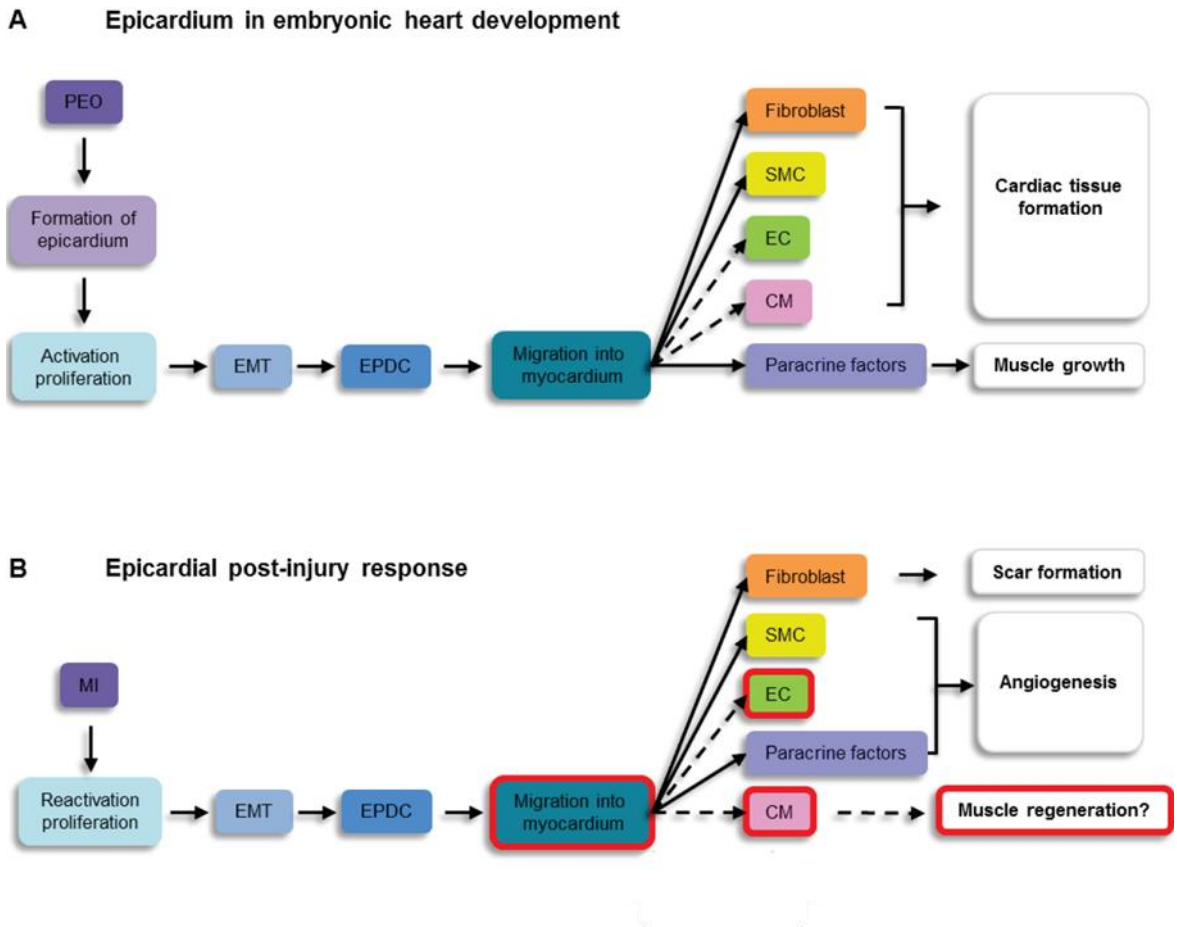

Figure 10 Epicardial-derived cells (EPDC) in the embryonic and injured mammalian heart

(A) Flow chart describing proepicardial (PEO) progenitor cell fates and functions following epicardial epithelial to mesenchymal transition (EMT) in embryonic development. **(B)** Flow chart diagram of adult heart epicardial response to myocardial infarction (MI) and EPDC fate and functions. EPDC transdifferentiate to fibroblasts and smooth muscle cells (SMC) and secrete cytokines. It remains unclear whether EPDCs adopt an endothelial cell (EC) or cardiomyocyte (CM) fate. Dashed lines and red boxed highlight outcomes that remain unclear at present. Image adapted from (Smits and Riley, 2014)

1.4.6.1 Epicardial derived paracrine signalling

An increasing body of evidence supports the epicardium as a central signal transducer for paracrine and autocrine signalling that orchestrates cellular events required to achieve zebrafish heart regeneration. Treatment of infarcted hearts with conditioned medium supplemented with epicardial secreted factors improves cardiac function and enhances coronary vasculature density (Zhou *et al*., 2011a). In the following paragraphs, I will highlight some of the epicardium-derived cytokines playing a conserved role across species in the response to cardiac damage as well as cytokines with promising therapeutic potential that were characterised in model systems.

The epicardium secretes retinoic acid (RA) both during development and following cardiac damage. Retinoic acid transduces signals *via* retinoic acid receptors (RARs) that form heterodimers, translocate to the nucleus and mediate transcription factor activities to regulate gene expression. In the adult mammalian heart, shortly after MI, the epicardium re-expresses embryonic-associated RA synthesising enzyme RALDH2 (also referred to as Aldh1a2 in the zebrafish) and the production of RA inhibitors is reduced (Bilbija *et al*., 2012; Zhou and Pu, 2011). Raldh2 is expressed by the zebrafish epicardium following cardiac damage, indicating conserved epicardial RA production between species. Additionally, Raldh2 is expressed by the endocardium, which is not observed in the mammalian heart after MI (Kikuchi *et al*., 2011b; Limana *et al*., 2010). In the zebrafish heart, epicardial expression of *radlh2* accumulates near the injury site and enhances cardiomyocyte proliferation (Kikuchi *et al*., 2011b). In contrast to its beneficial effects in zebrafish, RA encourages pathological inflammatory cell infiltration (Huang *et al*., 2012) and consequently mediates the fibroblast synthetic profile and ECM deposition in mammals (Figure 10)(Bilbija *et al*., 2012).

In the mouse, FGF2 (also referred to as basic FGF (bFGF)) and FGF9 are secreted by epicardial cells after MI and mediate autocrine and paracrine signalling (Zhou *et al*., 2011a). In line with its role in zebrafish, FGF signalling helps cardiac recovery in mammals. Mice lacking FGF2 exhibit increased infarct size caused by the lack of scar tissue formation and fibroblast proliferation that compromise cardiac function; this is compounded by limited angiogenesis (Virag *et al*., 2007). The reverse was observed in

FGF2 overexpressing mice, whereby greater fibroblast proliferation caused excessive scar deposition, and vascular density and increased cardiomyocyte hypertrophy, ultimately improving cardiac function (Virag *et al*., 2007). In the zebrafish, Fgf17b, derived from cardiomyocytes, signals through Fgfr2 in the epicardium to mediate epicardial EMT (Figure 9) (further described in section 1.4.6.2). In addition, Pdgf is essential for epicardial cell proliferation and neovascularisation, and is essential for the epicardial response to cardiac damage in zebrafish (Kim *et al*., 2010; Lien *et al*., 2006).

1.4.6.2 Epithelial to mesenchymal transition

Epithelial to mesenchymal transition (EMT) is the process whereby epithelial cells transdifferentiate to a mesenchymal phenotype and acquire a migratory profile. EMT has been described in several physiological and pathological processes and is particularly associated with cancer metastasis (Chaffer *et al*., 2016), during which epithelial cells delaminate from the epithelial layer, and migrate to other organ tissues (Figure 11). During mammalian cardiac development, epicardial cells undergo epicardial EMT in response to PDGF; they migrate into the underlying myocardium and transdifferentiate into vascular smooth muscle cells, cardiac fibroblasts and pericytes (Figure 10) (further discussed in section 1.1.1.4) (Lu *et al*., 2001). The re-expression of embryonic epicardial markers after cardiac injury in the adult heart has led to the hypothesis that the epicardium recapitulates developmental events such as EMT to facilitate revascularisation and fibrosis (Zhou *et al*., 2011a). This concept has been convincingly demonstrated by several other studies that have used lineage tracing to identify epicardial cell fate in the regenerating adult zebrafish heart (Aguiar and Brunt, 2015; Kikuchi *et al*., 2011a; Kim *et al*., 2010; Lepilina *et al*., 2006; Manuel Gonzalez-Rosa *et al*., 2012). A subpopulation of these epicardial cells undergo epithelial-to-mesenchymal transition and migrate into the damaged myocardium to provide vascular smooth muscle cells (Lepilina *et al*., 2006) and myofibroblasts (Chablais and Jazwinska, 2012) (Figure 11).

Myocardium-derived Fgf17b is reported to signal through epicardial Fgfr2 and Fgfr4 to initiate epicardial EMT and promote revascularisation of the injured area. Inhibition of Fgf signalling *via* dominant negative Fgfr transgenic fish resulted in reduced migration

of activated *tbx18*-positive epicardial cells into the injury area, implicating a role for Fgf induced epicardial migration. Kim *et al.* (2010) demonstrated that Pdgfbb, *via* Pdgfrβ, mediates a similar epicardial response during zebrafish heart regeneration. In primary epicardial cultures the authors showed that Pdgfbb enhances proliferation and stimulates epicardial tight junction disassembly, two key features observed in epicardial EMT during regeneration indicating a loss of epithelial identity. Inhibition of Pdgfbb signalling perturbs epicardial expression of EMT markers following injury and abrogates heart regeneration. This study also elucidated that Pdgf signalling was transduced, at least in part, by Rho-associated protein kinases in primary epicardial cultures.

Wt1 expression by activated epicardium targets the upregulation of *snai1* (encoding transcription factor Snail) and *twist*, which in turn, promotes a migratory phenotype essential for EMT (Martinez-Estrada *et al*., 2010). *Wt1b,* and not its *wt1a* ohnolog, is specifically expressed by epicardial cells after injury in the zebrafish (Aguiar and Brunt, 2015; Schnabel *et al*., 2011). However, not the entire epicardial cell population express *wt1b* after cardiac damage presumably indicating that only a subpopulation of epicardial cells undergo EMT (Manuel Gonzalez-Rosa *et al*., 2011; Peralta *et al*., 2014).

1.4.6.3 Endocardial response to injury

During zebrafish cardiac repair, endocardial expression of Raldh2 is observed within 3 hours of cardiac injury and is restricted to the injury site by 24 hours. The endocardium undergoes endothelial to mesenchymal transition (endoMT) which induces morphological changes, endothelial delamination from the endocardium and transdifferentiate to contribute fibroblast mural cells in the injury site proliferation (Kikuchi *et al*., 2011b). Although different to the zebrafish response, the mammalian heart is also known to elicit an endocardium response after MI. Endocardium-derived FGF-2 is implicated in cardiomyocyte proliferation and growth. It is expressed by the endocardium for up to 14 days post MI in the mammalian heart (Zhao *et al*., 2011) supporting a role for the endocardium in cardiac repair. Few studies have addressed the endocardial response to cardiac damage and regeneration, but clear evidence exists for a damage-induced response that likely helps recovery.

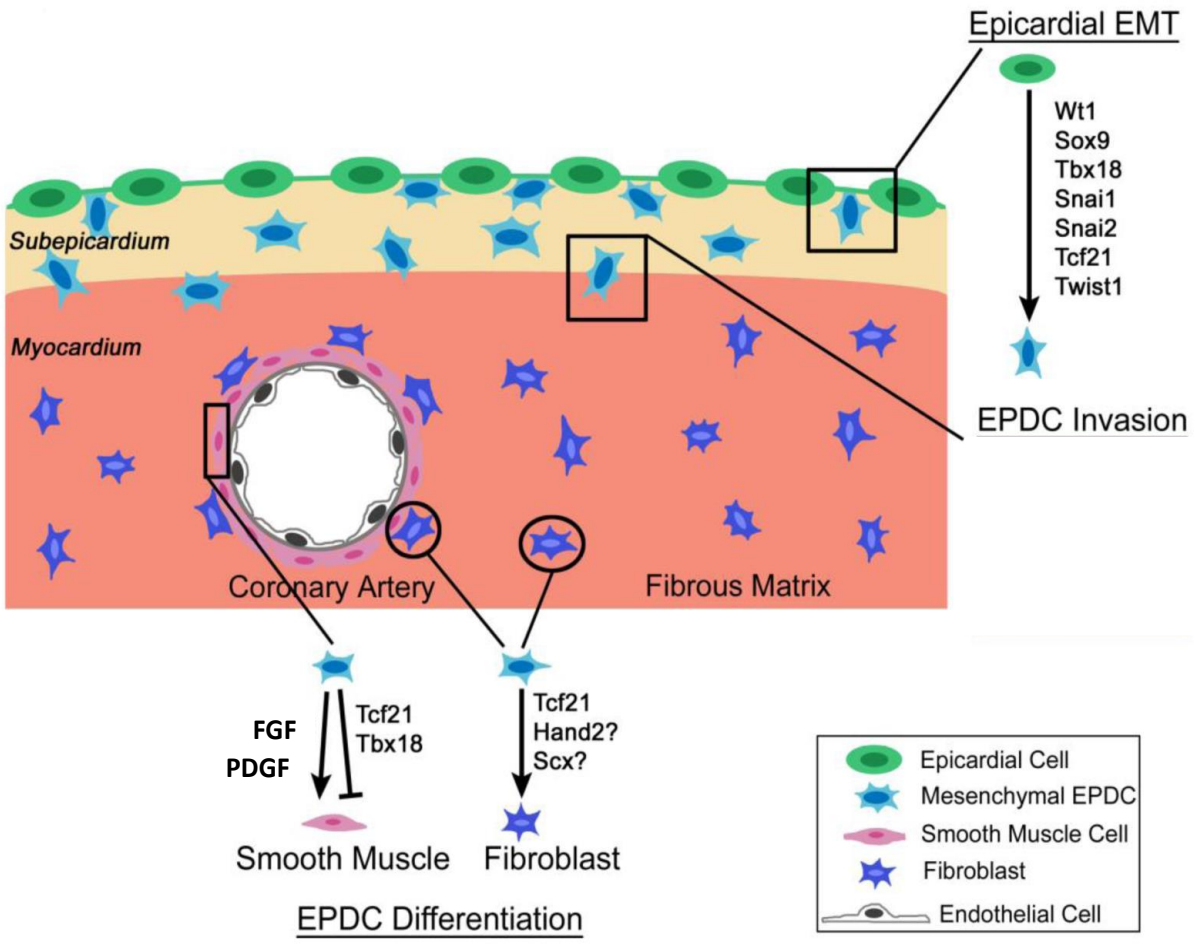

Figure 11 Epicardial epithelial to mesenchymal transition (EMT)

Schematic representation of epicardial EMT. Epicardial cells (green) express embryonic genes (listed to the right) that induce a mesenchymal profile and trigger delamination from the epicardium, giving rise to migratory epicardial derived cells (EPDCs) (light blue). EPDCs translocate to the myocardium and transdifferentiate into fibroblasts (dark blue) to synthesise extracellular matrix and pericytes/smooth muscle cells (pink cells) to support coronary vasculature maturation. The precise signal pathways that drive EPDC fate are undercharacterised. Image modified from Braitsch and Yutzey (2013)

1.5 Neuropilin as a potential contributor to zebrafish cardiac regeneration

It is evident that several cell types and signals co-ordinate zebrafish heart regeneration, however, there remain many candidate signalling pathways to be characterised. The co-receptor, neuropilin (NRP), has been reported to modulate signalling of a number of extracellular ligands, namely VEGF, PDGF, FGF and TGFβ (Evans *et al*., 2011; Glinka and Prud'homme, 2008; Liu *et al*., 2005; Pellet-Many *et al*., 2011; Soker *et al*., 1998). These signalling pathways have also been demonstrated to be essential regulators of zebrafish heart regeneration (Chablais and Jazwinska, 2012; Kim *et al*., 2010; Lepilina *et al*., 2006; Marin-Juez *et al*., 2016). However, the role of neuropilins in zebrafish heart regeneration has not been characterised to date.

1.5.1 Neuropilin structure

Neuropilins (NRPs) are type 1 transmembrane glycoprotein receptors. In humans, two NRP isoforms exist, NRP1 and NRP2, which share 44% protein sequence similarity (

Table **1**). The zebrafish karyotype contains 25 pairs of chromosomes; and the zebrafish genome encodes four neuropilins, *nrp1a*, *nrp1b*, *nrp2a* and *nrp2b* due to evolutionary teleost fish genome duplication (Amores *et al*., 1998; Phillips *et al*., 2006; Postlethwait *et al*., 1998). Zebrafish Nrp1a and Nrp1b ohnologs are the zebrafish orthologs for human NRP1 (hNRP1) and share 65% and 51% protein sequence similarity with hNRP1, respectively (

Table 1). A similar level of sequence similarity is observed between human NRP2 and zebrafish orthologs, Nrp2a and Nrp2b (57% and 59%, respectively) (

Table 1) (Bovenkamp *et al*., 2004).

NRP1 was originally identified in 1987 *via* an antibody screen in the developing xenopus brain and termed the A5 antigen (Takagi *et al*., 1987). Subsequently, its basic structural features were characterised (Fujisawa et al., 1989) and was named neuropilin, because the A5 antigen was found localised in the xenopus 'neuropile', a dense neuronal structure (Fujisawa et al., 1995; Takagi et al., 1991). NRP2 was later characterised in

1997 and identified as a NRP1 isoform because of structural similarities (Chen *et al*., 1997). Although both were initially reported in neuronal development, they have since been described as regulators of various additional physiological and pathological processes.

Table 1 Full-length NRP amino acid sequence similarity (%)

Protein % homology	zf Nrp1a	zf Nrp1b	Zf Nrp 2a	zf Nrp2b	hNRP1	hNRP2
zf Nrp1a (923 aa)	100	54.9	43.9	43.6	65.8	45.9
zf Nrp1b (959 aa)	54.9	100	47.3	47.1	51.5	41.6
zf Nrp2a (927 aa)	43.9	47.3	100	74.0	43.7	56.6
zf Nrp2b (920 aa)	43.6	47.1	74.0	100	43.4	59.3
hNRP1 (923 aa)	65.8	51.5	43.7	43.4	100	44.2
hNRP2 (926 aa)	45.9	41.6	56.6	59.3	44.2	100

h – human, zf – zebrafish, aa – amino acid

The neuropilins derive from two structurally conserved genes that encode the 923 amino acid (aa)-long NRP1 and the 926 aa-long NRP2 proteins, both with an approximate molecular mass of 130 kDa (Chen *et al*., 1997). The NRPs consist of a large extracellular domain (ectodomain), anchored to the cell by a single pass transmembrane domain and contain a small intracellular cytoplasmic domain (Figure 12). The ectodomain is formed by 5 protein homology domains: two CUB repeats (a1/a2) , two FA58C domains (b1/b2) and a MAM domain (c) (Takagi *et al*., 1991). The protein domain arrangement is conserved between species; they contain the identical ectodomain organisation (a1/a2, b1/b2, MAM).

The CUB domains share significant similarity with complement factor C1s/C1r, Uegf (sea urchin fibropellins) and Bone Morphogenetic Protein 1 (BMP1) proteins (Bork and Beckmann, 1993). Each of the CUB domains contain approximately 100 aa residues arranged in an anti-parallel β-barrel structure and require calcium to mediate electrostatic protein-protein interactions (Gaboriaud *et al*., 2011). NRP1 and NRP2 CUB domains are required for class 3 semaphorin binding to modulate axonal guidance (described in greater detail in section 1.5.5.1) (Gu *et al*., 2002).

The FA58C domains (b1/b2) are 150 aa regions that share structural similarity to the C-termini anion-binding structures of blood coagulation factors V and VIII. The b1 domain is essential for both semaphorin and VEGF binding (Appleton *et al*., 2007). The b2 domain further enhances NRP affinity for VEGF (Appleton *et al*., 2007; Gu *et al*., 2002).

The MAM (c) domain has homology to mephrin (a cell-surface glycoprotein), A5 antigen (the former name of NRP) and receptor tyrosine protein phosphatase μ and κ. The MAM domain has been previously implicated in neuropilin receptor oligomerisation and the formation of signal complexes to mediate semaphorin signal transduction to plexin-A1 (Nakamura *et al*., 1998; Takahashi *et al*., 1997). However, a recent study elucidated that the MAM domain alone is insufficient for receptor multimerisation and proposed that the MAM domain's function is to modify neuropilin domain positioning and optimise protein/protein interactions in signal complexes (Yelland and Djordjevic, 2016).

The cytoplasmic carboxyl (C)-terminal domain of neuropilins is made of 44 amino acid residues for NRP1 and 43 for NRP2, and does not possess any known enzymatic activity; thus, neuropilin complex formation with other receptors has been considered to be the primary mechanism for neuropilin signal transduction. This theory is supported by studies that showed no downstream signalling in response to VEGF stimulation of cells expressing NRPs but devoid of VEGFRs (Gluzman-Poltorak *et al*., 2000; Soker *et al*., 1998). The C-terminus ends with the protein sequence serine-glutamic acid (glutamate)-alanine (S-E-A); this motif interacts with PDZ (post synaptic density protein (PSD95), Drosophila disc large tumor suppressor (DlgA), and zonula occuldens-1 protein) homology domain-containing intracellular proteins. Further studies have demonstrated that the neuropilin C-terminus mediates interactions with a variety of cytosolic proteins,

best described as scaffold adaptor proteins, including synectin (also known as GIPC and neuropilin-interacting protein-1) (Cai and Reed, 1999). Synectin regulates the endocytosis of membrane receptors *via* myosin VI recruitment to form non-coated vesicles (Naccache *et al*., 2006). This mechanisms is thought to facilitate receptor signal transduction as VEGFRs propagate signalling most efficiently from intracellular vesicles (Lanahan *et al*., 2010). Furthermore, the PDZ domain has been implicated in VEGFR2 complex formation, as deletion of the SEA C-terminal sequence of NRP1 impairs VEGFR2 multimerisation (Prahst *et al*., 2008). The C-terminus can regulate receptor trafficking *via* rab proteins to facilitate endocytosis and has been linked to the turnover of focal adhesion components to aid cell motility (Seerapu *et al*., 2013). The NRP1 C-terminus is required for cytokine stimulation of tyrosine phosphorylation of the integrin adaptor molecule p130Cas phosphorylation that participates in the formation of a signalling platform to enhance cell motility, cytoskeletal organisation, cell survival and proliferation (Cai and Reed, 1999; Evans *et al*., 2011; Lanahan *et al*., 2010; Pellet-Many *et al*., 2011).

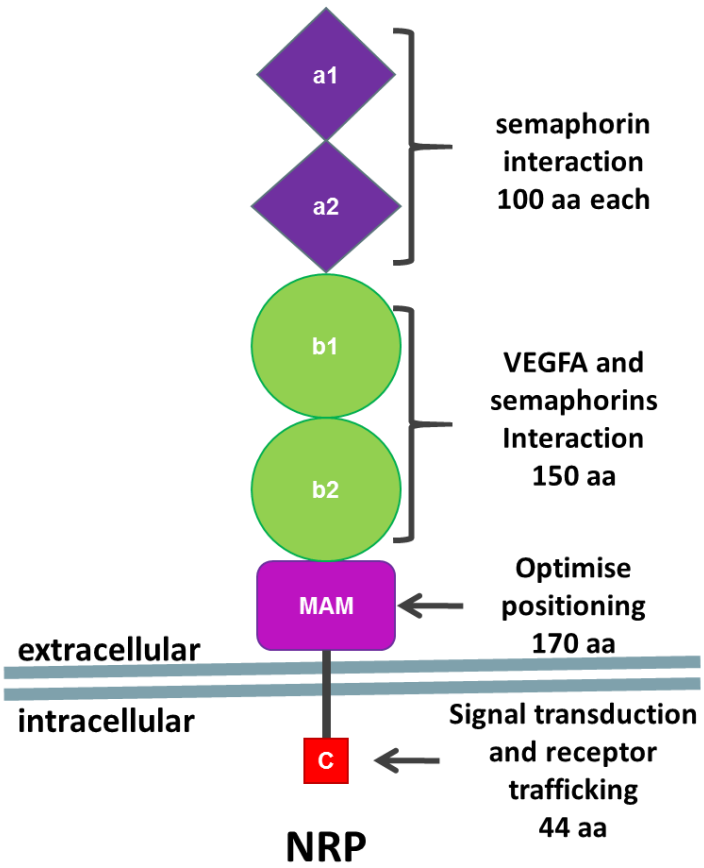

Figure 12 Neuropilin structure

Representative diagram depicting basic neuropilin structure. The ectodomain consists of the semaphorin-interacting a1 and a2 domains (CUB domains) (purple), VEGF-binding (and other heparin binding growth factors) b1 and b2 (FA58C) (green) and the MAM domain (pink) implicated in optimising receptor binding. The receptor has a single-pass transmembrane domain (grey) and a small cytosolic C-terminal domain (red) that mediates signal transduction with cytosolic proteins and regulates receptor trafficking. aa – amino acids

1.5.2 Neuropilin 1

1.5.2.1 Human NRP1

Full-length *NRP1* is a 120 kilo base pair (kb)-spanning gene located on chromosome 10p12 and encoding a 17 exons/16 introns gene transcribed into a 7kb mRNA (Rossignol *et al*., 2000). Several variants are differentially spliced to generate either a shorter transmembrane NRP1 lacking exon 16 (Tao *et al*., 2003) or a soluble NRP1 (sNRP1) species (Figure 13). sNRP1 is encoded by a 2.2-2.5kb-long mRNA sequence and translated to a 90kDa protein containing the CUB (a1/a2) and coagulation factor domains (b1/b2) (Figure 13) (Gagnon *et al*., 2000). Several sNRP1 exist as a 551- 704 amino acid peptide; termed s_{12}NRP1, s_{11}NRP1, s_{III}NRP1 and s_{IV}NRP1 referring the exons they contain. The soluble species retain the structural features required for ligand interaction but lack the MAM, intracellular and transmembrane domains and additionally encode a unique GIK (glycine-isoleucine-lysine) aa sequence (Figure 13). s_{12}NRP1 has been demonstrated to act as $VEGF_{165}$ antagonist/decoy for VEGF *in vitro* (Figure 14) (Gagnon *et al*., 2000). Although the endogenous physiological sNRP splice variant roles are still uncharacterised, soluble NRP species may alter NRP activity to be antagonistic as a monomer, but an agonist when dimerised, aiding delivery of ligands (Figure 14) (Yamada *et al*., 2001). Another two isoforms, s_{III}NRP1 (551aa) and s_{IV}NRP1 (609 aa) were later identified. They contain a similar structure (a1/2, b1/2) and are endogenously expressed in normal and cancerous tissue in humans (Cackowski *et al*., 2004). Soluble and full-length neuropilins are differentially expressed: full length NRP1 is found mostly in neuronal tissue and vessels, whereas, sNRP1 is not detected in endothelial cells (Rossignol *et al*., 2000).

Moreover full-length neuropilin is subject to posttranslational modifications that vary in different tissues; O-linked chondroitin sulphate addition at ser612 and N-linked glycosylation (CS-GAG) (Figure 13) are proposed to modify migratory capacity but further studies are required to elucidate the role of the modification (Frankel *et al*., 2008; Pellet-Many *et al*., 2011; Shintani *et al*., 2006). Ser612 is encoded by some sNRP1 isoforms, and not all undergo posttranslational modification by CS-GAG addition.

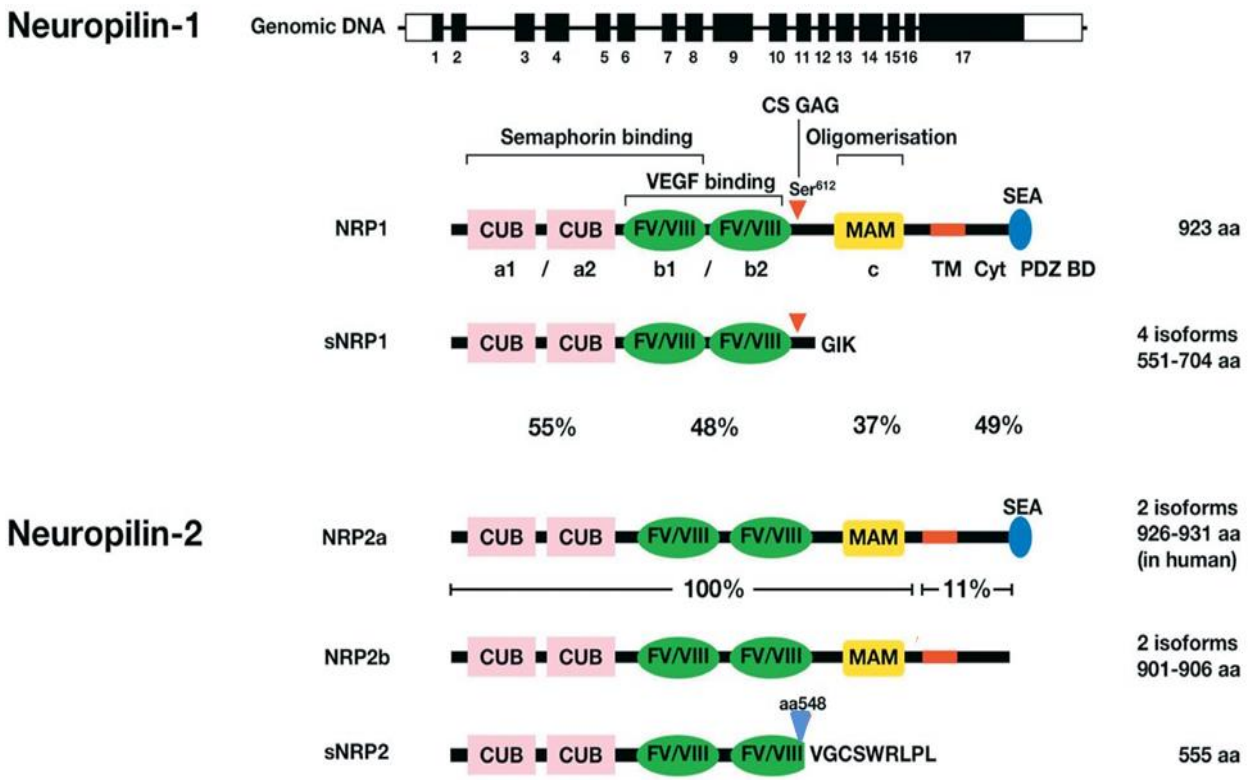

Figure 13 Neuropilin isoform homology

Illustrations representing neuropilin gene organization and protein structures. NRPs are encoded by a 17 exon gene (black rectangles). Both full-length NRP1 (923 amino acids (aa)) and NRP2 (926 - 931 aa) proteins contain a large ectodomain; two CUB (a1 and a2) domains (pink); two Factor V/VIII homology (b1 and b2) domains (green); a linker region; a MAM (c) domain (yellow); a single transmembrane domain (TM) (red); and a 43-44 aa cytoplasmic (Cyt) domain containing a C-terminal PDZ-binding domain motif (PDZ BD) (blue), with the sequence, SEA. The ectodomain mediates semaphorin and VEGF ligand interactions and optimises oligomerisation (indicated). NRP1 is subject to posttranslational O-linked CS-GAG modification (CS GAG) at Ser612 (red arrows). Soluble NRP1 (sNRP1) is truncated between the second Factor V/VIII and the MAM domain and ends with the three amino acids GIK. NRP2 exists as two main isoforms (NRP2a and NRP2b) that have identical ectodomains, but share only 11% transmembrane/C-terminal homology. NRP2b lacks the SEA PDZ-motif binding domain. A soluble NRP2 (sNRP2) is truncated at aa 548 (blue arrow) with an additional 9 aa (VGCSWRLPL). Sizes of NRPs and splice variants are indicated to the right. Amino acid homology between full-length NRPs is indicated as %values. Image modified from Pellet-Many *et al.* (2008)

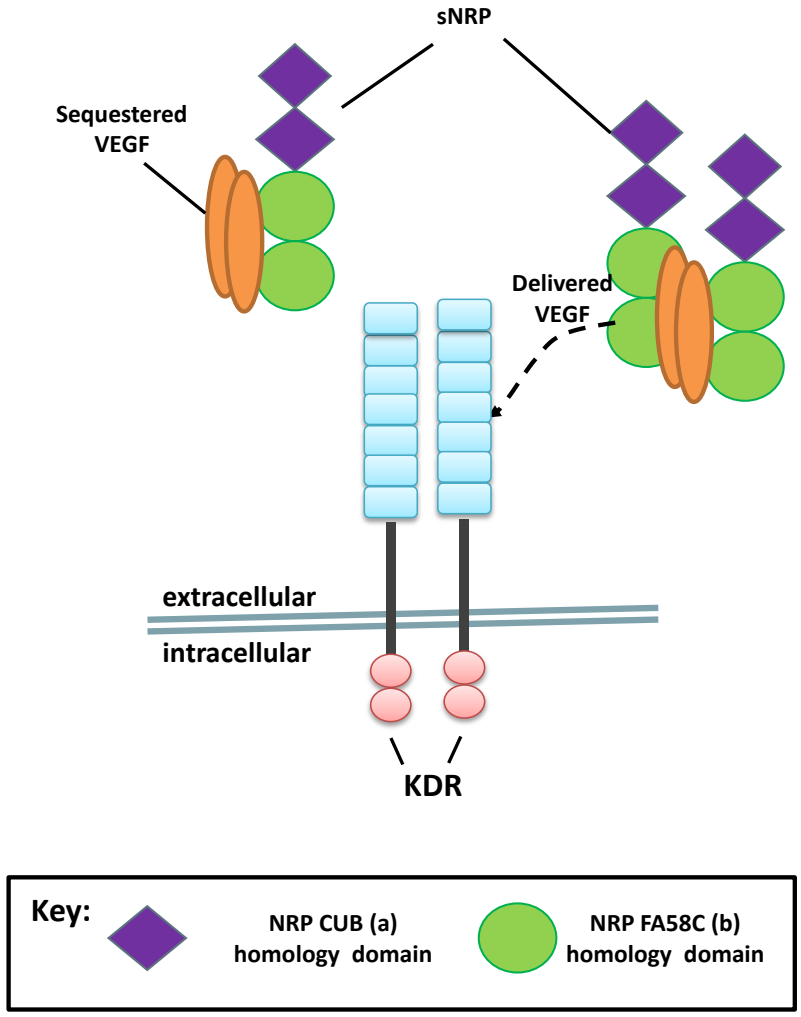

Figure 14 Soluble neuropilin mechanisms

Representative image of soluble neuropilin (sNRP) sequestration and delivery of vascular endothelial growth factor (VEGF) to receptors. When monomeric (left), sNRP acts a VEGF signalling antagonist. When sNRP is dimeric (right) it is thought to deliver VEGF to KDR (VEGFR2) rather than act as a decoy.

1.5.2.2 Zebrafish NRP1

Evolutionary teleost genome duplication gave rise to two zebrafish *nrp1* genes, *nrp1a,* and its ohnolog, *nrp1b.* The zebrafish *nrp1a* gene is located in linkage group 24 (chromosome 23), and encodes a 4 kb-long mRNA translated into a 923 aa protein of 125kDa (Bovenkamp *et al.*, 2004). The *nrp1b genes* is located in linkage group 2 (chromosome 8) and contains a 4.5 kb-long mRNA encoding for a 959 aa protein of

approximately 145kDa (Bovenkamp *et al*., 2004). A soluble Nrp1b (Nrp1b(s)) is endogenously expressed in the zebrafish. This isoform is 871 aa-long and translated into a 135kDa protein comprising the entire ectodomain, but lacking TM and C-terminus. It is therefore comparatively larger than the endogenous human sNRP1 isoforms that contain exclusively a1/a2, b1/b2 (Yu *et al*., 2004).

1.5.3 Neuropilin-2

1.5.3.1 Human NRP2

NRP2 is a 17 exons/16 introns gene located on chromosome 2q34, spanning over 112 kb and encoding a 926-931 aa-long protein. Two distinct isoforms, NRP2a and NRP2b, with identical ectodomains, are expressed in humans, however, their C-terminus and transmembrane domain exhibit only 11% protein sequence similarity (Figure 13) (Rossignol *et al*., 2000). NRP2a contains the SEA C-terminal sequence, whereas NRP2b is devoid of the PDZ-binding motif (Figure 13). Two NRP2a isoforms exist, $NRP2a_{(17)}$ and $NRP2a_{(22)}$ in humans, and four in mice (with the addition of $NRP2a_{(0)}$ and $NRP2a_{(5)}$), which are alternative splice variants resulting from the addition of 0, 5, 17 or 22 amino acids after amino acid 809 (between the MAM and transmembrane domain). The differential functions and roles of these isoforms caused by these insertions are undefined. Two endogenous isoforms of NRP2b also exist in humans. Similarly to NRP2a, insertions of either zero or 5 residues are added after amino acid 808, to generate $NRP2b_{(0)}$ or $NRP2a_{(5)}$, respectively (Rossignol *et al*., 2000).

Despite their identical extracellular domains, divergent roles for the different C-termini have evolved and their tissue expression varies. NRP2b is the isoform predominantly expressed in skeletal muscle, whereas NRP2a is seen in lungs, small intestine and kidneys, and both are present in the brain and heart (Rossignol *et al*., 2000). Lastly, a soluble NRP2 species, generated by alternative splicing, also exists. It is a 555 aa-long protein (62kDa) containing the a1/a2, b1 and a truncated b2 domain with a 9 aa insertion, and thus termed (s_9NPR2) (Figure 13) (Rossignol *et al*., 2000).

1.5.3.2 Zebrafish NRP2

The zebrafish *nrp2a* gene is located in linkage group 1 (chromosome 6) and encodes a 5.3 kb-long mRNA translated into a 927 aa-long protein (Bovenkamp *et al*., 2004). The *nrp2b* gene is located in linkage group 9 (chromosome 5) encodes a 4.8 kb gene and is translated into a 920 aa-long protein. The molecular weights of Nrp2a and Nrp2b have not yet been characterised in the zebrafish. Similarities to the Nrp1a and Nrp1b protein sequence would predict a molecular weight for Nrp2 of approximately 130kDa, however, post-translational modifications may alter molecular size. The zebrafish neuropilin 2 ohnologs both encode two small soluble splice variants, *nrp2a* express *nrp2a1* (1423bp, 309aa) and *nrp2a2* (437 bp, 84 aa). *nrp2b1* (759bp, 101 aa) and *nrp2b2* (704bp,188 aa) are splice variants (Bovenkamp *et al*., 2004), but their physiological role is unclear.

1.5.4 Neuropilins in development

1.5.4.1 Mammalian NRPs in development

Mammalian and zebrafish neuropilins have important roles in neuronal and vascular embryonic development. NRP1 null-mutant mice die *in utero* between embryonic day (E) 12 and E13.5 due to severe vascular and neuronal defects (Gerhardt *et al*., 2004; Kawasaki *et al*., 1999; Kitsukawa *et al*., 1997). Abnormal directionality of cranial and spinal efferent nerve fibres is also observed in NRP1 mutant mice (Kawasaki *et al*., 1999). NRP1 is also critical for vasculogenesis: null mutants display persistent *truncus arteriosus* of the great vessels due to septation defects, reduced vessel networks in the brain, and agenesis of great vessels such as the dorsal aorta (Kitsukawa *et al*., 1997; Kitsukawa *et al*., 1995). The NRP1-null mice vascular phenotype is recapitulated in transgenic mice that lack NRP1 specifically in endothelial cells; these mice die *in utero* around mid-to-late gestation (Gu *et al*., 2003). Conversely, excess neuropilin expression during development results in embryonic lethality with excess capillary growth, increased vascular permeability, haemorrhaging in the head and neck and a malformed heart, in addition to anarchic sprouting and defasciculation of nerves (Kitsukawa *et al*., 1995).

Doubly deficient NRP1/NRP2 knockout mice exhibit earlier embryonic mortality than the

single NRP1 knock out (E8 versus E12-13.5) and have a more severe vascular phenotype with large avascular areas in the yolk sacs, and head and trunk regions, and a lack of connections between blood vessel sprouts. (Takashima *et al*., 2002).

1.5.4.2 Zebrafish Nrps in development

In zebrafish, morpholino (MO) knockdown (KD) of neuropilins results in developmental defects. *nrp1* KD impairs angiogenesis of the intersegmental vessels (ISV) (analogous to mammalian capillary sprouting) (Lee *et al*., 2002) and leads to embryonic lethality (Jensen *et al*., 2015). Arteriovenous malformations, notably of the dorsal aorta and ISV are observed in zebrafish embryos injected with MO targeting *nrp1a, nrp1b* or *nrp2a* (Martyn and Schulte-Merker, 2004). In contrast, *nrp2b* morpholino knockdown causes more restricted impairment of vessel development, with effects on the caudinal vein and artery and cardiac oedema (Martyn and Schulte-Merker, 2004). Morpholino knockdown of *nrp1a* or *nrp2b* also results in axonal guidance defects in the developing zebrafish embryo (Wolman *et al*., 2004).

The zebrafish neuropilins display differential expression patterns during embryogenesis (see Table 2). However, they are predominantly localised to neuronal and vascular organs and tissues, with the addition of fin bud and mandibular expression. Taken together with higher vertebrate neuropilin expression patterns, the roles of neuropilins are largely conserved among species during development and provide evidence for retention of similar functions between species.

Table 2 *nrp* expression patterns in developing zebrafish embryo

Neuropilin isoform	Neuronal expression	Cardiovascular expression	Other localised expression	Morpholino knockdown phenotype	Reference
nrp1a	Vagus and spinal motorneurons, hypochord Retina, telecephalon, hypothalamus, hindbrain, otic sensory epithelium, epiphysis Lateral plate mesoderm, migrating cranial neural crest cells (nccs)	Heart Intersegmental vessels, tail angioblasts, dorsal aorta, posterior cardinal vein, caudal vein plexus	Gut, pronephros, mandibular Pharangeal arches Pectoral fin buds	Arteriovenous malformations. Intersegmental vessel sprouting irregularities	Bovenkamp (2004) Yu (2004) Lee (2002) Schulte-Merker (2004)
nrp1b	Hind brain Anterior neural tube, cranial ganglia, dorsal neural tube, lateral plate mesoderm	Dorsal aorta Endothelial cells, angioblasts	Melanophores Ventral fin	Arteriovenous malformations. Intersegmental vessel sprouting irregularities	Bovenkamp (2004) Yu (2004) Schulte-Merker (2004)
nrpb2a	Migrating cranial nccs, ventral cerebellum, anterior hindbrain, anterior neural tube, hypothalamus, epiphysis	Caudal vessels Cardinal vein	Pharangeal arches, pectoral fin buds	Arteriovenous malformations. Intersegmental vessel sprouting irregularities	Bovenkamp (2004) Yu (2004) Schulte-Merker (2004)
nrp2b	Migrating cranial nccs, mid- and hindbrain, lateral plate mesoderm, telecephalon, olfactory axonal trajectory, hypothalamus	Caudal vessel, heart	Melanaphores, mandibular, Gut endoderm, pharangeal arches	Posterior cardinal vein Cardiac oedema Reduced circulation Caudal artery shunting	Bovenkamp (2004) Yu (2004) Schulte-Merker (2004)

1.5.5 Neuropilins ligands and physiological functions

NRPs were initially characterised as co-receptors for semaphorins that mediate axonal guidance and were later implicated in limb and heart development (He and Tessier-Lavigne, 1997; Kitsukawa *et al*., 1997; Kitsukawa *et al*., 1995). NRPs interact with several ligands, notably class 3 semaphorins and VEGF family members to regulate neuronal cell guidance and angiogenesis respectively (Soker *et al*., 1998; Takahashi *et al*., 1999; Takahashi *et al*., 1998). NRPs are increasingly implicated in signalling of additional heparin-binding extracellular ligands (West *et al*., 2005) in various physiological processes, such as during inflammation (Glinka and Prud'homme, 2008; Tordjman *et al*., 2002), cancer metastasis (Adham *et al*., 2014; Evans *et al*., 2011; Grandclement *et al*., 2011) and smooth muscle cell migration (Pellet-Many *et al*., 2011). This section will briefly summarise neuropilin ligands and functions currently characterised.

1.5.5.1 Semaphorins

Semaphorins are a large family of 20 proteins, categorised into 5 classes and expressed as both membrane bound and soluble forms that regulate cell-cell contacts and axonal growth cone guidance *via* plexin receptors. The class 3 semaphorins (SEMA3) are secreted soluble peptides and require neuropilins as an obligate co-receptor to signal through type A plexins. Neuropilin co-receptors bind class 3 semaphorins *via* the a1/a2 and b1 ectodomains. These domains are essential for semaphorin signalling and presumably required for positioning, oligomerisation or optimal binding to their respective plexin receptor (Kitsukawa *et al*., 1997). The plexin-semaphorin-neuropilin signalling axis has been well characterised, in particular in the context of axonal guidance and patterning during development, but has been more recently identified to play roles in the vascular development of the aortic arch and outflow tract, lymphatic system, pulmonary veins and also in immune responses (Bouvrée *et al*., 2012; Plein *et al*., 2015; Suzuki *et al*., 2008; Worzfeld and Offermanns, 2014).

Different subsets of class 3 semaphorins preferentially bind to different neuropilin isoforms. SEMA3A signalling *via* NRP1-interaction was originally identified to cause neuronal growth cone collapse, and led to SEMA3A being initially named collapsin-1 (Luo *et al*., 1993). NRP1 is also able to bind SEMA3 classes B-F, although these interactions

have not been extensively characterised. NRP2 binding to SEMA3B, C and F is also implicated in axonal, vascular and immune cell physiology in mammals (Worzfeld and Offermanns, 2014).

NRP-semaphorin-plexin holoreceptors mediate intracellular signal cascades *via* the relief of plexin auto-inhibition, leading to the stimulation of Rho GTPase activity and thus causing neuron collapse (Negishi *et al*., 2005; Oinuma *et al*., 2004). The exact mechanisms by which NRP modulates semaphorin signalling remain poorly characterised; however, it is known that NRP1 and 2 can form complexes with plexin receptors independently of ligand availability (Rohm *et al*., 2000; Tamagnone *et al*., 1999). It has also been shown that the NRP1 C-terminus domain is dispensable for plexin receptor signalling (Nakamura *et al*., 1998).

Similar to mammals, zebrafish semaphorins regulate neuronal and vascular development. Semaphorin 3a1 affects the migration of angioblasts and the formation of the dorsal aorta (Shoji *et al*., 2003), and motor neuron patterning (Feldner *et al*., 2005). Additionally Nrp1a and 2b exert opposite modulation of axonal guidance in response to semaphorins: repulsion (Nrp1a mediated) or attraction (Nrp2b mediated) (Wolman *et al*., 2004).

1.5.5.2 Vascular endothelial growth factor

Vascular endothelial growth factors (VEGFs) are potent angiogenic glycoproteins that form dimers of approximately 40kDa (Leung *et al*., 1989). In mammals, 5 members of the VEGF families are known (VEGF-A, -B, -C, -D, and placental growth factor (PlGF)), and alternatively spliced variants give rise to several isoforms of these molecules. VEGFs signal through VEGF receptors (VEGFR) which are receptor tyrosine kinases (RTK). Three main VEGFRs have been identified: VEGFR1 (FLT-1(FMS-like tyrosine kinase)) and VEGFR2 (FLK-1 (Foetal Liver Kinase 1)/KDR (kinase insert domain-containing receptor)) regulate vasculogenesis (formation of blood vessels from haematopoietic stem cells) and angiogenesis (formation of new blood vessels from pre-existing vessels); VEGFR3 (FLT-4) is involved in lymphangiogenesis (Soker *et al.*, 1998). VEGFR interaction with VEGF dimers initiates VEGFR homo- or heterodimer complex formation that stimulates its intracellular tyrosine kinase domain activity and auto(trans)phosphorylation.

Phosphorylated tyrosine residues associate with intracellular proteins containing the SH1 (Src homology 1) domain to mediate downstream signal cascades such as ERK (extracellular signal-regulated kinases/MAPK (mitogen-activated protein kinase)) activation.

VEGFR2 (or KDR) is the VEGFR predominantly expressed in blood vessels. VEGFR1/2 bind with high affinity to VEGFA, B and PlGF. VEGFR3 is expressed in venous, lymphatic and capillary endothelia, as well as neuronal progenitors during development; it preferentially binds to VEGFC and D and can form homodimers or heterodimers with KDR (Dixelius *et al*., 2003). VEGFC signalling through VEGFR3 homodimers stimulates the ERK1/2 cascade, whereas VEGFR2/3 heterodimer interaction with VEGFC triggers Akt (RAC-alpha serine/threonine-protein kinase/PKB (protein kinase B)) signalling (Deng *et al*., 2015). The Akt signal axis is required for lymphangiogenesis, *via* the formation of a VEFGR3-VEGFC-NRP1 complex in cardinal vein lymphatic progenitors (Deng *et al*., 2015). VEGFC has also been shown to bind to NRP2 with high affinity and to participate in the formation of a VEFGR3-VEGFC-NRP2 complex (Xu *et al*., 2010). This complex plays a role in lymphangiogenesis and is associated with poor prognosis in cancer due to enhanced metastatic potential (Grandclement *et al*., 2011; Kawakami *et al*., 2002). Moreover, recent evidence uncovered a role for the VEGFC/NRP2 axis in autophagy and endocytic trafficking, improving cancer survival and triggering metastatic profile (Dutta *et al*., 2016; Stanton *et al*., 2013)

VEGFR1 is thought to act as an endogenous negative regulator of VEGFR2 signalling (Cao, 2009). Heterodimers formed with VEGFR1 do not stimulate ERK-induced calcium influx in endothelial cells (Cudmore *et al*., 2012), possibly because of weak VEGFR1 kinase activity (Ito *et al*., 1998). It is therefore proposed that VEGFR1 (FLT-1) acts as a decoy, sequestering VEGF away from VEGFR2 and therefore limiting signalling *via* the latter (Seetharam *et al*., 1995; Waltenberger *et al*., 1994). NRPs are unable to bind $VEGF_{121}$ in the absence of VEGFRs; the interaction of NRPs with VEGFRs is necessary to induce conformational changes for efficient $VEGF_{121}$ binding (Fuh *et al*., 2000; Gluzman-Poltorak *et al*., 2001).

NRPs act as a co-receptor that promotes VEGF-induced intracellular signal transduction by enhancing VEGFR affinity to its ligands. It does so by forming signal complexes, thus

bridging VEGF to VEGFRs and regulating intracellular vesicle trafficking (Figure 15). VEGFA signalling is central to embryonic development. In mice, haploinsufficiency leads to early embryonic lethality due to a lack of vascular and hematopoietic systems (Carmeliet *et al*., 1996). Neuropilin knockout mice models recapitulate some of the phenotypes observed in VEGFA mutant mice and highlight the critical influence of NRPs on VEGF signalling. The b1 domain is critical for NRP1 and 2 binding to VEGF and the b2 domain optimises binding, although it is dispensable for NRP1 binding (Gu *et al*., 2002). More precisely, NRP1 b1 domain binds to the VEGFA heparin-sulfate binding domain C-terminus (Pan *et al*., 2007).

The NRP C-terminus domain interacts with synectin which, in turn, interacts with myosin VI to mediate endocytosis of the VEGFR/NRP1/VEGF complex and is essential for VEGFR-mediated ERK activation and intracellular trafficking (Figure 15) (Lanahan *et al*., 2010). In contrast, NRP1 can also negatively regulate VEGFR2 signalling. When NRP1 interacts with VEGFR2 expressed by a neighbouring cell (binding in *trans*), VEGFR internalisation is blocked which results in reduced angiogenic signalling (Koch *et al*., 2014). NRP1 is required for $VEGFA_{165}$-mediated p38MAPK (p38 mitogen-activated protein kinase) activation for the induction of angiogenic sprouting and pericyte coverage (Kawamura *et al*., 2008). VEGF signalling in endothelial cells upregulates NRP1 expression *via* the VEGFR2 signalling pathway to enhance angiogenic EC proliferation (Oh *et al*., 2002). This upregulation of both VEGFR2 and NRP1 is relied upon by several physiological systems to facilitate vessel growth. For example, in regenerating livers following hepatectomy, hepatic endothelial cells redistribute VEGFR2 and NRP1 from perinuclear space to the membrane (Braet *et al*., 2004). Additionally, TNFα targets VEGFR2 and NRP1 in a similar manner to mediate the angiogenic properties of TNFα during inflammation (Giraudo *et al*., 1998).

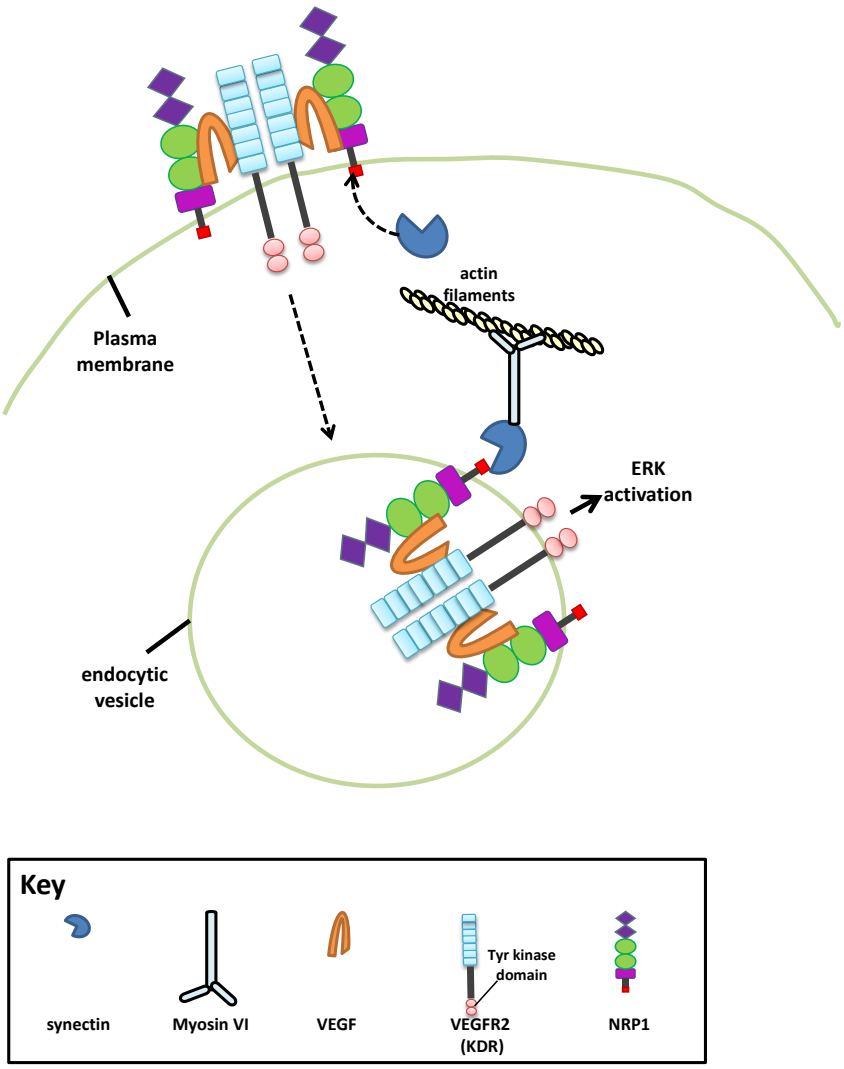

Figure 15 NRP trafficking of VEGFR2

Diagrammatic representation of NRP1 regulation of VEGFR trafficking. Upon ligand binding, receptor complex formation and trans-autophosphorylation (at the intracellular domains, red), the KDR receptor is internalised (black dotted arrow) to propagate signal (black arrow). NRP1 interacts with synectin via its C-terminal domain SEA (PDZ-recruiting) sequence. Synectin binds with myosin VI that mediate endocytic vesicle trafficking along cytoskeletal actin filaments.

As mentioned in the previous paragraphs, several VEGF-NRP1 pathways are implicated in angiogenesis, however NRP1 can also acts as a co-receptor to promote angiogenesis *via* VEGF-independent mechanisms. NRP1 can modulate angiogenesis by interacting with other molecules, such as hepatocyte growth factor (Sulpice *et al*., 2008), transforming growth factor (Hirota *et al*., 2015) and notch (Aspalter *et al*., 2015). Furthermore, NRP1 was shown to contribute to angiogenic sprouting by promoting tip cell formation *via* SMAD/ALK1/5 signalling inhibition (Aspalter *et al*., 2015).

VEGF signalling *via* NRP to regulate vessel growth is conserved in the zebrafish (Lee *et al*., 2002). In zebrafish, Vegfba signals through Nrp1 isoforms and is essential for vascular and neuronal development (Jensen *et al*., 2015). Vegfba knock down is embryonic lethal in the developing zebrafish due to cerebral vascular defects (Jensen *et al*., 2015), in contrast to mice where vegfb knockouts are viable but with only mild vascular defects (Bellomo *et al*., 2000). Interestingly, Vegfbb cannot compensate for *vegfba* morpholino knock down, however hypoxia-induced Vegfaa expression can rescue deleterious effects of Vegfba morpholino-mediated knockdown. These data provide some evidence for a more prominent role for Vegfb and Nrp1 signalling axis in developmental angiogenesis (as opposed to VEGFA driven angiogenesis during mammalian development) (Jensen *et al*., 2015).

1.5.5.3 Fibroblast growth factor

Fibroblast growth factors (FGFs) represent a large family of polypeptides, 22 fgf genes have been described in the human genome, and 10 *fgf* genes have been identified in the zebrafish (Bottcher and Niehrs, 2005; Griffin *et al*., 1995). All FGFs exhibit high affinity for heparin and mediate cellular responses *via* binding and activation of FGF tyrosine kinase receptors (FGFRs). FGF form dimers bridged by heparin sulphate proteoglycans (HSP). HSP stabilise the ligands and facilitate receptor dimerisation to mediate trans-autophosphorylation of intracellular tyrosine residues upon ligand interaction. Phosphorylated tyrosine residues interact with SH2 homology-containing intracellular proteins to relay signals. Two key signal cascades initiated by FGFs, are the phospholipase C and Ras/MAP (mitogen-activates protein) kinase (MAPK) pathways,

which stimulate protein kinase C (PKC), and ERK activity (Presta *et al*., 2005; Sternberg and Alberola-Ila, 1998), respectively. FGF signalling modulates a vast range of cellular and physiological processes during development, disease and homeostasis including cell migration, angiogenesis, proliferation, differentiation and cell fate specification (Thisse and Thisse, 2005).

It was reported that NRP1 does not bind the exon 7- lacking $VEGF_{121}$ isoform devoid of the heparin-binding domain, thus it was hypothesised that a heparin-like moiety is encoded by NRP that permits VEGF isoforms, containing heparin binding motifs, to interact (Ashikari-Hada et al., 2005; Pan et al., 2007). Additional proteins and growth factors encode heparin-binding motifs in their structure, such as fibroblast growth factor (FGF). Indeed, some FGF species have been reported to interact with neuropilin (FGF-1, -2 and -4), although, the physiological relevance and endogenous occurrence of these interactions remain largely unknown. FGF-2/NRP1 interactions enhance proliferation of HUVECs *in vitro* (West *et al.*, 2005), although there are conflicting reports on signalling changes in response to FGF-2 in HUVEC (Guttmann-Raviv *et al*., 2007). Furthermore, FGF can regulate NRP1 availability; FGF signalling increases neuropilin expression in vascular smooth muscle cells to enhance VEGF/KDR-induced cell motility (Liu *et al.*, 2005). FGF signalling *via* NRPs is not well characterised; further studies both *in vitro* and in animal models are needed to understand in which physiological or pathological context it is relevant.

1.5.5.4 Platelet derived growth factor

Platelet derived growth factor (PDGF) is a glycoprotein of approximately 14 kDa that forms dimers *via* a disulphide link to produce a 30 kDa peptide (Deuel *et al*., 1981). Five PDGFs exist, PDGF-A, –B, -C, -D and –AB, that signal through the two types of 180kDa PDGF receptor (PDGFR) tyrosine kinases, PDGFRα and PDGFRβ. The receptors are capable of forming homo- or hetero-dimers and specific PDGFRs combinations bind specific PDGF dimers. Upon ligand binding the PDGFR intracellular tyrosine kinase domain is activated, initiating trans-autophosphorylation and downstream signals that mediate cell division, motility, angiogenesis, wound-healing, inflammatory cell migration, proliferation and epithelial-to-mesenchymal transition (Pierce *et al*., 1991).

Platelet–derived growth factor is able to bind to NRP (Ball *et al*., 2007; Holmes and Zachary, 2005; Keck *et al*., 1989). PDGF-B and PDGFRβ null mice die shortly after birth due to severe cardiovascular abnormalities, haemorrhages, glomerular and renal dysfunction and breathing difficulty, thus presenting some common developmental defects of NRP1-null and VEGF-null mice (see 1.5.2 and 1.5.5.2) (Leveen *et al*., 1994; Lindblom *et al*., 2003). NRP1/PDGF interaction is important for vascular smooth muscle cell migration in response to PDGF-AA and –BB (Pellet-Many *et al*., 2011). NRP1 regulates PDGF-B-induced chemotaxis in hepatic stellate cells that transdifferentiate to myofibroblasts and contribute to the pathobiology of liver fibrosis(Cao et al., 2010a). These studies also confirmed NRP1/PDGFRβ co-localisation, suggesting complex formation, and that NRP1 overexpression enhanced cell migration *via* Rac1.

In line with its role in the potentiation of angiogenesis in mammals, Pdgf signalling *via* Pdgfrβ is essential for zebrafish ISV formation during development (Wiens *et al*., 2010). The authors observed impaired ISV development following both PDGFRβ morpholino knockdown and dominant negative receptor (lacking the intracellular kinase domains) expression. As observed in mammals, PDGFRα initiates PI3K activity in the mesoderm during gastrulation in zebrafish (Klinghoffer *et al*., 2002; Montero *et al*., 2003). Furthermore PDGFRα mediates endodermal myocardial fusion during cardiac morphogenesis in both mammals and zebrafish (Bloomekatz *et al*., 2016). Additionally, during zebrafish heart regeneration, Pdgf signalling is required for maturation of the neovasculature within in the lesion (Kim *et al*., 2010). Further studies are required to delineate the roles of Pdgfs and their receptors in zebrafish development and disease models; however, current reports provide compelling evidence for evolutionary conservation of physiological events stimulated by PDGF signalling in the zebrafish and higher vertebrates.

1.5.5.5 Transforming growth factor

The transforming growth factor beta (TGFβ) family of dimeric secreted polypeptides encodes 33 members in humans including TGFβ 1,2,3, activin, nodal and bone morphogenic proteins (Huminiecki *et al*., 2009). The ligands signal *via* binding and activation of TGFβ receptors (TGFβRs). TGFβRs represent a class of transmembrane

receptor kinases that phosphorylate serine and threonine residues. Upon ligand binding, TGFβRs receptors form a heterocomplex of two type I and two type II receptors to initiate downstream signal cascades. There are 7 type I and 5 type II TGFβ receptors (Massague, 2012). The type II receptors (activators) phosphorylate the type I receptors (signal-propagators) at the intracellular domain and permit SMAD effector protein interaction (Wrana *et al*., 1994). Type I receptors phosphorylate SMAD proteins that transduce the signal, primarily through nuclear translocation, with co-SMAD (SMAD4) to mediate gene regulation (Huse *et al*., 2001; Wrana *et al*., 1994). TGFβ 1,2 and 3 signal exclusively via type I receptor TβRI (ALK5) and type II receptor, TβRII (Moustakas and Heldin, 2009).

TGFβ signalling mediates a diverse range of physiological and pathophysiological functions, including morphogenesis, inflammation, fibrosis, angiogenesis, tumour metastasis and EMT (Derynck and Akhurst, 2007; Leask, 2007; Moustakas and Heldin, 2009; Scherz *et al*., 2008). TGFβ signalling drives the expression of EMT genes, such as *snail* and *twist,* via smad2/3 translocation to the nucleus, thereby enhancing dedifferentiation and transdifferentiation implicated in cancer metastasis (Kang *et al*., 2003; Xu *et al*., 2009). A central role in inflammation and fibrosis is governed by TGFβ (Frangogiannis, 2006) as it induces the transdifferentiation of myofibroblasts into a more synthetic phenotype thus increasing connective tissue deposition (Cao et al., 2010b; Leask, 2007; Lijnen et al., 2003).

NRPs involvement in the TGFβ signalling pathway has been well characterised. TGFβ is maintained in a latent inactive form whereby it is bound to latency associated peptide (LAP) and requires proteolytic activity or interactions with other proteins like integrins to release the active signal peptide. NRP1 can bind and activate LAP-bound latent TGFβ by mechanisms not yet fully understood, as well as active TGFβ and interact with TGFβRs (Glinka and Prud'homme, 2008). NRPs initiate signal complex formation to enhance TGFβ signal transduction and serve as TGFβ co-receptors (Glinka *et al*., 2011). NRP involvement in the TGFβ signal pathways has been described in cancer epithelial to mesenchymal transition (EMT) *in vivo.* NRP2 promotes TGFβ1-mediated EMT in colorectal cancer cells and is associated with a worse prognosis because of enhanced

metastatic potential (Grandclement *et al*., 2011; Kawakami *et al*., 2002). NRP1 and NRP2 modulate regulatory T (Treg) cell TGFβ signalling to promote SMAD3 signal transduction and enhance Treg suppression of immune response (Glinka and Prud'homme, 2008). The NRP1/TGFβ axis can also mediate an alternative cerebral angiogenesis, circumventing VEGFR2-mediated angiogenesis *via* ERK1/2, to generate neovessels in a VEGFR2-independent manner (Hirota *et al*., 2015).

The zebrafish *tgf*β receptors and *smad* genes underwent genome duplication (Postlethwait *et al*., 1998; Wu and Hill, 2009). The duplicated TGF signalling genes show overlapping and distinct expression patterns during development (Dick *et al*., 2000; Pogoda and Meyer, 2002), indicating additional functional roles for the genes, though these are currently poorly defined (Huminiecki *et al*., 2009). During zebrafish development TGFβ/SMAD3 signalling has been linked to spinal cord development (Casari *et al*., 2014) and left-right symmetry (Chocron *et al*., 2007; Sun *et al*., 2006).

1.6 Hypothesis

Although some cellular processes and mechanisms underlying zebrafish heart regeneration have been elucidated, in general these remain poorly characterised. Vegf, Fgf, Pdgf and Tgfβ, and are all cytokines implicated in zebrafish cardiac repair, and are all known neuropilin ligands. Additionally, cardiac damage switches on the re-expression of embryonic genes in the regenerating zebrafish heart, and, it is also known that neuropilins are expressed in the cardiovascular system during zebrafish embryonic development. It is also evident that the physiological roles of neuropilins extend beyond that of vascular and neuronal development, and, several biological processes occurring in zebrafish heart regeneration could involve neuropilins. For example, Neuropilins could be required for PDGF- and FGF- induced EMT of the epicardium, TGFβ/smad3 signalling that regulate fibrotic and inflammatory responses, as well as for VEGF-stimulated revascularisation of the injured area. Thus, I hypothesised that neuropilins are upregulated during and required for zebrafish heart regeneration.

1.7 Aims

Using the cryoinjury model of cardiac damage in zebrafish, I intended to carry out the following studies:

- Characterise the temporal expression of zebrafish neuropilin isoforms in the heart following cardiac damage using RT-qPCR.
- Investigate the spatiotemporal expression of neuropilins at time points coinciding with the inflammatory, reparative and regenerative stages of zebrafish heart regeneration.
- Identify the cell types expressing neuropilins during cardiac regeneration.
- Examine the role(s) Nrp1 may have in response to cardiac damage using a mutant fish lacking a functional *nrp1a* gene.

2 Materials and Methods

2.1 Animals

2.1.1 Husbandry

Procedures were performed in line with the Animals (Scientific Procedures) Act 1986 under project licence 70/7700. Zebrafish were raised at a density of 5 fish per litre in mixed sex populations, with a light-cycle (14 hours light + 10 hours of dark), water temperature (27-29^{o}C) and diet regulated by the Central University College London fish facility.

2.1.2 Animal details

Adult zebrafish between 6-18 months of age were used for experiments (see Table 3). Wild type *ABxTupLF* (AB X Tupfel Long Fin) and *nrp1a*$^{sa1485/sa1485}$ fish were used for *in vitro* culture, histological samples, RNA and protein expression analysis. Additionally, the following transgenic fish were used for histological preparations; *Tg(fli1a:GFP)* and *Tg(kdrl:mCherry)* (Chi *et al*., 2008) to identify endocardial cells, *Tg(wt1b:GFP)* (Perner *et al*., 2007) to detect activated epicardial cells and *Tg(cmlc2:GFP)* (Huang *et al*., 2003) to identify viable cardiomyocytes. TraNac zebrafish (gift from Paul Frankel, University College London) were crossed to produce embryos used for whole-mount *in situ* data.

Table 3 Details of zebrafish used in the study

Line name	Short name	Component identified	Obtained from	ZFIN ID	allele
AB X Tupfel Long Fin	***ABxTupLF***	Wild Type	Max-Planck, Tübingen, Germany	ZDB-GENO-990623-2	dt2
nrp1a$^{sa1485/sa1485}$	***nrp1a$^{sa1485/sa1485}$***	N/A	Zebrafish Mutation Project, Sanger Centre, Cambridge , UK	ZDB-ALT-120411-534	sa1485
Wilms' Tumour 1b: enhanced green fluorescent protein	***Tg(wt1b:GFP)***	Active epicardial cells	Fritz Lipmann Institute, Jena, Germany	ZDB-TGCONSTRCT-071127-1	li1
Cardiac myosin light chain: enhanced green fluorescent protein	***Tg(cmlc2:GFP)***	Viable cardiomyocytes	Institute of Molecular and Cell Biology, Taipei, Taiwan	ZDB-TGCONSTRCT-140716-2	mss5
Friend leukaemia integration 1a: enhanced green fluorescent protein	***Tg(fli1a:GFP)***	Endothelial cells	C.A.R.E.G institute, Ottawa, USA	ZDB-TGCONSTRCT-070117-94	is10
Kinase insert domain receptor like:mCherry	***Tg(kdrl:mCherry)***	Endothelial cells	Max-Planck, Tübingen, Germany	ZDB-ALT-081212-4	s896
Transparent (mpv17) x nacre (mitfa)	***TraNac***	Pigment mutation fish – transparent appearance	Cancer Research UK, London Research Institute, UK	ZDB-GENE-040426-1168 and ZDB-GENE-990910-11	Mpv17^{b18} and mitfa^{b692}

2.1.3 Zebrafish breeding

Zebrafish aged 3 months and above were used for breeding to generate new transgenic lines and maintain stocks. One male and one female fish of selected genotypes were placed into a 500 ml tank containing system water and fed with live brine shrimp for 10 minutes. Following feed, fish were transferred to a new 500 ml tank containing system water and breeding base insert (designed to separate eggs from fish) and left overnight. The following morning, fish were returned to tanks on system racks and eggs laid collected by removing insert and pouring tank water through a narrow-holed sieve to retain eggs. Collected eggs were transferred to petri dishes containing 0.01% methyl blue (in aquarium water) and stored in a 28^{o}C incubator. After 24 hours, unfertilised eggs were identified and removed using a plastic Pasteur pipette. Fertilised eggs, selected for fluorescence where appropriate, were transferred to a fresh petri dish containing system water with methyl blue and stored in a 28^{o}C incubator. At 4 days post fertilisation (dpf) zebrafish embryos (now fry at this stage) were returned to the UCL zebrafish facility and raised to adults according to establishment protocol.

2.1.4 Cryoinjury

Fish were anaesthetized in 0.02% (w/v) MS-222 (tricaine) (Sigma-Aldrich, A-5040) and transferred to a dampened sponge, ventral side up, under a microscope (Nikon, SMZ1500) and halogen fibre optic light (Schott, KL1500). Fine forceps were used to remove scales at the chest cavity and a small incision was made into the silvery pericardial sac to expose the ventricle (Figure 16A and B). The incised region was then dabbed dry of excess liquid and blood. A copper probe (0.75 mm Ø), cooled in liquid nitrogen, was gently pressed onto the tip of the ventricle for 5 seconds (Figure 16C). A Pasteur pipette containing system fish water was used to thaw and remove probe from the ventricle. Fish were returned to tanks containing system water supplemented with 10 µM lidocaine analgesic (Sigma-Aldrich, L5647) and a pasteur pipette was used to direct water towards the gills to improve recovery rate. Fish were left in lidocaine-containing water for 1 hour before placing them back to the general water system. Sham operations were performed as above, with the absence of probe application.

2.1.5 Fin clip

Fish were anaesthetized in 0.02% (w/v) MS-222 (tricaine) (Sigma-Aldrich, A-5040) then transferred to a petri dish. A small segment of the caudal fin was excised with a surgical scalpel and sterile forceps were used to transfer the fin sample to a clean Eppendorf tube, then residual aquarium water was removed. Fish were placed in 500 ml tanks containing aquarium system water to recover from anaesthesia and returned to a segmented grid tank (DC-96 R&D aquatics, #103) connected to aquarium system water for future identification. Genomic DNA was extracted from fin clips using the Phire Animal Tissue Direct PCR Kit (Thermo Scientific, F140WH) dilution protocol. Fin-clips were incubated in digestion solution (20 µl dilution buffer, 0.5 µl DNARelease), briefly vortexed, then digested at room temperature for 5 minutes before terminating the digestion at 98 °C for 2 minutes. Supernatant containing genomic DNA was transferred to a new Eppendorf and stored at -20^{o}C until required for genotyping.

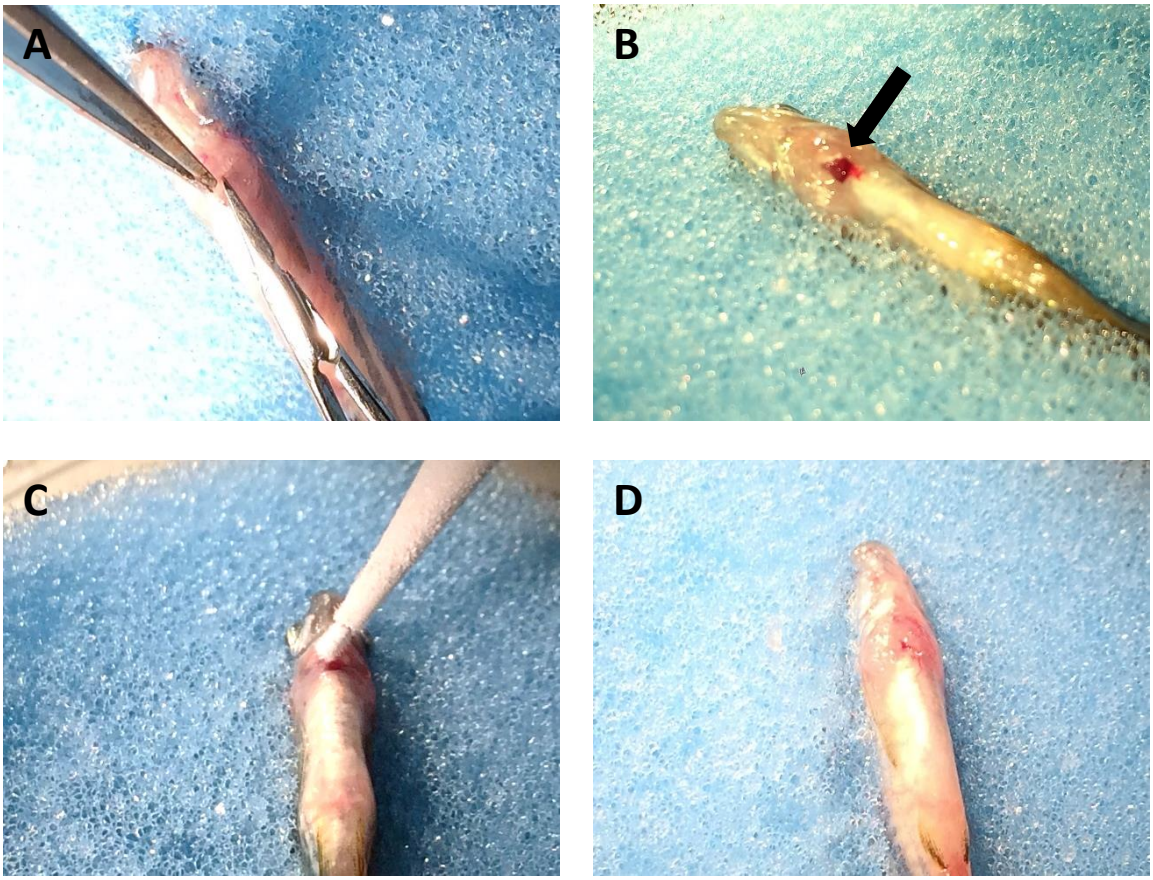

Figure 16 Cryoinjury procedure
Zebrafish are anaesthetised and placed into a dampened sponge and the heart location is identified by visibility of the heartbeat. The scales are removed from dissection area and **(A)** an incision is made to expose silvery pericardial sac. **(B)** Removal of the pericardial tissue exposes the ventricle at the surface of the thoracic region, excess blood and liquid is then dabbed dry. **(C)** A copper filament probe (0.75 mm Ø) cooled in liquid nitrogen is applied to the ventricle for 5 seconds and thawed with system water to aid removal. **(D)** The incision area is monitored briefly for successful injury and fish is returned to system water, supplemented with analgesic, for recovery.

2.2 Tissue collection

2.2.1 Heart collection

Operated fish hearts were collected at 1, 3, 7, 14, 30, 60 or 160 days post cryoinjury (dpci) for all protocols except *in vitro* epicardial culture whereby hearts were collected at 5 dpci. Fish were euthanised in tricaine (0.04% w/v). Gills were monitored for movement, the caudal fin pressed between fingers to initiate pinch reflex and reactions to vibration assessed. After cessation of all three responses, an incision was made between the gills to sever vessels and confirm death. The pectoral was cavity opened and heart excised with forceps at the *bulbus arteriosus*.

2.2.2 RNA preservation

The atrium and the *bulbus arteriosus* were removed from hearts, and the remaining ventricles were rinsed briefly in PBS and stored at -20^{o}C in RNAlater® stabilization reagent (Qiagen, Crawley, UK) until RNA extraction procedures.

2.2.3 Protein preservation

The atrium and the *bulbus arteriosus* were removed from hearts, and the remaining ventricles were rinsed briefly in PBS, placed in 1.5 ml Eppendorf tubes and snap frozen in liquid nitrogen. Samples were stored at -80^{o}C until processing for protein extraction.

2.2.4 Histology preparation

When possible, the entire heart (atrium, ventricle and *bulbus arteriosus*) was kept intact and placed in PBS/0.1 M KCl for 5 minutes to arrest heart in diastole before fixing with 4% (w/v) Paraformaldehyde (PFA) overnight at 4^{o}C. After fixation, hearts were rinsed several times in PBS. Samples were then dehydrated in biopsy cassettes (ProMarc Cellpath, J0109-10A) by immersion in a series of increasing ethanol concentrations (70, 80, 90 and 95%) to 100%, water-free alcohol using an automated tissue processor (Leica, TP1050). Samples were embedded in paraffin wax using a Tissue-Tek®TEC™ (Sakura) embedding station and mounted to cassette lids. Samples were cut in serial sections at 10 µm using microtome (Shandon finesse 325, Leica), mounted to slides and left to dry at room temperature (RT) overnight. Samples intended for Acid Fuchsin Orange G

(AFOG) staining and immunolabelling were mounted onto Superfrost® Plus (ThermoScientific, 630-0950) slides then stored at room temperature, those intended for *in situ* hybridisation were mounted onto Superfrost® ultra plus (ThermosScientific, 631-0099) slides and stored at -80^{o}C.

2.2.5 *In vitro* assay

The atrium and the *bulbus arteriosus* were removed from hearts, and the remaining ventricles were rinsed several times in HDMEM (DMEM (Dulbecco's Modified Eagle's medium), 23 mM HEPES (4-(2-hydroxyethyl)-1-piperazineethanesulfonic acid) and 15 mM NaCl) to remove residual blood, then stored temporarily in a petri dish at room temperature before promptly mounting to gel.

2.2.6 Embryo harvest

Zebrafish embryos that have a double mutation in the *transparent* and *nacre* genes (TraNac) were collected at 24, 48 and 72 hours post-fertilisation (hpf) into 1.5 ml Eppendorf tubes and then fixed in 4% PFA overnight at 4^{o}C. The following day embryos were rinsed with five 5-minute PBS washes and then transferred to 100% methanol for storage at -20^{o}C.

2.3 PCR

2.3.1 Principle of PCR

Polymerase chain reaction (PCR) is a molecular biology technique used to exponentially amplify DNA sequences. It relies on thermal cycling, with repeated heating and cooling of the reaction for DNA denaturation and replication, respectively. PCR generates a large quantity of a specific genetic sequence used as the starting point for many molecular biology protocols such as genotyping, cloning, virus synthesis and probe design.

To amplify a specific region of a gene, online databases, such as ncbi primer blast, can be used to design small 20-25 base pairs (bp) oligonucleotides (primers) that complement the gene of interest sequence within parameters required for the protocol. Often PCR requires amplicon products of less than 200 bp. The primers will be designed

to bind to the gene of interest on the template DNA in either the 3'-5' direction on the leading strand (forward primer) or in the 5'-3' direction on the lagging strand (reverse primer). The primers are often designed to anneal at high temperatures to increase specificity and reduce primer dimer formation.

Taq DNA polymerase was initially isolated from a thermophilic bacterium, *Thermus aquaticus*, that lives in geothermally heated bodies of water such as hot springs. The bacterium's enzymatic activities occur at temperatures exceeding 42°C (the temperature at which most mammalian proteins denature). It was consequently used to avoid the need of enzyme addition at each cycle and allowed the automated upgrade of the original PCR setting. The annealed primer provides a free 3' hydroxyl group from which DNA polymerases catalyse a hydrolysis reaction between the 5' phosphate group of the subsequent deoxynucleotide (dNTP) to form a covalent bond. These hydrolysis reactions repeat and the DNA polymerase synthesises a complementary strand of DNA from the template sequence, a process described as elongation (Figure 17). The *taq* polymerase can function at 72°C, incorporating up to 100 complementary oligonucleotides per second.

Often, commercially available *taq* polymerases are provided in an inactive form, whereby specific antibodies block non-specific amplification by the enzyme during reaction set up. An initial activation incubation at 95°C routinely precedes PCR reactions to denature the enzyme and activate *taq* polymerases. Following enzyme activation, the PCR reaction consists of a repeated series of temperatures, which mediate one of three PCR key stages; denaturation, annealing and extension (Figure 17). Denaturation is the initial stage, often at 95°C, to disrupt hydrogen bonds between anti-parallel double strands of DNA (dsDNA) molecules producing accessible DNA templates for primers to anneal to and simultaneously prevent DNA polymerase activity. Following denaturation, the temperature is lowered to approximately Tm-5°C (Tm, Melting temperature: Temperature at which half of the primers are annealed to the template DNA). Primers start to form bonds with the complementary target sequence, this is the second key stage: annealing. Finally, the extension step is carried out at 68-72°C, depending on the

polymerase used in the reaction. *Taq* polymerase binds to incomplete regions of double stranded DNA (at the primer-bound region) and synthesises a new strand of DNA, complementary to the template strand.

After one PCR thermal cycle, a new fragment of double stranded DNA stemming from both the forward and reverse primers is produced, therefore one copy of DNA template yields two copies of the desired DNA sequence. The cycle is repeated and the two newly synthesised double strands of DNA serve as the new template for the subsequent cycle. As there are now more templates available, more products are produced; 2 strands of double stranded DNA (dsDNA) will both be amplified and produce 4 new dsDNA PCR amplicons after a second cycle. An additional round of PCR will produce 8 amplicons from the initial 4 at the third cycle, 8 copies become 16 on the fourth cycle and so on. The process amplifies gene products exponentially, efficiently yielding millions to billions of copies of the target fragments of DNA.

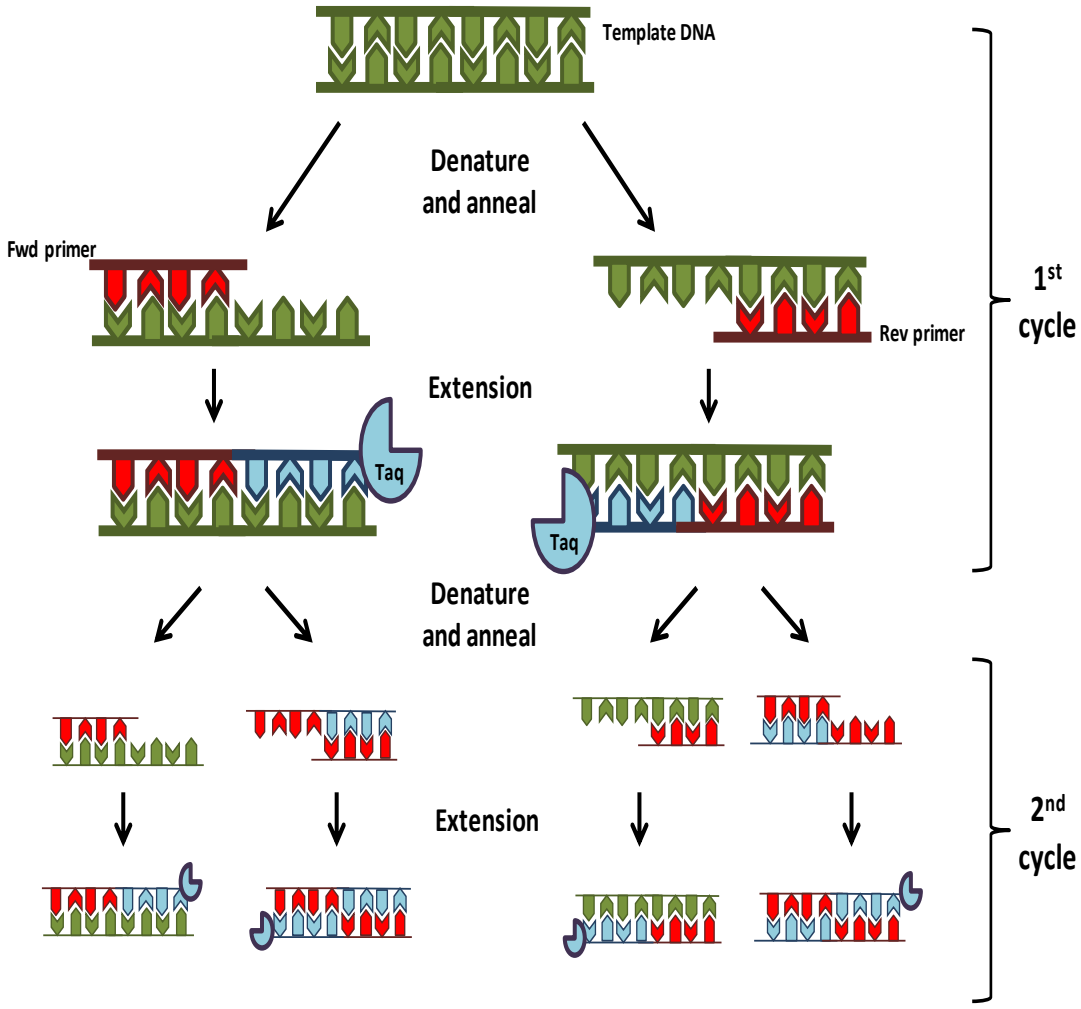

Figure 17 Polymerase Chain Reaction Schematic

Schematic representation of PCR thermal cycle DNA amplification. Template double stranded DNA (dsDNA) (green) from sample is denatured at high temperatures (95°C), the temperature is cooled (~60°C) to permit primers (red) to anneal its complementary sequence. Taq polymerases use primers as the origin to synthesise a new complementary strand of DNA from existing template (blue). Completion of denaturation, annealing and extension forms one thermal cycle and yields two strands of dsDNA (amplicons) from the original template. The second thermal cycle produces 4 amplicons from the original 2. This process is repeated over several cycles to yield millions to billions of identical amplicons.

2.3.2 Genotyping

2.3.2.1 Principle of Sanger sequencing

Sanger sequencing is commonly used to carry out genotyping and applies PCR principles to amplify a specific region of the gene of interest, however, it employs additional parameters to delineate the sequence of an unknown DNA template. The reaction mixture includes a small concentration of dideoxynucleotides (ddNTPs) that do not contain the 3' hydroxyl group required for the hydrolysis reaction catalysed by DNA polymerase during elongation. During sequencing, at an unpredictable point during the PCR, a ddNTP is incorporated during elongation at its 5' phosphate group, the absence of the 3' hydroxyl group for the next nucleotide results in the elongation termination.

The ddNTPs are labelled to be identified. The early sequencing method relied on radiolabelled ddNTPs; four separate PCR reactions would be carried out for the same gene, containing a single radiolabelled ddNTPs, one per nucleotide base (A, T, C and G) along with the unlabelled other dNTPs (Sanger *et al*., 1977). More recently, ddNTPs have been used where each base is labelled with a different fluorophore, and sequencing is now performed in a single reaction (Smith *et al*., 1986). The PCR reaction yields several amplicons of differing lengths depending on at which point the complementary ddNTPs was incorporated. The PCR reaction can then be ran in an acrylamide gel thereby separating the amplicons by size. The unknown sequence can be determined by reading the fluorescence of the different amplicons in ascending order of size. As PCR produces millions of replicates of a single product, sufficient copies of each possible fragment are generated to produce a detectable signal for hundreds of bases.

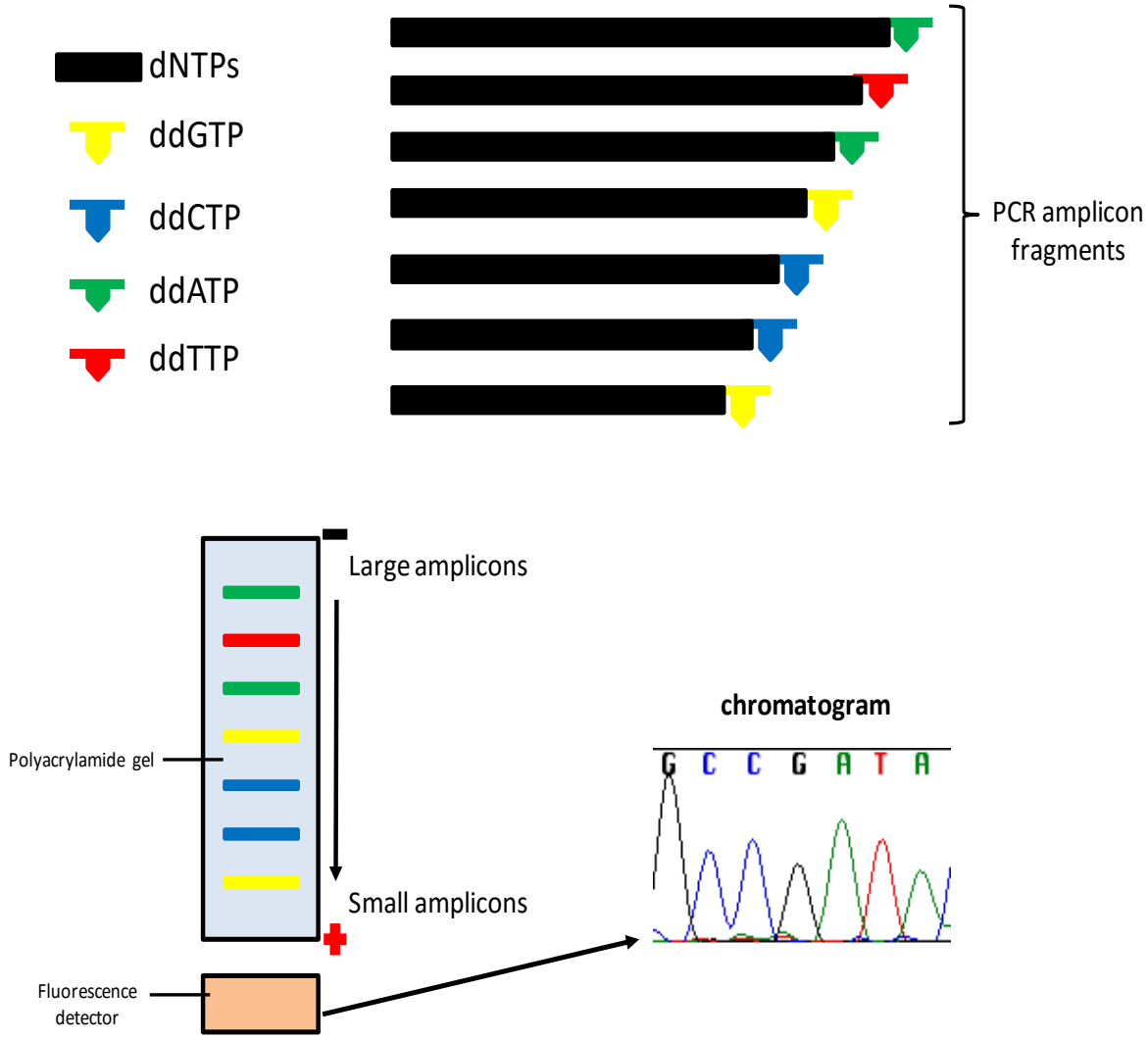

Figure 18 Sanger Sequencing

Schematic representation of Sanger sequencing. A PCR reaction is carried out with template DNA of unknown sequence. The PCR reaction contains both deoxyribonucleotides (dNTPs) and a low concentration of fluorescently labelled dideoxyribonucleotides (ddNTPs) that terminate elongation. Amplicon fragments of all possible lengths are generated in the PCR, each incorporating a fluorescent ddNTP. The PCR products are run in a polyacrylamide gel to separate amplicon fragments by size. A fluorescent detector records the light emitted by amplicons in sequential sizes and deduces which fluorescently labelled nucleotide is present. A chromatogram is produced indicating fluorescence and corresponding nucleotide to delineate the DNA sequence.

2.3.2.2 Experimental details

Genomic DNA (gDNA) from fin clip samples was diluted 1 in 10 with molecular grade water (HyClone™, SH30538.02). PCR reactions were carried out to amplify the portion of the *nrp1a* gene where *nrp1a*^{sa1485} nonsense mutation occurs. Maxima Hot Start Green PCR Master Mix (Thermo scientific, EP0601) 50 µl reactions were performed as per manufacturer's instructions containing 0.5 µM primers (forward (Fwd) TCCAGCAGCGGAGTCATCAAG, reverse (Rev) CCAGGGAATCCGTCCCAAAC (5'-3')) and 2 µl diluted gDNA. 20 µl aliquots of PCR products were analysed with agarose gel electrophoresis to confirm presence of a single PCR product. The remaining PCR reactions were purified with Zymo DNA clean and concentrator™ spin columns and DNA eluted in 12 µl molecular grade water and concentration and purity determined with NanoDrop 8000 spectrophotometer (Thermo Scientific). PCR products were sent for Sanger sequencing (Source bioscience services) at 2 ng/µl concentration, along with the forward primer of the PCR reaction. Sequencing data were analysed with Sequencher 5.3 software aligned to predicted sequence of mutation.

2.3.3 RT-qPCR

2.3.3.1 Principle of absolute RT-qPCR

Quantitative reverse transcription PCR (RT-qPCR) relies on the logarithmic generation of double stranded DNA fragments following each thermo cycle of PCR. The technique employs the use of a fluorescent signal (either a fluorescent/quencher signal reaction or non-specific double stranded DNA binding fluorophore) that correlates with the amount of DNA amplicons generated after each cycle. For the purposes of this study, the non-specific dsDNA-binding fluorophore SYBR® green was used. Upon interaction, the DNA-dye-complex absorbs blue light (λ_{max} = 497 nm) and emits green light (λ_{max} = 520 nm). The fluorescence emitted correlates with the amount of DNA amplicons produced during the PCR reaction.

Several variations of RT-qPCR exist, all require template DNA generated by reverse transcription of sample messenger RNA (mRNA) to produce complementary DNA

(cDNA). Most commonly used is the relative qPCR that simultaneously measures amplification of a reference gene along with the gene of interest and calculates a ratio between the two. Sample treatments are compared as differences between ratios of target gene with the reference gene (often described as a fold-change in expression).

For the purpose of my project, I used absolute qPCR. Absolute qPCR compares target gene expression with a combination of at least three reference genes which are used to produce a normalisation factor. Known numbers of amplicons (standards) are used to extrapolate the number of amplicons within the unknown samples, thus giving an indication of the level of gene expression. Whereas a two-fold change could mean from 10 to 20 copies, or 100,000 to 200,000 copies, absolute qPCR provides a quantitative value of amplicon copy numbers. Variability of qPCR is far greater at low copy numbers (e.g. 10-100 copies) than at high copy numbers. Knowing the level of expression gives some indication to the likely physiological relevance in gene expression changes.

qPCR standards are produced by amplifying the single gene product via PCR, they are then purified and quantified. Because the DNA sequence of the amplicon is known, the copy numbers per µl of that amplicon can be calculated from nanodrop concentration measurements. The PCR product is diluted to set concentrations from $1x10^7$ to $1x10^1$ copies per µl via serial dilutions. The standards are run to produce a standard curve by plotting the known copy numbers (x-axis) against the cycle threshold (ct) values (y-axis). Using standards also gives a simple way of directly checking the efficiency of the assay from the regression line of Cq vs. log standard concentration (Eff = 10-1/slope). The ct values of the experimental samples are aligned to the standard curve to extrapolate the copy number of the amplicon in the PCR reaction. Several reference genes are amplified following the same principle to gauge which are the most stable amongst all samples regardless of treatment, and a normalisation factor is generated by geNorm software using a minimum of three reference genes. The previously extrapolated experimental (unknown) sample copy numbers per reaction are multiplied by the normalisation factor to finally produce a “Normalised copy numbers per reaction” for genes of interest.

2.3.3.2 cDNA synthesis

All primers and standards were designed and purchased from qStandard services. Five ventricles were pooled from corresponding time points and treatments for RNA extraction. Ventricles were homogenised in 600 µl RLT buffer (Qiagen, 74106) in 1.4 mm ceramic bead-containing tubes (Peqlab precellys ceramic kit, 91-PCS-CKM) and mechanically disrupted in minilys® Tissue homogeniser (Bertin instruments). A further homogenisation step was carried out by passing homogenates through QIAshredder spin columns (Qiagen, 79654). Total RNA was extracted using RNeasy Mini Kit (Qiagen, 74104) spin columns. Spin column nucleic acid purification is based on silica gel membranes embedded within tubes. Nucleic acids are precipitated in ethanol and chelating reagents and cations within spin column buffers promote nucleic acid negatively charged backbones to bind silica columns. Residual homogenate components are then washed and removed from the membranes in a series of ethanol and salt washes *via* centrifugation, resulting in only precipitated nucleic acids bound to the silica gel membranes. Nucleic acids are then resuspended in a solvent, such as water, and collected in a final spin. RNA extraction for my studies were eluted from columns in a final volume of 30 µl. The quantity and purity of RNA were evaluated using a NanoDrop 8000 spectrophotometer (Thermo Scientific) and RNA integrity was assessed with a Bioanalyzer (Agilent). 500 ng of total RNA was treated with DNase to remove genomic DNA and cDNA synthesis was performed using QuantiTect® Reverse Transcription Kit (Qiagen) as per manufacturer's instructions. cDNA was stored at -20°C and diluted 10-fold with yeast transfer RNA (tRNA) (10 µg/ml) (Sigma, R8759) for subsequent PCR reactions.

2.3.3.3 qPCR

Absolute RT-qPCR reactions were performed by qStandard services using a Rotor-Gene PCR thermocycler (Qiagen). 10 µl reactions contained 0.5 M primers (Table 4), 5 µl Brilliant III (Agilent) and 1 µl diluted cDNA. All incubations included an initial denaturation step at 95°C for 5 minutes, followed by 40 two-step thermocycles of 95°C denaturation for 10 seconds, followed by combined annealing and extension at 57°C for

7 seconds. Product specificity was confirmed by running the amplified products on an agarose gel and thereafter during every qPCR run by melting curve analysis. qPCR standards were prepared by amplification of 10-fold diluted zebrafish ventricle cDNA; the single PCR amplicon was then isolated by agarose gel electrophoresis (E-gel® SizeSelect™ Gels, Life Technologies Ltd, Paisley, UK) and purified with microCLEAN (Microzone Ltd, 2MCL-1) purification kit. Quantity and purity of the DNA were evaluated using a NanoDrop 8000 spectrophotometer (Thermo Scientific). For all runs, a set of 10-fold serial dilutions of each internal standard ($10^1 – 10^7$ copies/µl) was used to generate a standard curve. All qPCR assays were linear within this concentration range with correlation coefficients (r^2) >0.95. Normalisation factors were calculated using the geNorm software by combining the values obtained for the three following reference genes: *gapdh*, *Rpl13a* and *eef1a1a* (see Table 4 for details) whose gene expression stayed constant regardless of time points or treatments in the zebrafish ventricles.

Table 4 qPCR primer details for housekeeper and neuropilin genes

Gene	Name	Accession Number	Primer Sequence 5'-3'	Melting temperature	Product length
rpl13a	Ribosomal protein L 13A	NM_212784	Fwd gtctgaaacccacacgcaaat Rev cgttctttttcagcctgcttagt	52 53	171
eef1a1a	Eukaryotic translation elongation factor 1a	NM_200009	Fwd ctcctctgggtcgttttgct Rev tatgtgtctctggagttggca	54 52	169
gapdh	Glyceraldehyde 3-phosphate dehydrogenase	NM_001115114	Fwd ttcctgagctcaatggcaagc Rev agacggactgtcagatccaca	54 54	85
nrp1a	Neuropilin 1a	NM_001040326 & NM_181497	Fwd ctccaacaaaccctaccaggt Rev tcggtgatgtccaccatgatttc	54 55	184
nrp1b	Neuropilin 1b	AY493415	Fwd gaccaaaagcagatggagggaa Rev catcttctgtattctctggatctttgc	55 57	176
nrp2a	Neuropilin 2a	NM_212965	Fwd gattctgacttcagctgggttatg Rev cgatgtacaggtagtttcccaaa	56 53	109
nrp2b	Neuropilin 2b	NM_212966	Fwd cagcattgagcttgagcagt Rev tcaggtcttcgctcagtcat	52 52	72
kdrl	kinase insert domain receptor like	NM_131472	Fwd ccttgagacgcagatgaatcc Rev ctgcgttatccaccctggtc	54 56	140
flt1	fms-related tyrosine kinase 1	NM_001014829 & NM_001257153	Fwd aactcacagaccagtgaacaaga Rev ttagccttctgtgggtatgtcca	53 55	156
vegfaa	Vascular endothelial growth factor Aa	NM_001190933	Fwd ccatctgtctgctgtaaaggct Rev gatgatgtctaccagcagctctc	55 57	130
vegfc	Vascular endothelial growth factor c	NM_205734	Fwd tgccatgcaggagcattcaga Rev gcctcctccgaccttgtttc	54 56	180
tgfb1a	Transforming growth factor beta 1a	NM_212965	Fwd gctggctctcatttgacgtg Rev ctctgcttgtctagccctga	54 54	157
pdgfra	Platelet-derived growth factor receptor alpha	NM_131459	Fwd tgataatctctacacaacgctgagt Rev ctcatagacatcactggacgcat	54 55	178
pdgfrb	Platelet-derived growth Factor receptor beta	NM_001190933	Fwd gctatcacaacaggactggttc Rev ctctgtgcgaaagtctggga	55 54	177
pdgfab	Platelet derived growth factor alpha b	NM_001076757	Fwd tgataatctctacacaacgctgagt Rev caggggtctgaggtcaaagtc	55 51	124
bcar1	Breast cancer anti-estrogen resistance protein 1	NM_001135133	Fwd gcactaccaacaaacggtatatgac Rev tggttctgattctccaggctct	56 55	132

2.4 Histology

2.4.1 Immunofluorescence

2.4.1.1 Principle of immunofluorescence

Immunofluorescence is a common laboratory technique relying on the use of antibodies to detect proteins in cells and tissues. Several antibodies can be used simultaneously to identify multiple molecules of interest within a sample, therefore allowing the detection of proteins localised to the same region (colocalised) of the cell or tissue. In the case of indirect immunofluorescence, the antibody specific for the antigen (the primary antibody) is unlabelled, and a second anti-immunoglobulin antibody (the secondary antibody), conjugated to a fluorophore, recognises the constant portion of the first antibody. If co-labelling is desired; primary antibodies generated in distinct species are applied to the same sample. Indirect immunofluorescence grants greater sensitivity than direct immunofluorescence (whereby the fluorophore is bound to the primary antibody) as multiple secondary antibodies can bind each primary antibody, resulting in an amplified signal. Moreover, it allows more flexibility with the choice of colour combinations and is relatively less expensive.

Fluorescent microscopes, fitted with lasers to excite the desired fluorophores and filters for emitted light, are used to localise the molecule of interest. Sequential images of a sample region are obtained for the different fluorophores and combined to produce a final image overlay. When proteins of interest colocalise, the colour in the overlay changes, *e.g*. if red and green staining are used, colocalisation will be indicated by a yellow stain.

2.4.1.2 Experimental details

Slides were placed in an oven at 60^{o}C for 10 minutes to soften paraffin wax, and then incubated twice in xylene for 10 minutes. Xylene is a strong organic solvent allowing the solubilisation of the paraffin. Sections were then rehydrated through graded washes of

ethanol in water, ending in a final rinse in pure water (100%, 95%, 90%, 70%, 30% and 2 times ddH_2O for 5 minutes each). Formaldehyde forms methylene crosslinks between proteins and is commonly used to fix tissues for histological preparations. The crosslinked proteins can mask epitope recognition by the primary antibodies, therefore two methods are commonly used to remove these bridges: heat-induced epitope retrieval (HIER) and proteolytic-induced epitope retrieval (PIER). I used HIER for all histology procedures in this project: sections were submersed in boiling citrate buffer (10 mM sodium citrate dehydrate, 5.4 mM HCl) with occasional boiling of samples in microwave for 10 minutes. Slides were then left to re-temper to room temperature for 10 minutes, washed 3 times in ddH_2O and once with Phosphate Buffer Saline Tween (PBST) (0.1% tween®20). Samples were permeabilised in PBS Triton X-100 (0.5% Triton X-100) for 15 minutes and washed again three times in PBST. Sections were blocked for 1 hour at room temperature in blocking solution (5% Bovine Serum Albumin (BSA)/10% donkey serum/PBST). Primary antibodies (details can be found in Table 5) were diluted 50-fold (100-fold for IgG controls as stock solutions are twice as concentrated) in blocking solution and incubated on samples overnight at 4^oC in humidifying chamber. The following day, slides were washed three times in PBST, incubated with two fluorescent secondary antibodies (anti-rabbit Alexa 488 (Life Technologies Ltd, A11034) and anti-mouse Alexa 555 (Life Technologies Ltd, A31570)) diluted 1 in 500 in blocking solution in light-insulated humidifying chamber for 1 hour at room temperature. Slides were then washed 3 times with PBST and incubated in 1% (w/v) Sudan black in ethanol for 15 minutes at room temperature to quench background fluorescence and finally rapidly rinsed 8 times with PBS. Slides were mounted with ProLong® Gold Antifade reagent with DAPI mounting medium (Life Technologies Ltd, P36931) and left overnight at room temperature in light-incubated conditions to set. Z-stack images were captured on a Leica TCS SPE1 confocal microscope system and processed using ImageJ software (Schneider *et al.*, 2012).

Table 5 Immunofluorescence antibody details

Antibody name	Structure labelled	Catalogue number	Company	raised in
Neuropilin-1 antibody [EPR3113]	Neuropilin-1 (c-terminus)	GTX62190	Genetex	rabbit
Mouse/Rat Neuropilin-2 Antibody	Neuropilin-2	AF567	R&D systems™ Biotechne®	goat
WT1 Antibody (6F-H2)	Wilms Tumor 1	NB110-60011	Novus Biologicals®	mouse
Monoclonal Mouse anti-GFP antibody	Green fluorescent protein	11814460001	Roche	mouse
Monoclonal Anti-Tropomyosin antibody	Tropomyosin	T2780	Sigma	mouse
mCherry Antibody (1C51)	mCherry	NBP1-96752	Novus Biologicals®	mouse
L-plastin	Lymphocyte cytosolic protein	In house antibody	Gift from imperial College London	rabbit
mlck	Mural cells	018M4800	Sigma	Mouse
aldh2	Retinoic acid dehydrogenase	GTX124302	Gentex	Rabbit
Mouse IgG	N/A	026502	Invitrogen	Mouse
Goat IgG	N/A	Sc-2028	Santa Cruz	Goat
Rabbit IgG	N/A	20009-1-200	Alpha diagnostics	Rabbit
Alexa anti mouse-555	Mouse IgG	A31570	Life Technologies	Donkey
Alexa anti goat-488	Goat IgG	A11055	Life Technologies	Donkey
Phalloidin FITC	actin	8953S	Cell Signalling	Donkey
Alexa anti rabbit-488	Rabbit IgG	018M4800	Sigma	Donkey

2.4.2 Acid Fuchsin Orange G

2.4.2.1 Principle of AFOG staining

Acid Fuchsin Orange G (AFOG) is a histological chemical stain that identifies the three following main tissue components: nuclei, cytoplasm and extracellular matrix. Incubation with phosphomolybdic acid is incorporated into the staining procedure to allow the dyes to interact with acidophilic macromolecules such as collagen. The different interactions of the AFOG dyes results in tissue components being labelled in distinct colours (described in Table 6).

Table 6 Acid Fuchsin Orange G staining key

Tissue component	Colour
Muscle and cytoplasm	Orange
Collagen	Blue
Fibrin	Red
Basement membrane	Pale blue
Vessels	Lively red
Nuclei	Black/dark brown
Erythrocytes	Yellow/brown

2.4.2.2 Experimental details

Slides were placed in the oven at 60^{o}C for 10 minutes to soften paraffin wax, and then incubated in xylene for 10 minutes, twice, to remove the paraffin. Sections were then rehydrated through graded ethanol in water, ending in pure water (100%, 95%, 90%, 70%, 30% and 2 times ddH_2O for 5 minutes each). Samples were then fixed in Bouin's fixative (Thermo Scientific, 57211) for 2 hours at 60^{o}C followed by overnight incubation at room temperature. The following day, slides were rinsed for 10 minutes under a

stream of tap water. Nuclei were stained with Weigert's iron haematoxylin (Amresco, 0701; Sigma F2877) and differentiated with three rinses in 1% hydrochloric acid (v/v) in 100% ethanol. Sections were treated for 5 minutes with 1% phosphomolybdic acid (w/v) in ddH_2O (Sigma-Aldrich, P7390). Slides were then incubated in AFOG staining solution (5g Methyl Blue (Sigma, 95290), 10g Orange G (Sigma, 0-3756), 15g acid fuchsin (Acros organics, 227900250) per litre ddH_2O, pH 1.09) for 10 minutes and briefly rinsed in ddH_2O 5 times. Slides were rapidly dehydrated in a series of increasing ethanols solutions (70%, 80%, 95%, and 100%) to xylene and DPX-mounted with glass coverslips for imaging in NanoZoomer automated slide scanner (Hamamatsu).

2.4.3 *In situ* hybridisation

2.4.3.1 Principle of in situ hybridisation

In situ hybridisation (ISH) is used to detect nucleic acid localisation within a sample, most commonly ribonucleic acids (RNA), and provides a specific detection technique to analyse gene expression patterns. In this project, *in situ* probes were designed to detect mRNA of specific genes. All or part of the target gene sequence intended for detection is amplified from cDNA to produce a sequence complementary to the mRNA expressed *in vivo.* The gene sequence is inserted into a vector and transformed into bacteria for amplification. After recovery of the recombined plasmid via DNA purification, an RNA polymerase reaction incorporating UTP ribonucleotides conjugated to digoxigenin (DIG) is performed to synthesise DIG-labelled RNA probes. The gene sequence can be synthesised to encode the 5'-3' and 3'-5' target gene sequence. The 5'-3' sequence will have the same sequence as the mRNA, termed the sense probe and will not bind to sample mRNA, this is often used as a blocking reagent or negative control. The 3'-5' sequence will have the complementary sequence to endogenous mRNA and will be able to bind *in situ*, this is known as the anti-sense probe and is used for specific gene detection. The anti-sense DIG-labelled probe hybridises with complementary mRNA expressed in the sample and an anti-DIG antibody conjugated to an enzyme (most commonly a peroxidase or alkaline phosphatase) or fluorescent reporter is used to

detect the hybridised probe. In the case of enzymatic detection, the signal is amplified using a reaction to produce a visible precipitate (Figure 19).

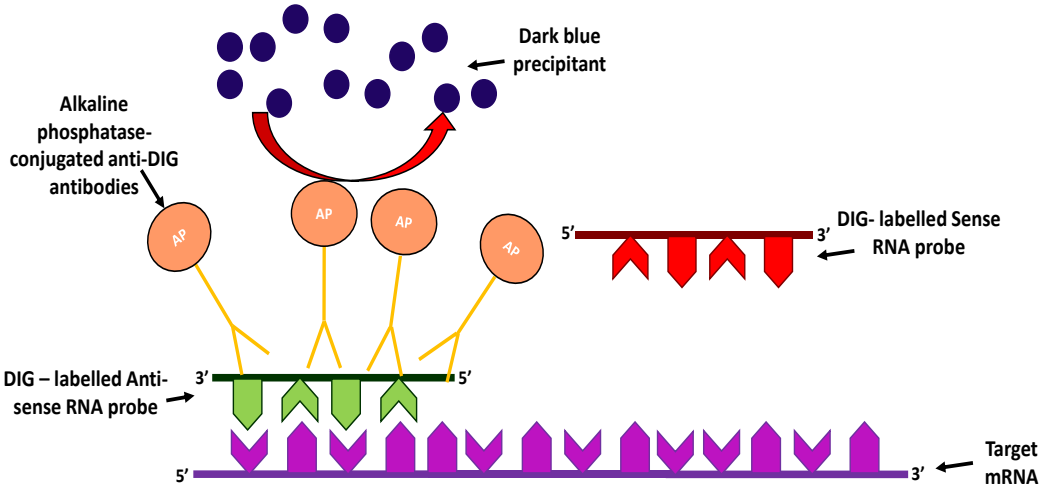

Figure 19 *In situ* hybridisation
Representative illustration of *in situ* hybridisation. Target mRNA expressed in the sample is bound by complementary digoxigenin (DIG)-labelled anti-sense RNA probes. Antibodies specific for DIG bind the RNA probes. Alkaline phosphatases conjugated to the antibody produce visible precipitate in the sample and mRNA localisation can be observed.

2.4.3.2 Dig-labelled RNA probe generation

cDNA derived from adult zebrafish heart samples were used as template to generate digoxigenin-labelled probes (see Table 7). cDNA diluted 10 fold was used for 50 µl Maxima Green Hot Start PCR reaction to amplify the probe sequence. The amplification of a single PCR product was confirmed by agarose gel electrophoresis, purified with Zymo DNA clean and concentrator™ spin columns (Zymo research, D4003) and the DNA concentration determined with a NanoDrop 8000 spectrophotometer (Thermo Scientific). Purified PCR products were ligated into 50 ng of pGEMT® vector (Promega, A3600) at a ratio of 3:1, insert: vector, using instant sticky ends ligase master mix (New England Biolabs, M0370L) as per manufacturer's instructions. The ligation reaction was used to transform One Shot® Top 10 competent E.coli. Successfully transformed

bacteria were identified through blue white screening and orientation of amplicon confirmed from mini prep plasmid isolation (Qiagen, 27104) and Source Bioscience Sanger Sequencing. Confirmed plasmids were isolated from bacteria via the midi prep procedure as per manufacturer's instructions (Qiagen, 12145) and plasmid concentration determined with NanoDrop 8000 spectrophotometer (Thermo Scientific). 1 µg of plasmid DNA was linearised by restriction digest; digestion was repeated twice, one reaction at either of the pGEMT® multiple cloning sites (for digest details see Table 7). The linear plasmid was purified in 30 µl molecular grade water with Zymo DNA clean and concentrator™ spin columns. Linearised plasmids were used to provide template for subsequent RNA polymerase reactions; one to generate a sense probe and the other reaction performed from the opposing pGEMT® RNA promoter (SP6 or T7) (see Table 7) to generate the anti-sense probe. 20µl reactions (containing 2 µl DIG-labelled RNA (roche, 11277073910), 11.5 µl linear plasmid, 2 µl 0.1 M DTT, 2 µl 10X RNA polymerase transcription buffer (NEB, B9012S), 0.5 µl RNasin® (Promega, N2111), 1 µl molecular grade water) were carried out to generate *in situ* probes. Probes were purified from reaction with Zymo RNA clean and concentrator™ spin columns, 30 µl probe was eluted in molecular grade water, concentration determined with NanoDrop 8000 spectrophotometer (Thermo Scientific), then aliquoted and stored -80^{o}C.

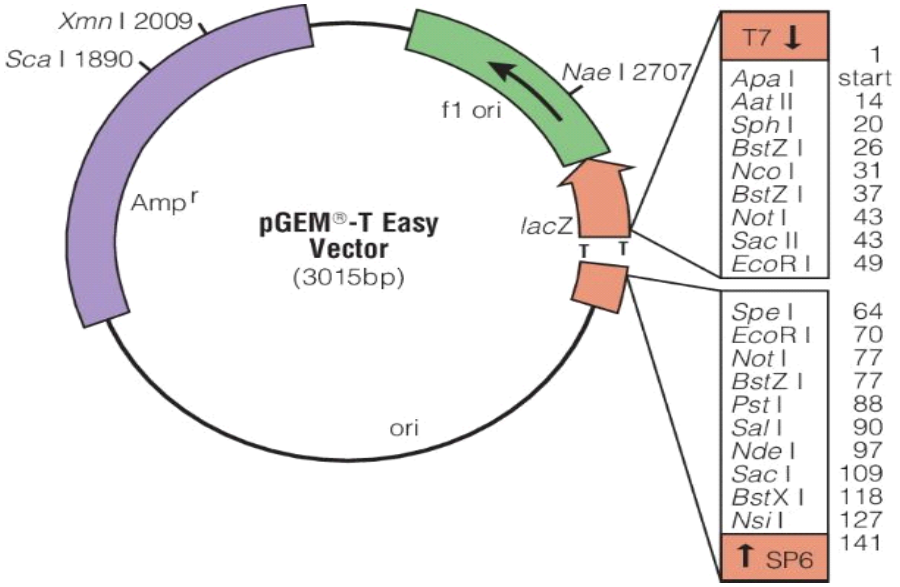

Figure 21 pGEM®T easy vector map

pGEM®T- Easy is a commercially available open vector. The vector has 3´-T overhangs at either end that provide a complementary base for taq polymerase PCR products containing 3'-A overhangs. pGEM®T- Easy also encode several restriction enzyme recognition sequences in succession in the multiple cloning site (MCS) preceded by either the T7 or SP6 RNA polymerase promoters.

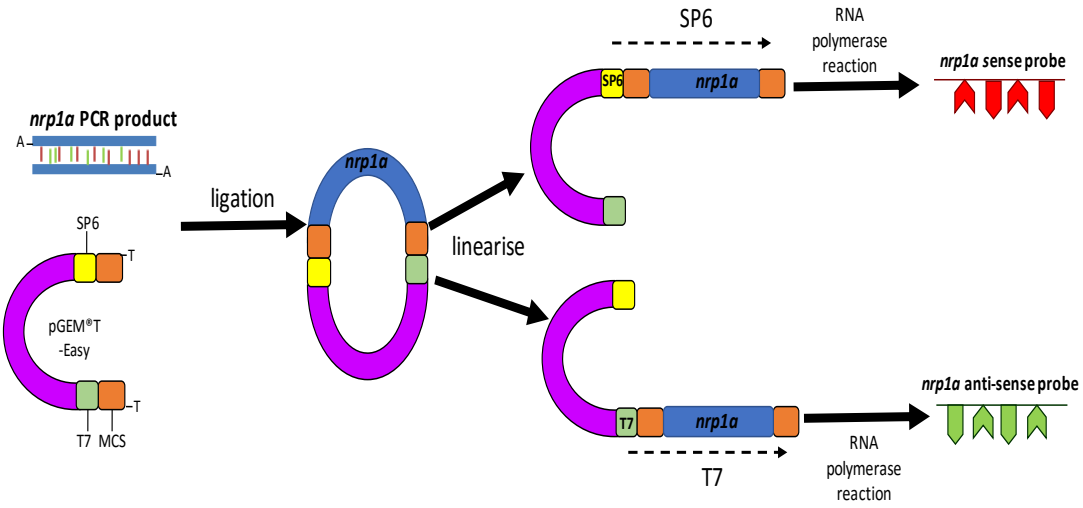

Figure 20 *In situ* probe synthesis

Schematic representation of *nrp1a* riboprobe synthesis. For the purpose of generating digoxigenin (DIG)-labelled RNA probes (riboprobes) for this study, regions of neuropilin genes were amplified from zebrafish cDNA in a taq polymerase PCR that leave 3'-A overhangs on products. Amplicons were ligated to pGEM®T-easy vector to the complementary 3' T overhangs of the open plasmid. Two restriction enzyme digest reactions were then carried out, one at either multiple cloning site (MCS) of the vector. Probes were synthesised with the appropriate RNA polymerase (SP6 or T7) in a reaction containing DIG-labelled UTP nucleotides to generate sense or anti-sense encoding probes.

Table 7: *In situ* RNA probe details

Gene	Primer sequence Fwd 5'-3' Rev 5'-3'	Probe length	Anti-Sense Enzyme	Anti-Sense RNA Polymerase	Sense Enzyme	Sense RNA polymerase
nrp1a	TACAGTGCCGCCTACTACAC CACGCTTCCGAGTACGAGTT	993	SalI	T7	NCOI	SP6
nrp1b	CAAAACCATGACACGCCAGA TGCCCTCACAGTTCACGATTT	997	NCOI	SP6	SalI	T7
nrp2a	AGACCAGCACGACACAGAAA GTGAGGGGTTTGGTGTGGTC	813	SalI	T7	SacII	SP6
nrp2b	ACCACCATTCCTGACACTGC GTGAGGGGTTTGGTGTGGTC	715	PstI	T7	SacII	SP6

2.4.3.3 Paraffin-embedded slides in situ hybridisation

Slides were placed in the oven at 60°C for 10 minutes to soften paraffin wax, and then incubated in xylene for 10 minutes, twice, to remove the paraffin. Sections were then rehydrated through graded washes of ethanol in diethyl pyrocarbonate–treated double distilled water (DEPC-H_2O)(100%, 95%, 90%, 70%, and 30%), transferred to PBS for 5 minutes and then fixed with 4% PFA at RT for 10 minutes. Slides were washed 2 times for 5 minutes in PBS and digested with proteinase K (10 µg/ml in PBS) at 37°C for 10 minutes. Enzymatic activity was stopped with a 10 minute incubation in glycine/PBS (2 mg/ml) and slides were further washed with PBS for 5 minutes and again fixed with 4% PFA for 5 minutes at RT. Sections were subsequently washed twice in PBS for 5 minutes and acetylated for 10 minutes with 0.25% acetic anhydride in 0.1 M triethanolamine (DEPC-treated) as an initial blocking step (to minimise non-specific binding of the negatively-charged probe to the positively charged glass slides). Slides were washed with PBS, then DEPC-H_2O for 5 minutes and 2 Frame-Seal™ Slide Chambers (Bio-Rad, SLF0601) borders were applied to the slides to enclose tissue sections. Hyb^+ solution (50% deionised formamide, 10% dextran sulphate, 1X Denhardt's, 5X Saline-Sodium Citrate (SSC), 1 mg/ml yeast tRNA, 0.1% Tween®20) was placed into chambers and slides incubated at 67°C for 2 hours in humidifying chamber (chamber humidifying solution 5XSCC/50% formamide in DEPC-H_2O). Hyb^+ was replaced with 100 µl hyb^+ containing either anti-sense (AS) or sense (S) digoxigenin-labelled probe (0.5 µg probe/ml) and incubated overnight at 67°C in humidifying chamber.

Slides were washed at 67°C in graded salt solutions (5X SSC/50% formamide, 2X SSC/50% formamide, 2X SSC and 0.2X SSC) for 30 minutes per wash. Slides were then washed with malate buffer (100 mM maleic acid, 150 mM NaCl, pH 7.5, 0.1% Tween®20) (MAB) 3 times, and sections blocked with 100 µl blocking solution (MAB/ 2% Boehringer blocking reagent/10% sheep serum) at RT for 2 hours. Blocking solution was replaced with 100 µl alkaline phosphatase-conjugated anti-DIG antibody (roche, 11 093 274 910) containing blocking solution (1:3000 dilution) and incubated overnight at 4°C in humidifying chamber (ddH_2O was used for chamber humidifying solution).

The following day, slides were washed with MAB 6 times for 15 minutes per wash, then equilibrated with 3 washes for 5 minutes in staining buffer (100 mM Tris pH 9.5, 50 mM $MgCl_2$, 100 mM NaCl, 0.1% Tween®20). Gene detection by alkaline phosphatase/ nitro-blue tetrazolium (NBT)/ 5-bromo-4-chloro-3'-indolyphosphate (BCIP) reaction (containing 5% polyvinyl alcohol) was carried out at 37°C in dark until dark purple precipitant was visible under stereomicroscope (Leica S8 APO). Upon substrate development, slides were washed in PBS, fixed with 4% PFA for 20 minutes at RT, washed a further 2 times in PBS before rapid dehydration in graded ethanols (70%, 80%, 95%, and 100%) to xylene for mounting with DPX and glass coverslips for imaging.

2.4.3.4 Whole-mount in situ hybridisation

Zebrafish embryos were dechorionated in 100% methanol, and rehydrated in graded methanols, then permeabilised with proteinase K (10 µg/ml) at RT for 20 minutes and further fixed in 4% (w/v) paraformaldehyde. Hybridisation buffer (50% formamide, 5X Saline-Sodium Citrate buffer (SSC), heparin (50 µg/ml), torula yeast tRNA (5 mg/ml), 0.1% Tween®20) was used to block embryos at 67°C for one hour. Probes were diluted to 0.5µg probe/ml in the same hybridisation buffer and denatured at 80°C for 3 minutes. Equilibrated embryos were then incubated in probe-containing hybridisation solution at 67°C overnight. Similarly, detection was performed using alkaline phosphatase-conjugated anti-DIG antibodies (Roche Life Science). Visualization was done using alkaline phosphatase substrate BM purple (Roche Life Science) in the dark at room temperature until a dark purple precipitant developed. Embryos were then post fixed with 4% (w/v) paraformaldehyde overnight at 4°C and stored in 80% glycerol/PBS for imaging.

2.5 Zebrafish primary *in vitro* epicardial culture

2.5.1 Assay

Thrombin-induced fibrinogen conversion to fibrin was performed in DMEM (gibco, 21063029) as described in (Kim *et al*.) (2012) to produce fibrin gel matrix. Gel matrix was set in either 24-well plates or 4-chamber slides (Lab-Tek II Chamber Slide System, 154526). The apices from dissected cryoinjured and sham-operated zebrafish hearts were placed in HDMEM (DMEM, 23 mM HEPES and 15 mM NaCl). Apices were rinsed several times with HDMEM at room temperature to remove residual blood. One apex per well/chamber was placed firmly on set fibrin gel matrices, ensuring epicardial surface contact with the gel. Excess DMEM was removed from heart tissue using a 10 µl pipette tip and left to adhere for 1 hour in a 28^{o}C tissue culture incubator. 1 ml of DMEM (supplemented with 0.5% FBS, 0.05% Normocin™ (Invivogen, ant-nr-1), penicillin (100 I.U./ml) and streptomycin (100 µg/ml) antibiotics (Sigma, P0781)) was added to the well or chamber and heart tissue cultured in a 28°C incubator (5% CO_2 and 100% humidity). Medium was changed every 2-3 days and cells were cultured for 7 days before harvesting epicardial outgrowths for protein extracts and immunofluorescence imaging.

2.5.2 Immunofluorescence

After 7 days culture, epicardial outgrowths were visible in all treatment groups. Medium was removed from slide chambers and rinsed twice with ice cold PBS. Cells were then fixed in 4% PFA at room temperature for 15 minutes and washed twice with PBST (0.1% Tween®20). Cells were permeabilised with PBS/triton X-100 (0.1% triton x-100) at room temperature for 10 minutes and further washed with PBST twice. Samples were blocked in blocking solution (1% BSA/10% donkey/PBST) at room temperature for 1 hour and incubated overnight at 4^{o}C with primary antibody diluted 1 in 200 (1 in 400 for IgG controls) (see Table 5 for antibody details) in blocking solution. The following day, samples were washed three times in PBST and incubated for one hour at room temperature with fluorescent secondary antibody (anti-rabbit Alexa 488 and Alexa Fluor® 546 conjugated phalloidin (Thermo Scientific, A11034 and A22283) in blocking solution (both 1 in 500) and insulated from light. Chambers were washed a further three

times in PBST to remove unbound excess antibodies. Boundaries were removed, heart tissue discarded and slides mounted with ProLong® Gold Antifade reagent with DAPI mounting medium (Life Technologies Ltd, P36931). Slides were left to set overnight at room temperature in light-insulated conditions and z-stack images captured on Leica TCS SPE1 confocal microscope system. Images were processed using ImageJ software (Schneider *et al*., 2012).

2.6 Rat epicardial culture and assays

Cultured rat epicardial cells described in (Wada *et al*.) (2003) were used to study epicardial cell signalling. Cells were grown in DMEM (Life Technologies Ltd, 41965-039) supplemented with 10% FBS, penicillin (100 I.U./ml) and streptomycin (100 µg/ml) antibiotics (Sigma, P0781). For signalling studies, cells were seeded to 6-well culture plates, when ~70% confluent, cells were infected with adenovirus encoding rat short hairpin RNA (shRNA) targeting either NRP1 or a control Scrambled (Scr), as described in Pellet-Many *et al.* (2015) at a multiple of infection (MOI) of 100. After 48 hours infection, cells were serum-starved for 16 hours and stimulated with various growth factors at concentrations and durations specified in Figure legends, before harvesting for western blotting analysis.

2.7 Western blotting

2.7.1 Principle of Western blotting

Western blotting is a common semi-quantitative molecular biology technique used to compare regulation of protein synthesis, post-translational modification and signalling. Homogenates of tissues or lysates of cells are made by mechanical disruption in a detergent containing solution to break cell membranes and release intracellular and membrane proteins. The proteins are often denatured to their primary peptide structure using a reducing agent (most commonly used Tris(2-carboxyethyl)phosphine (TCEP), dithiothreitol (DTT) or beta-mercaptoethanol) to remove disulphide bonds and heated to break secondary structures such as hydrogen bonds within the protein. The

samples are coated with an anionic surfactant, sodium dodecyl sulfate (SDS), to ensure all proteins have a negative charge. The proteins are then loaded into a polyacrylamide gel immersed in a conductive solution. An electric current is run through the gel and induces the migration of the negatively charged proteins towards the anode; this process is referred to as polyacrylamide gel electrophoresis (PAGE). The gel consists of a series of cross-linked polymers forming nanopores. The pore size is determined by the acrylamide concentration, a higher acryclamide concentration increases crosslinks and narrows the pore size. The denatured proteins are able to migrate through the polymer crosslinks, however, the rate of migration is restricted by their size (larger proteins migrate at a slower rate than the smaller proteins) and therefore gel electrophoresis allows the separation of proteins by size. A protein ladder with proteins of a known molecular weight and labelled with coloured dye is run alongside the samples as a reference, allowing the direct visualisation of the achieved separation.

Once the gel has run, proteins are transferred to a nitrocellulose or polyvinylidene fluoride membrane (PDVF), polymers with adhesive properties for proteins. This transfer process is also mediated in a chamber with an electric field driving the movement of proteins out of the gel and onto the membrane. The protein lysates are now immobilised on a stable platform that can be used to detect proteins of interest.

A primary antibody is used to target the protein or post-translational modification of interest, and a secondary antibody conjugated to horseradish peroxidase (HRP) enzyme is used to detect the primary antibody. In the final chemiluminescence reaction, HRP catalyses the oxidation of luminol into a reagent that emits light upon decay. Western blotting is often described as a semi-quantitative technique, with the amount of protein originally present in the lysate proportional to the amount of peroxidase enzyme bound to protein on the membrane, and so, to the amount of light generated and area and intensity of the band present on the film.

2.7.2 Lysate preparation

Proteins were extracted from samples with lysis buffer (consisting of RIPA buffer (Sigma, R0278) supplemented with proteinase inhibitor (cOmplete mini, Roche Diagnostics,

04693116001), phosphatase inhibitor cocktails (Sigma-Aldrich, P5726 and P2850), and TCEP (sigma, 646547)). For Western blot loading, lysates were mixed with 4x lithium dodecyl sulfate (LDS) loading buffer (Novex, NP0007) and radioimmunoprecipitation assay (RIPA) buffer, to obtain loading samples of equal volumes and protein content. All samples were then boiled for 3 minutes at 98^{o}C to denature proteins before loading to gels.

2.7.2.1 Zebrafish ventricles

Zebrafish heart lysates were obtained by homogenizing 3 ventricles of identical treatment and time points in 100 µl lysis buffer in 1.4 mm ceramic bead-containing tubes (Peqlab precellys, 91-PCS-CK14) using a MINILYS benchtop homogeniser (Bertin instruments). Homogenates were collected in 1.5 ml Eppendorf tubes and cellular debris separated by centrifugation at maximum speed for 15 minutes at 4^{o}C in a tabletop centrifuge. Homogenate supernatants were transferred to fresh Eppendorf tubes for subsequent use in Western blotting experiments. Protein lysate concentrations were determined with DC™ protein assay (Bio-Rad) to calculate the homogenate volume required for 1 µg protein/µl of sample to load to gels.

2.7.2.2 Rat epicardial cells

Following serum free or growth factor treatment of adenovirus infected rat epicardial cells, 6-well plates containing cells were placed on ice and washed with cold PBS twice, then all residual medium and liquid removed from wells with vacuum aspirator. 50 µl lysis buffer was added to each well and cell contents obtained by mechanical disruption with cell scrapper. The lysates were transferred to 1.5 ml Eppendorf tubes and vortexed. Cellular debris was pelleted from samples by centrifugation at maximum speed for 15 minutes at 4^{o}C in a tabletop centrifuge and the liquid homogenate was transferred to a fresh Eppendorf tube and stored at -20^{o}C before subsequent use in Western blotting experiments.

2.7.2.3 Zebrafish in vitro epicardial cells

Culture medium was removed from wells, explants were rinsed twice with ice cold PBS and residual liquid and medium were removed *via* vacuum aspiration. 15 µl lysis buffer was placed directly onto heart tissue (to ensure coverage of epicardial outgrowth), then the heart tissue promptly removed to allow lysis of underlying epicardial cell outgrowth. Lysates were collected to 1.5 ml Eppendorf tubes and care taken to minimise fibrin gel incorporation to lysate extract. Lysate from 3 outgrowths were pooled for cryoinjured samples and from 4 outgrowths for sham operated hearts. Cellular debris was pelleted from samples by centrifugation at maximum speed for 15 minutes at 4^{o}C in a tabletop centrifuge and the liquid homogenate was transferred to a fresh Eppendorf tube and stored at -20^{o}C before subsequent use in Western blotting experiments.

2.7.3 Western protocol

Lysate protein contents were separated by electrophoresis on 4–12% Bis-Tris polyacrylamide gels (novex, NP0322) in NuPage® SDS MOPS running buffer solution (Thermo scientific, NP0001) at 200 volts for 1 hour. Proteins were then electro-transferred onto PVDF membranes (Thermo scientific, LC2002) at 35 volts for 1.5 hours at room temperature in 20% methanol/2X transfer buffer (Thermo scientific, NP0006). Protein loading and transfer quality were briefly assessed with Ponceau S staining of the membrane. The membranes were then rinsed several times with distilled water and blocked with 5% (w/v) non-fat dried milk in PBS containing 0.1% Tween®20 (PBST) for one hour at room temperature on rocking platform. Membranes were incubated with primary antibodies (for details see Table 8) diluted 1000 fold in 5% milk/PBST overnight at 4^{o}C. The following day, membranes were further washed five times in PBST, incubated for 1 hour with horseradish peroxidase-labelled secondary antibody (Alfa diagnostic, 20320) in 5% milk/PBST (1 in 10,000 dilution) at room temperature for one hour. Proteins were detected using the ECL Plus™ Western blotting detection system and Hyperfilm ECL (both Amersham Biosciences).

2.8 Statistics

All statistical analysis were calculated with graphpad prism 6 software; using either unpaired t-test, one-way anova or two-way anova (specified in the Figure legend). Data compared for statistical analysis with a *P* value <0.05 were considered statistically significant. Graphs present data as means ± standard error of the mean (S.E.M), unless stated otherwise and were generated using graphpad prism 6.

Table 8 Western blotting antibody details

Antibody name	Structure labelled	Catalogue number	Company	raised in
Neuropilin-1 antibody [EPR3113]	Neuropilin-1 (c-terminus)	GTX62190	Genetex	rabbit
Mouse/Rat Neuropilin-2 Antibody	Neuropilin-2	AF567	R&D systems™ Biotechne®	goat
Mouse/Rat Neuropilin-1 Antibody	Neuropilin-1	AF566	R&D systems™ Biotechne®	goat
GAPDH Antibody (V-18)	Glyceraldehyde 3-phosphate dehydrogenase	sc-20357	Santa Cruz	goat
Phospho-p44/42 MAPK (Erk1/2) (Thr202/Tyr204)	Phosphorylated threonine 202 and tyrosine 204 Erk	9101L	Cell Signalling Technology	rabbit
p44/42 MAPK (Erk1/2)	Erk	9102L	Cell Signalling Technology	rabbit
HSP90	Heat shock protein 90	4874	Cell Signalling Technology	rabbit

3 Results chapter 1: Characterisation of neuropilin expression in adult zebrafish heart regeneration

Zebrafish have the remarkable capacity to regenerate their heart following injury and several investigations have set out to uncover the cellular and molecular mechanisms orchestrating this repair process. It has been reported that Pdgf, Tgfβ, Vegf and Fgf signalling are essential for zebrafish heart regeneration (Chablais and Jazwinska, 2012; Kim *et al*., 2010; Lepilina *et al*., 2006; Marin-Juez *et al*., 2016). These cytokines are also known ligands for neuropilin (NRP) co-receptors (Glinka and Prud'homme, 2008; Pellet-Many *et al*., 2011; West *et al*., 2005); however, the role of Nrps in zebrafish heart regeneration has not been characterised. Therefore, I investigated the expression, localisation and function of Nrps in zebrafish heart regeneration. This first chapter focuses on the gene expression of *nrp* isoforms in the cryoinjured zebrafish heart.

3.1 Establishing the zebrafish cryoinjury model of cardiac damage

In order to investigate the zebrafish heart regenerative response, I used the cryoinjury (also known as cryocauterisation) model of cardiac damage to induce cardiac damage. A platinum-filament probe cooled in liquid nitrogen is pressed against the ventricle apex, resulting in thermal shock-induced injury and the death of cardiac tissue in the targeted region (Figure 22B). I analysed the reproducibility of the cryoinjury model in my hands using transgenic zebrafish that encode green fluorescent protein (GFP) downstream of the *cardiac myosin light chain 2* (*cmlc2*) promoter (termed Tg(*cmlc2*:GFP)). In this model, viable cardiomyocytes express GFP (Figure 22C and D). Within 24 hours of surgery, the green fluorescence is significantly reduced in cryoinjured hearts (see Figure 22E), implicatining that cryoinjury results in loss of cardiomyocyte viability as a result of thermal shock.

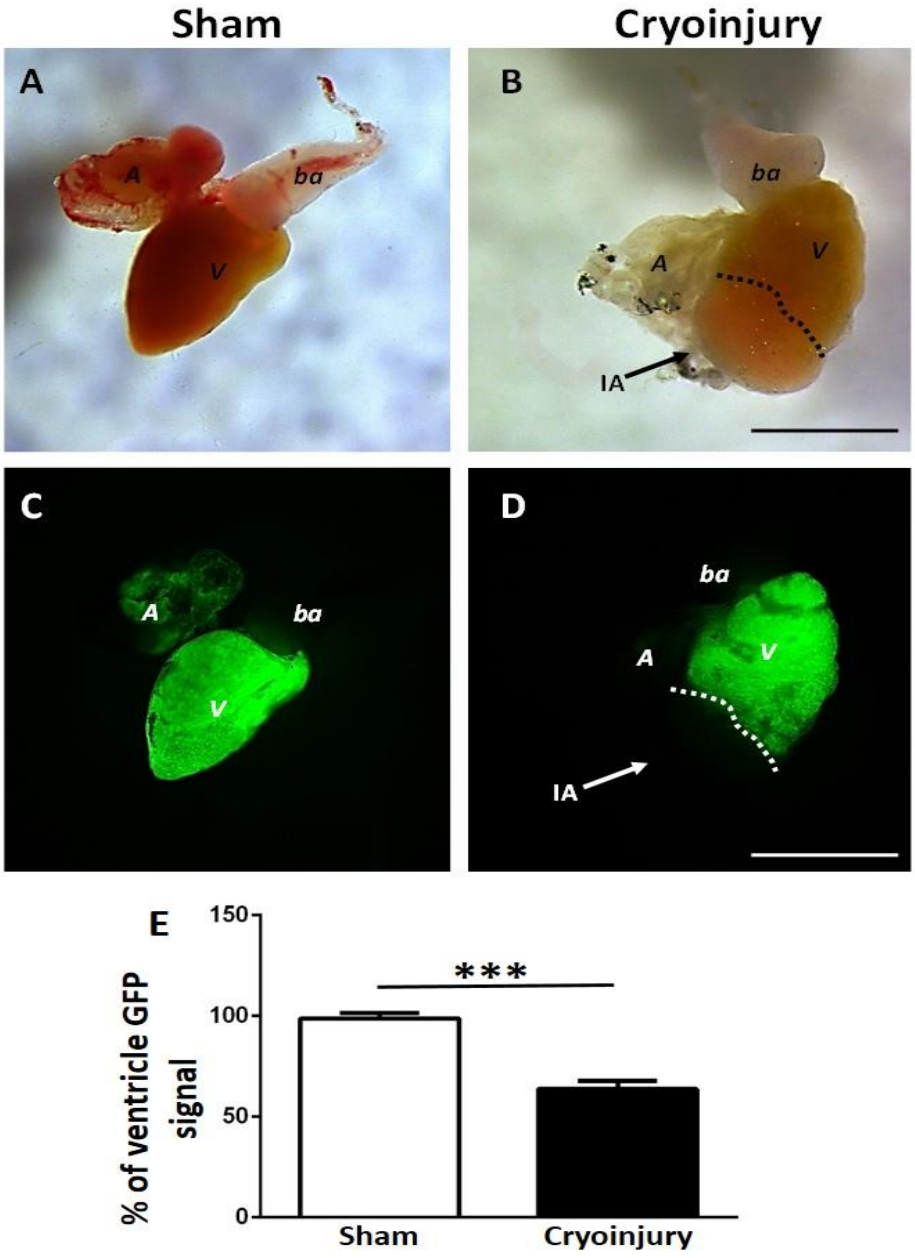

Figure 22 Loss of GFP signal in the cryoinjury lesion

Whole-mount images at 1 day post sham surgery **(A and C)** and 1 day post cryoinjury (dpci) **(B and D)** in transgenic *cardiac myosin light chain 2:GFP* (*Tg*(*cmlc2:GFP*)) zebrafish hearts, expressing GFP under a cardiomyocyte-specific promoter. Panels **A** and **B** show bright field images of the corresponding fluorescence images below **(C and D)**. The cryoinjured region is highlighted by black and white dotted lines and arrows **(B and C)**. Note the swollen and discoloured appearance **(B)** and absence of green fluorescence **(D)** in the injured ventricle region. *A – atrium*, *ba – bulbus arteriosus, V* – ventricle, IA – Injured area, scale bars 1 mm**. (E)** Quantification of GFP signal expressed as a percentage (%) of total ventricle area in sham (white bar) and cryoinjured (black bar) hearts $n = 5$ hearts $p = 0.0008$ (***$p<0.005$).

3.1.1 Heart regeneration after cryoinjury

The zebrafish heart is reported to fully regenerate up to 20% of the ventricle within 60 days after resection (Poss *et al*., 2002), or up to 25% ventricular mass after cryoinjury within 130 days (Gonzalez-Rosa and Mercader, 2012). There are numerous cryoinjury procedures reported using probes of varying size and material (Chablais *et al*., 2011; Gonzalez-Rosa and Mercader, 2012; Schnabel *et al*., 2011) introducing potential variability of injuries between reports. I set out to analyse the size and consistency of ventricular damage induced by the surgeries I performed and align injury features to those previously characterised in the literature.

3.1.2 Regeneration

Using Acid Fuchsin Orange G (AFOG) staining of serial sections to quantify injury size of hearts at 1 day post cryoinjury (dpci) (Figure 23B and H), I was able to achieve 25.2% (±5.6 % S.E.M., *n* = 5) ventricular damage. This is a similar injury size to the level of damage achieved by the authors who established and taught us the technique (Gonzalez-Rosa and Mercader, 2012). I monitored the regeneration of zebrafish hearts after injury and compared them with previously published data. The size of the injury (as a percentage of total ventricle size) was reduced at each consecutive time point, confirming regeneration occurs in the surgeries I perform. However, in my hands, from 30 dpci, regeneration slowed down and reached a plateau with an injury size comparable to the 60 dpci time-point (1.8% ± 0.98% S.E.M., *n* = 4 *versus* 2.2% ± 0.88% S.E.M., *n* = 8).

Moreover, a small scar deposit was observed in half of all 60 dpci samples, suggesting complete regeneration was not consistently accomplished in all surgeries within 60 days. This is consistent with other reports that state almost complete regeneration is achieved by 130 dpci using this approach (Gonzalez-Rosa and Mercader, 2012; Manuel Gonzalez-Rosa *et al*., 2011).

3.1.3 Scar composition

The composition of the injury was comparable to that reported by Manuel Gonzalez-Rosa and colleagues (2011). At 1 dpci, compared to the sham-operated hearts (Figure 23A), the injured region appears inflamed, and contains blood clots, yet retains myocardial trabeculations (Figure 23B). Also consistent with this study, fibrosis is evident in the injured area by 3 dpci and the epicardial layer is thickened (Figure 23C). I also analysed the outline and composition of the injury at 7 dpci. The expanded epicardial layer covering the entire injured region remains at 7 dpci, encasing more extensive fibrotic deposits consisting of a fibrin cap (red staining) with a collagen core (blue staining) on the luminal region of the injury (Figure 23D). At 14 dpci the scar composition is largely similar to that observed at 7 dpci, however, the overall injury is smaller due to the regenerating compact layer of cardiomyocytes infiltrating the outer boundaries of the injury (Figure 23E). At 30 dpci, as the heart undergoes the later stages of regeneration, healthier tissue is evident and the compact layer of the myocardium has fully recovered (Figure 23F), an observation noted by Gonzalez-Rosa *et. al.* (2011). Notably, the fibrin deposits of the scar tissue are cleared, leaving collagen deposits within the trabeculated region of the ventricle where damage was sustained (Figure 23F). When complete regeneration is evident, no blue collagen staining remains in the ventricle (Figure 23G). The progress of heart regeneration and the reduction in the damaged ventricular area are shown in Figure 23H.

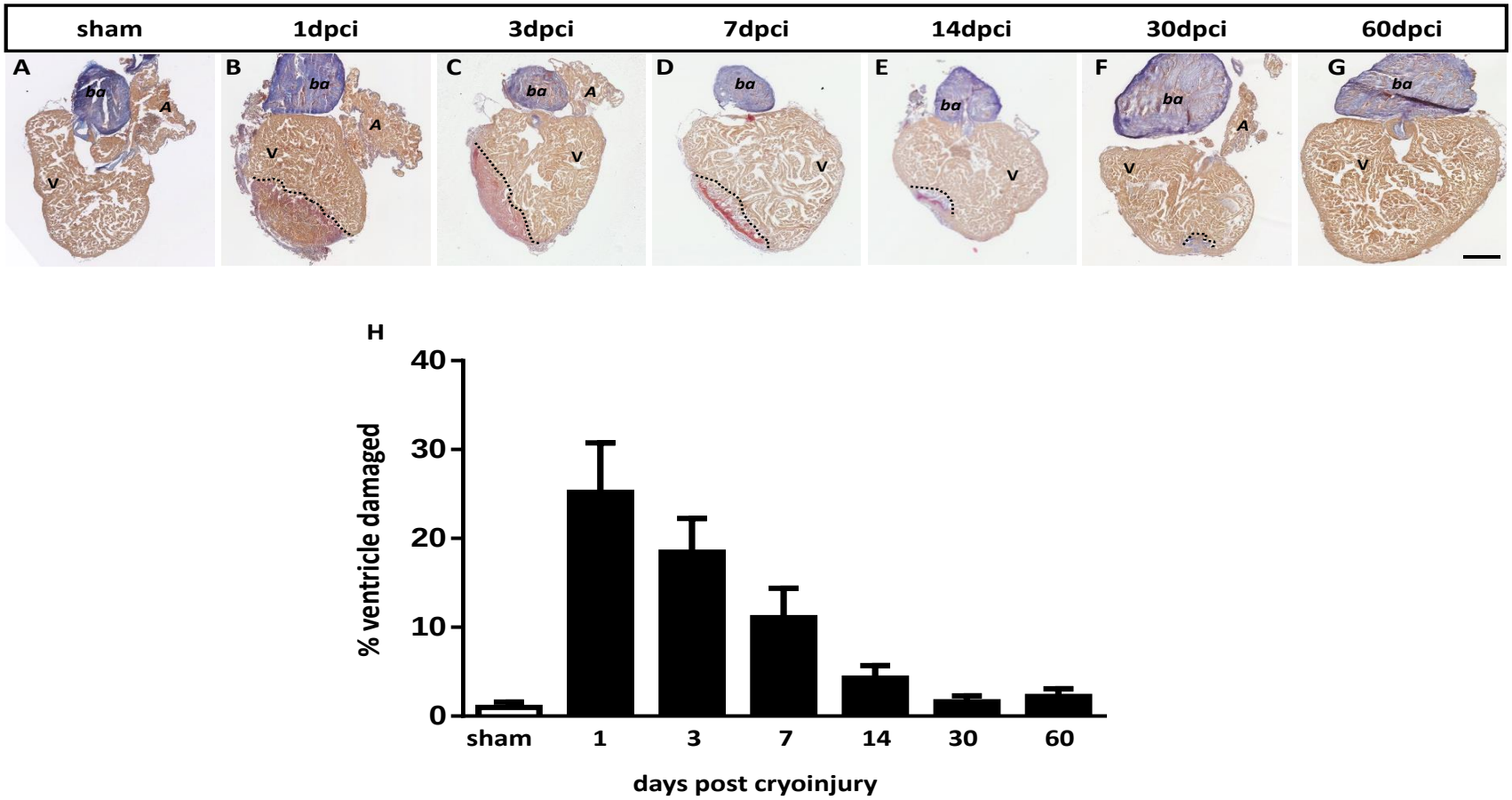

Figure 23 Recovery of Zebrafish heart following cryoinjury regeneration

(A-G) Acid Fuchsin Orange G (AFOG) staining of adult zebrafish hearts 1, 3, 7, 14, 30 and 60 dpci and sham surgery. Healthy cardiac muscle tissue is stained orange/brown, cytosolic components orange/yellow, fibrin red and collagen blue. The injury appears as an interruption of consistent orange colouring within the ventricle and demarcated with black dotted lines. The initial injury size observed at 1 day post cryoinjury (dpci) can be seen to reduce in area by 60dpci confirming regeneration occurring. *A* – Atrium, *ba* – bulbus arteriosus, *V* – ventricle, scale bar 250 µm **(H)** Quantification of total area of the ventricle damaged is presented as percentage ventricle damaged ± SEM ($n \geq 4$)

3.1.4 RT-qPCR quality measurements

3.1.4.1 RNA integrity

To assess the regulation of *nrp* isoform gene expression in the regenerating zebrafish heart following cryoinjury, absolute RT-qPCR was performed. Total RNA was extracted and its purity was initially assessed using a NanoDrop spectrophotometer (Thermo Fisher Scientific) by confirmation of a clear 260nm peak (the wavelength at which nucleic acids display maximal absorbance). To assure minimal reagent contamination the 260/280 ratio was also assessed and purity indicated by a value above 1.6. 24 randomly selected RNA samples were assessed for integrity by qStandard Ltd. using a Bioanalyzer (Agilent). The 18S and 28S ribosomal RNA bands are clearly visible and defined on the

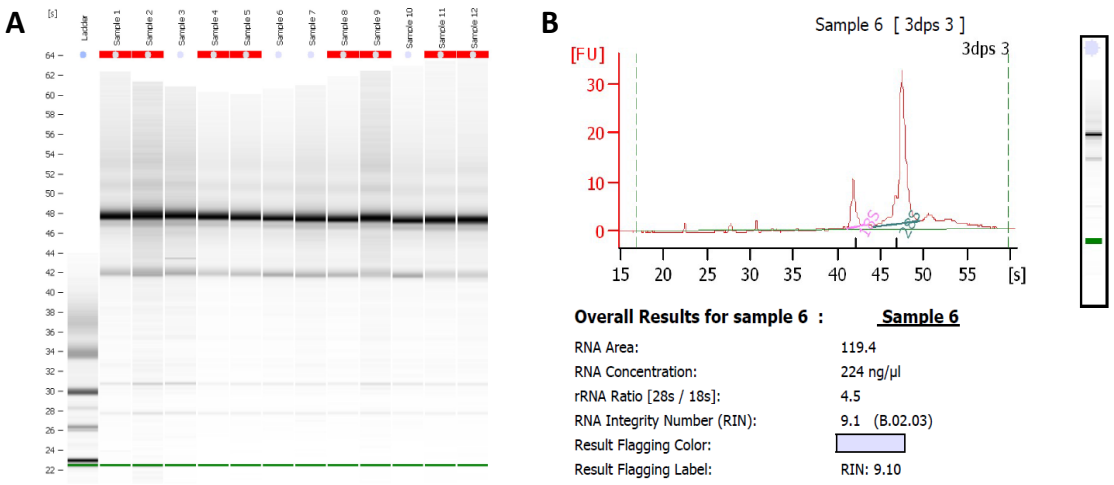

Figure 24 RNA integrity of zebrafish ventricle RNA extracts

(A) Zebrafish ventricle total RNA extract electrophoresis recorded on Agilent Bioanalyzer of 12 randomly selected samples. Two bands of high intensities are visible and represent the populations of 18S and 28S ribosomal RNA. Greater resolution of these bands indicates high quality RNA, while degradation of RNA would appear as smears between lower resolution bands. Fainter bands lower in the gel represent tRNA and mRNA. **(B)** Electropherogram depicting size distribution ([S]) of total RNA band fluorescent intensities ([FU]). Below the graph are listed the software-generated calculations of RNA concentration and RNA integrity (RIN). Values are calculated combining 18S and 28S fluorescent intensity peaks with the software algorithm. RIN values range from 1 to 10; the spectrum identifies 1 as degraded RNA and 10 as completely intact RNA. An RIN value of 7 or above is deemed suitable RNA for subsequent analytical techniques. *n* = 24

Bioanalyzer electrophoresis gel (Figure 24A). Bioanalyzer software algorithms calculate RNA integrity (RIN), incorporating the ratio of ribosomal electrophoresis band thickness and provides a number between 1 and 10; where 1 represents completely degraded RNA and 10 represents RNA of the highest integrity. Samples randomly selected for analysis produced RIN values of ≥9 (Figure 24B). High RIN values (>7) confirm minimal degradation during the RNA extraction procedure, and therefore, give confidence that the following reverse transcription to produce cDNA for the RT-qPCR will have complete and representative levels of mRNA templates.

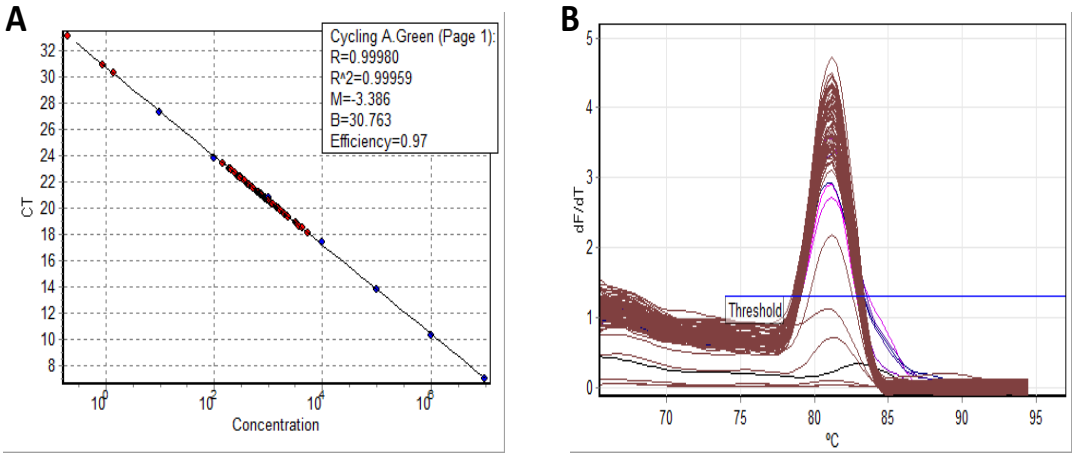

Figure 25 Absolute qPCR post-run analysis

Representative graphs of absolute qPCR quality measurements assessed following the final qPCR cycle. **(A)** Absolute qPCR standard curve applied to quantify copy numbers from samples. The standard curve is required to have an R^2 value of 0.95 or more for reliability. **(B)** Melt curve analysis is run at the end of the qPCR to ensure single peak observed to confirm one target gene PCR product amplified in the reaction.

3.1.4.2 Absolute qPCR standard curve and melt curve analysis

The majority of qPCRs were performed by qStandard Ltd., which provide additional analytical measurements to ensure qPCR efficiency and reliability. Standard curve amplification efficiency and melt curve analysis were systematically assessed for each qPCR. Standards containing known copy numbers of the gene of interest are run

simultaneously alongside the samples, allowing the extrapolation of the number of copies in the unknown samples. The target gene PCR amplification efficiency can be assessed *via* analysis of the standard curve. PCR at 100% efficiency amplifies all available DNA templates in each cycle and results in standard curve samples reaching the qPCR threshold at regular intervals. Placing standard curve values at a logarithmic scale against cycle threshold (ct) values generates a standard curve with a correlation coefficient (R^2) of 1.0 in 100% efficient qPCRs. The R^2 value ranges from 0 to 1, low R^2 indicates poor PCR efficiency and introduces inaccuracies in measurements, therefore only qPCRs with standard curves demonstrating 95% efficiency and $R^2 \geq 0.95$ were considered suitable for subsequent quantification. Figure 25A presents a software-generated standard curve (blue dots) following the completion of a $R^2 \geq 0.95$ qPCR run; sample ct values are plotted along the standard curve (red dots) to decipher gene of interest copy numbers in the reaction.

Melt curve analysis was performed for each qPCR reaction; it assesses the fluorescence of dissociating double stranded DNA amplicons at increasing temperatures. The fluorophore SYBR®green, used in the qPCR reaction, only fluoresces when bound to double stranded DNA (dsDNA). At a specific temperature (Tm), half of the amplicons will dissociate into single DNA strands and cause a sharp drop in fluorescence (or a peak if a graph of the negative first derivative of the melting-curve is plotted). For each gene, specific amplification of the single product was assessed. If another non-relevant product was generated, this would be evident *via* analysis of the melting curve (an additional peak would be visible). A single peak in the melt curve indicates a single PCR product in the reaction, confirming specific amplification of the target gene as demonstrated in Figure 25B.

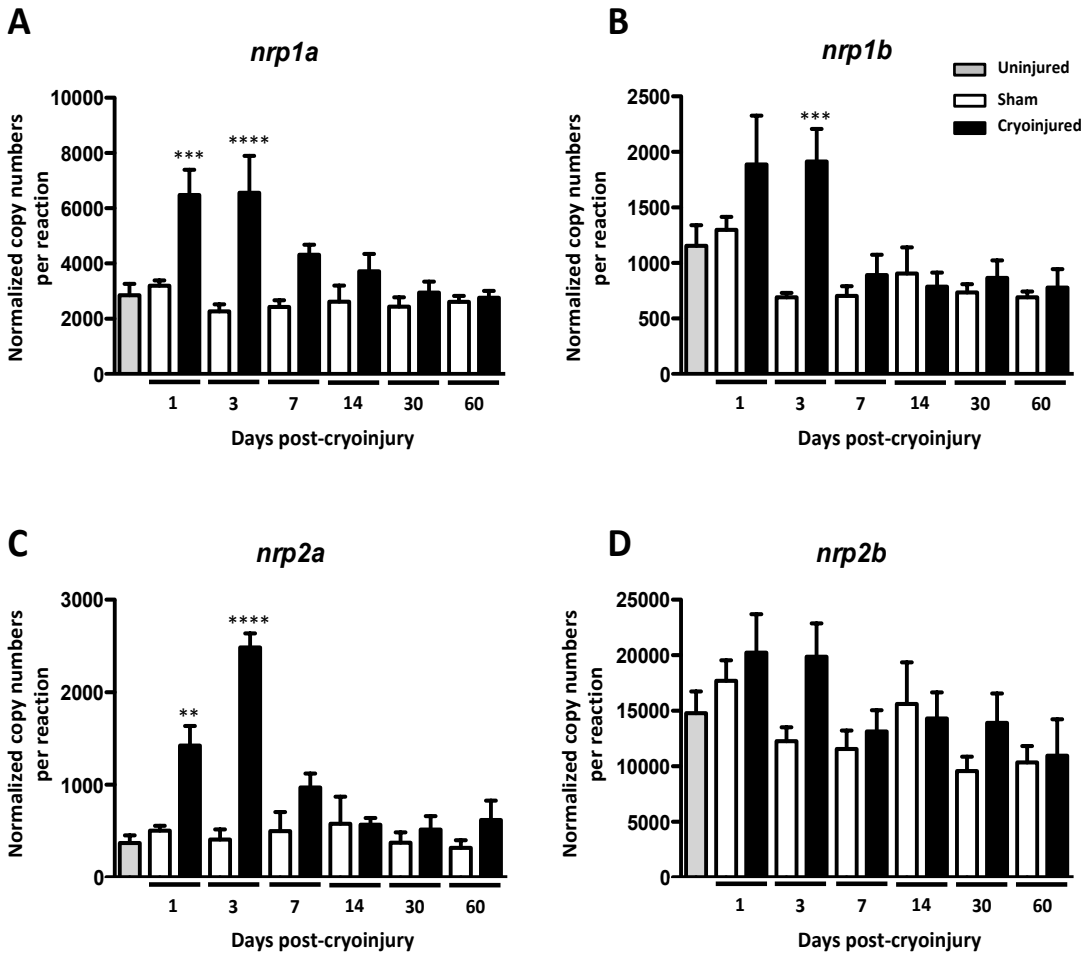

Figure 26. *nrp* gene expression in the cryoinjured zebrafish heart

Absolute Real Time quantitative PCR (RT-qPCR) analysis of *nrp1a* **(A)**, *nrp1b* **(B)**, *nrp2a* **(C)** and *nrp2b* **(D)** at 1, 3, 7, 14, 30 and 60 days following cryoinjury (black bars) or sham surgery (white bars). Basal expression of neuropilin isoforms were assessed with uninjured hearts (grey bars). Data are represented as means of normalised copy numbers per reaction ± S.E.M (error bars) **p<0.01, ***p<0.005, ****p<0.001. *n* = 4-5 with each *n* being a pool of 5 ventricles of identical treatment and time point.

3.1.5 RT- qPCR results

3.1.5.1 Neuropilin isoforms are upregulated after cryoinjury

Gene expression of all four neuropilin isoforms (*nrp1a, nrp1b, nrp2a, and nrp2b*) was evaluated in sham and cryoinjured ventricles at 1, 3, 7, 14, 30 and 60 days following sham operation and following surgery and cryoinjury, using absolute qPCR. Five zebrafish ventricles for each specific treatment and time point following sham operation and post-surgery were pooled, homogenised and used for RNA extraction and absolute RT-qPCR in order to generate a single value (i.e. $n = 1$). Gene expression in sham samples was assessed with one-way anova (Figure 26, white bars) and no significant changes in expression of any of the *nrp* isoforms was observed at different times following sham-operation. Also, the levels of *nrp isoform* expression between sham-operated and non-injured hearts (Figure 26, grey bars) were similar, indicating minimal effect of sham operation on *nrp* expression. Therefore, any change in gene expression following cryoinjury can very likely be attributed specifically to the cryoinjury of the heart.

A significant increase in expression of *nrp1a, nrp1b and nrp2a* was observed at earlier time points (1 and 3 dpci) following cryoinjury (Figure 26A-C). *Nrp1a* was significantly upregulated at 1 and 3 days post cryoinjury (dpci) ($p<0.005$ and $p<0.001$, respectively) by approximately 2-fold in comparison to the corresponding sham samples (Figure 26A). At 7 and 14 dpci *nrp1a* gene expression remained elevated but this increase was not statistically significant when compared with sham control samples. Finally, by 30 and 60 dpci, *nrp1a* expression returned to baseline levels. A significant increase in *nrp1b* was observed at 3 dpci only. It was also upregulated at 1 dpci but statistical significance was not reached at this time-point compared with sham control samples. *Nrp1b* expression returned to basal levels from 7 dpci onwards. *Nrp2a* was expressed at lower levels in the heart compared to other neuropilin isoforms, but was significantly upregulated at 1 and 3 dpci and returned to basal levels from 7 dpci onwards. Out of the four neuropilin isoforms, *nrp2b* had the highest level of basal expression, with baseline copy numbers at least ten times higher than for the other three *nrp* isoforms (Figure 26, grey bars), However, *nrp2b* expression was not significantly altered following cryoinjury compared

with sham samples, though some trend to an increase was observed at 3dpci (Figure 26D).

3.1.5.2 Vascular genes regulated following cryoinjury

I investigated the regulation of genes controlling angiogenesis because the revascularization of the injured area is an important process required for zebrafish heart regeneration (Kim *et al*., 2010; Marin-Juez *et al*., 2016). Moreover, neuropilins have an essential role in angiogenesis in mammals and zebrafish (Soker *et al*., 1998; Bovenkamp *et al*., 2004). Furthermore, NRP1 mediates VEGF and PDGF-BB signalling in endothelial cells and smooth muscle cells, respectively (Pellet-Many *et al*., 2011; Soker *et al*., 1998; Wang *et al*., 2003).

I could not detect a significant change in expression of *Vascular endothelial growth factor Aa* (*vegfaa)* after cryoinjury, though a non-significant increase was observed at 1dpci (Figure 27A)*. Vegfaa* is the zebrafish orthologue of VEGF-A, the most potent angiogenic cytokine in mammals. V*ascular endothelial growth factor C* (*vegfc*), which plays a major role in lymphangiogenesis, was significantly upregulated at 1 and 3 dpci (both $p<0.001$) and returned to baseline levels thereafter, consistent with previous publications (Lien *et al*., 2006) (Figure 27B). It should be noted that *vegfc* is expressed in the 100s of copy numbers at baseline (grey bar Figure 27B), whereas *vegfaa* basal expression is 10 times higher (Figure 27A).

The regulation of VEGF receptors (VEGFRs), *flt1* (orthologue of Human *Vegfr1*) and *kdrl* (orthologue of Human *Vegfr2*), was also assessed. No significant difference between sham and corresponding cryoinjury samples was observed for either gene at any time point post-cryoinjury (Figure 27C and D).

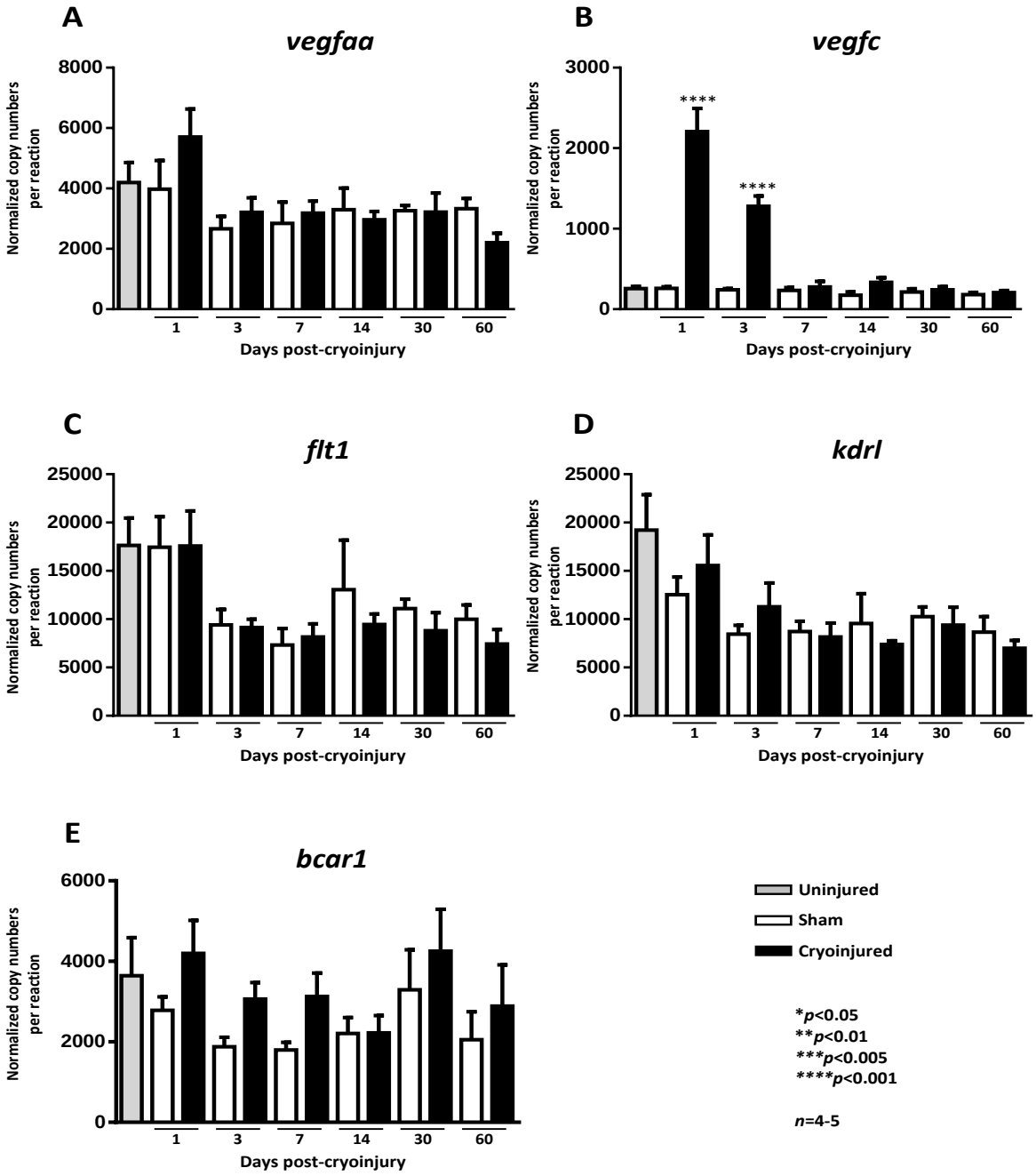

Figure 27 Regulation of genes associated with angiogenesis in the cryoinjured zebrafish heart

Absolute Real Time quantitative PCR (RT-qPCR) of *vegfaa* **(A)**, *vegfc* **(B)**, *flt1***(C)**, *kdrl* **(D)** and *bcar1* **(E)** at 1, 3, 7, 14, 30 and 60 days following cryoinjury (black bars) or sham surgery (white bars). Basal expression of genes was assessed with uninjured hearts (grey bars). Data are represented as means of normalised copy numbers per reaction ± S.E.M (error bars), **p*<0.05, **p<0.01, ***p<0.005, ****p<0.001. Each *n* is a pool of 5 ventricles of identical treatment and time point.

p130Cas is an intracellular adaptor molecule encoded by the *bcar1* gene implicated in angiogenesis, cytoskeletal dynamics and cell movement and its tyrosine phosphorylation is mediated via NRP1 in mammalian endothelial and vascular smooth muscle cells (Barrett *et al*., 2013; Evans *et al*., 2011; Pellet-Many *et al*., 2011). Although there was a trend for an increase in expression at 3, 7, and 14 dpci, these changes did not reach statistical significance (Figure 27E).

3.1.5.3 Expression of other cytokine ligands for Nrps and their receptors

Several cytokines are ligands for Nrps, and have previously been reported to be upregulated in response to zebrafish heart injury and implicated in heart regeneration, including *pdgfab* and receptor, *pdgfrβ,* and transforming growth factor beta (TGFβ). Therefore, I investigated the regulation of these genes both to confirm previous data, and to identify potential ligands and co-receptors for Nrps in the regenerating heart. Kim *et al* 2010 reported the upregulation of *platelet derived growth factor receptor beta* (*pdgfrβ*) but not *platelet derived growth factor receptor alpha* (*pdgfrα*) expression during zebrafish heart regeneration. Similarly, my results showed that *pdgfrα* displayed only a small non-significant trend for increased expression at 3 dpci (Figure 28A), whereas *pdgfrβ* expression was significantly upregulated at 1, 3 and 7 dpci and returned to baseline levels thereafter (Figure 28A). Using inhibitors of PDGFRs, Kim *et al* also reported platelet derived growth factor (PDGF) signalling as an essential regulator of epicardial response and revascularisation during zebrafish heart regeneration. My results also show a significant upregulation of *pdgfab* (encoding the PDGFab cytokine) at 3 and 7 dpci (Figure 28C), further supporting a role of PDGF signalling in cardiac regeneration. These data support the observations by Kim *et al*., implicating a role for PDGF in the early stages of zebrafish cardiac regeneration.

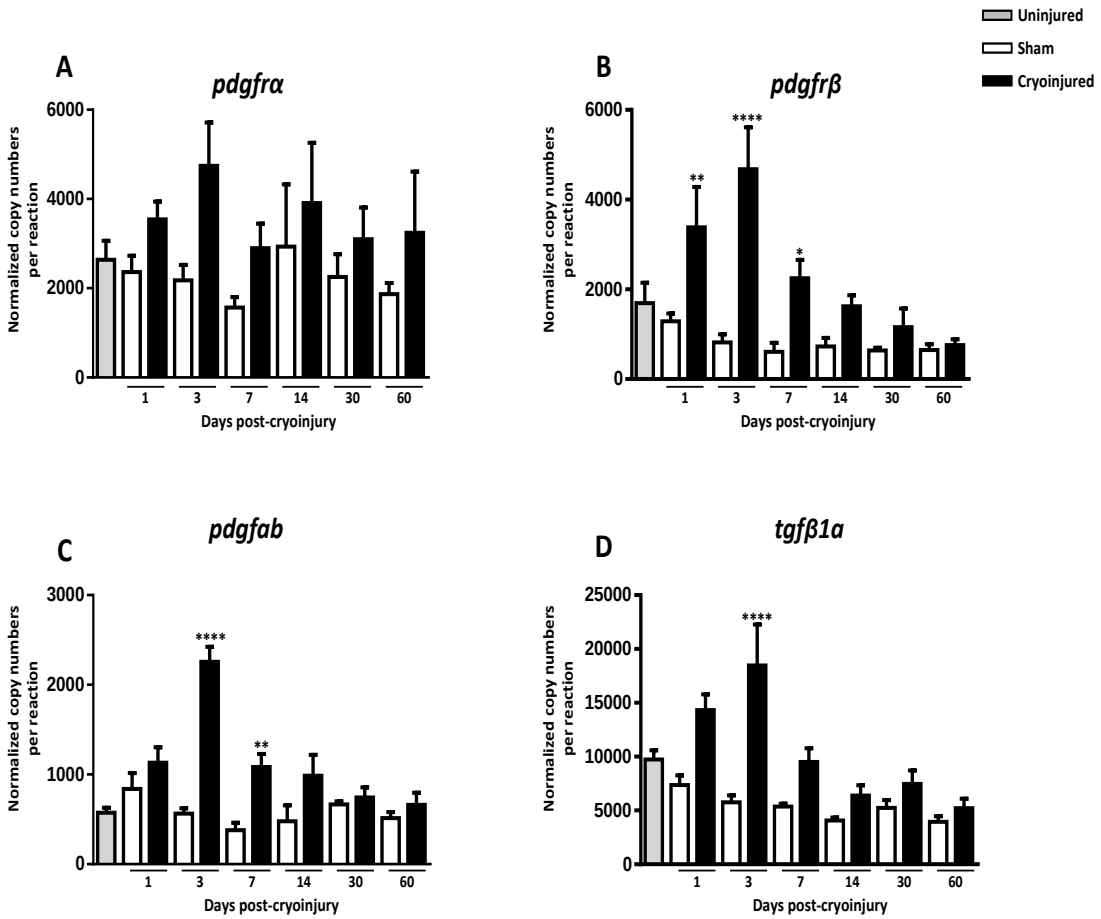

Figure 28 Gene expression of growth factors and receptors previously reported in the regenerating zebrafish heart

Absolute Real Time quantitative PCR (RT-qPCR) analysis of *pdgfrα* **(A)**, *pdgfr*β **(B)**, *pdgfab***(C)**, *tgfβ1a* **(D)** 1, 3, 7, 14, 30 and 60 days following cryoinjury (black bars) or sham surgery (white bars). Basal expression of genes was assessed with uninjured hearts (grey bars). Data are represented as means of normalised copy numbers per reaction ± S.E.M (error bars), *p<0.05, **p<0.01, ***p<0.005, ****p<0.001, *n* = 4-5 with each *n* being a pool of 5 ventricles of identical treatment and time point.

A study by Chablais and Jaźwińska (2012) identified transforming growth factor beta (TGFβ) signalling as an essential regulator of zebrafish heart regeneration, coordinating the inflammatory and fibrotic response and stimulating cardiomyocyte proliferation. My qPCR data shows that indeed, *tgfβ1a* expression is upregulated early at 3 dpci, during the inflammatory phase of repair (Figure 28D), in accordance with their findings.

3.1.6 *In situ* hybridisation

The vast majority of the ventricle mass is composed of cardiomyocytes, however other cell types, such as epicardial cells, fibroblasts, endothelial cells and leucocytes, are important for the cardiac regenerative response. All these cells express neuropilins, but represent relatively, a smaller proportion of the cells in the heart. qPCR provides information of quantitative mRNA expression, but cannot determine which specific cells or regions of the heart are expressing the target genes. Moreover, variation in gene expression by a smaller cell population may not be detected by qPCR of the entire ventricle due to variation from sample to sample. One way to selectively investigate gene expression of one particular cell type is to purify a specific cell population *via* fluorescence-activated cell sorting; alternatively, laser capture could isolate specific sample regions, for example healthy myocardium *versus* injured area. I addressed differential tissue gene expression using *in situ* hybridisation, which provides qualitative information on mRNA localisation and in which, staining intensities correlate to relative expression levels. However, variations in probe efficiencies and development times need to be considered when interpreting expression intensities.

3.2 Positive control riboprobe whole mount *in situ* hybridisation

Initially, I optimised the *in situ* protocol using whole-mount TraNac zebrafish embryos to confirm the procedure results in the specific binding of probes to target mRNA. I was provided with probes of genes reported to be activated in the epicardial and endocardial response to injury (*T-box18* (*tbx18*), *retinaldehyde dehydrogenase 2* (*raldh2)*, and *Wilm's tumor 1b* (*wt1b*)) as well as the cardiomyocyte marker *cmlc2* (kindly donated by Nadia Mercader, CNIC, Madrid). All four probes displayed staining patterns in agreement with the published literature (Figure 29), confirming the validity and stringency of my protocol.

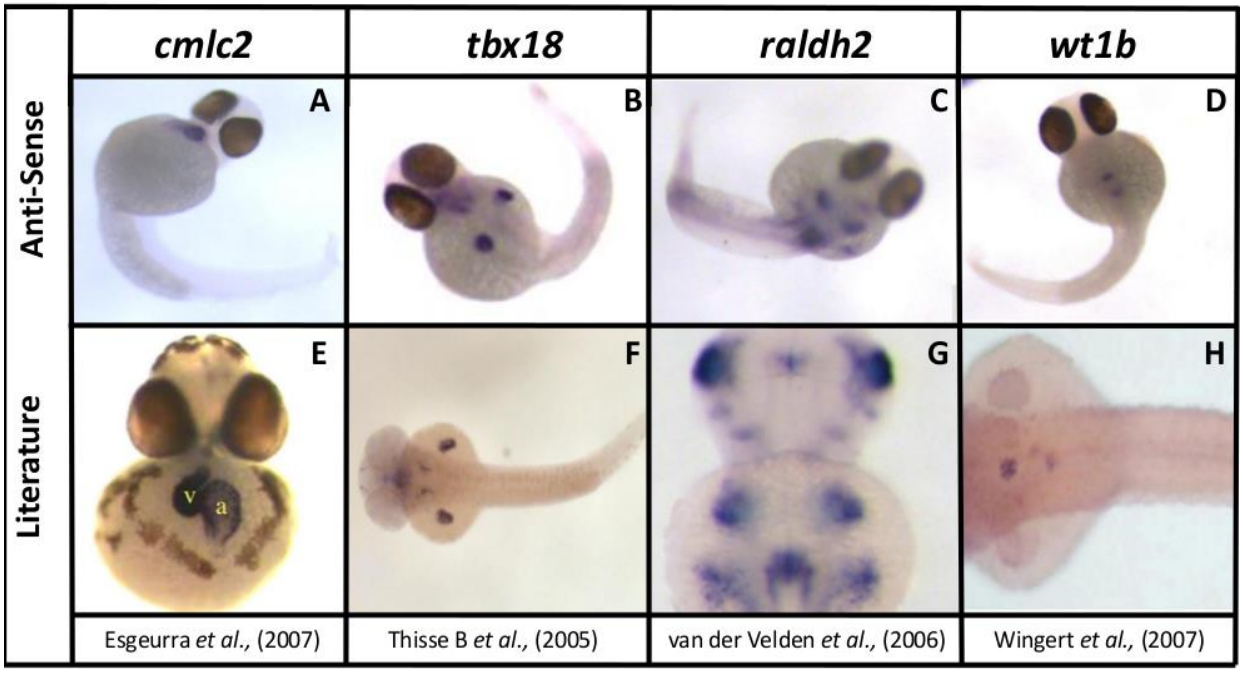

Figure 29 Positive riboprobe validation

In situ hybridisation of TraNac zebrafish 48 hours post fertilisation (hpf) with positive control anti-sense riboprobes (kindly donated by Nadia Mercader, CNIC, Madrid) targeted to; **(A)** *cmlc2*, **(B)** *tbx18*, **(C)** *raldh2*, **(D)** *wt1b* mRNA. Gene detection is comparable to that of the literature **(E-H)** and confirms riboprobe reliability and protocol parameter stringency. v- ventricle a-atrium

3.3 Neuropilin isoform probe validation using whole mount *in situ* hybridisation

Riboprobes of approximately 1000 bases were designed to specifically bind the mRNA of each *nrp* isoform. Additionally, I synthesized sense probes (negative controls) which were tested alongside the anti-sense whole mount *in situ* hybridisation reaction (Figure 30 A-D). As expected, sense probes failed to develop a signal, confirming their inability to bind mRNA and their use as reliable negative controls.

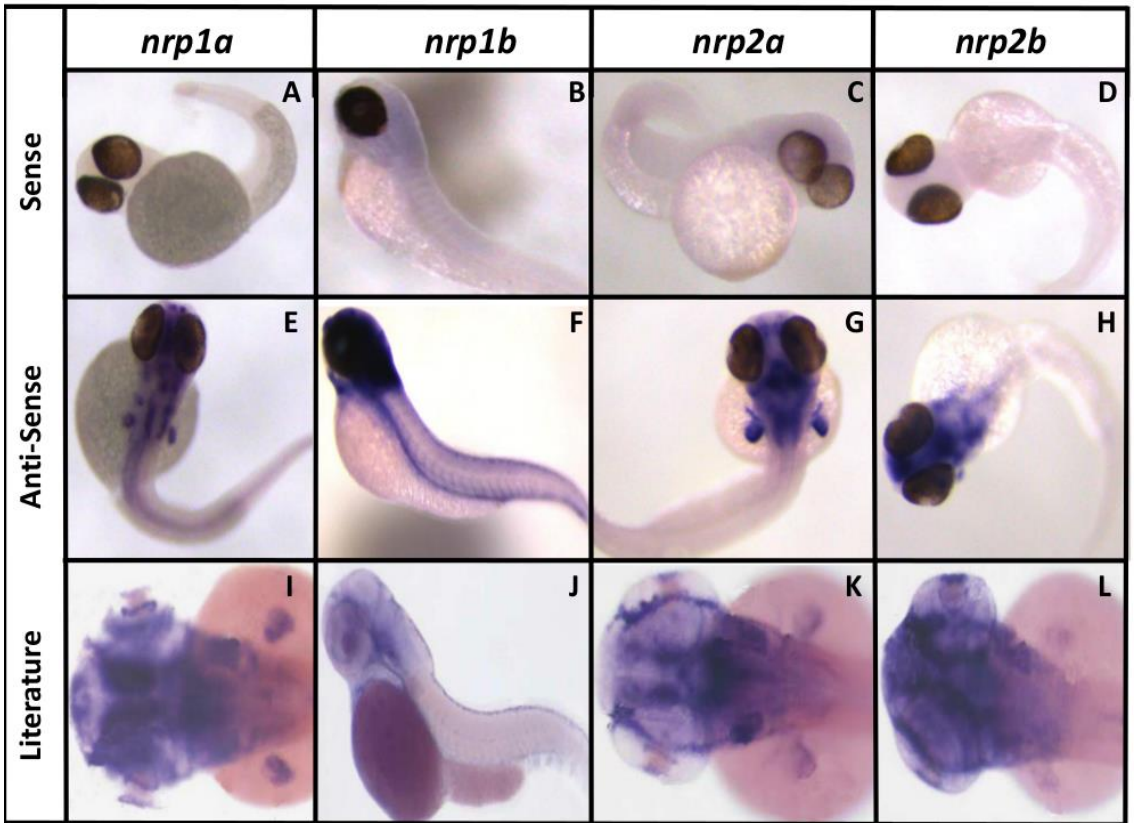

Figure 30 *nrp* riboprobe specificity validation

In situ hybridisation of TraNac transgenic zebrafish embryos 48 hours post fertilisation (hpf) with *nrp* sense riboprobes **(A-D)** and *nrp* anti-sense riboprobes **(E-H)**. A comparison to expression patterns reported by Bovenkamp *et al* (2004) in 48 hpf zebrafish embryos are presented in panels **I-L** (images obtained from (Bovenkamp et al., 2004). $n \geq 8$

I confirmed anti-sense riboprobe specificity using whole mount *in situ* hybridisation in TraNac zebrafish embryos 48 hours post fertilisation and compared the expression patterns with previous reports. I observed staining consistent with expression patterns characterised by Bovenkamp *et al.* (2004). All neuropilins are expressed in the brain (Figure 30E-L); yet additional differential staining is evident between isoforms suggesting different targets were bound by the different probes (Figure 30E-L). *Nrp1a* is also expressed in the fin buds, otic vesicles and hind brain in the developing embryo (Figure 30E), whereas *nrp1b* is expressed in the dorsal aorta and intersegmental vessels (Figure 30F), *nrp2a* expression is observed in the hind brain and fin buds (Figure 30G), and *nrp2b* expression is largely restricted to the brain and hind brain (Figure 30H) as well

as the heart (Martyn and Schulte-Merker, 2004). These data confirm differential expression of neuropilins in the embryo and verify riboprobe specificity.

3.4 Positive riboprobe localisation in the injured adult zebrafish heart

I tested the specificity of my positive control riboprobes in paraffin-embedded adult zebrafish heart sections. The positive probes are specific for cardiomyocytes (*cmlc2*), activated epicardium (*wt1b:GFP*) and endocardium (*raldh2* and *tbx18*), and were used to inform on localisation and potential cells types expressing the neuropilin isoforms.

The *cmlc2* riboprobe clearly identifies viable cardiomyocytes, whereas the injured area (Figure 31A, A'), the *bulbus arteriosus* and active proliferating epicardium (Figure 31A') remain devoid of staining. In contrast, *raldh2* and *tbx18* are developmental genes expressed by the endocardium and epicardium in the injured heart (Kikuchi *et al*., 2011b; van Wijk *et al*., 2012). Accordingly, both genes were localised to the epicardium and endocardium surrounding the injured region in my samples (Figure 31B,B',C,C'). *Wt1b* is a marker specific for epicardial cells undergoing EMT. The embryonic *wt1b* gene is re-expressed by a subpopulation of epicardial cells following cardiac damage. *wt1b in situ* staining can be observed near the injury and is indeed restricted to the epicardium (Figure 31D.D').

3.5 Neuropilin mRNA localisation in the injured zebrafish heart

Neuropilins are required for cardiogenesis in mice and zebrafish (Bovenkamp *et al*., 2004; Kitsukawa *et al*., 1995; Rossignol *et al*., 2000), however the localisation of neuropilin mRNA in the adult zebrafish heart has not been characterised in either basal conditions or during the regenerative response. After cardiac damage, embryonic genes are re-expressed by the zebrafish adult heart; therefore, I decided to investigate if neuropilins were similarly re-expressed in the heart following patterns observed throughout cardiogenesis. I investigated the localisation of the four zebrafish neuropilin isoforms in the injured adult heart using *in situ* hybridisation.

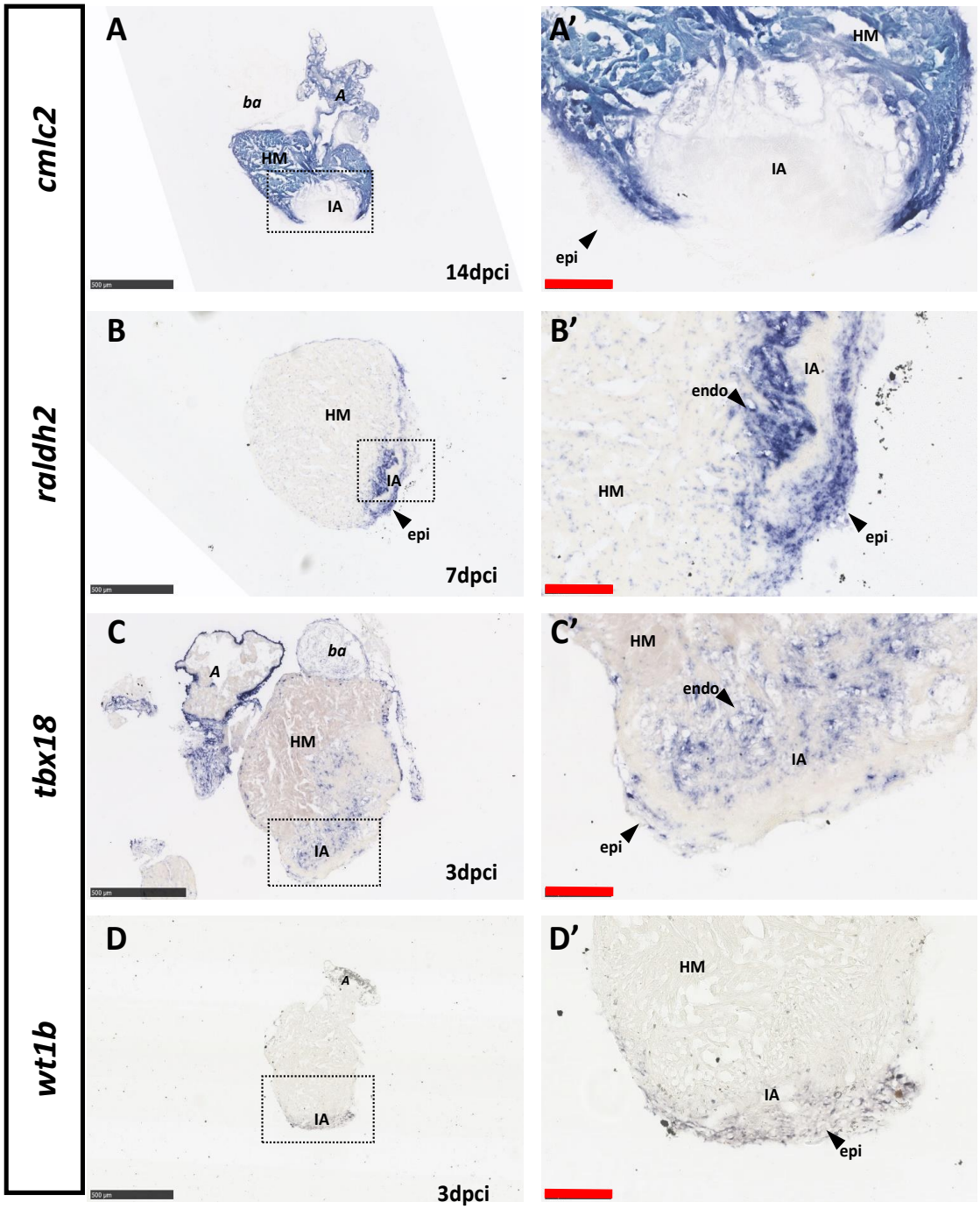

Figure 31. Positive riboprobe mRNA detection in the injured zebrafish heart

Adult zebrafish heart section were probed with positive control anti-sense riboprobes (kindly donated by Nadia Mercader, CNIC, Madrid) targeted to; **(A)** *cmlc2*, **(B)** *raldh2*, **(C)** *tbx18*, and **(D)** *wt1b,* previously characterised in zebrafish heart regeneration. *A* - atrium, *ba* - *bulbus arteriosus,* IA - injured area, HM - healthy myocardium, epi - epicardium, endo – endocardium black scale bar 500 µm, red scale bar 100 µm $n \geq 3$

3.5.1 Localisation of *nrp1a* mRNA in the regenerating zebrafish heart

Under basal control conditions *neuropilin* isoforms demonstrate differential expression (Figure 32A, F, K and P): *nrp1a* was expressed modestly within cardiomyocytes and a stronger signal was seen at the epicardium (Figure 32A). At 1 dpci, all neuropilin isoforms were detected within injured hearts and displayed a similar expression pattern (Figure 32B, G, L and Q) at the interface between the healthy myocardium and the injured area as well as in the epicardium surrounding the injury. Additionally, at 1dpci, *nrp1a* continued to show modest and diffuse expression within the entire myocardium, though the intensity of myocardial staining was fainter than at the injury interface. In contrast to the 1 dpci time-point, *nrp1a* expression was predominantly epicardial at 3 and 14 dpci (Figure 32B-D). Expression of *nrp1a* at the interface between injury and healthy myocardium persisted, however, at 3dpci, but was undetectable at 14dpci (Figure 32D). At 60 dpci, when almost complete regeneration should have occurred, *nrp1a* mRNA expression was very weak (Figure 32E). These data broadly support the qPCR measurements that revealed a significant upregulation of *nrp1a* at 1 and 3 dpci, with elevated yet not significant expression persisting until 14 dpci. The markedly upregulated expression of *nrp1a* localised at the epicardium and injury border at 1 and 3 dpci observed with *in situ* hybridisation, correlates with the significant gene upregulation detected in qPCR at those time points. Although expression of *nrp1a* mRNA is still evident at 14dpci, because its expression pattern is more restricted to the epicardium, this discrete upregulation was not sufficient to result in a significant increase of *nrp1a* gene expression in qPCR using the whole ventricle.

3.5.2 Localisation of *nrp1b* mRNA in the regenerating zebrafish heart

Following sham surgery, no evident expression of *nrp1b* mRNA was detected in the adult zebrafish heart (Figure 32F). At 1 dpci, *nrp1b* mRNA is markedly expressed at the interface between healthy myocardium and the injured area as well as at the epicardium (Figure 32G). This *nrp1b* mRNA distribution stays similar up to 14 dpci (Figure 32H and I). Nevertheless, in contrast to *nrp1a* and its striking epicardial expression, *nrp1b* mRNA is predominantly expressed at the injury/healthy myocardium interface throughout the

regenerative process. Finally, expression of *nrp1b* in the regenerated heart diminishes to basal levels by 60 dpci (Figure 32J) in accordance with the qPCR results.

3.5.3 Localisation of *nrp2a* mRNA in the regenerating zebrafish heart

According to our absolute qPCR results, *nrp2a* is the isoform with the lowest expression and, indeed, little *nrp2a* can be seen in the zebrafish heart following sham surgery (Figure 32K). However, acute *nrp2a* mRNA upregulation is observed at 1 and 3 dpci, and correlates with qPCR measurements. At 1 dpci, similarly to all neuropilin isoforms, *nrp2a* mRNA is discretely localised at the epicardium and injury/healthy myocardium interface (Figure 32L). *nrp2a* expression redistributes and exclusively localises to the epicardium by 3 dpci (Figure 32M). Consistent with qPCR data, *nrp2a* mRNA detection in the injured heart by *in situ* hybridisation is low at 14 dpci and 60 dpci (Figure 32N and O). The data suggests an acute role for *nrp2a* in the injury-activated epicardium and injury border.

3.5.4 Localisation of *nrp2b* mRNA in the regenerating zebrafish heart

Sham-operated hearts modestly express *nrp2b* in the entire ventricle (Figure 32P). At 1 dpci, *nrp2b* mRNA remains localised to the healthy myocardium additionally to upregulated expression at the injury/healthy myocardium border and by the epicardium surrounding the injury (Figure 32Q). Expression of *nrp2b* becomes predominantly localised within the injured region at 3 dpci (Figure 32R) and from 14 dpci onwards, *nrp2b* expression is comparable to expression in sham-operated hearts (Figure 32S and T).

Nrp2a and *nrp2b* display differential expression patterns in the regenerating heart; while *nrp2b* expression is evident within the injury, *nrp2a* is dominantly expressed by the epicardium, implicating differential roles for both isoforms in the cardiac response to damage.

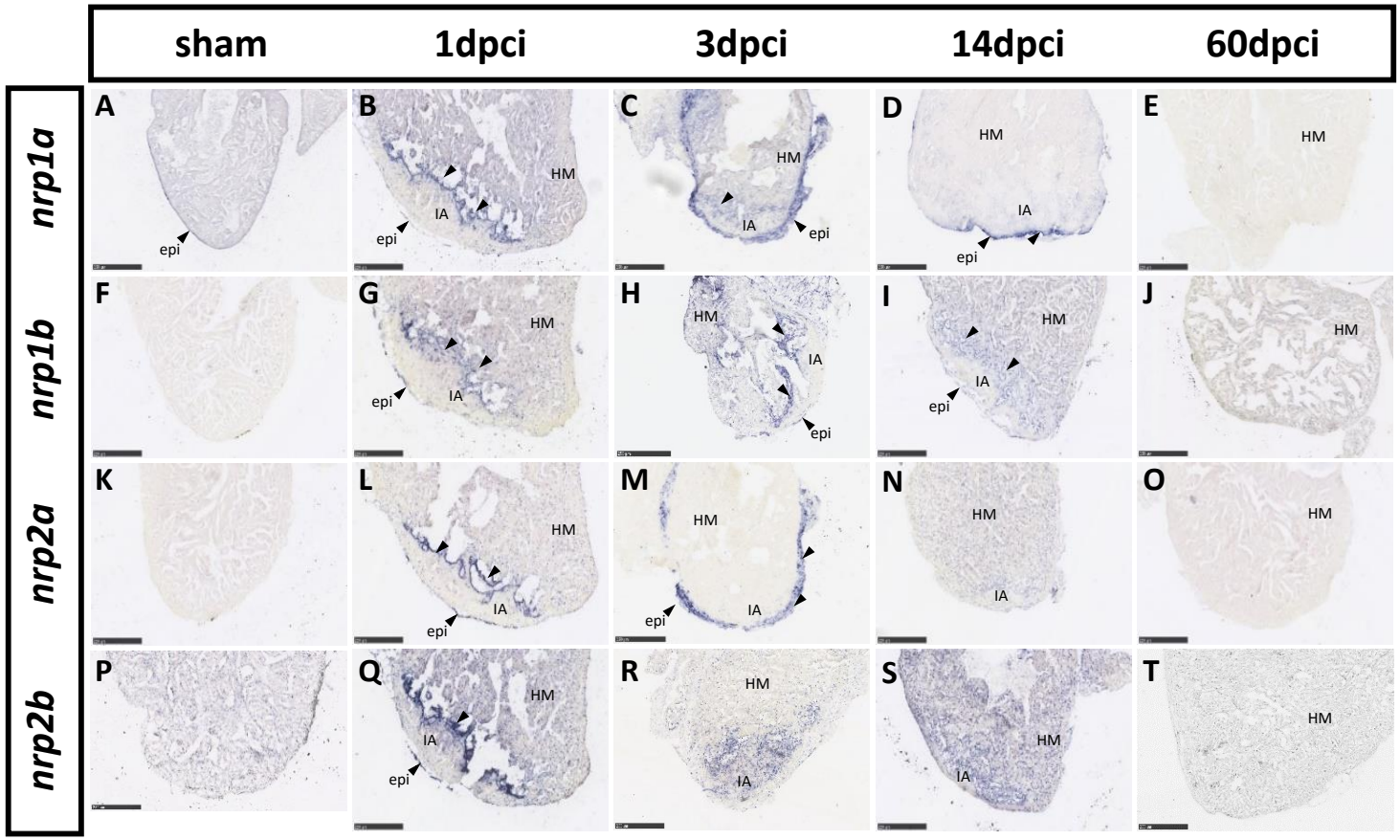

Figure 32 *nrp* mRNA localisation in the cryoinjured zebrafish heart

The localisation of *nrp* isoforms in the adult zebrafish heart were assessed after sham surgery **(A,F,K,P)** or 1, 3, 14, 60 days post cryoinjury (dpci) using *in situ* hybridization. Gene detection is observed as a dark blue stain within the section. IA = injured area, HM= healthy myocardium, epi = epicardium, arrows indicate gene expression within the epicardium or healthy myocardium to injury border. Scale bar 250µm. $n \geq 3$

3.6 Discussion

3.6.1 Technique validation

In this chapter I have demonstrated that I can generate reproducible cryoinjuries in the zebrafish heart. The damage causes loss of cardiomyocyte viability in a localised region of the ventricle. AFOG staining reveals inflammation 1 day following the injury and scar formation of similar composition as reported in the literature during the fibrotic response. By 60 dpci almost all injuries are resolved. In some isolated cases, a hint of scar was still observed by that time-point. Therefore, I have demonstrated that I am able to reproduce the cryoinjury model and trigger similar physiological responses as reported in the literature. I am also confident that I can injure the heart in a reliable and reproducible manner, affecting around 25-30% of the ventricle with limited variability.

3.6.2 Nrp mRNA regulation

The neuropilin isoforms, *nrp1a, nrp1b,* and *nrp2a* were all upregulated during the first three days following the injury. Upregulation suggest they all play a positive role in the zebrafish heart, and *in situ* hybridisation showed that these isoforms all localised at the injury interface and epicardium in the injured area 1 day following the injury. Despite these similar expression patterns, differential expression between these isoforms was noted, suggesting distinct roles may be played by different neuropilins in different cell types. Thus, *nrp1a* and *nrp2a* show marked expression in the activated epicardium, whereas expression of *nrp1b* was predominantly expressed at the injury interface. Localisation of the *nrp* isoform mRNA was persistent at regions of the heart at the injury border up to 14 dpci, further supporting a positive role of neuropilins in cells required for the regenerative response.

According to my qPCR analysis, in basal conditions, *nrp2b* is the most highly expressed isoform in the zebrafish heart. This suggest that it might play a role in cardiac homeostasis. Cardiac *nrp2b* is regulated in the heart during embryogenesis (Bovenkamp *et al*., 2004), but, according to the qPCR data presented here, *nrp2b* expression was not altered after injury. Nevertheless, *in situ* hybridisation indicated that *nrp2b* increased

markedly at the injury/healthy myocardium interface and within the injured region, supporting the conclusion that heart injury induces *nrp2b* upregulation, and suggesting that *nrp2b* also plays a role in the regenerative response of the zebrafish heart.

The data in this chapter indicate possibly different roles for neuropilins in the regenerating zebrafish heart with evidence suggesting epicardial cells that are activated after injury and cells at the injury border require neuropilin activity. A study carried out by Chablais and Jaźwińska (2012) categorises the first 4 days following cryoinjury as the inflammatory phase, in which TGFβ signalling co-ordinates leucocyte infiltration and clearance of cellular debris. It is therefore possible that the increase in neuropilin isoform gene expression within this timeframe is associated with a role for neuropilins in the inflammatory response after cardiac damage. The expression of *nrp* isoforms at the border regions of the injured area might be consistent with such a notion, since this is where inflammatory cells infiltrate the injury.

qPCR data does not provide information of specific heart area changes in gene expression; additionally, use of the entire ventricle for RNA isolation may mask smaller populations of expression changes.

The validity of the conclusion that *nrp* isoforms are upregulated in response to cryoinjury is reinforced by the demonstration in the same mRNA samples of upregulation of several other cytokines and their receptors, shown previously to be upregulated early (1-7 dpci) after zebrafish heart injury, including *pdgfab (*encoding the PDGFab cytokine), *platelet derived growth factor receptor beta* (encoding its receptor, Pdgfrβ), and *tgfβ1a* (2012).

My results also showed significant upregulation of vegfc 1-3 dpci, consistent with previous findings (Lien *et al*., 2006). Therefore, these findings also implicate a role for VEGFC in heart regeneration likely linked to lymphatic vessel development in the acute response to injury. Stimulating lymphangiogenesis to aid recovery from myocardial infarction and has been identified as a therapeutic approach (Henri *et al*., 2016; Klotz *et al*., 2015). Furthermore, it is known that NRP2 is required for lymphatic vessel

development and is a receptor for VEGF-C (Xu *et al*., 2010), and, indeed, in my model, *vegfc* follows a similar expression pattern to that of *nrp2a* (Figure 26C).

The analysis of gene expression suggests that *vegfaa* and its receptor kdr, the major endothelial ligand and co-receptor for Nrp1, respectively, are not upregulated during zebrafish heart regeneration. However, the use of the entire ventricle for qPCR may mask small and localised changes of *vegfaa* expression within the growing vessel in the injured area. Both *vegfaa* and *kdr* were expressed in high copy numbers, and thus localised changes in expression may be masked by performing qPCR of the entire ventricle rather than using a specific population of cells, obtained, for example, by fluorescence-activated cell sorting of endocardial and endothelial cells using a Tg(*fli1a*:GFP) fish. Marin-Juez *et al* very recently reported transient upregulation of *Vegfaa* at 1 dpci after cardiac cryoinjury, with a return to baseline expression by 3 dpci, and showed an important role for *Vegfaa* in inducing rapid revascularisation of the injured heart (Marin-Juez *et al* 2016). Though we found no significant upregulation of v*egfaa* following zebrafish cardiac cryoinjury concomitatnt with changes in *Nrp1* expression, our data did show a trend towards increased *Vegfaa* expression at 1 dpci, very similar to the findings of Marin-Juez and co-workers. Thus our findings could be consistent with a role for Nrp1 in mediating *Vegfaa*-driven angiogenesis in the regenerating heart. However, recent findings indicate that the role of NRP1 in mammalian developmental angiogenesis may be largely independent of VEGF, since NRP1 mutations which prevent VEGF-A binding impair post-natal angiogenesis but are compatible with normal embryonic development (Fantin *et al*., 2014). Establishing whether Nrp1 mediates angiogenesis in the regenerating heart through binding of Vegfa and heterocomplex formation between Nrp1 and Kdr will require studies of binding-deficient Nrp1a mutants.

Because of time and money constraints, I did not attempt to reproduce data related to FGF expression, which has also been implicated in the zebrafish regenerative response to cardiac damage and is also a neuropilin ligand. Although I investigated *vegfc* gene expression, regulation of its receptor, *flt4,* was not assessed. Due to the zebrafish

genome duplication, many genes have two ohnologs. I have investigated the expression of all neuropilin orthologs, but did not do so for all genes studied here. For example, PDGFAb has a distinct expression profile after cardiac damage in contrast to PDGFAa. Further investigation of expression of components of these signalling pathways, including *in situ* hybridisation analysis, would be of interest in future work.

3.6.3 qPCR

The absolute RT-qPCR was carried out by external services that use automated systems to minimise human errors, all measurements were run in duplicates, non-template controls and reverse transcriptase controls were included for every gene and the reactions. Often, RNA quality is not addressed in studies before cDNA synthesis and qPCR; however, degraded RNA can result in unreliable, inconsistent and misleading qPCR measurements. I selected randomly 24 RNA samples (approximately 30% of the total samples used to make cDNA in the qPCR) and evaluated their integrity, and all samples had RIN values above 9. Because the method used to extract RNA, the tissue and subsequent RNA storage were identical, I assumed that all of the remaining RNA samples were of similar integrity. It would have been preferable (but prohibitively costly) to assess the integrity of all RNA samples extracted to ensure high quality of all samples before qPCR quantification.

The absolute qPCR method informs of mRNA expression as copy number (rather than relative levels of expression), extrapolated from the reaction's cDNA content. The cDNA is generated from a reverse transcription reaction, which is of limited efficiency (only around 30% of RNA is reverse transcribed into cDNA) introducing a potential source of experimental variability. Gene variation in the high copy number values range are most likely to be less variable and translate as physiologically relevant *in vivo.* In general, qPCR cannot inform on whether the mRNA turnover is rapid or to what extent the mRNA is translated into protein, nevertheless, there is a correlation between mRNA expression and protein level and therefore physiological function associated to changes in gene expression.

The RNA isolated for the qPCR was derived from the entire ventricle. Cardiomyocytes dominate the cell population represented in the ventricle; however other smaller cell populations have important roles in the regenerative response. Therefore, expression pattern changes after cardiac damage in these smaller cell populations could be masked by gene expression by cardiomyocytes. One way to circumvent this, would be to isolate specific cell populations from transgenic fish with specific myocardial, epi- or endocardial marker by FACS and isolating RNA from purified cell type.

3.6.4 *In situ* hybridisation

I established the *in situ* hybridisation protocol to observe gene expression patterns in zebrafish heart samples. I confirmed that my technique leads to specific detection of target genes. Sense riboprobes did not stain samples, confirming them as a reliable negative control. Anti-sense neuropilins riboprobes stained whole mount embryos identically to previous reports in the literature confirming their specificity (Bovenkamp *et al*., 2004; Martyn and Schulte-Merker, 2004; Yu *et al*., 2004). The technique was then applied to paraffin embedded heart sections, positive control probes confirmed epicardial and endocardial activation, loss of cardiomyocyte viability and technique stringency.

I was provided some control riboprobes from another institute (CMIC, Madrid) and had limited information about the target sequence and I was unable to generate the negative control sense probes. However, these probes were used in previous publications which provided confidence about their specificity and therefore the sense probe would have been unlikely to provide any contradictory data.

The anti-sense riboprobes have different interaction properties depending on the target mRNA, therefore the staining intensity observed using the different riboprobes could be due to riboprobe binding efficiency, rather than expression levels. The *nrp* isoform staining intensities are not directly comparable between one another due to these variations in riboprobe affinity to target, only the localisation of probe detection can be compared.

Some sham hearts show slight expression of *nrps* whereas the expression is no longer evident at 60 dpci. This could be due to low grade activation of the epicardium during sham surgery which does not affect qPCR values on the entire ventricle, but that can be detected by ISH. Indeed, it has been reported that there is an epicardial and cardiomyocyte activation after even moderate disruption (de Preux Charles *et al*., 2016b; Itou *et al*., 2014). Alternatively, this might reflect downregulation of *nrp* expression at 60dpci relative to control expression.

3.6.5 Summary

In this chapter I have demonstrated:

- In my hands, the zebrafish cryoinjury procedure results in 25% ventricle damage and cardiomyocyte viability loss in the targeted region.
- Half of all cryoinjured fish fully replenish cardiac tissue and resolve the fibrotic scar within 60 days following cryoinjury.
- *nrp1a, nrp1b* and *nrp2a* are significantly upregulated within the first three days of cardiac damage, corresponding to the inflammatory phase.
- *nrp2b* is the dominant neuropilin isoform in the zebrafish heart.
- All *nrp* isoforms mRNA is localised at the injury healthy myocardium border at 1 day post cryoinjury (dpci). Thereafter, *nrps* display differential localisation patterns in the injured heart until 14 dpci and return to basal expression levels by 60 dpci.
- This chapter provides compelling evidence for positive yet distinct roles for neuropilins during the early cardiac regenerative response.

4 Results chapter 2: Cell-type specific nrp expression in zebrafish heart regeneration

In the previous chapter, I demonstrated that 3 of the 4 zebrafish *nrp* isoforms are acutely upregulated at 1 and 3 days post cryoinjury (dpci). Although *nrp2b* does not seem to be upregulated, it is the most highly expressed *nrp* isoform in the zebrafish ventricle. *In situ* hybridisation (ISH) revealed that all *nrp* isoforms are strongly localised to the injury-healthy myocardium border at 1 dpci, after which, the isoforms are differentially localised:

- *nrp1a* expression persists in the epicardium until 14 dpci,
- *nrp1b* is concentrated predominantly at the injury/healthy myocardium interface,
- *nrp2a* is distinctly epicardial at 3 dpci,
- *nrp2b* is localised within the injury and expressed throughout the myocardium.

qPCR and ISH strongly suggest positive but distinct roles for the neuropilins in regenerating zebrafish hearts. In this chapter, I set out to characterise Nrp protein expression and identify Nrp-positive cell types after cardiac damage in the zebrafish.

4.1 NRP C-terminus sequence similarities

The zebrafish has recently emerged as a popular vertebrate model to study cardiovascular diseases. However, commercially available reagents, notably antibodies, that specifically detect zebrafish antigens are limited. Evolutionary genome duplication in the zebrafish has resulted in frequent occurrence of duplicate genes, adding further complexity, and making it more difficult to distinguish between the protein products of ohnologs (a gene duplicate originating from whole genome duplication) of high levels of sequence similarity.

A

NRP1

```
-CACSHSGMSDRNLSALENYNFELVDGVKLKKDKLNSQNSYSEA  43aa zf Nrp1a
YCACAHT--TNRNLSALENYNFELVDGVKLKKEKLSAQKSYTEA  42aa zf Nrp1b
YCACWHNGMSERNLSALENYNFELVDGVKLKKDKLNTQSTYSEA  44aa human NRP1
```

B

NRP2

```
YCTCSYGGLTSRSSTTLENYNFELYDGIKHKVKLNQQRCCSEA 43aa zf Nrp2a
YCTCSYGGLTSRSSTTLENYNFELYDGIKHKVKLNQQRCCSEA 43aa zf Nrp2b
--TCSYSGLSSRSCTTLENYNFELYDGLKHKVKMNHQKCCSEA 41aa human NRP2
```

C

	zf Nrp1a	zf Nrp1b	zf Nrp2a	zf Nrp2b	Human NRP1	Human NRP2
zf Nrp1a	100	74.4	55.8	55.8	86.0	58.5
zf Nrp1b	74.4	100	50.0	50.0	72.7	46.3
zf Nrp2a	55.8	50.0	100	100	54.5	82.9
zf Nrp2b	55.8	50.0	100	100	54.5	82.9
Human NRP1	86.0	72.7	54.5	54.5	100	53.7
Human NRP2	58.5	46.3	82.9	82.9	53.7	100

Figure 33 NRP C-terminus amino acid sequence alignment

A) Alignment of human NRP1 against zebrafish (zf) Nrp1a and Nrp1b c-terminus protein sequence. **(B)** Alignment of human NRP2 against zebrafish (zf) Nrp2a and Nrp2b C-terminus protein sequence. Amino acids that differ between the two species but classified in the same amino acid group are highlighted in purple. Amino acid differences of unrelated molecular properties are highlighted in yellow. **(C)** Percentage protein sequence homology between zebrafish (zf) and human NRP isoforms c-termini were calculated using ClustalW sequence alignment software.

The NRP 42-44 amino acid C-terminal cytoplasmic domain is highly conserved between species and provides a suitable epitope for some commercially available and validated NRP antibodies. I compared the amino acid sequences of zebrafish and human NRP C-termini to predict if human-targeting NRP antibodies were likely to cross-react with zebrafish Nrps (Figure 33). Immunogen sequence similarities of 80% and above are considered to have high cross-reactivity potential.

Human NRP1 has 86% and 72.7% C-terminus sequence similarity to zebrafish Nrp1a and Nrp1b (respectively) (Figure 33A,C), suggesting that Nrp1a will likely cross react more with antibodies targeted to the C-terminus of human NRP1 than will Nrp1b. The zebrafish Nrp2 ohnologs have an 82.9% C-terminal amino acid sequence similarity to human NRP2 (Figure 33B,C), also supporting the potential cross-reactivity of human NRP2 C-terminal targeting antibodies to Nrp2a and Nrp2b. Amino acids that differ between the two species often belong to the same amino acid group and therefore possess similar chemical properties, suggesting they may retain comparable molecular interactions with antibodies (purple highlight Figure 33A and B).

The zebrafish Nrp1a and Nrp1b ohnologs share 74% C-terminus protein sequence similarity, whereas Nrp2a and Nrp2b C-termini have complete sequence homology. This is consistent with a previous hypothesis suggesting that the genetic drift that has occurred between *nrp1a* and *nrp1b* genes is greater than between the *nrp2* ohnologs (Bovenkamp *et al*., 2004). Therefore, with respect to antibody specificity, both Nrp2a and Nrp2b isoforms are predicted to indistinguishably bind to antibodies that detect zebrafish Nrp2 C-termini. However, antibodies targeting the C-terminus of human NRP1 may not cross-react with both zebrafish Nrp1a and Nrp1b. Moreover, because the Nrp1 ohnologs have different molecular weights, they can be identified as two separate bands when performing immunoblotting.

There is approximately 50% amino acid sequence similarity between the zebrafish Nrp1 ohnologs and the human NRP2 C-terminus, a similar level of C-terminus sequence

similarity as observed between human NRP1 and human NRP2 (52.7%). This strongly suggests that antibodies targeting the C-terminus of human NRP1 will unlikely cross react with the C-terminus of zebrafish Nrp2.

Taken together, the C-terminus amino acid sequence suggests there is a high probability that antibodies targeted to human NRP C-terminus will cross react with the corresponding zebrafish Nrp ortholog, although it is uncertain which ohnolog will be identified and whether the antibodies will non-specifically cross-react with other zebrafish proteins.

4.2 Neuropilin protein regulation in the cryoinjured heart

qPCR and ISH data confirm regulation of *nrp* mRNA expression in response to cardiac damage. mRNA regulation is correlated to changes in protein levels. I observed an acute (1 and 3 dpci) upregulation of *nrp* mRNA in the zebrafish ventricle after cryoinjury and thus predicted this would be accompanied by protein upregulation at similar time points. To assess this hypothesis, immunoblotting was performed to measure protein expression in lysates from sham-operated *versus* cryoinjured ventricle at 1,3,7,14 and 30 days post-surgery.

GAPDH was used as a loading control for Western Blot as absolute qPCR measurements indicate stable GADPH expression regardless of treatment or time point (data not shown), suggesting that GADPH protein expression should also remain consistent. Several antibodies targeted to human, rat and mouse NRP1 or NRP2 C-termini were tested for cross-reactivity with zebrafish NRPs. Unfortunately, NRP2 immunoblots showed that NRP2 antibodies bound off-target zebrafish proteins (data not shown). However, a NRP1 antibody was validated and could identify two separate bands at approximately 130 and 150kDa (Figure 34A). These Nrp1 zebrafish doublets have been previously described by Bovenkamp *et al.,* who identified the lower molecular weight band as Nrp1a at 125kDa, and the upper higher molecular weight band as Nrp1b at 145kDa. The variation in Nrp1a and Nrp1b molecular weight, despite protein sequence similarity, are probably due to differential post-translational modifications. Indeed,

work from others in our group has shown that NRP1 was post-translationally modified by the addition of a single glycosaminoglycan residue (either chondroitin sulphate or heparin sulphate) at Serine 612 in vascular smooth muscle cells and some cancer cells (Frankel *et al*., 2008; Pellet-Many *et al*., 2011).

Nrp1a and Nrp1b band intensities were measured with the ImageJ software and normalised to GAPDH. Quantification of the two Nrp1 bands as a doublet shows a trend for NRP1 upregulation at 3 and 7 dpci and reaches statistical significance at 14 dpci in comparison to sham control samples (Figure 34B). The quantification of the single Nrp1a band hints a trend towards upregulation at 7 dpci, which is not concomitant with the timing from my qPCR results showing an earlier upregulation of *nrp1a* at 1 and 3 dpci (Figure 34C). Since translation occurs after transcription, the increased mRNA levels most likely precede the increase in protein expression. The quantification of the single Nrp1b band shows a significant upregulation at 3 dpci and reverts to basal sham expression levels thereafter (Figure 34D). Nrp1 upregulation during the first 14 days following cardiac damage is observed both at mRNA levels (qPCR analysis) and protein levels (immunoblotting) and thus support a role for Nrp1 role in the early regenerative process, concomitant with the inflammatory and reparative phases. At later stages of the regenerative response (30 dpci and later), neuropilin levels return to basal level expression, similar to sham expression in qPCR, ISH and Western blot analysis, indicating that neuropilin's role is more important during the immediate and early cardiac responses following injury.

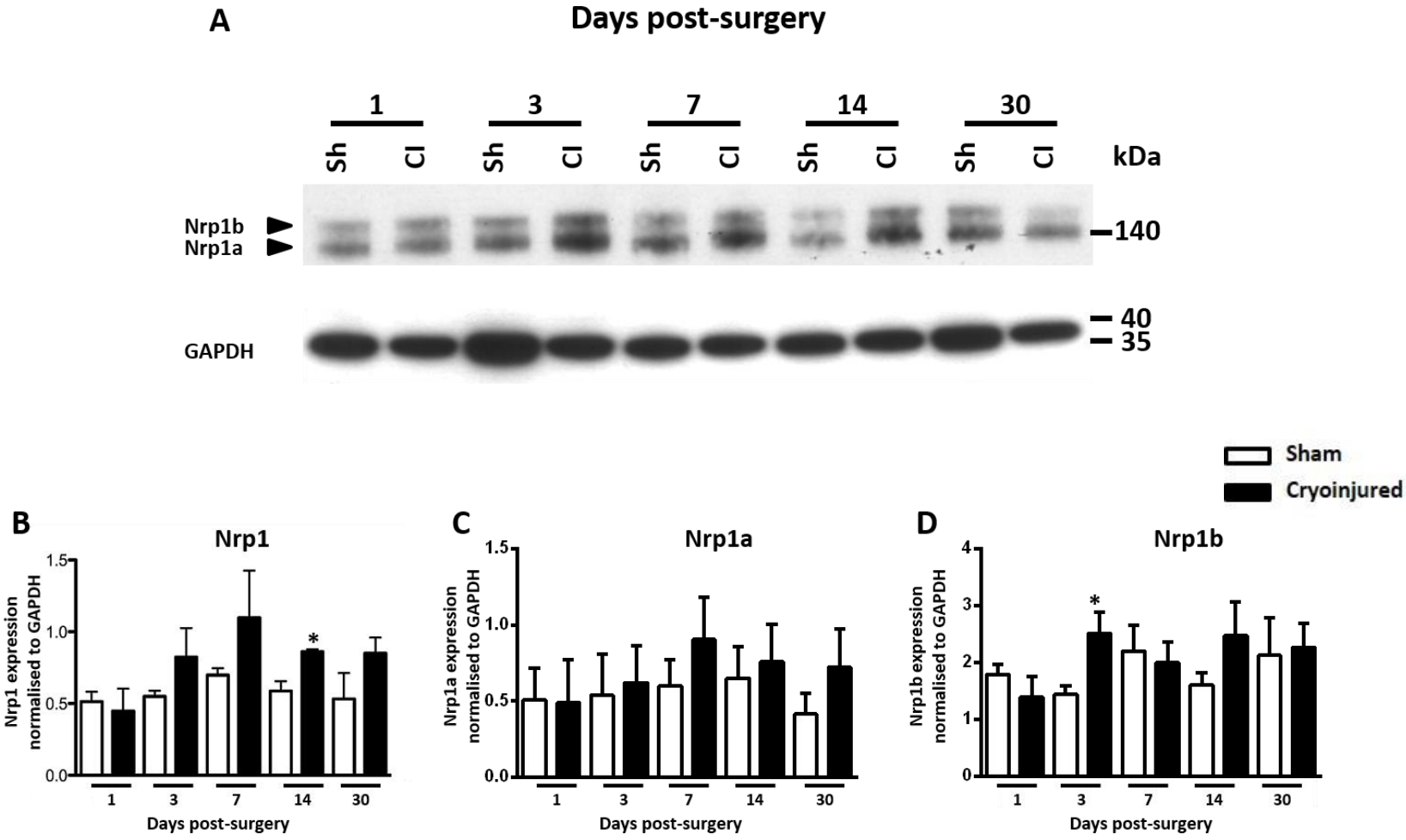

Figure 34 Nrp1 is regulated in cryoinjured zebrafish ventricle

(A) Adult zebrafish ventricle lysates were obtained 1, 3, 7, 14 and 30 days following sham surgery (Sh) or cryoinjury (CI). Lysates were immunoblotted for Nrp1 and Gapdh. Nrp1a bands are visible at approximately 130kDa and Nrp1b at approximately 150 kDa (indicated). Quantification of **(B)** both bands, **(C)** Nrp1a lower band and **(D)** Nrp1b upper band 1, 3, 7, 14 and 30 days following sham surgery (white bars) or cryoinjury (black bars). Data are represented as means of band intensities normalised to GAPDH ± S.E.M (error bars) *p<0.05; n = 4 with each n being a pool of 3 ventricles of identical treatment and time point.

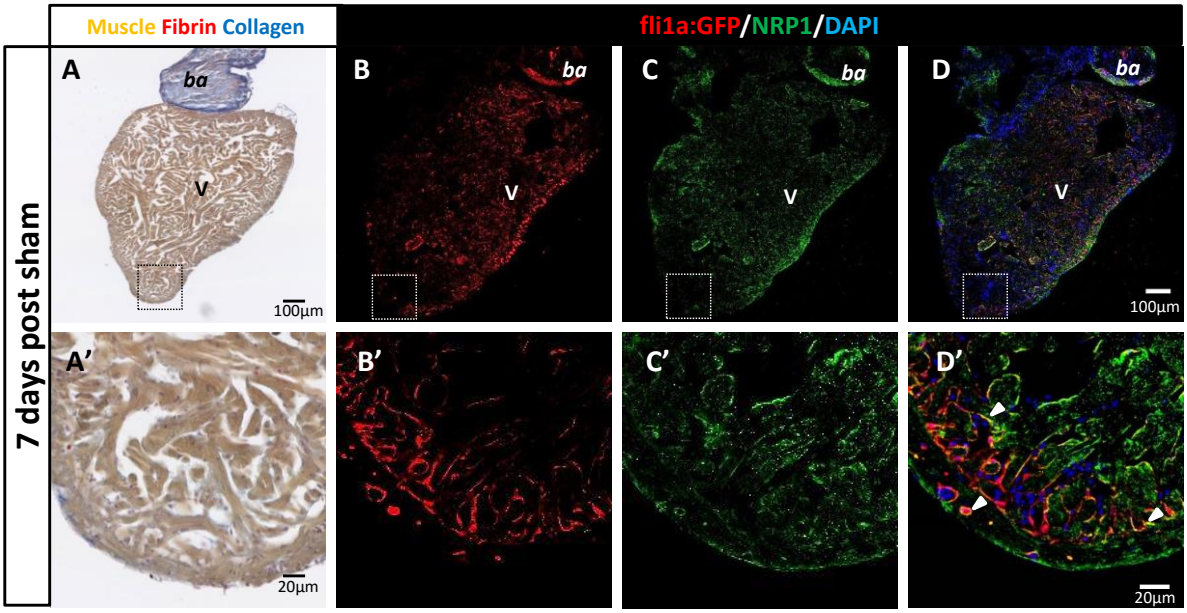

Figure 35 Nrp1 colocalises with endothelium and endocardium in sham-operated hearts

AFOG staining **(A and A')** and immunofluorescence images **(B-D and B'-D')** of *Tg(fli1a:GFP)* zebrafish heart 7 days post sham surgery. AFOG staining confirms the integrity of cardiac tissue and gives reference to the heart structure. *fli1a* expression by endothelium and endocardium are immunolabeled with GFP-targeted antibody (red) (B and B') and Nrp1 expressing regions stained green **(C and C').** Overlay of the two colours are displayed with DAPI nuclei staining **(D and D')**. White arrows indicate areas of colocalisation. Dotted boxes highlight magnified region. v – ventricle *ba- bulbus arteriosus n* = 5

4.3 Neuropilin localisation in the regenerating zebrafish heart

ISH identified increased *nrp* expression localised at regions in close proximity to the injured area. Therefore, I further investigated which cell types express Nrps in the regenerating heart with immunofluorescent staining.

4.3.1 Nrp1 expression in the endocardium

Immunofluorescence staining detecting Nrp1 and GFP in sham-operated Tg(*fli1a:GFP*) zebrafish heart sections was performed (Figure 35A). The endocardium lining the ventricle lumen and coronary vessel endothelial cells in the myocardium compact layer

express *fli1a* (Figure 35B and B'). Co-staining reveals Nrp1 in the epicardium and endocardium (Figure 35C,C'), and Nrp1 colocalisation with GFP-positive coronary vessel endothelial cells within the compact myocardial layer and the endocardium of sham-operated *Tg(fli1a:GFP)* hearts (Figure 35D,D'). Nrp1 expression that does not colocalise with GFP positive cells is seen in the quiescent epicardial monolayer (Figure 35D').

Sections from cryoinjured *Tg(fli1a:GFP*) zebrafish hearts 1 dpci were evaluated with immunofluorescence, and corresponding serial sections were stained with AFOG (Figure 36A,A') or used for *nrp1a* and *nrp1b* anti-sense riboprobe ISH (Figure 36B,B',C,C'). GFP immunofluorescence shows endothelial cells forming new vessels at the edges of the injured area (Figure 36D, D'). Nrp1 colocalises with all GFP positive cells of neovessels in the injured area suggesting a role for Nrps in early revascularisation after cardiac damage (Figure 36E, E', F, F'). ISH staining of *nrp1a* and *nrp1b* shows mRNA expression localised within the injury that could in part reflect Nrp1-positive neovasculature (Figure 36B' and C').

An endocardial GFP signal was largely absent within the injury core, however viable Nrp1 endocardium remained evident in healthy cardiac tissue at the injury border (white arrows) (Figure 36F'). Furthermore, NRP1 immunofluorescent staining demonstrated greater intensity within the viable endocardium at the injury interface (Figure 36E') and recapitulates ISH staining patterns that implicate a neuropilin expression increase at the injury border at 1 dpci (Figure 36B' and C'). The data suggest a requirement for Nrp1 upregulation in the endocardium proximal to the injury immediately after imsult. The endocardium responds within hours of cardiac damage essential for the regenerative process (Kikuchi *et al*., 2011b).

Nrp1 expression patterns in the injured region were analysed at 7 dpci in *Tg(fli1a:GFP)* zebrafish (Figure 37A, A'). At this point of the regeneration process, revascularisation continues to develop in the injured area (Lepilina *et al*., 2006; Marin-Juez *et al*., 2016) and endocardium activation is established (Kikuchi *et al*., 2011b). At 7 dpci, endocardial cells proximal to the injury exhibited a rounded morphology (Figure 37B,B') consistent with previous characterisation of the endocardial endoMT in response to ventricular

amputation (Kikuchi *et al*., 2011b). Moreover, a subpopulation of endocardial cells were observed protruding into the injured area (Figure 37B' white arrows); these cells are likely being activated to form new vessels or provide new endocardium for the regenerating cardiac tissue by transiently transdifferentiating into mesenchymal cells. A higher vessel density stemming from the epicardium was evident (Figure 37B and B'), but the core of the injury remained largely avascular.

Similar to my observations at 1 dpci, Nrp1 colocalised with all *Tg(fli1a:GFP)* positive cardiac tissue (Figure 37D,D') at 7dpci, suggesting Nrp1 is required for endocardial activation and vessel development in the regenerating zebrafish heart from 1 dpci to 7 dpci. Additional staining of Nrp1 was observed at the periphery of the injury in a layer of GFP negative cells. The location and appearance of these latter cells suggested that they might be of epicardial origin since the epicardium has been previously reported to undergo extensive proliferation in response to injury (Kikuchi *et al*., 2011b; Manuel Gonzalez-Rosa *et al*., 2012; Schnabel *et al*., 2011). This indicates that distinct cell types other than endocardial and endothelial cells express Nrp1 in the regenerating zebrafish heart.

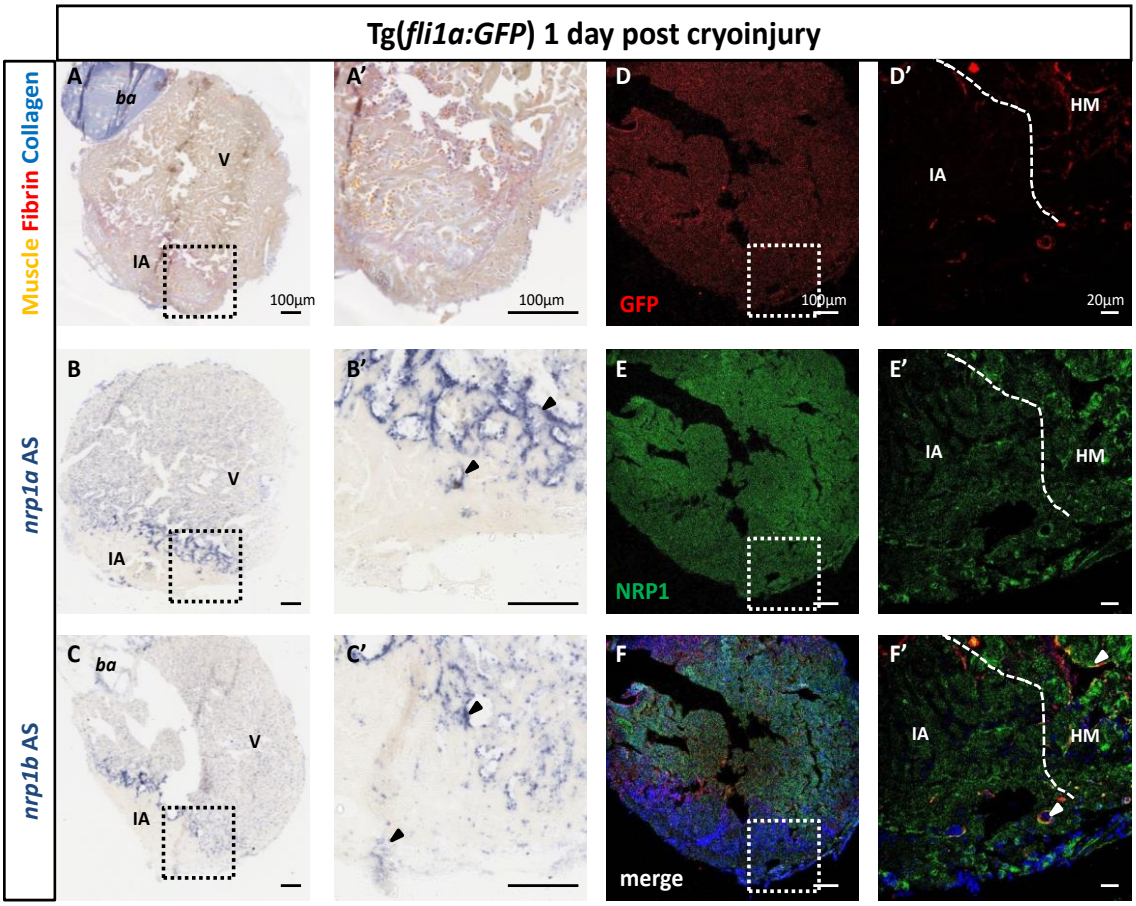

Figure 36 Nrp1 is expressed by the activated endocardium and neovasculature during the inflammatory phase (1 dpci)

AFOG staining **(A and A')**, *in situ* hybridisation **(B, B', C and C')** and immunofluorescence of *Tg(fli1a:GFP)* zebrafish heart 1 day post cryoinjury (dpci). AFOG staining gives reference to the heart structure and cryoinjury-location (A and A'). *nrp1a* and *nrp1b* mRNA detection are observed as dark blue staining (B, B', C and C'), black arrows indicate mRNA expression within the injury and at the injury/healthy myocardium border. GFP positive cells highlight *fli1a* expression by viable endothelium and endocardium labelled in red **(D and D')** and Nrp1 expressing regions of the heart in green **(E and E')**. Overlay of the two colours are displayed with DAPI nuclear staining **(F and F')**. White arrows indicate areas of colocalisation. Dotted boxes highlight magnified regions. Dashed lines define injury interface. *v* – ventricle *ba- bulbus arteriosus* IA- injured area HM- healthy myocardium *n* = 3

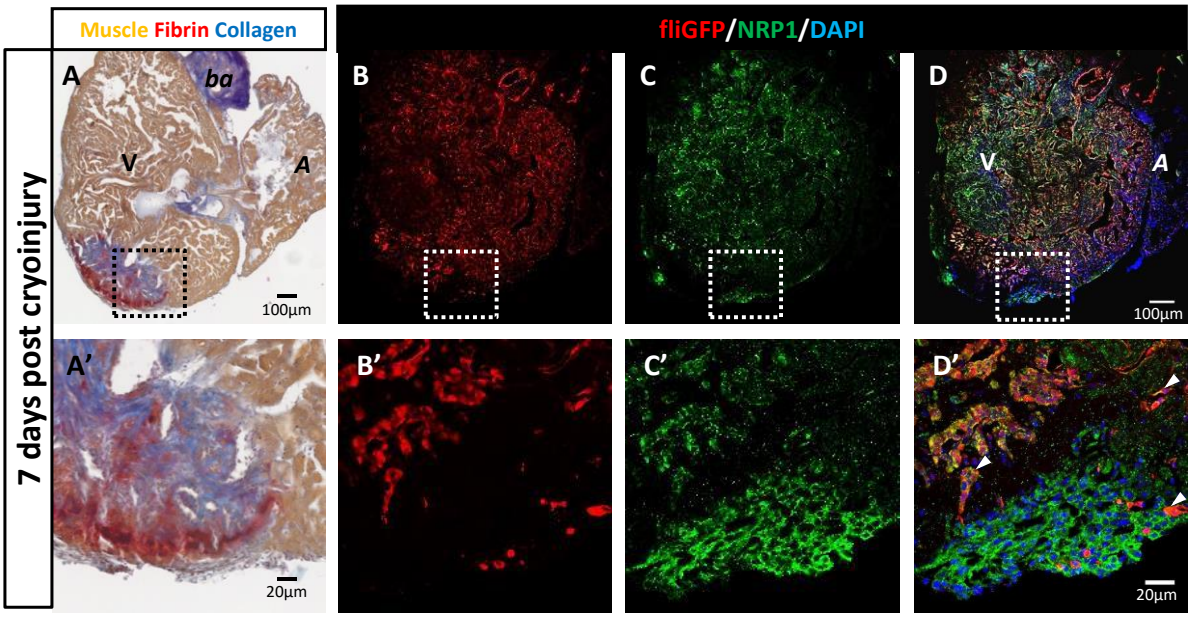

Figure 37 Nrp1 is expressed by the activated endocardium and neovasculature during reparative phase

AFOG staining **(A and A')** and immunofluorescence images **(B-D and B'-D')** of Tg(*fli1a:GFP*) zebrafish heart 7 days post cryoinjury (dpci). AFOG staining identifies cardiac damage and gives reference to the heart structure and cryoinjury-location. *fli1a* expression by endothelium and endocardium are immunolabeled with anti-GFP antibody (red) (B and B') and Nrp1 expressing cells are shown in green **(C and C')**. Overlay of the two colours are displayed with DAPI nuclei staining **(D and D').** White arrows indicate areas of colocalisation. Dotted boxes highlight magnified region. *v* – ventricle *ba- bulbus arteriosus A* – atrium *n* = 3

I studied the expression and colocalisation of Nrp1 using an additional transgenic endothelial/endocardial reporter line that express the mCherry fluorophore downstream of the *kdrl* (*kinase insert domain receptor like*, also known as *vascular endothelial growth factor receptor-2*) promoter in 7 dpci hearts (Figure 38A,A'). ISH was used in serial sections to localise *nrp1a* mRNA expression in these hearts (Figure 38,B',C,C'). mCherry positive cells were almost exclusively endocardial with limited expression by coronary vessels in the compact myocardium, indicating a lack of coronary vessel Kdrl expression in the zebrafish heart (Figure 38D'). Nrp1 colocalised with mCherry positive cells throughout the entire endocardium including the endocardium within the regenerating injured area (Figure 38E,E',F ,F') consistent with the *Tg(fli1a:GFP*)/Nrp1 co-staining data presented (Figure 37). This further strengthens the hypothesis that Nrp1 is constitutively expressed by the endocardium in zebrafish hearts and that Nrp1 could act as a potential endocardial marker.

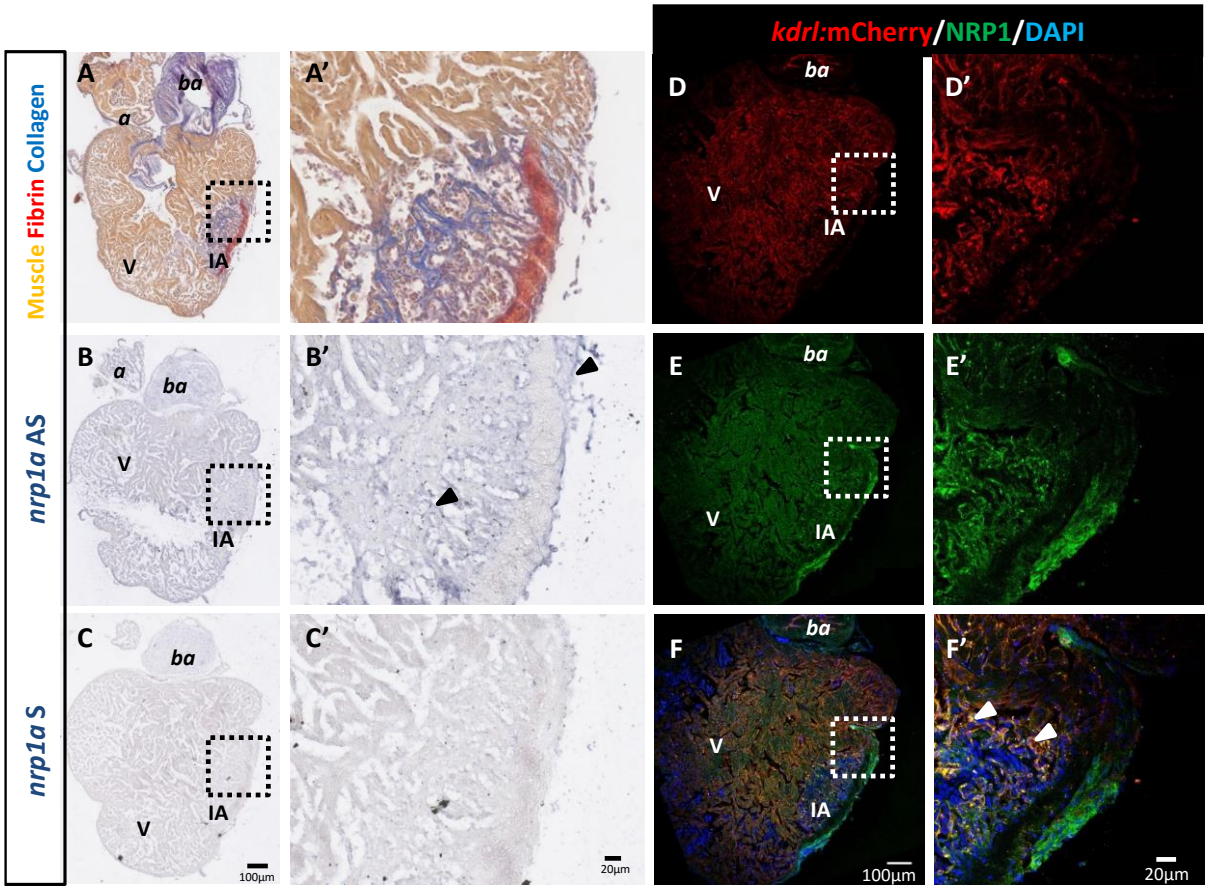

Figure 38 Nrp1 expression in the endocardium at 7dpci

AFOG staining **(A and A')**, *in situ* hybridisation (ISH) **(B, B', C and C')** and immunofluorescence (D-F) of Tg(*kdrl:mCherry*) zebrafish heart 7 days post cryoinjury (dpci). AFOG staining gives reference to cryoinjury location and tissue composition (A and A'). ISH of *nrp1a* anti-sense riboprobe (*nrp1a* AS) (B and B') and negative control sense (*nrp1a* S) riboprobe (C and C'), signal is observed as a dark blue stain within the section (B and B'), black arrows indicate mRNA expression. *kdrl* expression by viable endocardium is immunolabeled with anti-mCherry antibody (red) **(D and D')** and Nrp1 expressing cells are labelled green **(E and E')**. Overlays of the two colours are displayed with DAPI nuclei staining **(F and F')**. White arrows indicate areas of colocalisation of Nrp1 and *kdrl*-mCherry. Dotted boxes highlight magnified regions. *v* – ventricle *ba*- bulbus arteriosus *a* – atrium IA- injured area *n* = 3

4.3.2 Nrp1 expression in the myocardium

The expression of Nrp1 by cardiomyocytes was assessed in sham-operated and cryoinjured adult zebrafish heart sections. Cardiomyocytes form the majority of the ventricle mass. Viable cardiomyocytes were identified with tropomyosin and injury location was identified where damaged tissue lacked tropomyosin expression (Figure 39C' and D'). In sham-operated hearts, Nrp1 expression by cardiomyocytes was limited; tropomyosin and Nrp1 staining patterns were mostly discrete from one another (Figure 40B). Nrp1 expressing cells predominantly encase the trabeculated folds of the myocardium, distinctive pattern of the endocardium, or form a monolayer at the periphery of the heart, characteristic of the epicardium (Figure 39B).

Following cardiac damage Nrp1 expression remained largely absent from cardiomyocytes; however Nrp1 expression was evident in cardiomyocytes protruding into the injured area from the sub-epicardial layer (Figure 39D white arrows).

4.3.3 Nrp1 expression in the epicardium

The epicardium is a quiescent mesothelial cell monolayer that surrounds the entire heart. In the zebrafish, after cardiac damage, the epicardium becomes activated, proliferates and re-expresses developmental genes such as *tbx18*, *raldh2* and *wt1b*. The activated epicardium produces cytokines to mediate epicardial epithelial-to-mesenchymal transition (EMT) (Kikuchi *et al.*., 2011; Manuel Gonzalez-Rosa *et al.*., 2012; Masters and Riley, 2014), orchestrate inflammatory cell recruitment (Han *et al.*., 2014) and induces cardiomyocyte proliferation (Chen *et al.*., 2002; Kikuchi *et al.*., 2011; Lepilina *et al.*., 2006). The mammalian epicardium responds to cardiac damage (Zhou *et al.*., 2011) and, during development expresses NRP1 (Partanen *et al.*., 1999). In my studies, neuropilin ISH and immunofluorescence staining patterns strongly indicated epicardial expression of Nrp1. Thus, localisation of neuropilin to the epicardium was assessed in sham-operated and cryoinjured *Tg(wt1b:GFP)* zebrafish, in which GFP expression is controlled by the promoter for the activated epicardial marker, *wilms' tumor 1b* (*wt1b*). In sham-operated control *Tg(wt1b:GFP)* zebrafish heart sections (Figure 40A,D), GFP signal was absent consistent with the conclusion that epicardial cells

were not in an activated state, and confirming the quiescence of the epicardium following sham surgeries (Figure 40B' and C'). In sham-operated hearts, as seen previously, Nrp1 was expressed by the endocardium and also expressed within the quiescent and discrete epicardial monolayer (Figure 40C). 7 days after cardiac damage, there was a robust increase in the number of wt1b:GFP positive cells within the activated epicardium, all of which also expressed Nrp1. Activated wt1b:GFP positive epicardial cells expressed Nrp1 after cardiac damage (Figure 40F white arrows). A subset of activated epicardial cells expressed wt1b:GFP (Figure 40F and Figure 41H), as previously described (Peralta *et al.,* 2014).

The localisation of Nrp1 immunofluorescent staining within the epicardium was compared to *nrp1a* AS ISH staining (Figure 41). *nrp1* mRNA was strongly expressed at the border between healthy myocardium and the injured tissue as well as having an epicardial-wide expression at 3 dpci (Figure 41E), similar to protein expression of Nrp1 observed using immunofluorescent staining at 3 dpci (Figure 41C,G).

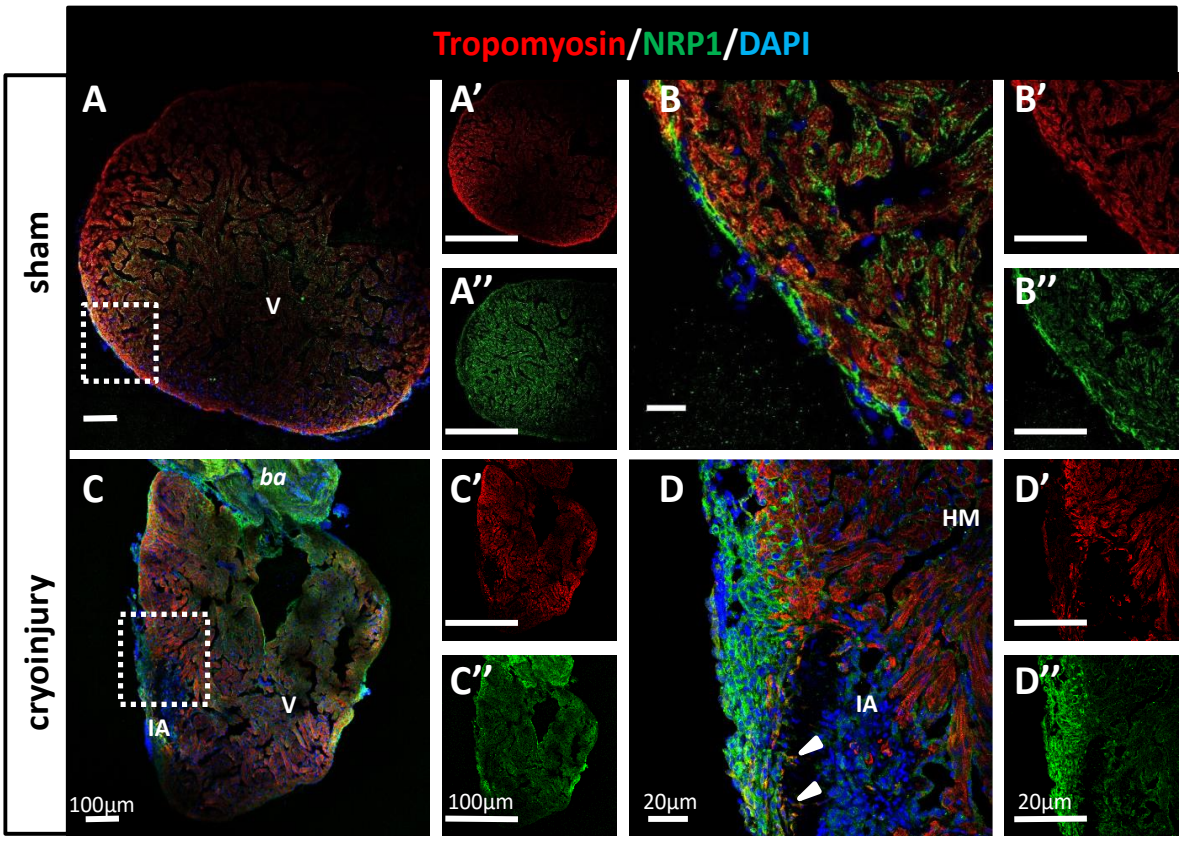

Figure 39 NRP1 is expressed in migrating sub-epicardial cardiomyocytes

Immunofluorescence of adult zebrafish heart sections 7 days post sham surgery **(A and B)** or 7 days post cryoinjury **(C and D).** Viable cardiomyocytes were labelled with tropomyosin and stained in red (A'-D'). Nrp1 expressing cells are shown in green (A''-D''). Overlay of the two colours are displayed with DAPI nuclei staining (A-D). Dotted boxes highlight magnified region. White arrows indicate colocalisation. v – ventricle *ba- bulbus arteriosus* IA – injured area HM- healthy myocardium *n* = 3

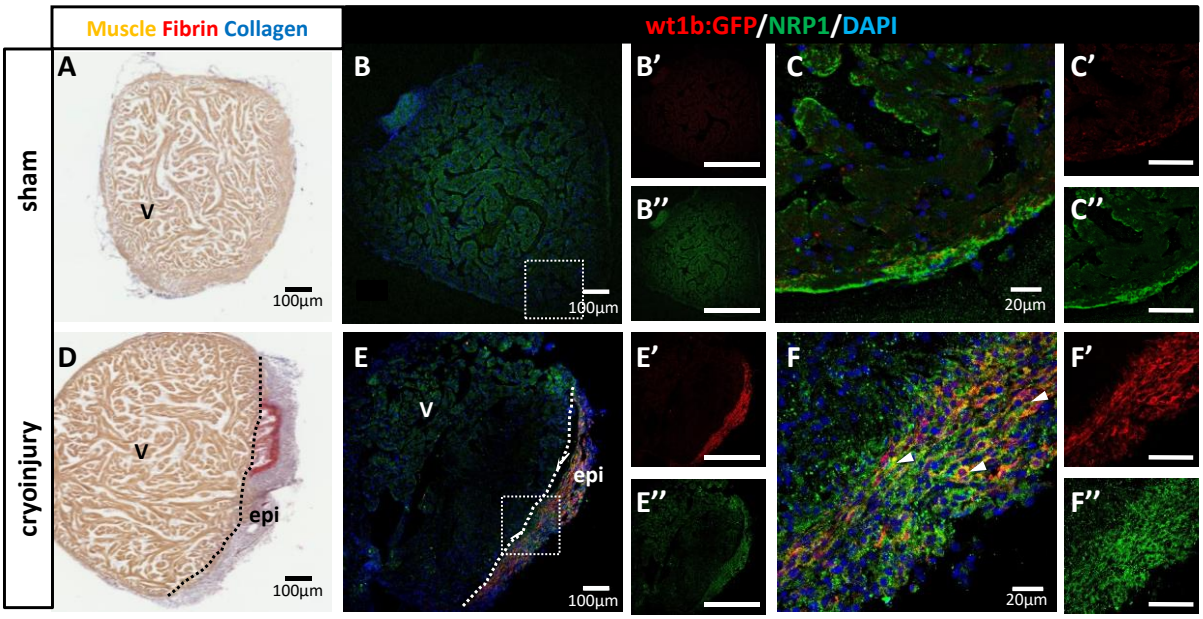

Figure 40 Nrp1 is expressed by epicardial cells

AFOG staining **(A and D)** and Immunofluorescence **(B, C, E and F)** of *Tg(wt1b:GFP)* zebrafish heart sections 7 days post sham surgery (A-C) or 7 days post cryoinjury (D-F). AFOG staining confirms cryoinjury location and gives reference to tissue composition (healthy myocardium - orange, collagen – blue, fibrin – red, basement membrane – pale blue). Injury-activated epicardial cells were detected with anti-GFP antibody (B', C', E' and F') (red). Nrp1 expressing cells are shown in green (B'', C'', E'' and F''). Overlay of the two colours are displayed with DAPI nuclei staining (B, C, E and F). Dotted boxes highlight magnified region. Dotted lines indicate injury border with healthy myocardium. White arrows indicate areas of colocalisation. v – ventricle *ba- bulbus arteriosus* IA – injured area epi= epicardium *n* = 4

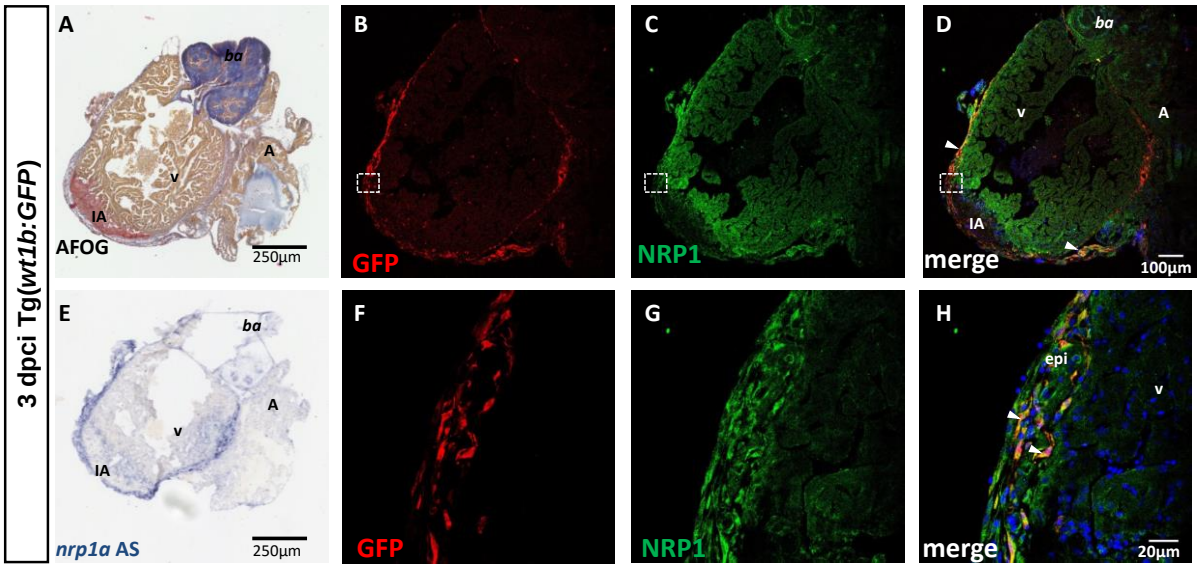

Figure 41 *nrp1a* mRNA localisation is reflected by Nrp1 immunostaining

AFOG staining **(A)**, *nrp1a in situ* hybridisation (ISH) **(E)** and immunofluorescence **(B-D and F-H)** of *Tg(wt1b:GFP)* zebrafish heart 3 days post cryoinjury (dpci). AFOG staining show tissue composition and gives reference to injury location (healthy myocardium - orange, collagen – blue, fibrin – red, basement membrane – pale blue) (A). ISH of *nrp1a* anti-sense riboprobe (*nrp1a* AS) shows localisation of nrp1a mRNA observed as a dark blue stain within the section (E). Activated epicardium that express wt1b are GFP positive and are probed with anti-GFP antibody (red) (B and F) and Nrp1 expressing regions of the heart in green **(C and G)**. Overlay of the two colours are displayed with DAPI nuclei staining (E and E'). White arrows indicate colocalisation. Dotted boxes highlight magnified regions. *v* – ventricle *ba- bulbus arteriosus A* - atrium IA- injured area epi- epicardium AS *n* = 3

4.3.4 Nrp2 expression in the endocardium

The ISH and qPCR data showed that *nrp*2a was upregulated at 1 and 3 dpci and that mRNA expression was initially localised to the injury borders and epicardium before re-distributing to become almost exclusively epicardial at 3 dpci. Whereas *nrp*2b is expressed widely by the myocardium, by cells within the injury, at the injury border and in the epicardium.

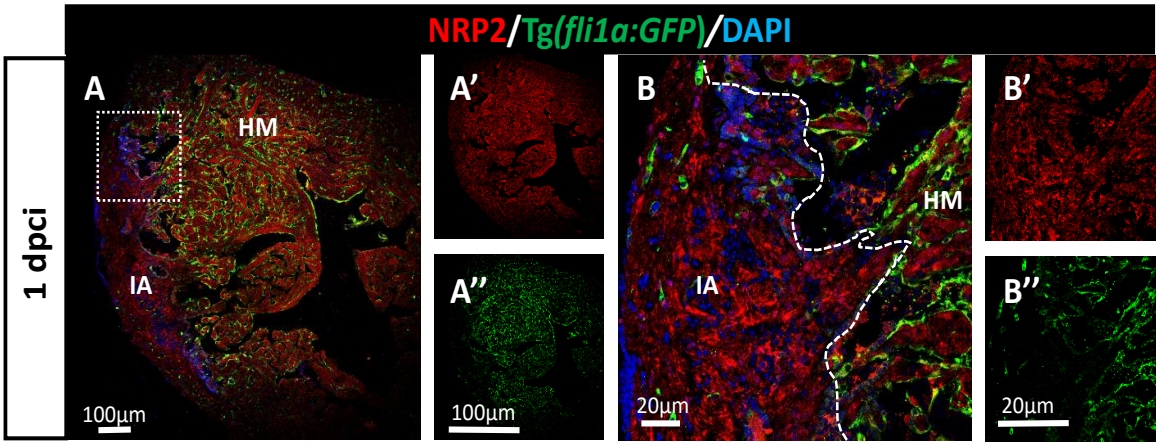

Figure 42 Nrp2 expression is limited in endothelium and endocardium

Immunofluorescence of Tg(*flia:GFP*) adult zebrafish heart 1 day post cryoinjury (dpci). *fli1a* expression by viable endothelium and endocardium are immunolabeled with anti-GFP antibody (green) **(A'' and B'')** and Nrp2 expressing regions of the heart in red **(A' and B')**. Overlay of the two colours are displayed with DAPI nuclei staining **(A and B)**. Dotted box highlights magnified region. Dotted line indicates healthy myocardium and injury border.IA- injured area HM- healthy myocardium *n* = 2

4.3.5 NRP2 antibody cross-reactivity to zebrafish

Nrp2 was difficult to confirm by Western Blot; several NRP2 bands were detected using Western blot analysis, thus making antibody specificity questionable. I next tried to assess Nrp2 expression using immunofluorescence in *Tg(fli1a:GFP)* zebrafish heart sections. Nrp2 and GFP staining were segregated from each other 1 dpci at the injury border (Figure 42B). These data suggest that the ISH staining pattern of *nrp2a* and *nrp2b* observed at 1 dpci at the border between the injured tissue and the healthy myocardium was not due to endocardial expression was instead due to another cell type; alternatively, there may be a lag between *nrp2* mRNA expression and NRP2 protein translation in the endocardium.

4.3.6 Nrp2 in inflammatory cells after cardiac damage

At 1 dpci the zebrafish heart is in the inflammatory phase of the regeneration process, during which innate immune cells infiltrate the injury and clear cellular debris (Chablais and Jazwinska, 2012; Evans *et al*., 2013). Inflammatory cells express NRP2 (Aung *et al*., 2016; Ji *et al*., 2009; Stepanova *et al*., 2007), therefore Nrp2 expression by leucocytes was investigated using immunofluorescence. The leucocyte marker, L-plastin, was used to identify inflammatory cells. Under basal sham-operated conditions, detection of L-plastin is sparse in the zebrafish heart (Figure 43B). At 1 dpci, a cluster of L-plastin positive leucocytes was observed in and around the injured area (Figure 43C' and D'). Co-staining of Nrp2 with L-plastin revealed that, at 1 and 7 dpci, these infiltrating leucocytes were Nrp2 positive (Figure 43D and F).

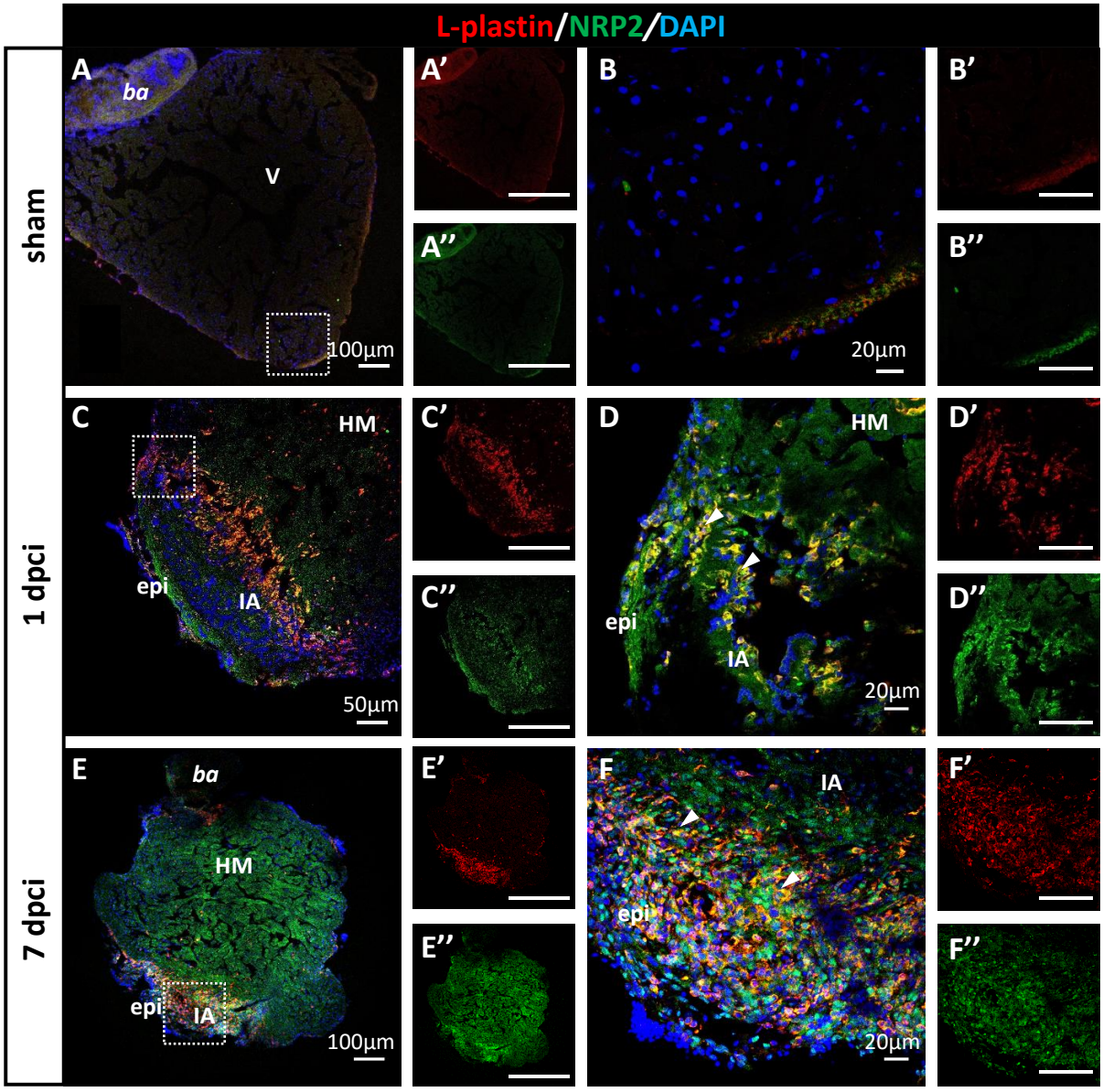

Figure 43 Inflammatory cells express Nrp2

Sham-operated **(A and B)**, 1 dpci (day post cryoinjury) **(C and D)** and 7 dpci **(E and F)** adult zebrafish hearts sections stained with immunofluorescence. Samples were immunolabeled for leukocyte marker L-plastin (red) (A' - F') and Nrp2 (green) (A'' – F''). Overlay of the two colours are displayed with DAPI nuclei staining (A - F). Dotted box highlights magnified region. White arrows indicate colocalisation.v – ventricle, *ba- bulbus arteriosus,* epi – epicardium, IA- injured area HM- healthy myocardium n = 2-3

4.3.7 Nrp2 expression in cardiomyocytes

Nrp2 immunofluorescence staining was observed throughout the entire myocardium. This is aligned with the qPCR data that suggests that *nrp2b* is highly expressed in the zebrafish heart under basal conditions and the ISH data showing *nrp2b* mRNA expression in the entire ventricle. Therefore, I investigated Nrp2 expression by cardiomyocytes. Immunofluorescent staining confirmed expression of Nrp2 by healthy cardiomyocytes in both basal sham conditions and after cryoinjury (Figure 44). Additionally, Nrp2 colocalised with proliferating and migrating cardiomyocytes that infiltrate and replenish the injured area (Figure 44F). Nrp2 immunofluorescent staining also appeared to detect sarcomeric structures in cardiomyocytes (Figure 44F). This suggests a homeostatic role for Nrp2 in healthy cardiomyocytes consistent with previous studies that report Nrp2 being expressed in the developing zebrafish heart (Bovenkamp *et al*., 2004). The bulk of Nrp2 protein expression by cardiomyocytes detected via immunofluorescence is likely due to *nrp2b* expression, given the ISH and qPCR data.

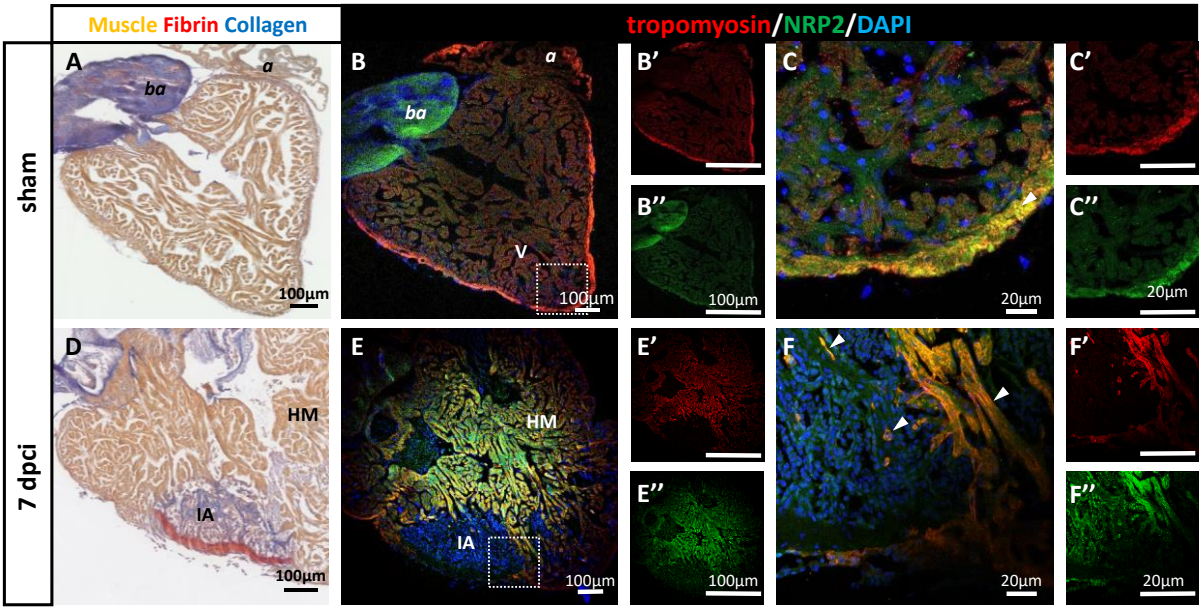

Figure 44 Nrp2 localises with viable cardiomyocytes

AFOG staining **(A and D)** and immunofluorescence **(B, C, E and F)** of wild type zebrafish hearts 7 days post sham surgery (A-C) and 7 dpci (days post cryoinjury) (D-F). AFOG staining shows tissue composition and gives reference to injury location (healthy myocardium - orange, collagen – blue, fibrin – red, basement membrane – pale blue). Immunofluorescence show viable cardiomyocytes immunolabeled in red (B'-F') and Nrp2 expressing regions in green (B''-F''). Overlay of the two colours are displayed with DAPI nuclei staining (B, C, E and F). Dotted box highlights magnified region. White arrows indicate colocalisation. HM – Healthy myocardium, *ba*- bulbus arteriosus, *a*- atrium, IA- injured area, v-ventricle *n* = 2 (sham), 3 (cryoinjured)

4.3.8 Nrp2 expression in endo and epithelial –to mesenchymal transition in the zebrafish heart

ISH indicated a striking *nrp2a* epicardial expression at 3 dpci, whereas *nrp2b* is predominantly present within the injury with some expression in the epicardium. I set out to investigate Nrp2 expression in injury-activated epicardium and endocardium. *Raldh2* is expressed by both the activated epicardium and endocardium following injury and contributes to EMT (Kikuchi *et al*., 2011b). Raldh2 positive cells expressed Nrp2 in both the endocardium and epicardium at 7 dpci, supporting a role for Nrp2 in the endocardial and epicardial EMT (Figure 45), a physiological process previously identified to require NRP2 in another pathophysiological setting (Grandclement *et al*., 2011). These data contrast with expression of Nrp2 in endothelium and endocardium at 1 dpci in *Tg(fli1a:GFP)* hearts, which showed Nrp2 detection was discrete from GFP positive cells (Figure 42). It is possible Nrp2 is expressed in the endocardium and epicardium at time points later than 1dpci when epicardial and endocardial activation is established.

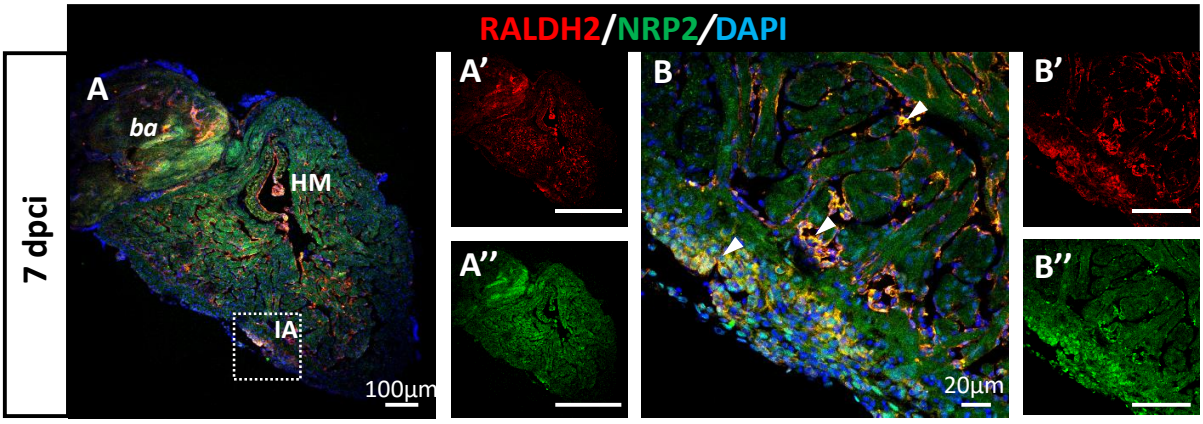

Figure 45 Activated endocardium and epicardium express Nrp2

Immunofluorescence image of adult zebrafish heart 7 days post cryoinjury (dpci). Activated epicardium and endocardium are labelled with Raldh2 **(A' and B')** (red) and NRP2 expressing regions of the heart in green **(A'' and B'')**. Overlay of the two colours are displayed with DAPI nuclei staining **(A and B)**. Dotted box highlights magnified region. *ba- bulbus arteriosus*, IA-injured area, HM- healthy myocardium *n* = 2

4.4 Discussion

4.4.1 Nrp1 regulation

The Human NRP1 cytoplasmic C-terminus sequence shares high amino acid sequence similarity to the zebrafish Nrp1a and Nrp1b C-termini (86% and 72% respectively). Immunoblotting for the Nrp1 C-terminus detected two bands in zebrafish hearts: a lower molecular weight Nrp1a band and higher molecular weight Nrp1b band. Quantified together Nrp1 protein was significantly upregulated in zebrafish ventricle lysates at 14 dpci. Whereas individual band analysis showed no statistical difference in the regulation of Nrp1a, Nrp1b upregulation was statistically significant at 3 dpci. The close proximity of Nrp1a and Nrp1b bands introduced potential for variation in Western blot band quantification due to the difficulty in delineating isolated ohnolog signal. Furthermore, similar to the qPCR studies, the samples measured for protein analysis were derived from the entire ventricle, and thus reflect total heart Nrp1 expression, which may mask smaller localised regions of high expression. Additionally, immunoblotting is a semi-quantitative technique, meaning that a standard curve is needed to interpolate the unknown protein levels in the experimental samples, something I was unable to do. Finally, Western Blotting is not a technique of high sensitivity able to detect subtle changes. A more sensitive and quantitative technique, such as ELISA, could be applied to quantify Nrp1 concentration in the ventricle samples.

Because the Western blot sample consists of whole ventricle protein lysate of the entire ventricle, mainly made up of cardiomyocytes, localised changes of NRPs in the discrete endocardium and epicardium might be concealed. This was clearly evident when localisation of Nrp1 expression was analysed using immunofluorescent (IF) staining. Concordant with qPCR results, Nrp1 protein levels returned to basal expression by 30 dpci.

It is not possible to distinguish which Nrp1 isoform is detected via immunofluorescence. However, ISH expression patterns correlate with the localisation of Nrp1 observed using immunofluorescent staining, and therefore support antibody cross-reactivity to both

Nrp1a and Nrp1b. Immunofluorescence imaging demonstrates that, under basal conditions, Nrp1 localised to the epicardium, endocardium and *fli1a*-expressing endothelium of coronary vessels in the myocardium compact layer. Whereas, Nrp1 expression by cardiomyocytes is low. Taken together, this suggests that Nrp1 has a constitutive role in the homeostasis of the endocardium, epicardium and coronary vasculature in the zebrafish heart, but probably not in cardiomyocytes themselves.

After cardiac damage, activation of the endocardium in close proximity to the injury occurs within 24 hours and is required for zebrafish heart regeneration (Kikuchi *et al*., 2011b). All or most *fli1a* and *kdrl* expressing endocardium also expressed Nrp1 after injury. This was including cells protruding into the cryoinjured region from the border between the injury and the healthy myocardium, implicating a role for Nrp1 in the endocardial response to cardiac damage. Additionally, early *fli1a* positive vessels that help revascularize the injured area from as early as 1 dpci, were also all positive for Nrp1 and continued to express Nrp1 in the neovasculature at 7 dpci, indicating that Nrp1 expression and upregulation is involved in revascularisation of the injured heart. The lack of coronary vessel *kdrl* expression in the zebrafish hearts analysed here (Figure 38D'), is an unexplained observation, as arterial *kdrl* expression has been reported in the zebrafish heart coronary arteries 24 hours after cryoinjury (Marin-Juez *et al.*., 2016) and other tissues (Kumar *et al*., 2016). It is possible that, at 7 dpci, *fli1a* expressing vessels in the injured area are not arterial, but may be capillaries, venous or lymphatic vessels and thus might not express the mature arterial marker *kdrl.*

The epicardium is also known to be essential for regulating the heart regeneration process (Lepilina *et. al.*, 2006). After injury the epicardium becomes activated and proliferates and interestingly, I noted that Nrp1 was expressed in all epicardial cells after cardiac damage. Nrp1 could potentially serve as an epicardial marker in both its quiescent and activated states. A subpopulation of *wt1b*-expressing epicardial cells initiate EMT; they trans-differentiate and gain a migratory phenotype required for mesenchymal cell contribution to the regenerative process (Peralta *et.al.*, 2014). All

wt1b-positive epicardial cells undergoing EMT also expressed Nrp1, suggesting Nrp1 is required for the trans-differentiation and/or the migration of these cells.

Cardiomyocytes expressed low levels of Nrp1 after cardiac damage and some sub-epicardial cardiomyocytes migrating into the injured region expressed Nrp1. Pre-existing cardiomyocytes provide the majority of new cardiomyocytes in the regenerating zebrafish heart (Jopling *et al*., 2010), with a subpopulation proposed to be derived from epicardial cells and cardiac stem cells (Ellison *et al*., 2013; van Wijk *et al*., 2012). However, the accuracy of these lineage tracing studies have been questioned by other groups that identified different fates for epicardial cells and limited cardiac progenitor populations (Jopling *et al*., 2010; Manuel Gonzalez-Rosa *et al*., 2012). Cardiomyocytes in close proximity to the injury are stimulated to dedifferentiate, proliferate and invade damaged cardiac tissue to replenish the cardiomyocyte population (Itou *et al*., 2012b; Jopling *et al*., 2010). Proliferating and migrating cardiomyocytes localise to the sub-epicardial area at the injury (Kikuchi *et al*., 2010), that results initially in the formation of a new compact myocardium, and they then invade the underlying scar tissue to regenerate the trabeculated myocardium (Manuel Gonzalez-Rosa *et al*., 2011). Nrp1 expression in protruding cardiomyocytes from the sub-epicardial compact layer could indicate a role for Nrp1 in migrating cardiomyocytes that repopulate the damaged area or the subpopulation of epicardial cells implicated in contributing to new cardiomyocytes.

Though basal Nrp1 expression by cardiomyocytes was low in comparison to the more prominent Nrp1 expression by the endocardium and epicardium, increased Nrp1 staining in injured hearts suggests its potential role for the migration of cardiomyocytes from the sub-epicardial layer into the injured area following cardiac damage. These data also support my Western blot and qPCR observations that show trends for NRP upregulation but do not reach significance.

Thus, in the injured heart, Nrp1 likely plays a role in several cell types critical for the regenerative process. A common characteristic shared by the endocardium, epicardium, sub-epicardial cardiomyocytes and vessels during regeneration is that they are all

required to gain a migratory phenotype to elicit their regenerative function. Nrp1 has previously been implicated in cell migration in various cell types (Banerjee *et al*., 2006; Evans *et al*., 2011; Frankel *et al*., 2008; Pellet-Many *et al*., 2011; Seerapu *et al*., 2013; Soker *et al*., 1998) and therefore could also play a role in response to migratory cues in the regenerating zebrafish heart.

Unfortunately, due to antibody incompatibility, Nrp1 colocalisation with the marker of active endocardium, Raldh2, was not possible; nevertheless, the data presented in this chapter strongly indicates Nrp1 as playing a role in these cells (Figure 37 and Figure 38). Nrp1 is clustered at the border between the healthy myocardium and the injury, a region that contains both activated endocardial cells and inflammatory cells. Previous studies support a role for Nrp1 in the immune response (Aung *et al*., 2016; Ji *et al*., 2009; Tordjman *et al*., 2002). However, I was unable to assess the expression of Nrp1 by leukocytes because the L-plastin and Nrp1 antibodies were both raised in rabbits, therefore it is possible that Nrp1 may also be expressed by infiltrating inflammatory cells.

4.4.2 Nrp2 regulation

Zebrafish Nrp2a and Nrp2b C-termini protein sequences are homologous and share 82.9% sequence similarity with Human NRP2 implicating important evolutionary conservation of the NRP2 cytoplasmic domain. Unfortunately, antibodies used for NRP2 Western blot analysis of ventricle lysates failed to demonstrate specific cross-reactivity to zebrafish NRP2 orthologues and was not quantifiable. However, a signal was detected using immunofluorescent staining and Nrp2 localisation was therefore evaluated in zebrafish heart sections using this approach.

Under sham-operated conditions, Nrp2 expression was evident within the myocardium, with low basal expression by the endocardium and epicardium. Following cardiac damage, I noted Nrp2 being expressed by infiltrating leukocytes, suggesting its role for the initial inflammatory response after cardiac damage. The majority of leucocytes in the inflammatory response are innate immune cells such as macrophages and

monocytes derived from circulating blood (Chablais and Jazwinska, 2012; Evans *et al*., 2013), and my results suggest these cells either constitutively express Nrp2, or upregulate Nrp2 after recruitment to the damaged area. Evidence from other models and tissues suggests that Nrp2 is constitutively expressed by inflammatory cells (Aung *et al*., 2016; Ji *et al*., 2009; Stepanova *et al*., 2007). The ISH staining that identified *nrp2a* and *nrp2b* mRNA within and proximal to the injury at 1 dpci may therefore be due to infiltrating leucocytes. Thus Nrp2 upregulation and mRNA re-distribution to the injury area indicates a role for Nrp2 in inflammation following cardiac injury.

Injury-activated epicardium and endocardium, identified by Raldh2 expression, also expressed Nrp2. Additionally, NRP2 was constitutively expressed by viable cardiomyocytes in normal conditions and following cardiac damage, including in migrating cardiomyocytes that infiltrate the injured area. Thus, Nrp2 likely plays a homeostatic role in zebrafish cardiomyocytes but also has an injury-induced role in inflammation and endocardial and epicardial EMT.

It is uncertain whether immunofluorescent staining exclusively detected zebrafish Nrp2 in my studies, or may also reflect non-specific protein binding. However, Nrp2 immunofluorescent staining was located to similar regions of the heart that were highlighted using ISH patterns supporting the conclusion that immunofluorescent staining reflected genuine Nrp2 detection. For example, small round Nrp2 positive cells within the injury express the leucocyte marker L-plastin and are also present within the injury-activated epicardium, which reflects observations of *nrp2* gene localisation in ISH (Figure 32). *Nrp2* mRNA expression was observed within the myocardium using ISH, which is further supported by Nrp2 immunofluorescent staining which appeared to detect sarcomeric structures in cardiomyocytes (Figure 44F). Therefore, Nrp2 antibody likely cross-reacts with zebrafish Nrp2 in immunofluorescent staining, but not using immunoblotting, perhaps due to antibody epitope recognition of zebrafish Nrp2 in the more native rather than the reduced unfolded state.

4.4.3 Summary

In this chapter I have established the following:

- Zebrafish NRPs are upregulated in response to cardiac damage, and may therefore play positive roles in the zebrafish regenerative response.
- Nrp1 and Nrp2 display differential expression patterns in basal conditions and in regenerating zebrafish hearts
- These data suggest that the isoforms carry out specific roles and have differing physiological responses in homeostasis *versus* regeneration.
- Expression patterns reflected ISH mRNA detection confirming ISH data to accurately predict Nrp protein regulation in the zebrafish heart.

5 Results Chapter 3: Heart Regeneration in *nrp1a* mutant zebrafish

Thus far, my data has demonstrated that all neuropilin orthologs are acutely upregulated in response to cardiac damage at both the mRNA and protein levels suggestive that they play a positive role in zebrafish heart regeneration. Neuropilins localise in close proximity to the damaged tissue or within the injury during the inflammatory and reparative phases of the regeneration process, with marked expression in the endocardium and epicardium. To investigate Nrp1 function in zebrafish heart regeneration, I studied a *nrp1a* mutant fish expressing a truncated and thus non-functional Nrp1a. This chapter focuses on the characterisation and regenerative capacity of this *nrp1a* mutant fish.

5.1 *nrp1a* mutant fish identification

The Sanger Wellcome Trust zebrafish mutagenesis project (ZMP) has generated several fish lines with point mutations in the sequence of protein encoding genes. The N-ethyl-N-nitrosourea (ENU) mutagen has been used to treat male zebrafish to create random mutations in the genome during spermatogenesis. Male zebrafish were then bred with wild type females and offspring screened for genetic mutations and a founder fish that transmit the mutation through the germline was identified (See section 1.3.1.2).

I obtained the *nrp1a*^{sa1485} mutant zebrafish line from the ENU ZMP. This mutant fish encodes a nonsense point mutation (where a Cytosine replaces an Adenine base) resulting in the generation of an early stop codon at amino acid 206 out of 923 amino acids of the Nrp1a sequence (Figure 46A). This mutation yields a truncated Nrp1a protein lacking the cytoplasmic C-terminus, transmembrane domain, MAM domain, b1, b2 and half of the a2 ligand interacting domains, resulting in a non-functional and soluble Nrp1a fragment (Figure 48A). At the time when I acquired the *nrp1a*$^{sa1485/sa1485}$ mutant fish, no other fish neuropilin mutant lines were available. Initially, genomic DNA

extracted from adult fish fin clips was used to identify heterozygous *nrp1a*$^{sa1485/+}$ mutant fish *via* sequencing. Heterozygous fish were then incrossed, and a random selection of 48 hpf embryos were genotyped from the offspring (Figure 46A). The offspring genotypes followed a Mendelian ratio distribution of the three genetic outcomes indicating that homozygous inheritance of the *nrp1a* mutation is not embryonic lethal by 48 hpf (Figure 46B). Because of the occurrence of evolutionary genome duplication, four neuropilin isoforms are encoded by the zebrafish genome (Postlethwait *et al*., 1998); thus redundancy due to the presence of the *nrp1b* ohnolog may compensate for the loss of full-length Nrp1a function during development.

Embryos were raised to adulthood and homozygous mutants were identified *via* sequencing. This further confirmed that the homozygous inheritance of the mutation and loss of Nrp1a function is not embryonic lethal. The homozygous mutants were incrossed to establish a homozygous *nrp1a*$^{sa1485/sa1485}$ line. A 42% survival rate of the offspring was noted, which is significantly lower than the ~90% survival rate observed for established wild type lines. This suggests possible underlying complications during development that were not detected by my initial observational and qualitative analysis.

5.2 *nrp1a* mutant line characterisation

Nrp1a gene expression was assessed by RT-qPCR in adult *nrp1a*$^{sa1485/sa1485}$ zebrafish heart lysates (Figure 47A) and expression patterns were evaluated in *nrp1a*$^{sa1485/sa1485}$ 24 hpf embryos using ISH (Figure 47B). Both showed a marked reduction of *nrp1a* mRNA expression (Figure 47), suggesting that the nonsense mutation results in downregulation of *nrp1a* mRNA expression. This may be due to an adaptive response to loss of Nrp1a function. According to previous reports, *nrp1a* is expressed during embryogenesis and in wild type adult hearts (Yu *et al*., 2004). However, *nrp1a*$^{sa1485/sa1485}$ mutant embryos displayed no obvious morphological abnormalities in the absence of full-length Nrp1a. These results strongly suggest that genetic redundancy occurs: the presence of the *nrp1b* ohnolog might compensate for the reduced Nrp1a activity required for heart development. These data also confirm that the point mutation has a sustained and

marked effect on *nrp1a* gene expression from early development continued throughout adulthood.

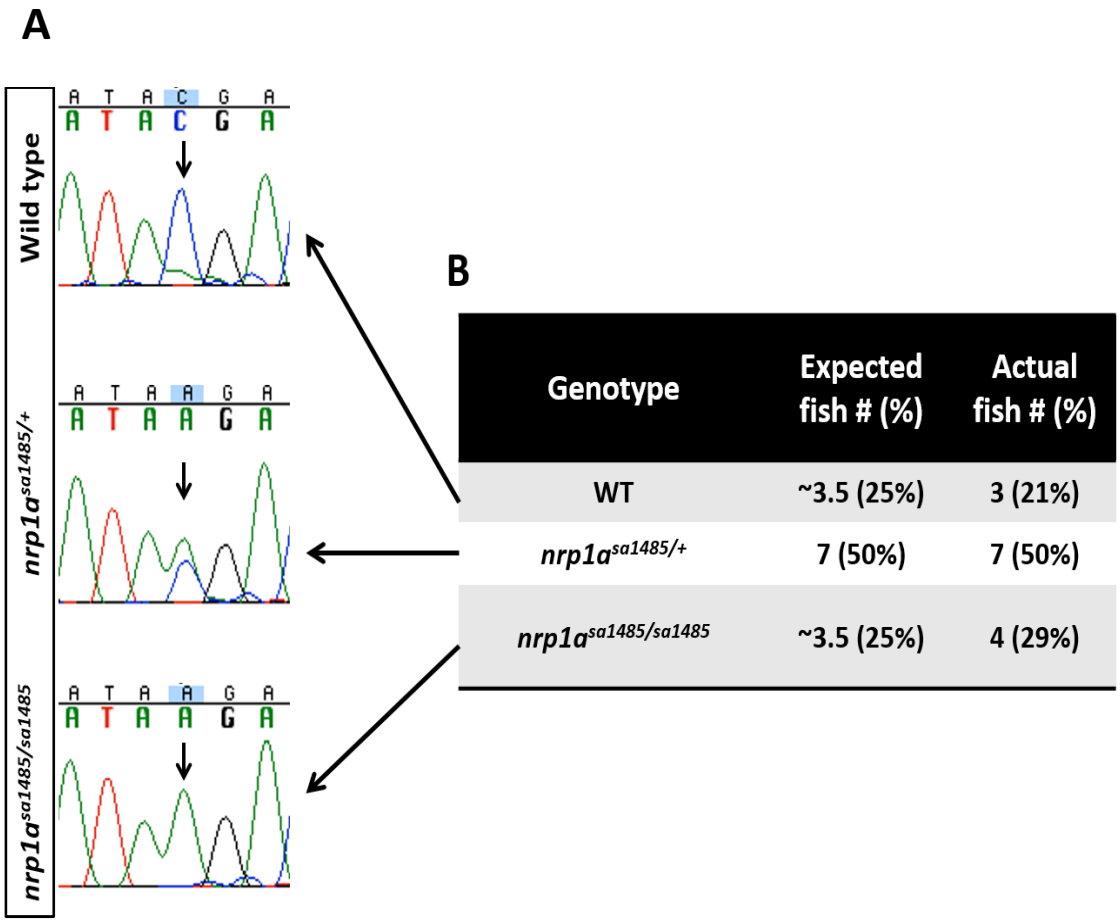

Genotype	Expected fish # (%)	Actual fish # (%)
WT	~3.5 (25%)	3 (21%)
nrp1a$^{sa1485/+}$	7 (50%)	7 (50%)
nrp1a$^{sa1485/sa1485}$	~3.5 (25%)	4 (29%)

Figure 46 *nrp1a* mutant sequencing

(A) Sequencing chromatograms of wild type, heterozygous (*nrp1a*$^{sa1485/+}$) and homozygous (*nrp1a*$^{sa1485/sa1485}$) mutant embryos 48 hpf. An Adenine replaces a Cytosine base causing the generation of the early stop codon (nonsense mutation) TAA, rather than the Tyrosine (TAC) codon at amino acid 206. **(B)** The table displays the genotypes of 14 zebrafish embryos 48 hpf alongside the expected mendelian ratio occurrence after heterozygous fish incross. Wild type and homozygous mutants are expected to account for 25% of the genotypes each (~3.5 out of 14), whereas heterozygous mutants should account for 50%. The outcome of genotyping is described in the third (actual fish number) column.

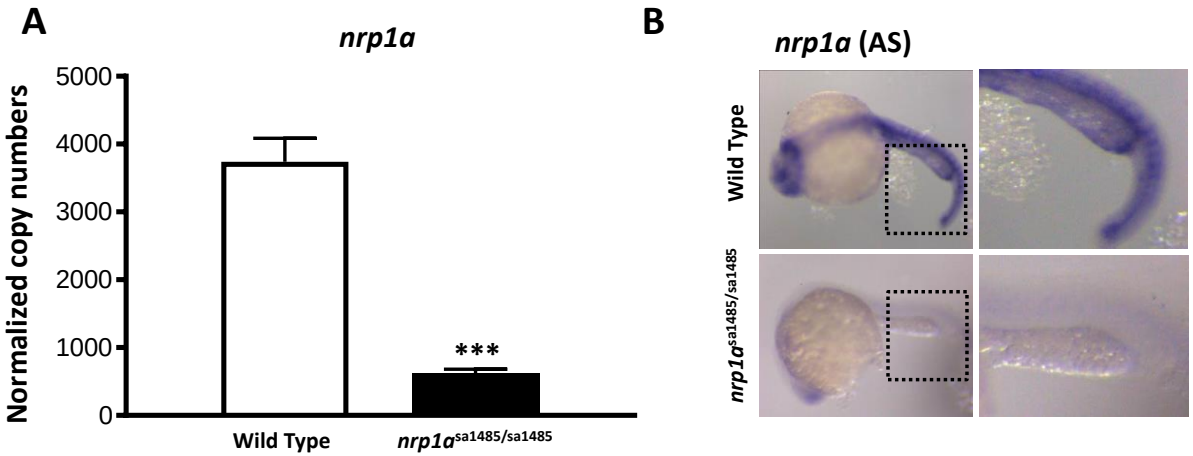

Figure 47 *nrp1a* mRNA expression in homozygous *nrp1a*$^{sa1485/sa1485}$ mutants

(A) Absolute RT-qPCR of wild type (white bar) and *nrp1a*$^{sa14854/sa1485}$ homozygous mutant (black bar) adult zebrafish hearts under basal conditions. Data are represented as means of normalised copy numbers per reaction ± S.E.M (error bars) ***p<0.005 *n* = 4 with each *n* being a pool of 3 ventricles. **(B)** *nrp1a* anti-sense (AS) *in situ* hybridisation of wild type (upper row) and *nrp1a*$^{sa14854/sa1485}$ homozygous mutant (bottom row) 24 hpf embryos carried out simultaneously. Black dotted boxes indicate magnified region enlarged to the right.

5.3 Nrp1a expression in the *nrp1a*$^{sa1485/sa1485}$ mutant line

Protein expression levels of adult ventricle lysates obtained from wild type and homozygous *nrp1a*$^{sa1485/sa1485}$ zebrafish hearts were evaluated using Western blot. An antibody targeting the human NRP1 C-terminus was used to detect Nrp1 ohnologs and verify the loss of full-length protein expression as a result of the mutation.

Zebrafish Nrp1 is detected as a doublet on immunoblots, with a lower Nrp1a molecular weight band at ~120kDa, and a higher Nrp1b molecular weight band at ~140 kDa (Figure 48A). The lower Nrp1a band is clearly not expressed by the *nrp1a*$^{sa1485/sa1485}$ mutants, confirming loss of the full-length Nrp1a protein expression.

The Nrp1b protein was expressed by the *nrp1a*$^{sa1485/sa1485}$ adult hearts (Figure 48B) and though its expression appeared to be reduced compared to WT fish, this reduction was not statistically significant (Figure 48C). These data indicated that Nrp1b expression in the adult *nrp1a*$^{sa1485/sa1485}$ fish is not markedly affected by the mutation and that there is no compensatory upregulation of one Nrp1 ohnolog in response to the loss of the other.

It is possible that alternative pathways mediate cellular mechanisms to compensate for loss Nrp1a loss in the adult zebrafish heart, or that the role of Nrp1a is redundant under basal conditions.

5.4 *nrp1a*$^{sa1485/sa1485}$ anatomical characterisation

The superficial anatomical measurements of wild type zebrafish were compared to those of age-matched *nrp1a*$^{sa1485/sa1485}$ mutants to identify any phenotypes that might arise from the mutation. *Nrp1a*$^{sa1485/sa1485}$ mutant fish were phenotypically indistinguishable from wild type fish (Figure 49A), they displayed normal behaviour and were fertile. There was no significant difference in fish body length (base of caudal fin to tip of mouth) (Figure 49B). Neither was there a difference in heart size when the area of whole ventricles collected were measured (Figure 49C) or the heart to body length ratio (Figure 49D). There was a trend for mutant fish to be smaller than wild type

controls but sample size was small and there were a few outliers in both groups. Thus, the loss of full length Nrp1a does not affect zebrafish growth or development. More detailed studies investigating the fish anatomical features and physiological functions that require full-length Nrp1a, such as the vessel development during embryogenesis and neuronal development, should be performed.

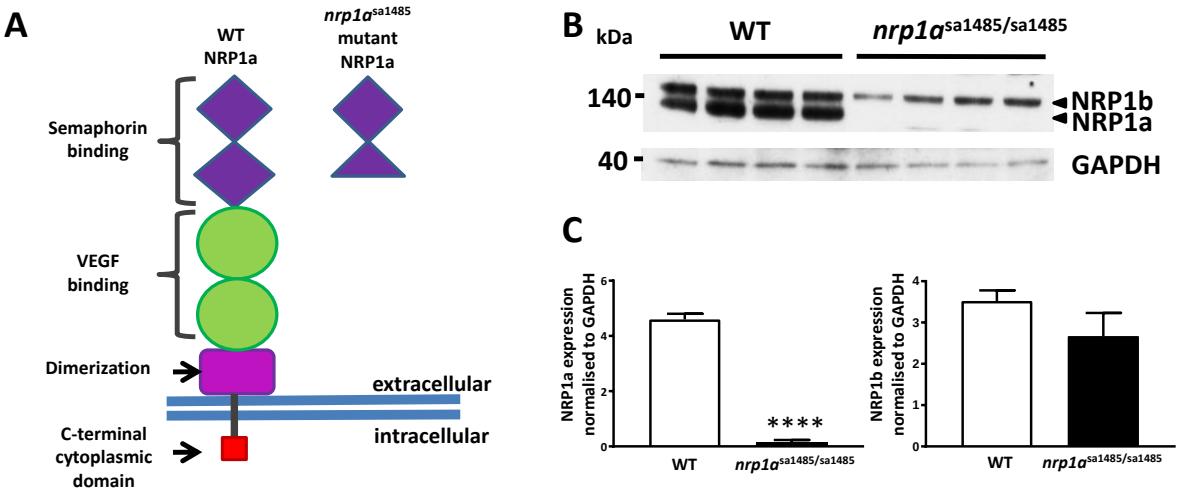

Figure 48 Nrp1a protein analysis of the *nrp1a* homozygous mutant

(A) Schematic representation of wild type (WT) (left) and *nrp1a*$^{sa14854/sa1485}$ (right) Nrp1a structure. The point mutation results in the insertion of a premature stop codon at amino acid 206, which generates a truncated Nrp1a fragment. The Nrp1a mutant encodes the a1 and part of the a2 extracellular semaphorin binding domain. **(B)** Western Blot of WT or *nrp1a*$^{sa14854/sa1485}$ homozygous mutant adult zebrafish ventricle lysates under basal conditions. Lysates were immunoblotted for the Nrp1 cytoplasmic domain and Gapdh. Note the absence of C-terminus detection in the *nrp1a*$^{sa14854/sa1485}$ samples **(C)** WT (white bars) and *nrp1a*$^{sa14854/sa1485}$ (black bars) adult zebrafish ventricle Western Blot quantification normalised to GAPDH, of Nrp1a band (left graph) and Nrp1b band (right graph). Data are represented as band density means ± S.E.M ****p<0.0001 n = 4 with each n being a pool of 3 ventricles.

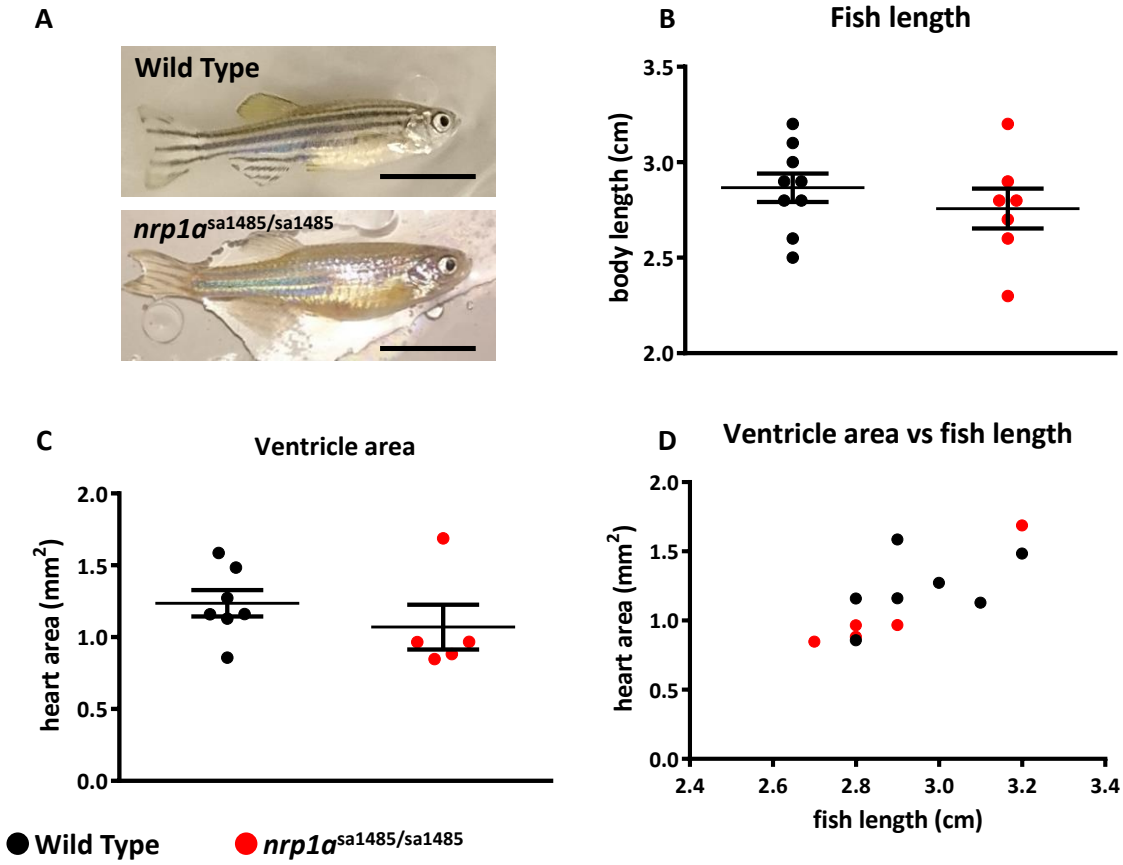

Figure 49 Wild type and mutant fish measurements

(A) Representative picture of WT (upper panel) and *nrp1a*$^{sa1485/sa1485}$ mutant zebrafish (lower panel) scale bar 1 cm. The body length, **(B)** and heart size **(C)** of age matched wild type (black dots) and *nrp1a* mutant (red dots) zebrafish were measured and comparison of body length to heart size made **(D)**. Scatter graph values are displayed as means ±S.E.M and individual measurements of fish indicated as black (wild type) or red dots (*nrp1a*$^{sa1485/sa1485}$ mutants).

5.5 Regenerative capacity in *nrp1a*$^{sa1485/sa1485}$

Under basal conditions the *nrp1a* mutants appeared normal and comparable to WT controls (Figure 50A and H). To evaluate the mutant response to cardiac damage, cryoinjuries were performed and the extent of the injury and viable cardiac tissue quantified using AFOG staining (Figure 50A-N). At 1 dpci both wild type and mutants sustained a similar proportion of damage to the heart (25.2 ± 5.5% and 22.6 ± 5.2%, respectively) (Figure 50O). The mutant heart demonstrated progressive reduction of injury size over time, confirming that they retain some regenerative capacity in the absence of full length Nrp1a (Figure 50O, black bars). However, my data revealed a clear reduction in the extent of decrease of the injured area in mutant as compared to WT hearts (Figure 50K-N). Statistical analysis of these data by two-way anova revealed a significant delay in regeneration of mutant hearts in comparison to wild type hearts (p = 0.038). Specific time-point comparison of injury size showed a significantly larger injury remaining at 14 and 30 dpci in mutant hearts compared to wild type hearts (Figure 50E,F, L and M), indicating Nrp1a is required for efficient cardiac repair (Figure 50O). Additionally, the mutants displayed abnormal epicardial morphology throughout regeneration. Wild type epicardium proliferates and encases the entire injured region. In the mutant fish, the epicardial response was abnormal: the epicardium appeared to proliferate, evident as a a thickened layer of cell on the surface of the heart, but did not consistently surround the injured region (Figure 50J and L). Rather, the epicardium clustered at the periphery of the injury, however further experiments would be required to confirm whether clusters of cells on the heart surface are of epicardial origin or blood cells. Moreover, the scar resolution process in the mutants also differed from that in wild type fish. The fibrin cap is the first fibrotic tissue cleared from the scar, but fibrin deposits (observed as red staining in injury area denoted by black dotted line) were still evident at 30 and 60 dpci in mutant fish though not in wild type (Figure 50F, G, M and N).

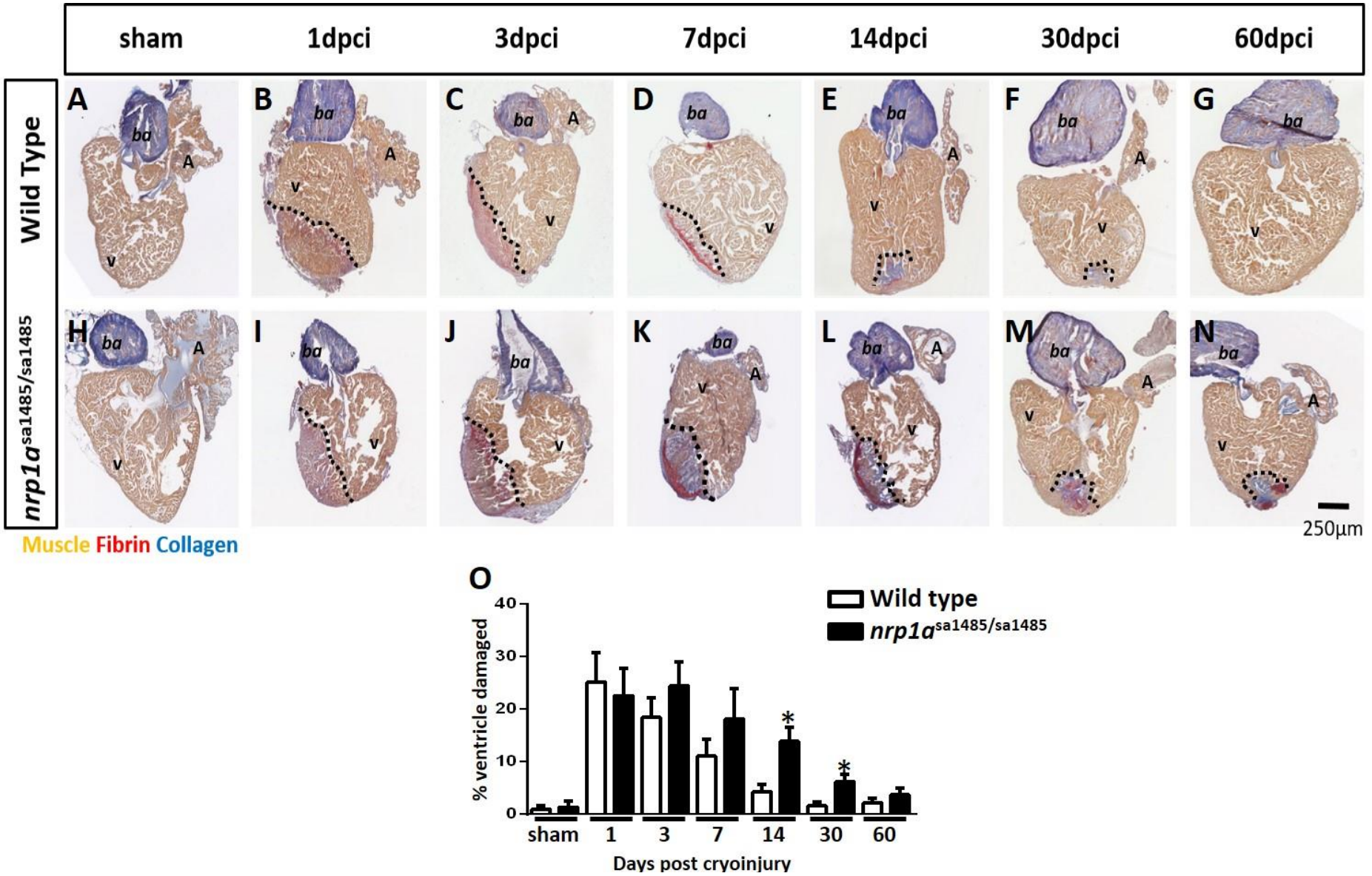

Figure 50 Recovery from cryoinjury is delayed in the *nrp1a* mutant

Wild type **(A-G)** and *nrp1a*$^{sa1485/sa1485}$ mutant **(H-N)** fish were cryoinjured and injury size (denoted by black dotted line) determined with AFOG staining. Black arrows indicate adipose deposits. White arrows indicate epicardial clusters **(O)** Total ventricle injury area was quantified and % ventricle damage presented as mean percentage (± S.E.M) *n* = 4-6 **p*<0.05. *V*- ventricle, *A*-atrium, *ba- bulbus arteriosus*

Additionally, I also observed differences in regeneration of the compact layer and wound closure. The compact myocardium regenerates simultaneously to the removal of the fibrin cap (Gonzalez-Rosa and Mercader, 2012; Kikuchi *et al*., 2010). When a continuous layer of cardiomyocytes encloses the residual collagen scar, the wound is regarded as closed, whereas incomplete compact myocardial coverage is described as an open wound (see Figure 51A). In the advanced stages of regeneration (30 and 60 dpci), a larger proportion of mutant hearts remained as an open wound compared with wild type hearts at 30 and 60 dpci (Figure 51B). This indicates a failure of the compact myocardium to migrate and/or proliferate efficiently towards the subepicardial layer in order to close the wound in *nrp1a* mutant fish.

Mutant sham-operated hearts also displayed abnormal fat deposits rarely observed in wild type fish (Figure 50A and H, black arrows). Adipose tissue composition and morphology were not quantified, however.

These data indicated that after cryoinjury, loss of full-length Nrp1a impairs the regenerative response, and results in abnormal epicardial morphology and scar composition in comparison to WT fish hearts. This points to a key role of Nrp1a in epicardial response and scar resorption during the regenerative process.

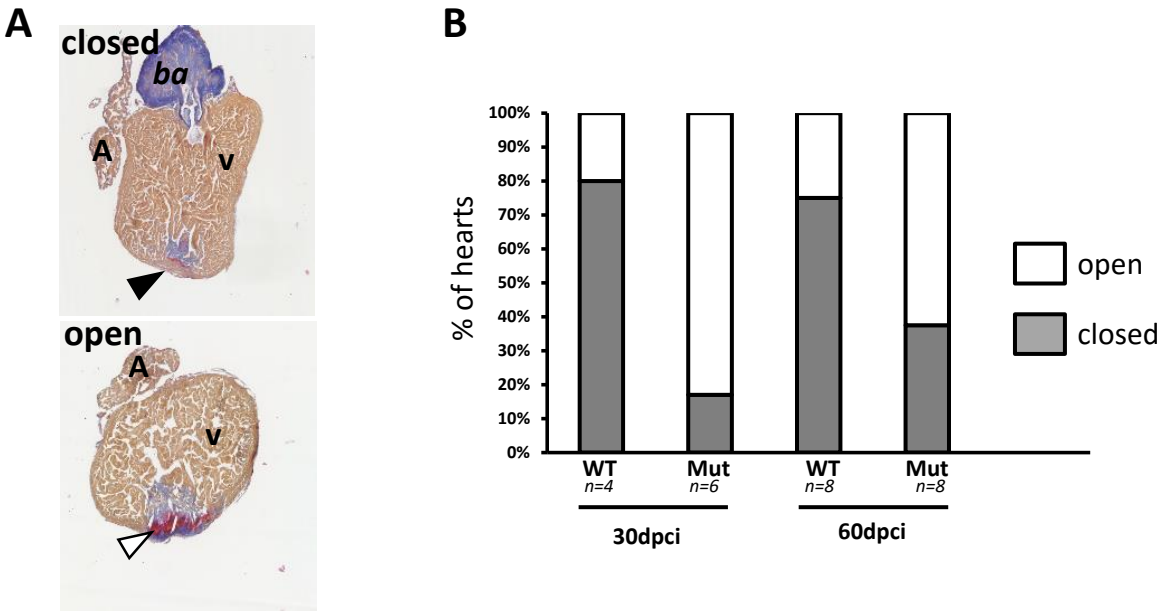

Figure 51 Wound closure in *nrp1a* mutant

A) Example of a closed (upper image) and open (bottom image) adult cryoinjured zebrafish heart. The compact layer of the myocardium regenerates initially and encloses the fibrotic scar tissue (black arrow); open wounds do not display a continuous myocardial compact layer and the wound remains at the surface of the ventricle (white arrow). **(B)** Open (white) and closed (grey) wounds were quantified in wild type (WT) and *nrp1a* mutant (Mut) hearts at 30 and 60 dpci. Values are displayed as percentage of samples in either category. A – atrium, V-ventricle, *ba – bulbus arteriosus*

5.1 Discussion

In this chapter I set out to identify and characterise a *nrp1a* mutant zebrafish line reported to express a nonsense mutation resulting in truncated Nrp1a molecule. The mutation generates a soluble Nrp1a fragment that cannot interact with intracellular scaffolding proteins or receptors, nor bind any known ligands. After identification of homozygous mutants *via* sequencing, I analysed *nrp1a* mRNA and Nrp1a protein expression in the zebrafish and evaluated regenerative capacity.

5.1.1 *Nrp1a* mutants are viable

Mutant fish are viable, present no gross phenotype under basal conditions and the genotype is detected at expected mendelian ratio from a heterozygous cross. However, there may be undetected underlying problems encountered during development as the nursery survival rate is approximately half to that of wild type fish. It is well established that *nrp1a* is expressed in several other organs during zebrafish development, especially in the nervous system (Bovenkamp *et al*., 2004; Martyn and Schulte-Merker, 2004; Yu *et al*., 2004). The phenotype of *nrp1a*$^{sa1485/sa1485}$ fish described here is not in line with previous studies that investigated the effects of *nrp1a* knock down using morpholinos, and showed abnormal vessel growth and high embryonic lethality (Bovenkamp *et al*., 2004; Dell *et al*., 2013), features not recapitulated in the ENU *nrp1a*$^{sa1485/sa1485}$ mutants. Conflicting observations between morpholino gene silencing and germline-acquired mutations are common, and the morpholino approach is likely to have deleterious off-target effects (Kok *et al*., 2015; Schulte-Merker and Stainier, 2014). Additionally, morpholinos could have off target and toxic effects that also affect development (Rossi *et al*., 2015). A zebrafish embryo encompasses 500 ng of total RNA, 2-5% of which is mRNA (25 ng). Assuming that at any given time there are more than 100 different and equally represented mRNA transcripts present in a cell (Dawid, 1987), only 2.5 pg of a specific mRNA species is available for targeting. MO injections typically deliver a minimum of 1 ng anti-sense oligonucleotide (Nasevicius and Ekker, 2000). Assuming further that the target mRNA has an average length of 1.25 kb, whereas the MO is a 25-mer, this equates to a 20,000-fold molar excess of MO versus target mRNA. It is

therefore most likely that this vast excess of MO will bind other RNA or other macromolecules resulting in false positive phenotypes. Conversely, a recent study examined intersegmental vessel (ISV) sprouting in a *nrp1a* mutant embryo generated *via* TALEN mutagenesis. The mutation also results in a truncated soluble Nrp1a fragment and showed no adverse defects in ISV growth (Kok *et al*., 2015), in agreement with my observations that show no deleterious or obvious morphological abnormalities caused by *nrp1a* gene disruption in the *nrp1a*$^{sa1485/sa1485}$ fish under basal conditions.

The *nrp1a*$^{sa1485/sa1485}$ mutants expressed a truncated and soluble Nrp1a, which could potentially retain some physiological activity by associating with some unknown molecules, which may in part explain the viability of these mutants. Soluble Nrp1a is endogenously expressed in the zebrafish (Bovenkamp *et al*., 2004), however the physiological function of this splice variant has not been investigated. Nevertheless, my data shows that full length Nrp1a is not essential for normal zebrafish development, implicating possible redundancy due to genome duplication and the existence of the *nrp1b* ohnolog or other compensatory adaptions and mechanisms. Further work is required to investigate this, including examination of the phenotype and response to cardiac injury of *nrp1b* mutant fish, and evaluation of expression and function of other pathways that could potentially compensate for loss of Nrp1a, such as components of Vegf angiogenic signalling pathways. Alternatively, Nrp1a signalling and activity may not have a role in embryonic development and in homeostasis in the adult zebrafish heart, and these roles may be performed by Nrp1b. Analysis of *nrp1b* mutant fish would reveal such a role. Nrp1b is the ohnolog of Nrp1a and theoretically could compensate for Nrp1a activity loss, however it has been suggested that the two genes have undergone extensive genetic drift to the extent that they demonstrate different embryonic expression profiles and post-translational modifications, which gives them distinguishably different molecular weights (Bovenkamp *et al*., 2004)(Figure 48A). They present differential localisation in the developing zebrafish embryo and during cardiac regeneration, implicating distinct roles for the two isoforms. Nrp1b protein expression is unaffected by the loss of function of Nrp1a in adult ventricle lysates, indicating that

Nrp1b is not upregulated to compensate for the limited Nrp1a activity, but any compensatory ability of this ohnolog cannot be precluded.

5.1.2 Nrp1a expression downregulated in homozygous mutants

It is clear that from an early developmental stage (24 hpf) the mutant fish actively downregulates *nrp1a* expression. This might be due to a negative feedback, perhaps from the truncated mutant protein, or exerted during protein translation, that results in constitutive downregulation of *nrp1a* gene expression; the mechanisms behind this remain unclear.

Despite the gene and protein regulation of *neuropilin1a* being reduced in mutants, wild type and mutant adult fish are very similar suggesting that, under physiological conditions mutants that survive to adulthood are healthy. The adult fish showed a trend to be smaller than wild type fish, but were indistinguishable from wild type fish in other measurements and observations; thus the *nrp1a* mutation does not seem to trigger a detrimental adult phenotype. My examinations were mainly focused on cardiac and body size. Therefore, because the mutation is a global knockout, and *nrp1a* is expressed by many tissues, I cannot rule out the existence of a phenotype resulting from loss of function Nrp1a (for example within the nervous system) that I did not investigate.

5.1.3 *Nrp1a* mutants have reduced survival and delayed regenerative response

Mutant *nrp1a* hearts show a delayed regenerative response after cryoinjury, supporting the conclusion that full-length Nrp1a is required for normal heart regeneration. Since regeneration did occur in the *nrp1a* mutants, this isoform is not essential for the regenerative process. However, the *nrp1a* mutants also exhibited delayed recovery of the compact myocardium illustrated by an impaired ability of the compact myocardium to migrate and/or proliferate efficiently towards the subepicardial layer in order to close the wound. Furthermore, *nrp1a* mutants displayed abnormal scar resolution indicated by the persistence of fibrin deposits at later stages of the regenerative process (30 and 60 dpci). Abnormal protrusions of proliferating epicardium were occasionally observed in the regenerating mutant hearts that may indicate a further consequence of functional

Nrp1a loss in the regenerating heart (Figure 50J and L). These findings, together, indicate a key role for *nrp1a* in zebrafish heart regeneration.

The mutant zebrafish heart did finally regenerate overall, though this may be due to compensation by *nrp1b*, which was expressed in the mutant hearts. It is possible therefore, that Nrp1 may play a more vital role in heart regeneration, obscured by loss of only a single ohnolog. This could be examined in double nrp1a/nrp1b mutants, though these would be predicted to be embryonic lethal. However, this could be circumvented using an inducible (e.g. by tetracycline, or tamoxifen) knock-out.

I also observed that mutant sham-operated hearts displayed abnormal fat deposits rarely observed in wild type fish (Figure 50A and H), though these were not quantified. Cardiac adipose tissue characterisation is limited in the literature, being briefly described in one publication (Hu *et al*., 2001). NRP1 is proposed to play a role in white adipose tissue nerve growth in conjunction with sema3A (Giordano *et al*., 2003) and macrophage recruitment through sema3E secretion(Shimizu *et al*., 2013), therefore neuropilin may regulate white adipose tissue of the heart. These observations regarding adipose morphology may shed light on possible phenotypes caused by lack of full-length Nrp1a in the zebrafish heart under resting conditions, but require further investigation.

5.5.1 Summary

In this chapter I have demonstrated:

- *nrp1a*$^{sa1485/sa1485}$ homozygous mutant zebrafish are viable and appear normal under physiological conditions.
- Heart regeneration was severely delayed in mutant following cryoinjury.
- Mutant hearts indicate an impaired epicardial phenotype in response to injury.

.

6 Results chapter 4: Role of NRP1 in the epicardium

In the previous chapters have described the upregulation of the different neuropilin isoforms in the cryoinjured zebrafish heart. I have noted a clear expression of Nrp1 in uninjured heart and found that its expression was notably increased by both the epicardium and the endocardium following injury. I have characterised a *nrp1a* mutant fish line expressing a non-functional soluble Nrp1a fragment. The *nrp1a*$^{sa1485/sa1485}$ fish exhibited a delayed resolution of the cryoinjured lesion; displayed an impaired regeneration of the compact myocardium layer as well as an abnormal epicardial morphology. Therefore, my results in the preceding chapters suggest a functional epicardial role for Nrp1. In this chapter I decided to further investigate the role of Nrp1 in the epicardium in more detail using primary epicardial cells.

6.1 Neuropilin activity in epicardial cells

6.1.1 Epicardial *in vitro* assay validation

During the reparative phase of regeneration, a fibrin cap is laid down in the injured area, below the epicardium (Chablais *et al*., 2011; Manuel Gonzalez-Rosa *et al*., 2011). A subset of epicardial cells undergoes EMT, migrates through the subepicardial fibrin scar matrix (as shown in Figure 40) and eventually transdifferentiate into mural or fibroblasts cells (Lepilina *et al*., 2006; Manuel Gonzalez-Rosa *et al*., 2012).

Primary epicardial cells from zebrafish ventricle explants can be cultured *in vitro* on fibrin gels that mimic *in vivo* conditions of cardiac repair (Kim *et al* 2012). The zebrafish ventricle apex is placed on a fibrin gel and left to adhere for a short period before medium is added to the sample (see section 2.5). Within 24 hours, epicardial cells can be seen infiltrating the matrix surrounding the apex tissue (Kim *et al* 2012) and, after a week, larger outgrowths can be visualised (Figure 52A). I performed this procedure with three transgenic lines (*Tg(fli1a:GFP), Tg(cmlc2:GFP),* and *Tg(wt1b:GFP)*) and imaged outgrowths using fluorescence microscopy to identify the population of migrated cells

(Figure 52B). No GFP signal was detected in the outgrowths from *Tg(fli1a:GFP) or Tg(cmlc2:GFP)* apices strongly indicating that the outgrowths do not contain endothelial cells or cardiomyocytes (Figure 52B). GFP positive cells were evident in the outgrowths from *Tg(wt1b:GFP)* zebrafish ventricle apices (Figure 52B), confirming that the method yields an epicardial population.

To confirm the identity of the outgrowing cell population, I immunostained the samples for Raldh2 and found that all cells were Raldh2 positive (Figure 53 green panel upper row), further validating their epicardial identity. In *Tg(wt1b:GFP)* apices, the degree of GFP expression was heterogeneous, all cells showing some GFP expression, but only a proportion of outgrowing cells were strongly GFP-positive (Figure 53 green panel, second row); this is consistent with previous reports showing that only a subpopulation of epicardial cells express *wt1b* after cardiac damage (Manuel Gonzalez-Rosa *et al*., 2011; Peralta *et al*., 2014). Staining of F-actin cytoskeletal filaments was used to highlighted the epicardial cell morphology, a cobblestone-like appearance was observed and the cells grow as a monolayer, similar to that described by Kim *et al*. (2012) (Figure 53). F-actin staining also revealed the cells are in close contact between each other, characteristic epithelial cell monolayers (Figure 53). Taken together, these results strongly indicate that the outgrowths consist primarily of an epicardial cell population.

I also examined Nrp1 expression in these epicardial outgrowths and observed that all cells were Nrp1 positive (Figure 53), which is in line with immunofluorescence images of heart sections, described earlier (see 4.3.3),showing Nrp1 positive epicardial cells in both cryoinjured and sham operated hearts *in vivo*. These observations support the conclusion that Nrp1 is expressed in epicardial explants and that this model would allow me to examine the functional role of Nrp1 in epicardial cells. In zebrafish epicardial cell outgrowths, Nrp1 was localised predominantly to the perinuclear region, but also within the cytoplasm and at the membrane as suggested from its co-localisation with F-actin (white arrows, Figure 53).

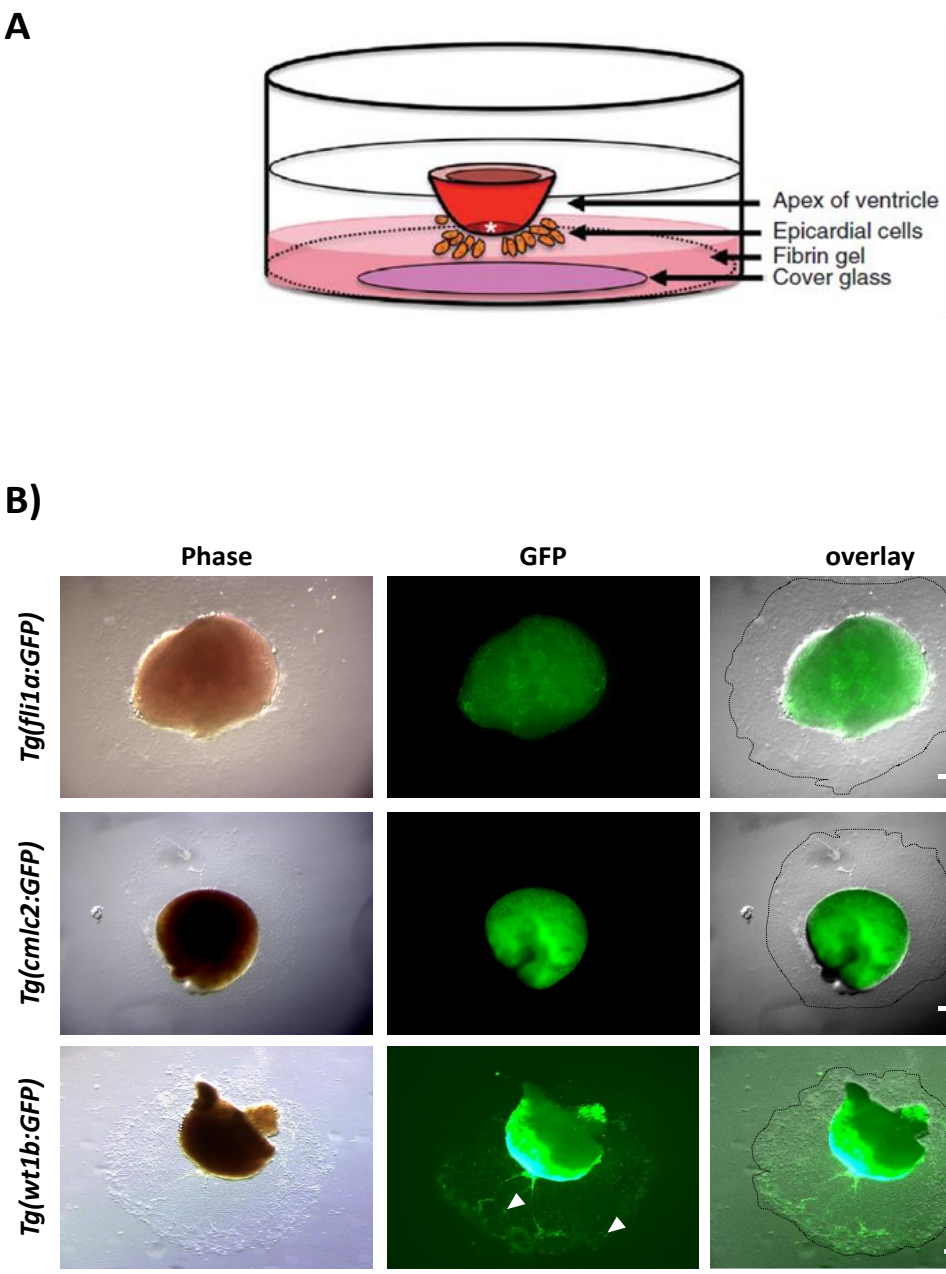

Figure 52 Epicardial outgrowth *in vitro* assay validation

(A) Schematic representation of epicardial cell *in vitro* culture. The ventricle apex is placed into a tissue culture well onto a fibrin gel matrix (ensuring epicardium contact with matrix). Once adhered, culture medium is added and epicardial cells migrate radially onto the matrix away from cardiac tissue. An optional cover glass slip can be inserted into the gel for histological assays. (See 2.5.1 for detailed assay description). Star indicates damaged area. image modified from Kim *et al.* (2012). **(B)** Epicardial outgrowths from *Tg(fli1a:GFP)* (upper row), *Tg(cmlc2:GFP)* (middle row), and *Tg(wt1b:GFP)* (bottom row) cryoinjured fish after 7 days in culture. Outgrowths are displayed under phase light (left column), GFP fluorescence (middle column) and overlaid images (right column), black dotted lines indicate outgrowth boundary. Scale bar 500µm.

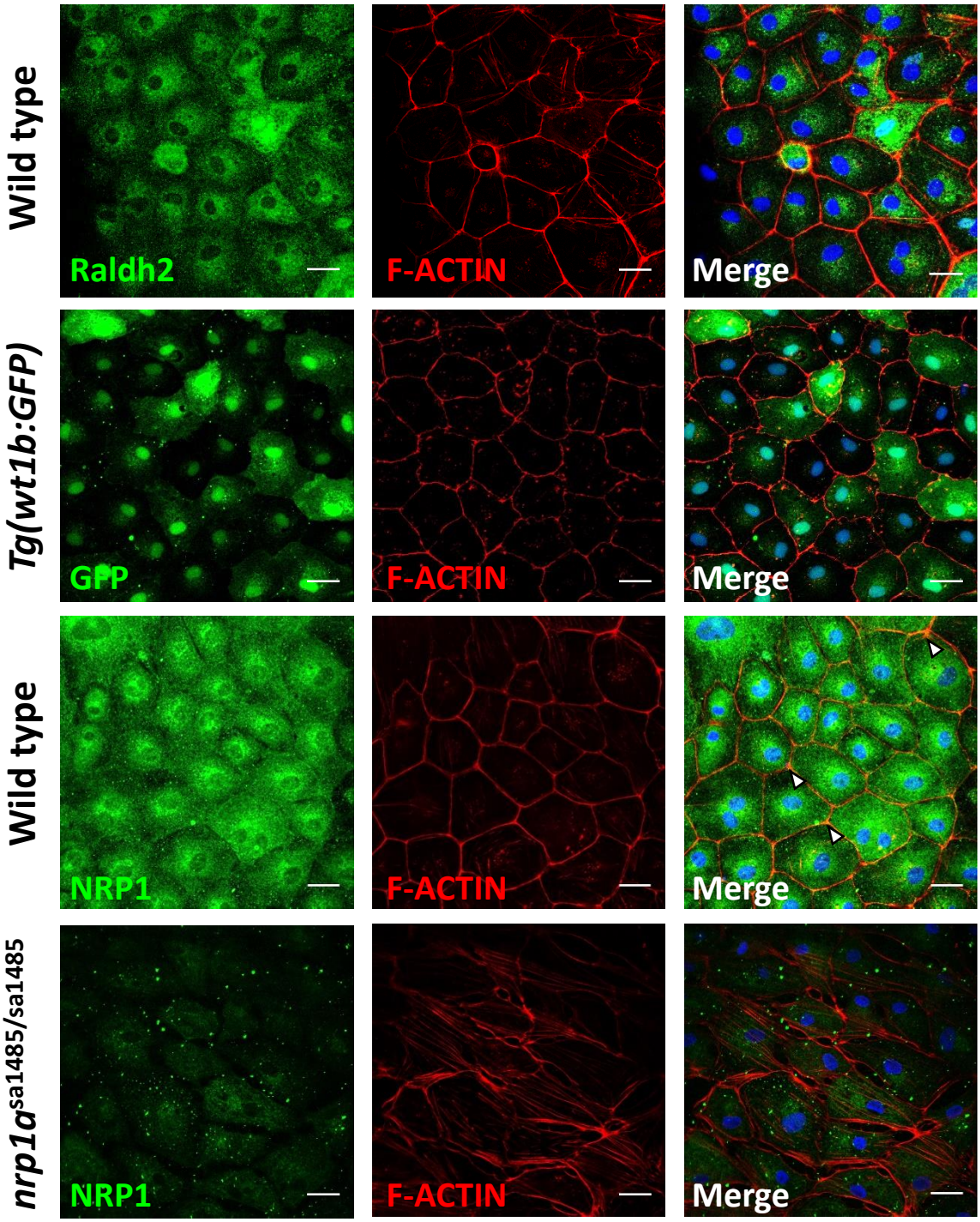

Figure 53 Epicardial outgrowth immunofluorescent cytochemistry

Ventricle apices were collected 5 dpci and cultured *in vitro* for 7 days from wild type (first and third row), *Tg(wt1b:GFP)* (second row), and *nrp1a*$^{sa1485/sa1485}$ (bottom row) fish. Epicardial outgrowths were immunostained for either Raldh2 (first row) (*n = 3*), GFP (second row) (*n = 2*) or NRP1 (third (*n = 4*) and fourth (*n = 2*) row) (green) and phalloidin conjugated to Alexa-555 to identify F-ACTIN cytoskeleton (red). DAPI (blue) staining was applied to help locate individual cells and overlaid with green and red channels (third column). White arrows indicate regions of colocalisation. Scale bar 20 µm.

Epicardial outgrowth morphology and Nrp1 expression were also examined in explants from *nrp1a*$^{sa1485/sa1485}$ mutant hearts (Figure 53 bottom row). Nrp1 showed that Nrp1 expression was much weaker in the mutant compared to wild-type hearts, (Figure 53 bottom row), indicating that Nrp1a is the Nrp1 isoform predominantly expressed in epicardial outgrowths. It was also observed that, although the *nrp1a*$^{sa1485/sa1485}$ mutant epicardial cells presented a cobblestone morphology, however, the F-actin staining pattern was altered, suggestive of discontinuous cell-cell adhesions, possibly due to disruption of tight junctions.

6.1.2 Cryoinjured heart epicardial expansion

Injury-induced epicardial activation, proliferation and migration (Lepilina *et al*., 2006) results in increased epicardial expansion from resected hearts compared with sham operated hearts as previously reported (Kim *et al*., 2012). Nevertheless, there has been no previous description of the effect of cryoinjury on epicardial outgrowths *in vitro*, thus I compared the outgrowths of cryoinjured hearts against sham-operated hearts (Figure 54A). I quantified the epicardial expansion area from the apex circumference and found that cryoinjured samples expanded to approximately double the area (3.9 ± 0.37 mm^2) of outgrowths from sham-operated apices (2.01 ± 0.23 mm^2) (Figure 54 B). The significant increase (p = 0.0003) in epicardial outgrowth following cardiac damage supports previous observations in resected hearts (Kim *et al*., 2012). Additionally, I assessed the extent of epicardial activation in sham and cryoinjured outgrowths from *Tg(wt1b:GFP)* apices (Figure 54A). A clear trend for increased fluorescence in cryoinjured hearts was observed, however, a single outlier in both treatment groups caused large variation, and thus, the data recorded was not statistically significant (p = 0.0713, n = 4) (Figure 54C). Increasing the number of experimental repeats may lead to statistically significant GFP signal increase.

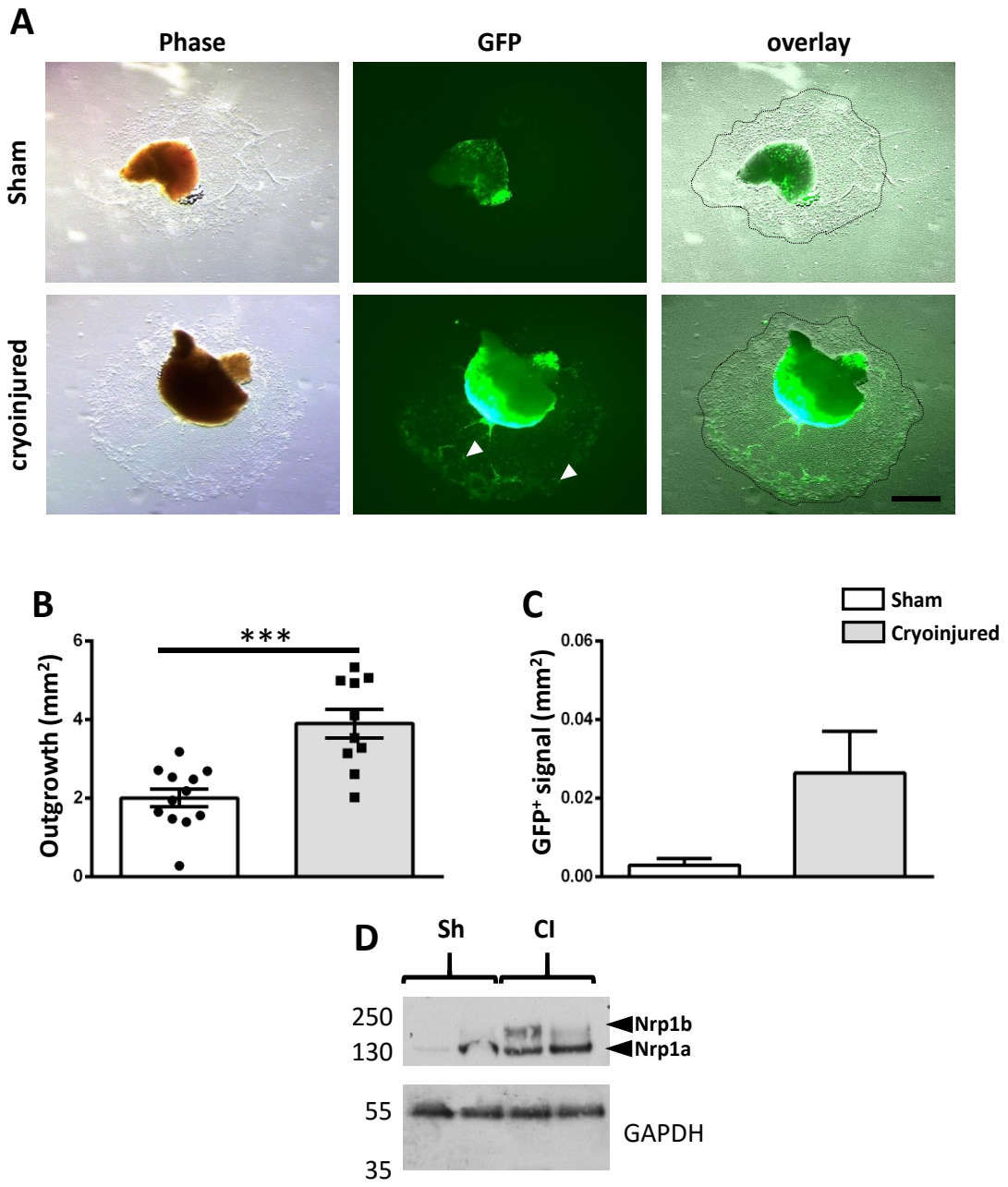

Figure 54 Cryoinjury induces epicardial expansion and activation.

(A) The apices of *Tg(wt1b:GFP)* zebrafish ventricles were collected 5 days post sham surgery or cryoinjury and cultured on fibrin gels for 7 days. Preparations were imaged under phase and green-fluorescence microscopy, then overlaid to visualise GFP-positive epicardial outgrowth (white arrows). Scale bar 500µm. **(B)** Epicardial outgrowths from sham (white bar) and cryoinjury (grey bar) surgeries in wild-type zebrafish hearts were quantified. Data are represented as mean outgrowth areas in mm^2 ± S.E.M ***$p \leq 0.0005$ ($p = 0.0003$), $n = 10\text{-}12$. **(C)** Epicardial outgrowth GFP-positive signal was measured in explants from sham (white bar) and cryoinjured (grey bar) *Tg(wt1b:GFP)* zebrafish hearts. Data are represented as mean GFP-positive areas in mm^2 ± S.E.M ($p = 0.0713$), $n = 4$ **(D)** Lysates obtained from sham-operated (Sh) and cryoinjured (CI) *in vitro* epicardial outgrowths from wild-type zebrafish hearts were immunoblotted for Nrp1 and Gapdh $n = 2$

Following 7 days *in vitro* culture, sham-operated and cryoinjury epicardial samples were harvested and protein lysates examined by Western blot analysis. The lysates were immunoblotted for Nrp1, using Gapdh as a loading control (Figure 54D). Epicardial lysates obtained from cryoinjured samples expressed increased Nrp1 levels compared with sham-operated samples. However, statistical analysis of the Western blot data was not possible due to the insufficient number of experimental replicates. Observations from immunofluorescence images that displayed increased Nrp1 levels in the epicardium after cardiac damage (see Figure 32 and Figure 40) would support higher Nrp1 expression in cryoinjured outgrowth lysates; however, I could not draw a definitive conclusion from the current *n* numbers.

6.1.3 Epicardial outgrowth is impaired in the absence of *nrp1a*

I next examined the epicardial outgrowths in wild type and *nrp1a* mutant fish apices following sham surgery and cryoinjury (Figure 55A-D). Epicardial outgrowths were observed in *nrp1a* mutant fish samples from both surgical procedures (Figure 55B and D). Epicardial outgrowth area quantification revealed no increase in epicardial expansion following cryoinjury in mutant zebrafish (p = 0.859), whereas a significant increase was displayed by explants from wild type cryoinjured hearts as compared with sham-operated hearts consistent with data in Figure 54 (Figure 55E; p = 0.0061). Wild type and mutant epicardial expansions from sham-operated explants were similar (p = 0.9732). Furthermore, a significant decrease in cryoinjury-induced epicardial expansion was observed in mutants when compared with wild type (p = 0.0203): wild type outgrowth area (4.35 ± 0.53 mm^2) was almost two times greater than that of mutants (2.65± 0.46 mm^2). These observations indicate that cryoinjury-induced epicardial expansion is severely impaired in the absence of full-length Nrp1a, but that under basal conditions, Nrp1a activity is dispensable for epicardial outgrowth *in vitro.* The data indicate a role for Nrp1a in either epicardial migration or proliferation after cardiac damage.

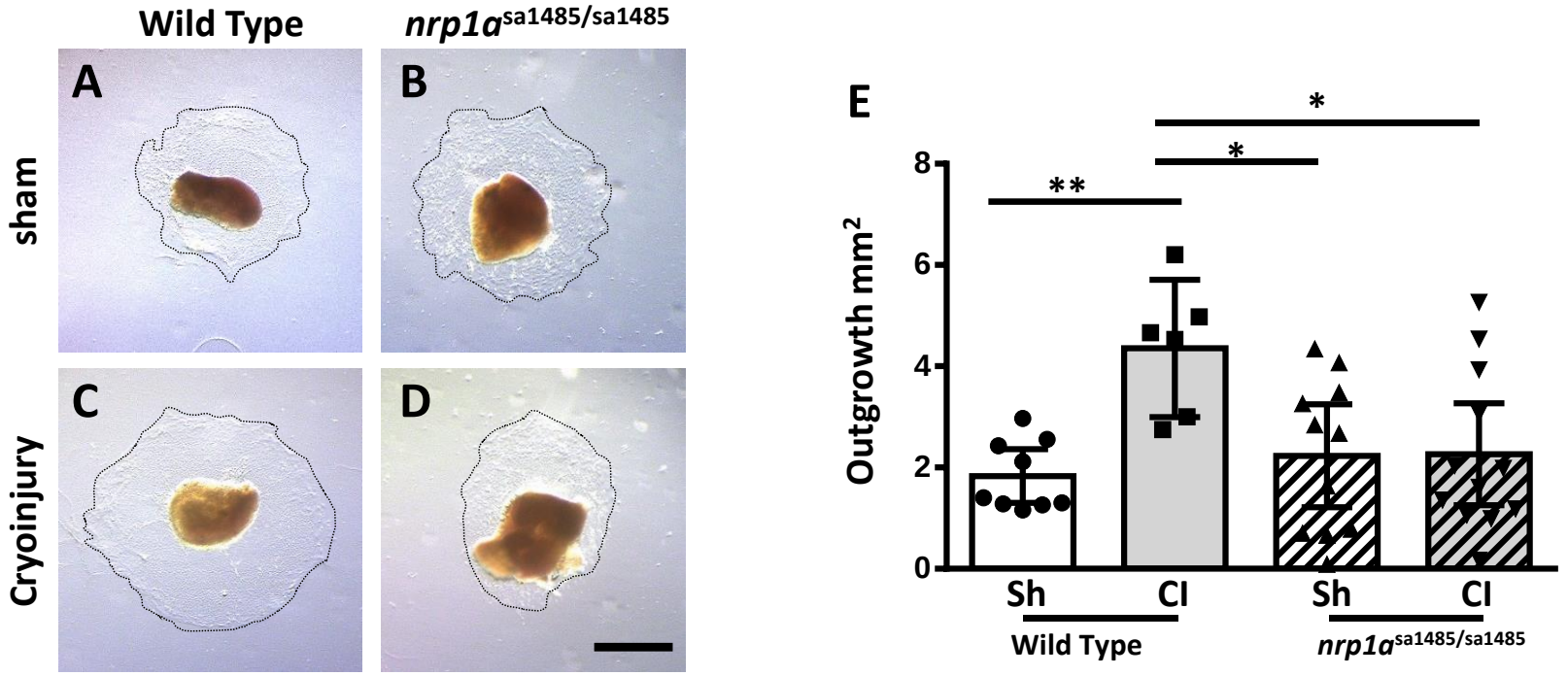

Figure 55 Epicardial migration is impaired in *nrp1a* mutants

The apex of wild type **(A**, **C)** and *nrp1a*$^{sa1485/sa1485}$ **(B**, **D)** zebrafish ventricles were collected 5 days post sham surgery **(A**, **B)** or cryoinjury **(C, D)** and cultured on fibrin gels for 7 days. Epicardial cells migrate into the fibrin gels (dotted black lines). Scale bar 1 mm. **(E)** Epicardial outgrowths were measured for each condition after 7 days culture, data are represented as mean outgrowth ± S.E.M (n = 5-12) *$p < 0.05$, **$p < 0.001$

6.1.4 Epicardial proliferation is unaffected by Nrp1a

To investigate whether the lack of injury-induced epicardial expansion observed in *nrp1a* mutants is due to impaired proliferation or migration, I assessed epicardial cell proliferation in heart sections. Samples obtained from WT and mutant hearts 7 dpci were immunostained for proliferative cell nuclear antigen (PCNA) and Raldh2 (expressed in activated endocardium and epicardium following injury)(Figure 56A). Raldh2 positive cells of the epicardium were counted, and the proportion of PCNA positive cells calculated. Quantification showed no significant difference in epicardial proliferation between WT and *nrp1a* mutant cryoinjured hearts ($p > 0.999$) (Figure 56B). These observations suggest that Nrp1a does not play a role in injury-induced epicardial proliferation, and that, therefore, the impaired expansion is likely a result of compromised migration and/or EMT that enhances the migratory potential of the epicardium.

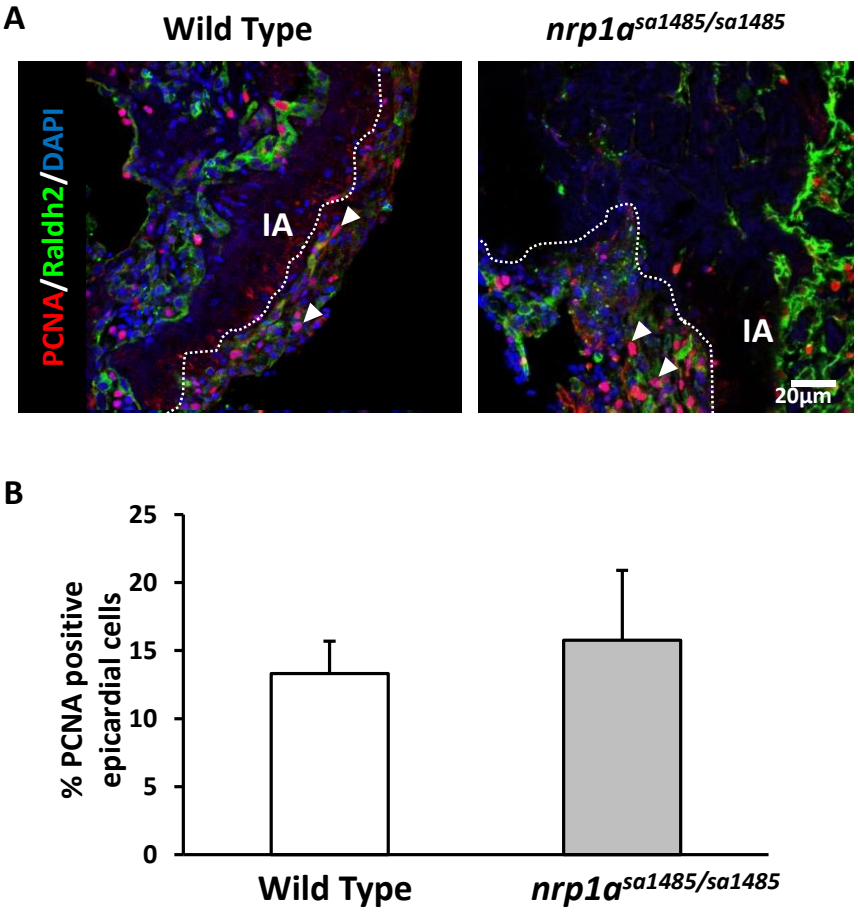

Figure 56 Epicardial proliferation in nrp1a mutants

(A) Immunofluorescence of wild type and mutant hearts 7 dpci immunostained for PCNA and Raldh2. White dotted line demarcates Raldh2 positive epicardium border, arrows indicate PCNA positive epicardial cells. IA- injured area. **(B)** Percentage of PCNA positive epicardial cells in WT versus mutant hearts 7dpci. *n*=3 where each *n* is a mean of 3 fields of view from one heart. *p*>0.05

6.1.5 Rat epicardial cell *in vitro* studies

Reagents and pharmacological inhibitors specific to zebrafish are limited. Additionally, the culture of epicardial cells is an intricate procedure and requires a minimum of 3 to 5 hearts to generate sufficient protein lysate usable for Western blotting. Therefore, to better understand the role of NRP in the regulation of candidate signalling pathways in the epicardium, I carried out *in vitro* experiments using adult rat epicardial cells (these cells were a generous gift from Dr Nicola Smart and were previously described in Wada *et al.* (2003)). Cells were infected with adenovirus containing either scrambled (Scr) or NRP1 targeted (Sh1) short hairpin (Sh) RNA (shRNA) (viruses were generated as described in Pellet-Many *et al.* (2015)). Upon stimulation by growth factors, cells were lysed and immunoblotted for ERK phosphorylation.

VEGF is a well characterised ligand for NRP1 (Soker *et al*., 1998) and has been associated with mammalian embryonic epicardial EMT (Tomanek *et al*., 2006) and migration (Tao *et al*., 2013). Therefore, I assessed the effect of NRP1 knockdown on epicardial VEGF response. There was a trend for an increased ERK phosphorylation following VEGF stimulation (Figure 57A), but this did not reach statistical significance ($p = 0.1179$, $n = 3$) (Figure 57B). Similarly, a trend for reduced VEGF response was observed after NRP1 knockdown (Figure 57A), but was not found to be statistically significant ($p = 0.5122$). These experiments are in the process of being repeated using siRNA, which may lend greater statistical weight to the results generated so far and decipher whether VEGF signalling is being mediated by NRP1 in the epicardium.

Pdgfbb was demonstrated to mediate epicardial EMT *via* Pdgfrβ following ventricular resection essential for cardiac repair in zebrafish. PDGF is also a recognised NRP1 ligand (Banerjee *et al*., 2006; Dhar *et al*., 2010; Pellet-Many *et al*., 2011). Thus, I examined rat epicardial cell responses to PDGFBB. I assessed the phosphorylation of one of the PDGF downstream targets, ERK, following PDGF stimulation. PDGFBB clearly increased ERK phosphorylation indicating that rat epicardial cells respond to PDGF and target the MAPK/ERK pathway (Figure 57C). PDGFBB stimulation induced a significant increase in ERK phosphorylation when compared with serum free (SF) conditions ($p = 0.0367$)

(Figure 57D). NRP1 knockdown showed reduced ERK phosphorylation after PDGFBB stimulation when compared with scrambled RNA in 2 out of the three repeated experiments (Figure 57C). However, a large variation in protein band quantification and the low number of repeat experiments resulted in no clear trend or overall effect after NRP1 knockdown on PDGFBB in rat epicardial cells (p = 0.1529) (Figure 57D).

It has been previously reported that Fgf signalling in the epicardium is essential for zebrafish epicardial EMT to mediate neovascularisation of the injured area (Lepilina *et al*., 2006); moreover, FGF is implicated as a NRP1 ligand (West *et al*., 2005). Therefore, I further examined rat epicardial cell responses to FGF. Both Scr and Sh1 treated rat epicardial cells demonstrated a robust increase in ERK phosphorylation upon FGF stimulation (Figure 58A). This demonstrated that ERK is a downstream target of FGF signalling in epicardial cells, as previously characterised in proepicardial cells (van Wijk *et al*., 2009; Vega-Hernandez *et al*., 2011). Indeed, FGF stimulation induced a significant increase in ERK phosphorylation when compared with serum free (SF) conditions (p ≤0.0001). NRP1 knockdown did not affect ERK phosphorylation after FGF stimulation when compared with Scr-treated rat epicardial cells (p = 0.3770 n = 3) (Figure 58)

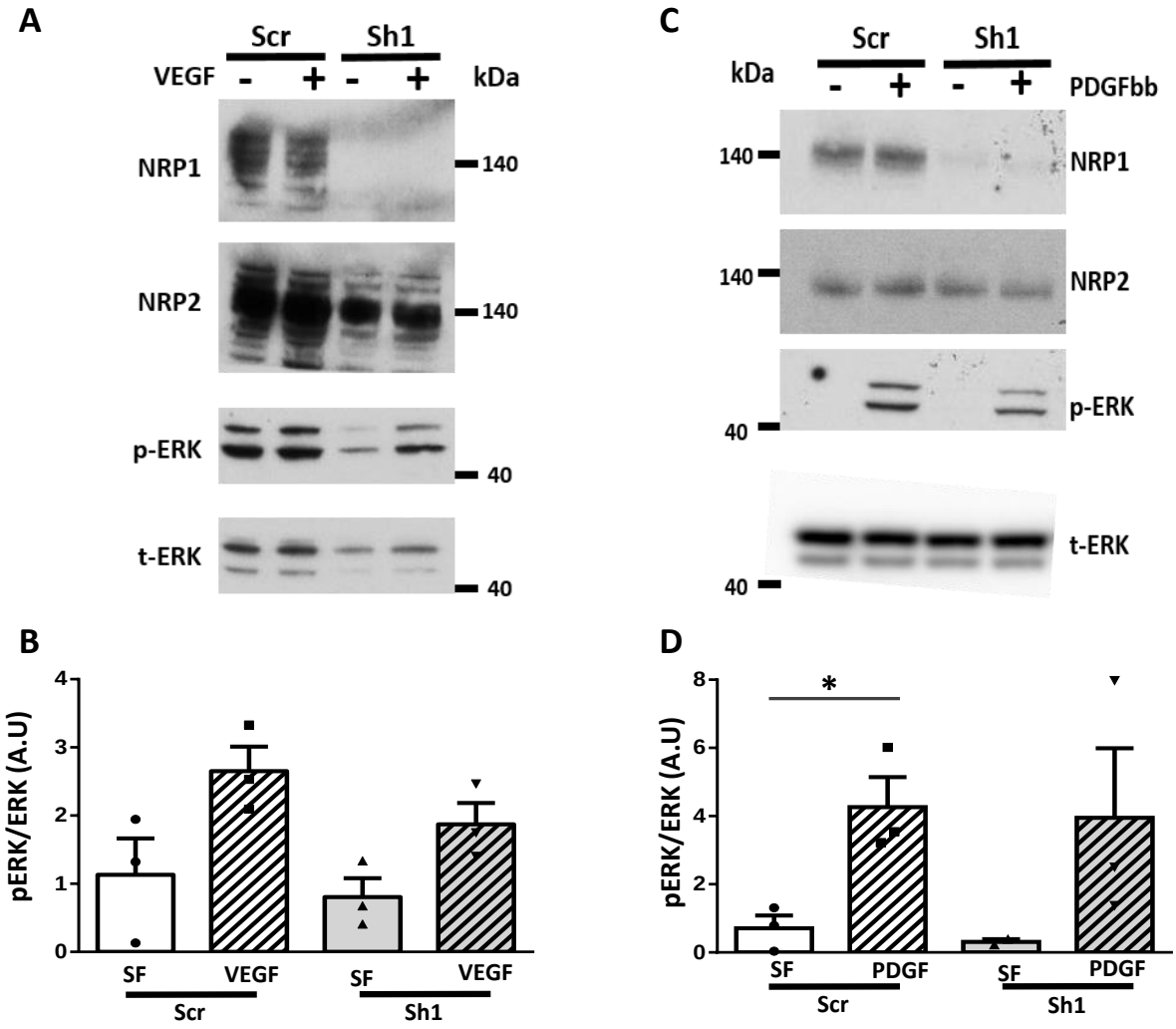

Figure *57* Rat epicardial signalling *in vitro*

Western blot analysis of rat epicardial cells infected with adenovirus containing either scrambled (Scr) control or NRP1 (Sh1) short hairpin RNA and stimulated with VEGF **(A)** or PDGFBB **(C)**. Quantification of band intensities are represented as phosphorylated ERK/total ERK ratios ±S.E.M **(B and D)**. White bars represent scrambled samples; grey bars represent Sh1 samples. Solid fill bars represent non-stimulated cells (SF- serum free) and striped bars represent growth factor stimulated samples. $n = 3$ $*p \leq 0.05$

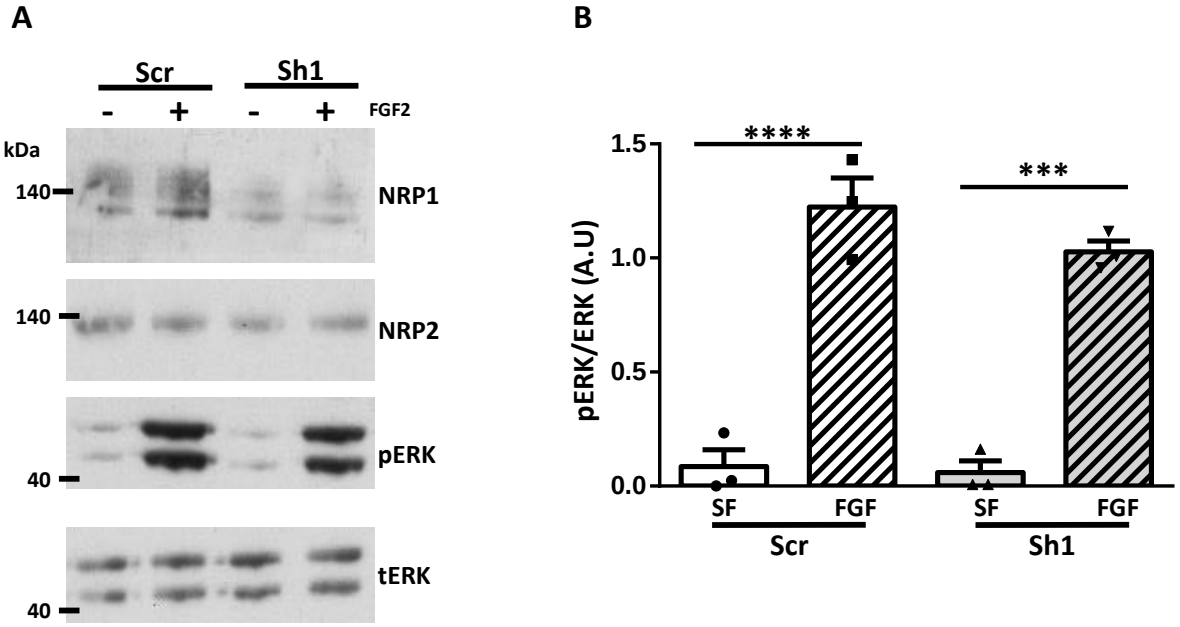

Figure 58 Rat epicardial FGF signalling *in vitro*

(A) Western blot analysis of rat epicardial cells infected with adenovirus containing either scrambled (Scr) control or NRP1 (Sh1) short hairpin RNA and stimulated with FGF **(B)** Quantification of band intensities are represented as phosphorylated ERK/ERK ratio ±S.E.M. White bars represent scrambled samples; grey bars represent Sh1 samples. Solid fill bars represent non-stimulated cells (SF- serum free) and striped bars represent growth factor stimulated samples. n= 3 ****$p < 0.0001$, ***$p \leq 0.0001$

6.2 Discussion

6.2.1 Epicardial cells are cultured *in vitro* from ventricle apices

Because the heart contains a heterogeneous population of cells, I used three transgenic GFP reporter lines to confirm the identity of the outgrowth cell population from cryoinjured ventricle apices. Outgrowth GFP signal was exclusively detected in cryoinjured *Tg(wt1b:GFP)* samples in agreement with data showing that *Wt1b* is expressed by a subpopulation of activated epicardial cells *in vivo* after injury (Peralta *et al*., 2014). *Wt1b* encodes a transcription factor that drives expression of EMT markers such as snai1 and N-cadherin in mammals (Martinez-Estrada *et al*., 2010).

Retinaldehyde-specific dehydrogenase type 2 (Raldh2) is a cytosolic enzyme that produces the hormone, retinoic acid. In zebrafish, it is expressed in the epicardium and endocardium during cardiogenesis and re-expressed after cardiac damage (Keegan *et al*., 2005; Kikuchi *et al*., 2011b). Epicardial outgrowths from cryoinjured hearts displayed uniform cytoplasmic Raldh2 protein expression, indicating they are made of cells of epicardial lineage (Figure 53). Raldh2 is also expressed in the endocardium after injury (Kikuchi *et al*., 2011b), therefore Raldh2 positive cells could also originate from the endocardium. Nevertheless, given the absence of GFP signal from *Tg(fli1a:GFP)* apices (Figure 52B,) and by ensuring that only the ventricle apex outer surface is in contact with the fibrin gel matrices, it is unlikely that the Raldh2 positive cells represents an endocardial-derived population. Though it cannot be ruled out that some minimal cell contamination by other cell types, such as fibroblasts, might be present. The 'cobblestone' monolayer morphology of the explant outgrowths was strongly indicative of an epicardial phenotype, and did not suggest contamination by mesenchymal cells. Together, these data validated the presence of epicardial cells in the outgrowths, demonstrated the induction of Wt1b expression after cryoinjury in the *in vitro* heart explant setting, and confirmed that this was a useful model for examining the role of Nrp1 in epicardial outgrowth and associated cell functions.

6.2.2 Epicardial expansion is increased in cryoinjured ventricle apices *in vitro*

The finding in this chapter that cryoinjured explants undergo significantly larger epicardial expansions compared to shams agrees with observations from the authors who developed the cardiac explant protocol using resected hearts. In resection, as in cryoinjured hearts, the epicardium proliferates extensively and, a subpopulation delaminates from the epicardial layer to migrate into the subepicardial fibrin scar (Lepilina *et al*., 2006; Poss *et al*., 2002). The injury-induced increase in epicardial expansion observed *in vitro* cultures likely recapitulates the epicardial cell behaviour, exhibiting a migratory phenotype following injury. These cells move into the fibrin gel that mimics the subepicardial fibrin scar tissue produced following cardiac damage. It is interesting to note that epicardial cells migrate outwards, in the direction of the matrix, whereas *in vivo* they migrate into the sub epicardial space. The cardiac tissue is present throughout the protocol, yet the epicardial cells migrate into the matrix. Endogenous paracrine signals that direct epicardial cells into the underlying damaged region may compete with the culture medium growth factors or external gel fibrin to influence epicardial cells to migrate into the gel.

Given that the epicardial cells of damaged hearts exhibit a migratory phenotype, it is intriguing that cells also migrate from sham-operated hearts. Indeed, the epicardium initiates a robust response after extensive cardiac damage, but sham operations have also been demonstrated to elicit an epicardial response, though to a lesser extent (Itou *et al*., 2014). Therefore, the epicardium is likely partially activated during the sham-operation following tissue handling and the opening of the chest cavity during the preparation of the sham protocol. Furthermore, the process of making explants and culturing them will likely induce some degree of activation and outgrowth. As sham surgery inflicts less extensive tissue damage in comparison with cryoinjured samples, the epicardium is only mildly activated and expands to a lesser extent than injured heart epicardial cells. This is supported by observations of sham versus cryoinjured hearts from *Tg(wt1b:GFP)* fish. A clear increase of GFP signal was detected in cryoinjured explant outgrowths when compared with shams, indicating greater epicardial activation

following cardiac damage. This system provides a good model to study epicardial activation whereby cells exhibit a similar physiological response to injury *in vitro.*

6.2.3 Epicardial cells express Nrp1 *in vitro*

All epicardial cells from the zebrafish cardiac explants were Nrp1 positive and were localised to the cytoplasm, the perinuclear region and at the membrane. Epicardial cells derived from *nrp1a*$^{sa1485/sa1485}$ mutant hearts were immunostained with an antibody specific for the NRP1 C-terminus. Nrp1 signal from immunostained mutant epicardial cells was notably decreased in comparison with WT hearts. Moreover, Nrp1 signal localised at the membrane and perinuclear region observed in WT outgrowths, was no longer evident in the mutants. This suggests that Nrp1a localises, at least, to the membrane and perinuclear region in zebrafish epicardium, and also likely within the cytosol. The data also implies that the most predominantly expressed Nrp1 isoform in zebrafish epicardial cells is Nrp1a. This observation is also supported by Western blot experiments that showed a stronger Nrp1a band in epicardial cell lysates (Figure 54D) and strong *nrp1a* mRNA localisation in the epicardium using ISH (see Figure 32).

Nrp1a mutant epicardial outgrowths displayed abnormal F-actin filament morphology that could point to a role for Nrp1a cell-cell or cell-ECM interactions. Immunofluorescence demonstrated co-localisation of Nrp1 with F-actin at the cell-cell contact edges of membranes. Additionally, NRP1 is implicated in cytoskeleton regulation and focal adhesion turnover activity, *via* p130Cas and synectin interactions (Naccache *et al*., 2006; Seerapu *et al*., 2013). An abnormal F-actin cytoskeleton was observed twice in the two experiments performed. Nevertheless, it cannot be ruled out that the fibrin gel in these preparations was distorted and that this affected cytoskeleton organisation. Further experiments are required to determine whether the cytoskeleton of *nrp1a* mutant fish consistently display abnormal morphology. Additional staining with tight junction markers present in the epicardium such as E-cadherin and Zonula occuldens-1 (ZO-1) could be carried out to obtain a clearer tight junction structure. A role for Nrp1a in epicardial cell integrity and cytoskeletal function could provide explanation for the abnormal epicardial phenotype occasionally observed *in vivo* (see Figure 50).

6.2.4 Nrp1a is required for injury-induced epicardial activation

Under basal conditions *nrp1a* does not affect *in vitro* epicardial migration suggesting alternative pathways, or that compensation by Nrp1b is sufficient to mediate epicardial expansion from sham operated apices. As described in section 6.2.2, following cryoinjury, the epicardium becomes activated, thus enhancing the migratory response of epicardial cells. This injury-induced increased epicardial expansion does not occur in *nrp1a*$^{sa1485/sa1485}$ outgrowths, suggesting a requirement for Nrp1a in injury-induced epicardial activation. Outgrowth occurs *via* epicardial cell migration and proliferation. My data implicate a role for Nrp1a in the migration of epicardial cells rather than in their proliferation, since the latter was shown to be unaffected in the absence of Nrp1a *in vivo*. Several reports have associated NRP1 activity with EMT and cell migration in mammalian cells (Chu *et al*., 2014; Evans *et al*., 2011; Pellet-Many *et al*., 2011; Tao *et al*., 2013; Tomanek *et al*., 2006), two mechanisms key to the epicardial response to cardiac damage. It is unclear, at this stage, whether Nrp1a plays a role in epicardial EMT initiation and/or migratory potential. Thorough characterisation of the expression of EMT and mural cell markers (such as *snail, slug,* N-cadherin and alpha fibronectin, smooth muscle actin), and of components of signalling pathways involved in migration, both in cultured epicardial cells and *in vivo* in WT and *nrp1a* mutant fish, will be necessary to clarify Nrp1 cellular and molecular mechanisms involved in epicardial migration and/or EMT.

6.2.5 Candidate signalling pathways mediated by NRP1 in rat epicardial cells

Unfortunately, more extensive studies using the rat epicardial cells were prevented due to time constraints and difficulties with reproducibility during protocol optimisation (virus titres and availability). Nevertheless, the data hint at a role for NRP1 in the regulation of epicardial cell VEGF and PDGFBB responses. NRP1 not does not appear to modulate FGF-induced MAPK/ERK signal pathway in rat epicardial cells. FGF2 was used in this study as it has been previously characterised to induce an epicardial response *in vitro* (van Wijk *et al*., 2009), whereas Fgf17b was identified as the isoform required for zebrafish heart regeneration *in vivo* (Lepilina *et al*., 2006); thus the different FGF

isoforms may induce differential pathway stimulation and vary in their NRP1 dependence.

Further analysis of the rat epicardial cells stimulated with other candidate signal molecules (such as TGFβ) could shed light on molecular pathways activated in zebrafish epicardial cells during regeneration. I examined solely the MAPK/ERK signal pathway, however, this is only one of the many downstream pathways triggered following growth factor stimulation. The MAPK/ERK signal pathway is associated with cell proliferation. From my previous observations in zebrafish heart sections, it seems unlikely that NRP1 is required for epicardial proliferation; hence, the lack of significant effect on ERK phosphorylation following NRP1 knockdown in rat epicardial studies support these data. The role of Nrp1a in zebrafish injury-activated epicardium was deduced to be more likely due to modulation of EMT and/or migration; therefore, it would be important to study candidate downstream targets associated with EMT (such Snail and Vimentin) and migration (such as p130Cas, Focal adhesion kinase and Paxillin). Lastly, NRP1 is a co-receptor, and likely enhances the RTK ligand interaction response, and may facilitate receptor autophosphorylation. Therefore, examining the extent of receptor phosphorylation in the NRP1-depleted cells may give an indication as to whether NRP1 plays a direct role in receptor activation.

The rat immortalised epicardial cell line was derived from embryonic samples (Wada *et al*., 2003), and will likely model the embryonic-profile adopted by epicardial cells following cardiac damage. *In vitro* studies in zebrafish epicardial cells present several problems. First of all, the number of zebrafish hearts required for epicardial protein and signalling analysis is impractically large due to the small cell numbers generated from a single apex. Additionally, pharmacological reagents and antibodies specific to zebrafish are limited, but more readily accessible for mammalian samples. As the rat epicardial cell line is immortalised, signalling data can be obtained at high throughput and at a greater scale. On the other hand, a cell line does not exactly recapitulate the behaviour of primary cells. The intention was to take the data collected from rat epicardial signalling studies and validate them in zebrafish epicardial physiology. Although

conservation of key signal pathways amongst vertebrates seem largely conserved, it is uncertain whether the rat epicardial cell line initiates the same signal pathways that would occur *in vivo* in the zebrafish.

6.3 Summary

In this chapter I have demonstrated that:

- I can successfully carry out an *in vitro* assay to culture epicardial cells from adult zebrafish heart explants
- Cryoinjury increases the rate of *in vitro* epicardial expansion
- Epicardial cells express Nrp1 in the perinuclear region, cytosol and at the membrane and its expression increases after cardiac damage
- Nrp1a is required for injury-induced epicardial expansion, likely linked to migration and cell-cell junction regulation.
- NRP1 may be important for the mammalian epicardium response to PDGFBB and VEGF, but current data is too limited to be able to draw firm conclusions.

7 Discussion

The candidate pathways and molecular mechanisms that govern zebrafish heart regeneration remain poorly characterised. It is recognised that during regeneration, the heart adopts a more embryonic profile and that cell signals produced by cardiomyocytes, inflammatory cells, endocardium and the epicardium co-ordinate many key cellular responses essential to regeneration (de Preux Charles *et al*., 2016a; Evans *et al*., 2013; Kikuchi *et al*., 2011b; Lepilina *et al*., 2006). Amongst the cardiac repair-promoting cytokines are Vegfaa, Pdgfbb, Tgfβ and Fgf, required to orchestrate epicardial activation, neovascularisation and cardiomyocyte proliferation, key aspects of regeneration (Chablais and Jazwinska, 2012; Kim *et al*., 2010; Lepilina *et al*., 2006; Marin-Juez *et al*., 2016). All of these growth factors are implicated as neuropilin ligands (Glinka and Prud'homme, 2008; Pellet-Many *et al*., 2011; Soker *et al*., 1998; West *et al*., 2005). Neuropilins are multifunctional co-receptors initially identified for axonal guidance and vascular development, and have since been linked to regulation of other physiological processes (Kawasaki *et al*., 1999; Kitsukawa *et al*., 1995; Takashima *et al*., 2002). Neuropilins have not previously been investigated in the context of zebrafish heart regeneration, and neuropilin activity in the zebrafish heart is poorly characterised. To build upon current knowledge of the regenerative response, I set out to characterise the expression and function of neuropilins during zebrafish heart regeneration. The key findings of this PhD study are as follows:

- Neuropilin isoforms are upregulated within the injured area of the ventricle.
- Nrp1 localises to the active endocardium and epicardium, neovasculature and migrating subepicardial cardiomyocytes during the regenerative process.
- Mutant *nrp1a* zebrafish, lacking full length Nrp1a, are viable and present no morphological phenotype, but display a delayed and aberrant regenerative response.

- I have identified a novel role for Nrp1a in the epicardial activation associated with zebrafish heart regeneration.

7.1 Relevance and quantification of the zebrafish cryoinjury model

I chose to perform the cryoinjury model of cardiac damage in the zebrafish because, unlike the resection model (another very commonly used regeneration technique), cryoinjury damages the heart in a localised region without the removal of cardiac tissue. However, thermal shock-induced cardiac damage by the cryoinjury model does not exactly recapitulate the ischemic injury and the pathophysiological mechanisms of myocardial infarction (MI)-induced cardiac damage in humans. Both result in inflammation and a similar fibrotic tissue composition, and cause necrosis and apoptosis of cardiomyocytes amongst other cardiac cell types (Christia *et al*., 2013; Dobaczewski *et al*., 2010; Manuel Gonzalez-Rosa *et al*., 2011). Coronary vessel occlusion would be the most appropriate procedure to induce cardiac damage, however this is technically impossible to achieve in the zebrafish. The zebrafish heart is very small, approximately 1 mm in width, location and ligation of the major coronary vessels would be technically challenging and difficult to create a reproducible injury. Moreover, the zebrafish heart is highly trabeculated, therefore the coronary vasculature is not the only means by which the cardiomyocytes have access to oxygen which could diffuse from the blood present in the ventricle.

The physiology of the zebrafish heart differs to mammalian hearts, they have a two-chambered heart that beats at a lower pressure and higher frequency than typically observed in humans, however these parameters are comparable considering the differences in organism size (Tsai *et al*., 2011). These functional differences could contribute to conditions that favour regeneration in the zebrafish over that of adult mammals. Additionally, although the zebrafish heart is proportional for its size, the number of cardiomyocytes lost after cardiac damage in the zebrafish is minimal in comparison to humans after MI. The sheer number of cardiomyocytes required to

replenish cardiac damage in humans may also contribute to the limited regenerative response, whereas zebrafish have less cardiomyocytes overall to replace.

In this study, heart regeneration was measured using sections of several different hearts; this required the sacrifice of each fish before analysing the cardiac damage, rather than monitoring regeneration of the same heart in a longitudinal study. This means that variations between surgeries may not be accounted for, although initial analysis of my surgical technique showed that I could injure the heart in a reproducible manner. One way to monitor regeneration the zebrafish longitudinally would be to use optically clear fish, such as the TraNac, expressing a cardiomyocyte reporter, such as *cmlc2: GFP* and capture heart fluorescence of the same fish at different time points following the injury. However, as the heart is beating in the live animal, an algorithm would have to accurately image and quantify fluorescence.

I selected 6 serial sections that span across the entire heart to quantify overall injury size. It would be possible quantify injury of all sections of the entire heart, however, in order to comply with the principles of the 3Rs (Replacement, Reduction and Refinement), I used some of the serial heart sections for other staining procedures, such as immunofluorescence and *in situ* hybridisation. Therefore, injury size may not be exact, but will be an accurate representation of the percentage of the heart damaged.

Although software plugins are available to quantify scar tissue in an automated manner, the quantification was carried out manually because it is technically more accurate. As a result, some small degree of bias may inadvertently have been introduced, as I was not fully experimentally blinded for the quantification of the heart injuries. Nevertheless, I have discussed the quantification method with Prof Nadia Mercader, who first established the model, and followed the technique reported in the literature.

I did not specifically and systematically record additional measurements for every single fish used in the study. For example, the length and weight of each fish was not recorded for each corresponding heart collected and the exact size of the heart before sectioning was not recorded. Heart size is correlated to animal size; therefore, some animals may

sustain different extents of injury due to natural variations in size. Nevertheless, we used animals of similar ages and sizes. Overall anatomical features and comparison of heart size were recorded and analysed for a representative sample of individuals (WT and also mutant fish) and we did not find any difference between the groups of animal used.

Finally, I did not record fish density in the tank following the surgeries. The number of fish in the tank would affect how much food each of them receive as a similar ration is given to each tank regardless of fish density. It is not known if nutritional access affects regenerative capacity.

Quantification of the cryoinjuries showed that, although the size of the injured area reduced over time, 100% of hearts did not fully recover and on average at 60 dpci 2% of the ventricle mass remained with a scar. This is a minimal scar; however, it does highlight that the extent of some injuries may have been more severe than others or that the regenerative capacity of fish varies slightly between animals. Previous studies on zebrafish heart regeneration report complete regeneration between 60 and 130 dpci depending on extent of lesion and injury method (Manuel Gonzalez-Rosa *et al*., 2011; Poss *et al*., 2002)

7.2 Neuropilins are upregulated after cardiac damage

Neuropilin expression has been characterised in the embryonic zebrafish heart (Bovenkamp *et al*., 2004; Martyn and Schulte-Merker, 2004; Yu *et al*., 2004). In this project I provide the first description of neuropilin expression in the uninjured and regenerating injured adult zebrafish heart at both the mRNA and protein levels. Data gathered throughout this study show that several cells types are Nrp-positive pre- and post-cardiac damage (Table 9). Evidence for a possible homeostatic role of *nrp1a* and *nrp2b* in the normal uninjured heart is provided by expression of these isoforms in uninjured hearts. Following cardiac damage all *nrps* exhibited localised expression adjacent to or within the injury, indicating an injury-induced response and a likely positive role of Nrps in heart regeneration.

I have demonstrated for the first time that 3 of the 4 *neuropilin* isoforms are upregulated in the zebrafish ventricle within the first three days of cryoinjury. The first three days following cardiac damage mark the inflammatory phase of regeneration. During the inflammatory response after cardiac injury, leucocytes infiltrate the injured area (Chablais and Jazwinska, 2012; de Preux Charles *et al*., 2016a; Fang *et al*., 2013); concomitantly, neovessels invade the lesion (Marin-Juez *et al*., 2016), and the epicardium is activated (Kikuchi et al., 2011b; Wang et al., 2013b), these events are essential to propagate subsequent regenerative processes. Neuropilins have been implicated in the innate and adaptive immune response (Dejda *et al*., 2014; Fantin *et al*., 2010) and could serve to modulate Vegf signals secreted by and leucocytes and hypoxic cells at the inflammation site (Leibovich *et al*., 1987; Yoshida *et al*., 1997). Furthermore, NRP is associated with vascular permeability increase in a VEGF- dependent and independent manner (Roth *et al*., 2016; Wang *et al*., 2003). These reports support a possible link of the neuropilin contribution to the inflammatory component of cardiac damage *via* response to locally secreted Vegf, that facilitate leucocyte migration and extravasation from circulating blood through Nrp1 positive endocardium.

Furthermore, neovascularisation, which commences within 15 hours of cardiac damage, has recently been shown to depend on Vegfaa signalling (Marin-Juez *et al*., 2016). Immunofluorescence imaging of *Tg(fli1a:GFP)* zebrafish hearts at 1 dpci revealed that neovessels infiltrating the injured area express Nrp1. NRPs form holoreceptors with VEGF and VEGFRs to mediate angiogenesis (Soker *et al*., 1998; Takashima *et al*., 2002) and have been shown to regulate vessel development in the zebrafish embryo (Martyn and Schulte-Merker, 2004). These reports support the potential role of Nrps in mediating neovascularisation in the injured area in response to VEGF.

Over 600 genes are differentially expressed after cardiac damage in the zebrafish heart (Lien *et al*., 2006). Of the selected genes examined through qPCR in this study, *vegfc* was one of the most strikingly upregulated. Increase of VEGFC in ischaemic tissue has also been previously identified in other species (Witzenbichler *et al*., 1998). Interestingly my mRNA analysis showed that the temporal patterns of *nrp2a* and *vegfc* expression

paralleled each other. Convincing evidence exists for NRP2 in VEGFC-mediated lymphangiogenesis and EMT (Gemmill *et al*., 2017; Jeltsch *et al*., 1997; Kawakami *et al*., 2002; Parker *et al*., 2015) and could point to Vegfc/Nrp2-mediated lymphangiogenesis *via* the VEGF-C receptor, vegfr3, though the latter was not measured. Re-establishment of lymphatic vessels is necessary for draining excess fluid after inflammation and aids cardiac recovery (Klotz *et al*., 2015). It is possible *Vegfc* could form a complex with Vegfr3 and Nrp2 to replenish lymphatic vessel supply to the injury lesion in zebrafish heart regeneration to aid cardiac repair. In zebrafish hearts, both *vegfc* upregulation and neovascularisation are stimulated within a day of the injury, concomitantly with *nrp2a* expression. Furthermore, VEGF-C stimulates endothelial PDGFbb expression to regulate capillary integrity (Onimaru *et al*., 2009). An additional function of Vegfc in zebrafish response to cardiac damage could be to enhance Pdgfbb secretion that induces epicardial EMT and cardiomyocyte migration.

Table 9 Cellular expression of *nrps* in adult zebrafish heart

	Basal		Cardiac damage	
Cell type	**Nrp1**	**Nrp2**	**Nrp1**	**Nrp2**
Cardiomyocytes	-	+	+	+
Endocardium	+	-	++	-
Epicardium	+	-	++	++
Leucocytes	?	?	?	+
Fibroblasts	?	?	?	?
Endothelium	+	-	+	-
Lymphatic vessels	?	?	?	?
Nerves	?	?	?	?
Mural cells	?	?	?	?

7.3 Regeneration is delayed in Nrp1a mutant

I established a homozygous *nrp1a* mutant fish line and confirmed that the mutation resulted in the loss of full length Nrp1a. No morphological abnormalities were identified upon superficial examination of mutants, and growth and behaviour were similar to those of wild type fish. However, it was noted that *nrp1a* mutant survival to adulthood was approximately half that seen in wild types. Therefore, homozygous inheritance of the *nrp1a*$^{sa1485/sa1485}$ mutation is not embryonic lethal in zebrafish, but does compromise survival to maturation, possibly suggesting some effect on development. The mutation is global; therefore, all tissues in the *nrp1a*$^{sa1485/sa1485}$ zebrafish express the truncated Nrp1a. It is possible that other organ systems, that require *nrp1a,* don't fully mature until adulthood such as the nervous system and adaptive immune system, but these were not investigated in this study. Depending on the mutagenesis method employed and gene targeted, disruption of one allele in a zebrafish may result in clear phenotypes, or does not induce deleterious phenotypes due to genome duplication and redundancy (Kok *et al*., 2015; Postlethwait *et al*., 1998; Schulte-Merker and Stainier, 2014). Despite the presence of *nrp1b* in the *nrp1a*$^{sa1485/sa1485}$ mutants there must be underlying late stage developmental events that require *nrp1a* and cannot be compensated for by *nrp1b,* resulting in premature mortality. Further investigations are required to understand why survival to adulthood is diminished in the *nrp1a* mutant zebrafish.

Following cardiac damage, the mutants demonstrated delayed compact layer recovery and scar resolution when compared with wild types. This is, to my knowledge, the first report of an impairment of heart regeneration resulting from ENU mutagenesis of a single allele. At this stage, it is not certain how regeneration is delayed, nor were there any indications as to why the delay does not cause mortality. It could be postulated that Nrps are required for efficient signal interpretation and enhanced sensitivity to growth factors to mediate heart regeneration, thus loss of Nrp1a causes regeneration to take place over a longer duration. It is interesting to note that while *in situ* hybridization of wild type hearts revealed overlapping *nrp* isoform expression in the first 3 days following cardiac damage, only *nrp1a* remained expressed in the epicardium proximal to the

lesion at 14 dpci, coincident with the time at which *nrp1a* mutants begin to present delayed regeneration. It could be possible that overlapping expression by other *nrp* isoforms in the early stages of cardiac repair can compensate for full length Nrp1a loss. Upon the time point by which *nrp1a* is exclusively expressed in the epicardium, a phenotype arises due to lack of other *nrp* isoforms available to carry out compensatory mechanisms.

It is also plausible that evolutionarily genetic drift between Nrp1a and Nrp1b has resulted in loss of gene redundancy. The two genes diverged over 100 million years ago (Postlethwait *et al*., 1998) and have since acquired different post-translational modifications that have resulted in distinct protein mass and present differential developmental tissue expression. During cardiac regeneration, the isoforms do not display identical localisation, exemplified by their differential expression in epicardial cells. Moreover, Nrp1b is not upregulated in response to loss of full-length Nrp1a. These differences point to divergent physiological roles for the two Nrp1 ohnologs, and could potentially lead to an inability to fully compensate for one another.

Nrp1a mutants presented impaired compact myocardium recovery following cardiac damage. After cryoinjury, new myocardium is derived from pre-existing spared cardiomyocytes at the periphery of the lesion. The cardiomyocytes dedifferentiate, proliferate and invade the subepicardial fibrin deposits to enclose the collagen scar tissue and heal the compact myocardium (Jopling *et al*., 2010; Kikuchi *et al*., 2010). According to immunofluorescence co-staining generated in this study, cardiomyocytes are for the most part Nrp1 negative, and Nrp1 expression was observed exclusively in the migrating cardiomyocytes in the subepicardial space. It was more recently shown that cardiomyocytes migrate toward PDGF signals produced by endocardial progenitor cells during embryonic development (Bloomekatz *et al*., 2017). Furthermore, Pdgfbb signalling is essential for zebrafish heart regeneration, perturbed cardiomyocyte recovery and wound closure impairment were reported in the absence of PDGF signals (Kim *et al*., 2010). NRP is a co-receptor for PDGF and has been demonstrated to modulate chemotaxis in response to PDGF in smooth muscle cells and metastatic breast

cancer cells (Banerjee *et al*., 2006; Pellet-Many *et al*., 2011). Zebrafish cardiomyocytes adopt an embryonic profile after cardiac damage (Jopling *et al*., 2010) and therefore likely recapitulate developmental cardiomyocyte behaviour during regeneration. Therefore I present a model whereby the dedifferentiated migrating subepicardial cardiomyocytes express Nrp1 in order to enhance PDGF-induced chemotaxis (Figure 59A and B). In *nrp1a* mutants the loss of full-length Nrp1a impedes this mechanism and limits efficient cardiomyocyte migration, and results in delayed wound closure observed in the mutants.

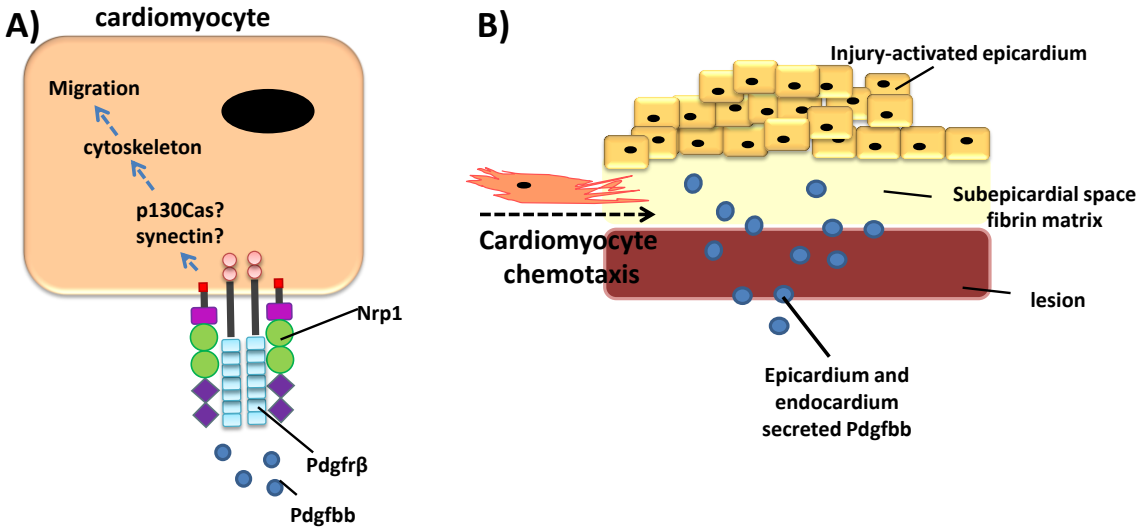

Figure 59 Pdgf-induced cardiomyocyte migration

Schematic representation of **(A)** Pdgf signalling in Nrp1-positive dedifferentiated cardiomyocytes. Pdgfbb form holoreceptor complexes with Pdgfrβ and Nrp1. The signal is propagated by Nrp1 *via* intracellular docking protein p130Cas and synectin to rearrange cytoskeleton and focal adhesions to **(B)** mediate cardiomyocyte chemotaxis in the direction of Pdgfbb gradient. Activated endocardium and epicardium proximal to injury lesion secrete Pdgfbb and direct migrating cardiomyocytes through the fibrin matrix into the underlying subepicardial space leading to the recovery of compact myocardium and wound closure.

7.4 Novel Nrp1 role in epicardium

Epicardial activation is a central mediator of cardiac repair paracrine and autocrine signals that coordinate cardiomyocyte proliferation, revascularisation and induce epicardial EMT (Lepilina *et al*., 2006). The epicardial *in vitro* studies carried out in this study report previously undescribed neuropilin expression in the adult zebrafish epicardium, and the first description of neuropilin expression in the epicardium of any adult species. A novel neuropilin role in the injury-activated response is supported by impaired epicardial outgrowth after cardiac damage in the absence of full-length Nrp1a. These data also for the first time identify a perturbed epicardial function resulting from a single allele mutation.

Loss of full-length Nrp1a impaired epicardial expansion, but did not alter epicardial proliferative capacity. Given that NRPs influence cell migration and EMT in other physiological settings (Chu *et al*., 2014; Evans *et al*., 2011; Frankel *et al*., 2008; Pellet-Many *et al*., 2011), I propose that Nrp1a enhances migratory signals from the underlying injured tissue and facilitates directed epicardial cell movement (Figure 60). Furthermore it is possible that epicardial EMT governed by FGF and PDGF require Nrps to act as a co-receptor for these signals (Figure 60).

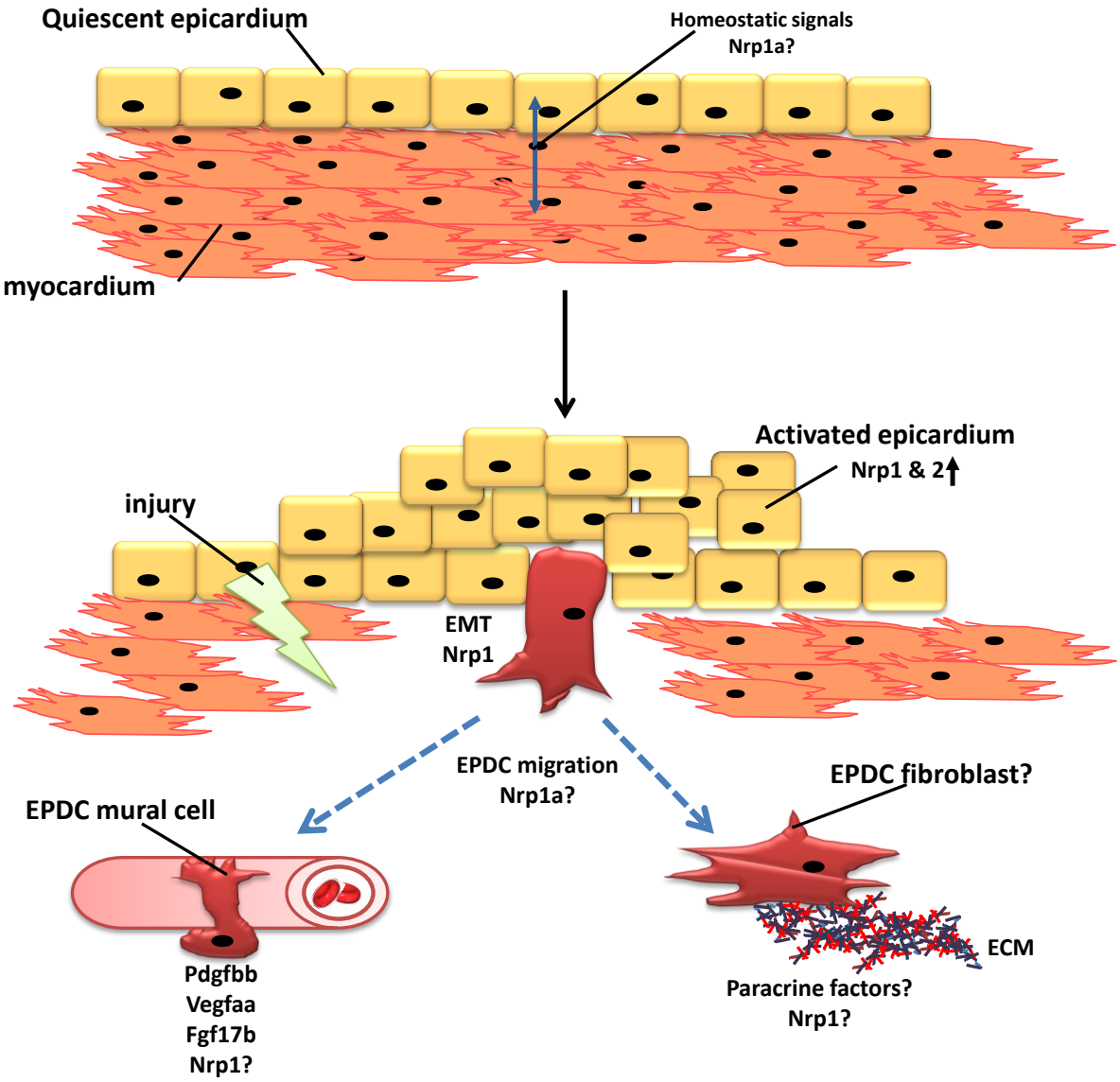

Figure 60 Nrp1a function in the epicardium

Diagrammatic representation of hypothesised epicardial neuropilin functions in zebrafish quiescent and injury-activated epicardium. Nrp1a is endogenously expressed in the epicardium of uninjured hearts to regulate cardiac homeostasis. Upon injury, activated epicardium increase Nrp1a (and Nrp2a) in order to enhance epicardial sensitivity to paracrine signals and increase EMT potential. Nrp1a facilitates epicardial derived cell (EPDC) chemotaxis into underlying subepicardial space towards neovessels and mediate transdifferentiation to pericytes to support vessel maturation. It is unclear at this stage whether Nrp1a may induce EPDC transdifferentiation to cardiac fibroblasts to produce extracellular matrix (ECM) that provide scaffolding for neomyocardium.

7.5 Future directions

I have characterised neuropilin expression patterns in the adult zebrafish heart under basal conditions and during regeneration. I then followed on to describe regenerative phenotypes observed in mutants lacking *nrp1a*. I was unable to fully define the molecular pathways Nrps modulate and what roles Nrps mediate in the cell types identified to express them during regeneration. Taking into consideration the data gathered throughout my thesis, several questions remain and additional experiments could help further characterisation of the role of neuropilins in zebrafish heart regeneration.

7.5.1 Neuropilin mutant lines

To understand neuropilin functions in zebrafish heart regeneration, I used *nrp1a* mutants, primarily due to availability of this line. Data generated in this project with *in situ* and qPCR support previous studies that document differential expression patterns of all four *nrps* (Bovenkamp *et al*., 2004; Martyn and Schulte-Merker, 2004; Yu *et al*., 2004), and point to distinct *nrp* isoform physiological functions. Generating fish with functional mutations in the *nrp1b* gene could provide complementary information and help to define the *nrp1* ohnolog-specific contribution to zebrafish heart regeneration. A *nrp1b*^{fh278} fish is now available for purchase from the Zebrafish International Resource Center (ZIRC) ENU project. A point mutation induces in a non-sense mutation codon at amino acid 116 resulting in a premature stop in the a1 (first CUB) domain in the *nrp1b*^{fh278} mutant allele. This will likely yield non-functional soluble Nrp1b fragments that cannot interact with known Nrp1 ligands. I began to establish the *nrp1b*^{fh278} mutant fish line towards the end of my project; however, identification of a homozygous mutant was not achieved before my studies concluded. Availability of the *nrp1b*^{fh278} line creates the possibility to generate *nrp1a* and *nrp1b* double mutants, although complete *nrp1* deletion will likely cause lethality as seen in nrp1 mammalian mutants (Takashima *et al*., 2002) and morpholino knockdown (Martyn and Schulte-Merker, 2004). However, if the zebrafish survive to adulthood in the absence of both *nrp1* ohnologs, it would also be interesting to study regenerative mechanisms in Nrp1-/- fish, which would likely cause

a more robust phenotype and better reflect a mammalian NRP1 null physiological response.

Due to fish line availability and antibody compatibility, *nrp1* was the primary focus of this study; however, *nrp2* isoforms also show regulated expression in the adult zebrafish heart after cardiac damage. Additionally, *nrp2b* is the dominantly expressed isoform of all four *nrps* in the cardiac tissue under healthy and injured conditions, consistent with developmental cardiac expression of *nrp2b* (Bovenkamp *et al*., 2004). Moreover, *nrp2b* was not upregulated in qPCR, but showed clear redistribution of expression to the endocardium and within the lesion using *in situ* hybridisation. *Nrp2a* was strikingly upregulated at 1 and 3 dpci in the qPCR and at 3 dpci *nrp2a* was exclusively epicardial in expression. This presents another example of likely differential roles of *nrp* ohnologs; it appears that *nrp2b* may constitutively regulate cardiomyocyte activity, whereas *nrp2a* plays a role in injury-activated epicardium. Publications describing NRP2 activity in the adult myocardium and epicardium have not been described, other than in development, where NRP2 is expressed by a sub-population of cardiovascular precursors that can differentiate to endothelial, smooth muscle and cardiomyocyte cell types (Ding *et al*., 2015). Mutant fish for *nrp2a* are now available to purchase through ZIRC, but a mutant for *nrp2b* is still unidentified. I attempted to generate *nrp2b* mutant zebrafish using CRISPR technology but was unsuccessful at inducing disruption of the genomic DNA sequence. Compelling evidence suggests a role for *nrp2* in zebrafish heart development, adult homeostasis and regenerative processes, its role in heart regeneration warrants investigation. I predict a phenotype would arise from the disruption of the *nrp2* genes that would present cardiac deformities and altered function in the absence of *nrp2b,* and lymphatic vessel supply and epicardial EMT may also be impaired without *nrp2a*.

7.5.2 Role of neuropilins in specific cells types

Neuropilins were identified in several cardiac cell types in the zebrafish heart during this study (Table 9); however the Nrp functions in these cells remain to be elucidated. Further validation of the *nrp1a* mutant phenotypes could be performed with rescue experiments. For example, in the *in vitro* epicardial outgrowth assay, transfection of cells with *nrp1a* transcript could be performed. If injury-induced epicardial expansion is restored upon exogenous *nrp1a* mRNA delivery in *nrp1a*$^{sa1485/sa1485}$ mutants, it would confirm Nrp1a a key regulator of this process.

To extend my current observations in the *nrp1a* mutant it would be beneficial to generate cell-type specific reporter lines in the mutants or carry out immunofluoresence with cell-type specific markers. Nrp1 was shown to be constitutively expressed by endocardium and coronary vessels and likely plays a role in angiogenesis after cardiac damage. Using a *Tg(fli1a:GFP):nrp1a* mutant or immunostaining for endothelial-specific markers such as Tie2 or ERG would enable me to visualise vessels. Quantification of neovessels would allow me to compare vascular density in the injured area at varying timepoints in both wild type and mutant hearts, and conclude whether Nrp1a is necessary for revascularisation. These studies have been commenced, but are currently at a preliminary stage.

Cardiomyocyte proliferation and migration could also be assessed in the mutants and compared with wild type. I hypothesise Nrp1a to play a role in dedifferentiated subepicardial cardiomyocyte migration towards Pdgfbb gradient in the injury (Figure 59). To test this hypothesis, I could generate a *nrp1a* mutant that expresses the *Tg(cmlc2:GFP)* and isolate and culture primary cardiomyocytes *in vitro* (Figure 61)(Sander *et al*., 2013). They could then be stimulated with different growth factors and their cell movements tracked by images captured at regular intervals using a tissue incubator installed with a fluorescent microscope (such as the Incucyte Zoom, Essen Bio). The imaging software could then calculate rates of migration and compare different treatments. I have carried out the cardiomyocyte *in vitro* culture as demonstrated in Figure 61, but no functional studies have commenced using this model.

I could support *in vitro* observations with tropomyosin immunostaining of regenerating wild type and mutant heart sections; these data could then be used to calculate and compare subepicardial cardiomyocyte numbers in the different genotypes. Moreover, an *in vitro* model of myocardial infarction in zebrafish cardiomyocytes has been developed using hypoxic chambers: hypoxia stimulates cardiomyocyte proliferation (Sander *et al*., 2013). I could investigate how loss of Nrp1a affects cardiomyocyte proliferation in response to ischemic stress.

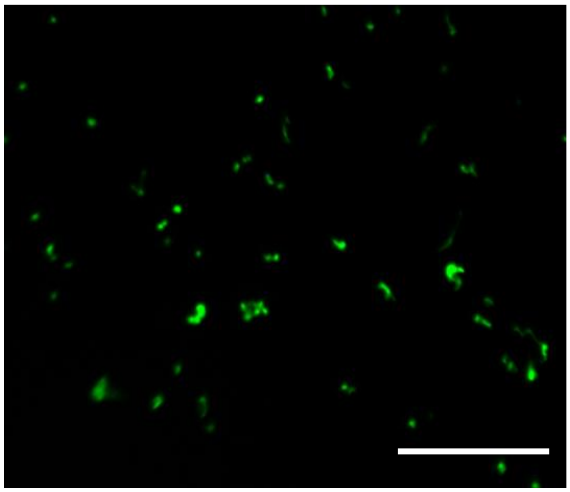

Figure 61 Zebrafish cardiomyocyte *in vitro* culture

Image captured of primary cardiomyocyte culture derived from *Tg(cmcl2:GFP)* adult zebrafish hearts visualised under green fluorescence. Cells can be isolated and cultures for several weeks on fibrin gels. Scale bar 250µm.

This study revealed that epicardial migration was perturbed in *nrp1a* mutant outgrowths. Understanding the role of full-length Nrp1a in epicardial activation could be expanded by generating a mutant that expresses an activated-epicardial reporter transgene such as *Tg(wt1b:GFP)*, in which the GFP signal would be detected in activated epicardial cells undergoing EMT only. Comparison of activated epicardial-specific GFP

expression in wild type and *nrp1a* mutant cryoinjured heart outgrowths would provide some evidence as to whether Nrp1a is required for epicardial wt1b expression, and thus likely regulate EMT. I would predict that Nrp1a plays a role in EMT and that the GFP signal would be reduced in *nrp1a* mutant outgrowths. Other EMT markers could then be analysed using Western Blot or immunofluorescent staining to compare EMT markers of the epicardial outgrowths.

Neuropilins were originally identified in brain and nervous tissue; nerves innervate the subepicardial and subendocardial tissue to regulate heart rate according to physiological demands (Volders, 2010; Zipes, 2008). After cryoinjury transmural damage causes death of all cardiac layers in the affected region; thus nerves will likely need to regenerate in the repairing cardiac tissue. During embryonic development semaphorin3a (SEMA3A) is expressed in the heart to mediate innervation of cardiac tissue (Chen *et al*., 2013; Ieda *et al*., 2009). It could be expected that Sema3a will be re-expressed during regeneration of the zebrafish heart. Type 3 semaphorins (such as SEMA3A) require neuropilins as obligate co-receptors to signal through plexin receptors and mediate axonal guidance (Gu *et al*., 2002; Takahashi *et al*., 1999). It would be interesting to investigate re-innervation of cardiac tissue following cryoinjury and monitor nerve induced regulation of cardiac electrophysiology in the heart in the absence of *nrp* isoforms. Furthermore SEMA3C has been associated with endothelial to mesenchymal transition during embryogenesis (Plein *et al*., 2015), and its expression could be recapitulated in the zebrafish activated endocardium that also undergoes endoMT in response to cardiac damage to contribute mural cells and fibroblasts (Kikuchi *et al*., 2011b).

7.5.3 Neuropilin signalling and function in heart regeneration

Persistent scar, delayed wound closure and impaired epicardial expansion were the main functional phenotypes identified during regeneration in the *nrp1a* mutants. It is unclear from my studies whether these would cause impaired cardiac function after regeneration in *nrp1a*-deficient fish. I would like to apply further organ functional assays to the mutants such as ECG, echocardiography or MRI to assess cardiac output parameters and electrical conductivity after cryoinjury.

The ultimate aim of this project was to dissect the mechanisms underlying zebrafish heart regeneration. However, the results from this study may have implications for human heart regeneration, and therefore future work should seek to test the applicability of my findings to humans recovering from MI. It will therefore be important to characterise and evaluate mammalian neuropilin expression and function in the adult mammalian heart. I'd like to translate the findings of this thesis to mammalian models of regeneration. Neonatal mice can regenerate heart tissue up to seven days following birth (Porrello *et al.,* 2011) and have shown partial regeneration after cryoinjury (Mizutani *et al*., 2016; Polizzotti *et al*., 2016; Strungs *et al*., 2013). I could assess NRP expression profiles in neonatal mammals and generate inducible cell type-specific NRP knockouts to investigate whether NRP function is important in mammalian heart regeneration.

Functional assays and signalling experiments of adult zebrafish primary epicardial cultures is limited due to low cell numbers in outgrowths and lack of reagents specific to zebrafish proteins and pathways. One way to circumvent limitations of epicardial *in vitro* zebrafish studies, would be to model epicardial physiology in an established and immortalised rat embryonic epicardial cell line (Wada *et al*., 2003). These studies were commenced during the thesis, but it was not possible to generate data supporting robust conclusions. The intention of these studies was to identify candidate epicardial signal pathways modulated by NRPs using pharmacological agents and transfections. Neuropilin expression can be manipulated using siRNA and adenovirus *in vitro* and growth factors can be exogenously supplied into the culture medium to stimulate isolated pathways. This permits the opportunity to characterise NRP activity in response to specific signals. Additionally, functional assays are possible in the rat epicardial cell line. For example, NRPs are regulators of cell migration and the transwell migration assay could be applied to epicardial cells *in vitro* to monitor epicardial cell chemotaxis towards a gradient of candidate chemokines (Figure 62) following NRP-knockdown or upregulation. The number of migrated cells toward stimulant could help deduce the physiological role of neuropilins in epicardial migration. I would expect the chemotactic

response to be impaired in the absence of NRPs and provide a mammalian system that supports observations in zebrafish epicardial outgrowths.

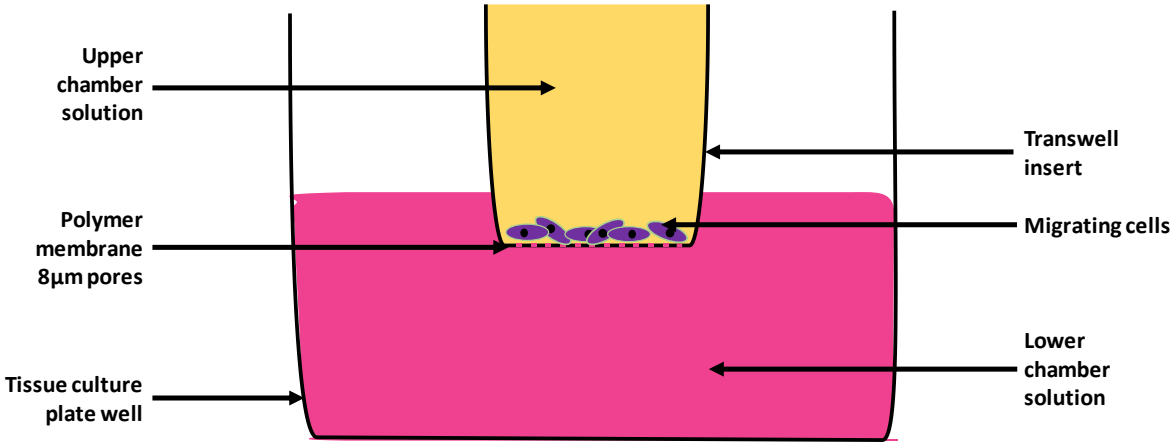

Figure 62 Schematic representation of transwell migration assay

An insert containing cells intended for assessment of migration properties in a serum-free medium is placed into a tissue culture plate well. The well contains either serum-free medium (for control experiments) or serum-free medium supplemented with chemotactic stimuli (such as growth factors). Cells that respond to the chemoattractant migrate through the insert pores towards the chemotactic signals and adhere to the other side of the membrane.

7.5.4 Implications for translational research

Given that Nrp1a and possibly other Nrps are important for cardiac recovery, they could serve as therapeutic targets in mammalian cardiac repair post-MI. This would require strong pre-clinical evidence for a role of NRPs in mammalian heart regeneration, which could be obtained in the neonatal mouse model, and also evidence that NRPs are implicated in the human heart following MI. For example, it could be examined whether NRP expression changes in human hearts after MI, if samples were available. Direct targeting of Nrps to promote a regenerative response would be difficult to achieve unless a way could be found specifically to 'activate' NRPs. NRP expression could be increased by delivery of viral vectors encoding NRPs. However, previous attempts to

stimulate therapeutic angiogenesis in ischaemic heart disease by over-expressing VEGF-A, for example, has not produced clear patient benefit (Zachary and Morgan, 2011).

7.6 Conclusions

The current models I propose for the role(s) of neuropilins in zebrafish heart regeneration are as follows. Nrp1a contributes to quiescent epicardial homeostasis, whereas Nrp2b is required for cardiomyocyte maintenance. Following cardiac damage, Nrp1a and Nrp2a are upregulated in the epicardium to increase epicardial sensitivity to injured tissue paracrine and autocrine factors. Their targeted expression also serves to enhance EMT and mediate chemotaxis of EPDCs into lesions to contribute mural cells and facilitate neovasculature maturation. The epicardial EMT response is likely recapitulated in the endocardium to promote endothelial to mesenchymal transition and this also requires Nrps to detect cellular cues. Invading neovessels require Nrp1 to respond to Vegfaa signals that induce angiogenesis to replenish blood supply in the injury lesion. Furthermore, Nrp1 expression is implicated in the response of migrating cardiomyocytes to mediate Pdgfbb-induced cell migration into the subepicardial fibrin matrix to facilitate compact myocardium recovery. Loss of *nrp1a* results in reduced compact myocardium replenishment and dampened epicardial activation and outgrowth expansion, which ultimately delay cardiac regeneration.

References

Adham, S. A. I., I. Al Harrasi, I. Al Haddabi, A. Al Rashdi, S. Al Sinawi, A. Al Maniri, T. Ba-Omar, and B. L. Coomber, 2014, Immunohistological Insight into the Correlation between Neuropilin-1 and Epithelial-Mesenchymal Transition Markers in Epithelial Ovarian Cancer: Journal of Histochemistry & Cytochemistry, v. 62, p. 619-631.

Aguiar, C., and K. R. Brunt, 2015, Wilms' tumor 1 (re)activation in evidence for both epicardial progenitor and endothelial cells for cardiovascular regeneration: Journal of Molecular and Cellular Cardiology, v. 84, p. 112-115.

Ali, S. R., S. Hippenmeyer, L. V. Saadat, L. Luo, I. L. Weissman, and R. Ardehali, 2014, Existing cardiomyocytes generate cardiomyocytes at a low rate after birth in mice: Proceedings of the National Academy of Sciences, v. 111, p. 8850-8855.

Amores, A., A. Force, Y. L. Yan, L. Joly, C. Amemiya, A. Fritz, R. K. Ho, J. Langeland, V. Prince, Y. L. Wang, M. Westerfield, M. Ekker, and J. H. Postlethwait, 1998, Zebrafish hox clusters and vertebrate genome evolution: Science, v. 282, p. 1711-4.

Appleton, B. A., P. Wu, J. Maloney, J. Yin, W. C. Liang, S. Stawicki, K. Mortara, K. K. Bowman, J. M. Elliott, W. Desmarais, J. F. Bazan, A. Bagri, M. Tessier-Lavigne, A. W. Koch, Y. Wu, R. J. Watts, and C. Wiesmann, 2007, Structural studies of neuropilin/antibody complexes provide insights into semaphorin and VEGF binding: Embo j, v. 26, p. 4902-12.

Armstrong, P. W., C. B. Granger, P. X. Adams, C. Hamm, D. Holmes, Jr., W. W. O'Neill, T. G. Todaro, A. Vahanian, and F. Van de Werf, 2007, Pexelizumab for acute ST-elevation myocardial infarction in patients undergoing primary percutaneous coronary intervention: a randomized controlled trial: Jama, v. 297, p. 43-51.

Ashikari-Hada, S., H. Habuchi, Y. Kariya, and K. Kimata, 2005, Heparin Regulates Vascular Endothelial Growth Factor165-dependent Mitogenic Activity, Tube Formation, and Its Receptor Phosphorylation of Human Endothelial Cells: Comparison Of The Effects Of Heparin And Modified Heparins: Journal of Biological Chemistry, v. 280, p. 31508-31515.

Aspalter, I. M., E. Gordon, A. Dubrac, A. Ragab, J. Narloch, P. Vizán, I. Geudens, R. T. Collins, C. A. Franco, C. L. Abrahams, G. Thurston, M. Fruttiger, I. Rosewell, A. Eichmann, and H. Gerhardt, 2015, Alk1 and Alk5 inhibition by Nrp1 controls vascular sprouting downstream of Notch: Nature Communications, v. 6, p. 7264.

Aung, N. Y., R. Ohe, H. Meng, T. Kabasawa, S. Yang, T. Kato, and M. Yamakawa, 2016, Specific Neuropilins Expression in Alveolar Macrophages among Tissue-Specific Macrophages: PLoS ONE, v. 11, p. e0147358.

Baeyens, N., C. Bandyopadhyay, B. G. Coon, S. Yun, and M. A. Schwartz, 2016, Endothelial fluid shear stress sensing in vascular health and disease: The Journal of Clinical Investigation, v. 126, p. 821-828.

Baker, K., K. S. Warren, G. Yellen, and M. C. Fishman, 1997, Defective "pacemaker" current (Ih) in a zebrafish mutant with a slow heart rate: Proc Natl Acad Sci U S A, v. 94, p. 4554-9.

Bakkers, J., 2011, Zebrafish as a model to study cardiac development and human cardiac disease: Cardiovasc Res, v. 91, p. 279-88.

Ball, S. G., C. A. Shuttleworth, and C. M. Kielty, 2007, Vascular endothelial growth factor can signal through platelet-derived growth factor receptors: The Journal of Cell Biology, v. 177, p. 489-500.

Banerjee, S., K. Sengupta, K. Dhar, S. Mehta, P. A. D'Amore, G. Dhar, and S. K. Banerjee, 2006, Breast cancer cells secreted platelet-derived growth factor-induced motility of vascular smooth muscle cells is mediated through neuropilin-1: Mol Carcinog, v. 45, p. 871-80.

Barrangou, R., C. Fremaux, H. Deveau, M. Richards, P. Boyaval, S. Moineau, D. A. Romero, and P. Horvath, 2007, CRISPR provides acquired resistance against viruses in prokaryotes: Science, v. 315, p. 1709-12.

Barrett, A., C. Pellet-Many, I. C. Zachary, I. M. Evans, and P. Frankel, 2013, p130Cas: a key signalling node in health and disease: Cell Signal, v. 25, p. 766-77.

Beck, G., and G. S. Habicht, 1991, Primitive cytokines: harbingers of vertebrate defense: Immunol Today, v. 12, p. 180-3.

Becker, J. R., T. Y. Robinson, C. Sachidanandan, A. E. Kelly, S. Coy, R. T. Peterson, and C. A. MacRae, 2012, *In vivo* natriuretic peptide reporter assay identifies chemical modifiers of hypertrophic cardiomyopathy signalling: Cardiovascular Research, v. 93, p. 463-470.

Becker, T., M. F. Wullimann, C. G. Becker, R. R. Bernhardt, and M. Schachner, 1997, Axonal regrowth after spinal cord transection in adult zebrafish: Journal of Comparative Neurology, v. 377, p. 577-595.

Bedell, V. M., Y. Wang, J. M. Campbell, T. L. Poshusta, C. G. Starker, R. G. Krug Ii, W. Tan, S. G. Penheiter, A. C. Ma, A. Y. H. Leung, S. C. Fahrenkrug, D. F. Carlson, D. F. Voytas, K. J. Clark, J. J. Essner, and S. C. Ekker, 2012, *In vivo* genome editing using a high-efficiency TALEN system: Nature, v. 491, p. 114-118.

Bellomo, D., J. P. Headrick, G. U. Silins, C. A. Paterson, P. S. Thomas, M. Gartside, A. Mould, M. M. Cahill, I. D. Tonks, S. M. Grimmond, S. Townson, C. Wells, M. Little, M. C. Cummings, N. K. Hayward, and G. F. Kay, 2000, Mice lacking the vascular endothelial growth factor-B gene (Vegfb) have smaller hearts, dysfunctional coronary vasculature, and impaired recovery from cardiac ischemia: Circ Res, v. 86, p. E29-35.

Berdougo, E., H. Coleman, D. H. Lee, D. Y. Stainier, and D. Yelon, 2003, Mutation of weak atrium/atrial myosin heavy chain disrupts atrial function and influences ventricular morphogenesis in zebrafish: Development, v. 130, p. 6121-9.

Bergmann, O., R. D. Bhardwaj, S. Bernard, S. Zdunek, F. Barnabe-Heider, S. Walsh, J. Zupicich, K. Alkass, B. A. Buchholz, H. Druid, S. Jovinge, and J. Frisen, 2009, Evidence for Cardiomyocyte Renewal in Humans: Science, v. 324, p. 98-102.

Bernhardt, R. R., E. Tongiorgi, P. Anzini, and M. Schachner, 1996, Increased expression of specific recognition molecules by retinal ganglion cells and by optic pathway

glia accompanies the successful regeneration of retinal axons in adult zebrafish: J Comp Neurol, v. 376, p. 253-64.

Berse, B., L. F. Brown, L. Van de Water, H. F. Dvorak, and D. R. Senger, 1992, Vascular permeability factor (vascular endothelial growth factor) gene is expressed differentially in normal tissues, macrophages, and tumors: Molecular Biology of the Cell, v. 3, p. 211-220.

Bilbija, D., F. Haugen, J. Sagave, A. Baysa, N. Bastani, F. O. Levy, A. Sirsjo, R. Blomhoff, and G. Valen, 2012, Retinoic acid signalling is activated in the postischemic heart and may influence remodelling: PLoS One, v. 7, p. e44740.

Bloomekatz, J., R. Singh, O. W. Prall, A. C. Dunn, M. Vaughan, C. S. Loo, R. P. Harvey, and D. Yelon, 2017, Platelet-derived growth factor (PDGF) signaling directs cardiomyocyte movement toward the midline during heart tube assembly: Elife, v. 6.

Bloomekatz, J., R. Singh, O. W. J. Prall, A. C. Dunn, M. Vaughan, C.-S. Loo, R. P. Harvey, and D. Yelon, 2016, PDGF signaling directs cardiomyocyte movement toward the midline during heart tube assembly: bioRxiv.

Bork, P., and G. Beckmann, 1993, The CUB domain. A widespread module in developmentally regulated proteins: J Mol Biol, v. 231, p. 539-45.

Bottcher, R. T., and C. Niehrs, 2005, Fibroblast growth factor signaling during early vertebrate development: Endocr Rev, v. 26, p. 63-77.

Bouvrée, K., I. Brunet, R. del Toro, E. Gordon, C. Prahst, B. Cristofaro, T. Mathivet, Y. Xu, J. Soueid, V. Fortuna, N. Miura, M.-S. Aigrot, C. H. Maden, C. Ruhrberg, J. L. Thomas, and A. Eichmann, 2012, Semaphorin3A, Neuropilin-1, and PlexinA1 Are Required for Lymphatic Valve Formation: Circulation research, v. 111, p. 10.1161/CIRCRESAHA.112.269316.

Bovenkamp, D. E., K. Goishi, N. Bahary, A. J. Davidson, Y. Zhou, T. Becker, C. G. Becker, L. I. Zon, and M. Klagsbrun, 2004, Expression and mapping of duplicate neuropilin-1 and neuropilin-2 genes in developing zebrafish: Gene Expression Patterns, v. 4, p. 361-370.

Braet, F., M. Shleper, M. Paizi, S. Brodsky, N. Kopeiko, N. Resnick, and G. Spira, 2004, Liver sinusoidal endothelial cell modulation upon resection and shear stress *in vitro*: Comp Hepatol, v. 3, p. 7.

Braitsch, M. C., and E. K. Yutzey, 2013, Transcriptional Control of Cell Lineage Development in Epicardium-Derived Cells: Journal of Developmental Biology, v. 1.

Brette, F., G. Luxan, C. Cros, H. Dixey, C. Wilson, and H. A. Shiels, 2008, Characterization of isolated ventricular myocytes from adult zebrafish (Danio rerio): Biochem Biophys Res Commun, v. 374, p. 143-6.

Brooks, W. W., S. S. Shen, C. H. Conrad, R. H. Goldstein, and O. H. L. Bing, 2010, Transition from compensated hypertrophy to systolic heart failure in the spontaneously hypertensive rat: Structure, function, and transcript analysis: Genomics, v. 95, p. 84-92.

Brown, D. R., L. A. Samsa, L. Qian, and J. Liu, 2016, Advances in the Study of Heart Development and Disease Using Zebrafish: J Cardiovasc Dev Dis, v. 3.

Brown, L. F., D. Dubin, L. Lavigne, B. Logan, H. F. Dvorak, and L. Van de Water, 1993, Macrophages and fibroblasts express embryonic fibronectins during cutaneous wound healing: The American Journal of Pathology, v. 142, p. 793-801.

Bryant, D. M., C. C. O'Meara, N. N. Ho, J. Gannon, L. Cai, and R. T. Lee, 2015, A systematic analysis of neonatal mouse heart regeneration after apical resection: Journal of Molecular and Cellular Cardiology, v. 79, p. 315-318.

Bui, A. L., T. B. Horwich, and G. C. Fonarow, 2011, Epidemiology and risk profile of heart failure: Nat Rev Cardiol, v. 8, p. 30-41.

Buja, L. M., and D. Vela, 2008, Cardiomyocyte death and renewal in the normal and diseased heart: Cardiovascular Pathology, v. 17, p. 349-374.

Burns, C. G., D. J. Milan, E. J. Grande, W. Rottbauer, C. A. MacRae, and M. C. Fishman, 2005, High-throughput assay for small molecules that modulate zebrafish embryonic heart rate: Nat Chem Biol, v. 1, p. 263-264.

Bussmann, J., J. Bakkers, and S. Schulte-Merker, 2007, Early endocardial morphogenesis requires Scl/Tal1: PLoS Genet, v. 3, p. e140.

Cackowski, F. C., L. Xu, B. Hu, and S. Y. Cheng, 2004, Identification of two novel alternatively spliced Neuropilin-1 isoforms: Genomics, v. 84, p. 82-94.

Cai, C.-L., J. C. Martin, Y. Sun, L. Cui, L. Wang, K. Ouyang, L. Yang, L. Bu, X. Liang, X. Zhang, W. B. Stallcup, C. P. Denton, A. McCulloch, J. Chen, and S. M. Evans, 2008, A myocardial lineage derives from Tbx18 epicardial cells: Nature, v. 454, p. 104-U4.

Cai, C. L., X. Liang, Y. Shi, P. H. Chu, S. L. Pfaff, J. Chen, and S. Evans, 2003, Isl1 identifies a cardiac progenitor population that proliferates prior to differentiation and contributes a majority of cells to the heart: Dev Cell, v. 5, p. 877-89.

Cai, H. B., and R. R. Reed, 1999, Cloning and characterization of neuropilin-1-interacting protein: A PSD-95/Dlg/ZO-1 domain-containing protein that interacts with the cytoplasmic domain of neuropilin-1: Journal of Neuroscience, v. 19, p. 6519-6527.

Cao, S., U. Yaqoob, A. Das, U. Shergill, K. Jagavelu, R. C. Huebert, C. Routray, S. Abdelmoneim, M. Vasdev, E. Leof, M. Charlton, R. J. Watts, D. Mukhopadhyay, and V. H. Shah, 2010a, Neuropilin-1 promotes cirrhosis of the rodent and human liver by enhancing PDGF/TGF-β signaling in hepatic stellate cells: The Journal of Clinical Investigation, v. 120, p. 2379-2394.

Cao, Y., 2009, Positive and Negative Modulation of Angiogenesis by VEGFR1 Ligands: Science Signaling, v. 2, p. re1.

Cao, Y., A. Szabolcs, S. K. Dutta, U. Yaqoob, K. Jagavelu, L. Wang, E. B. Leof, R. A. Urrutia, V. H. Shah, and D. Mukhopadhyay, 2010b, Neuropilin-1 Mediates Divergent R-Smad Signaling and the Myofibroblast Phenotype: The Journal of Biological Chemistry, v. 285, p. 31840-31848.

Carmeliet, P., V. Ferreira, G. Breier, S. Pollefeyt, L. Kieckens, M. Gertsenstein, M. Fahrig, A. Vandenhoeck, K. Harpal, C. Eberhardt, C. Declercq, J. Pawling, L. Moons, D. Collen, W. Risau, and A. Nagy, 1996, Abnormal blood vessel development and lethality in embryos lacking a single VEGF allele: Nature, v. 380, p. 435-439.

Casari, A., M. Schiavone, N. Facchinello, A. Vettori, D. Meyer, N. Tiso, E. Moro, and F. Argenton, 2014, A Smad3 transgenic reporter reveals TGF-beta control of zebrafish spinal cord development: Developmental Biology, v. 396, p. 81-93.

Chablais, F., and A. Jazwinska, 2012, The regenerative capacity of the zebrafish heart is dependent on TGF beta signaling: Development, v. 139, p. 1921-1930.

Chablais, F., J. Veit, G. Rainer, and A. Jazwinska, 2011, The zebrafish heart regenerates after cryoinjury-induced myocardial infarction: Bmc Developmental Biology, v. 11.

Chaffer, C. L., B. P. San Juan, E. Lim, and R. A. Weinberg, 2016, EMT, cell plasticity and metastasis: Cancer Metastasis Rev.

Chang, N., C. Sun, L. Gao, D. Zhu, X. Xu, X. Zhu, J. W. Xiong, and J. J. Xi, 2013, Genome editing with RNA-guided Cas9 nuclease in zebrafish embryos: Cell Res, v. 23, p. 465-72.

Chen, H., A. Chedotal, Z. He, C. S. Goodman, and M. Tessier-Lavigne, 1997, Neuropilin-2, a novel member of the neuropilin family, is a high affinity receptor for the semaphorins Sema E and Sema IV but not Sema III: Neuron, v. 19, p. 547-59.

Chen, H. I., B. Sharma, B. N. Akerberg, H. J. Numi, R. Kivela, P. Saharinen, H. Aghajanian, A. S. McKay, P. E. Bogard, A. H. Chang, A. H. Jacobs, J. A. Epstein, K. Stankunas, K. Alitalo, and K. Red-Horse, 2014, The sinus venosus contributes to coronary vasculature through VEGFC-stimulated angiogenesis: Development, v. 141, p. 4500-12.

Chen, R.-H., Y.-G. Li, K.-L. Jiao, P.-P. Zhang, Y. Sun, L.-P. Zhang, X.-F. Fong, W. Li, and Y. Yu, 2013, Overexpression of sema3a in myocardial infarction border zone decreases vulnerability of ventricular tachycardia post-myocardial infarction in rats: Journal of Cellular and Molecular Medicine, v. 17, p. 608-616.

Chen, T. H. P., T. C. Chang, J. O. Kang, B. Choudhary, T. Makita, C. M. Tran, J. B. E. Burch, H. Eid, and H. M. Sucov, 2002, Epicardial induction of fetal cardiomyocyte proliferation via a retinoic acid-inducible trophic factor: Developmental Biology, v. 250, p. 198-207.

Chi, N. C., R. M. Shaw, S. De Val, G. Kang, L. Y. Jan, B. L. Black, and D. Y. R. Stainier, 2008, Foxn4 directly regulates tbx2b expression and atrioventricular canal formation: Genes & Development, v. 22, p. 734-739.

Chocron, S., M. C. Verhoeven, F. Rentzsch, M. Hammerschmidt, and J. Bakkers, 2007, Zebrafish Bmp4 regulates left–right asymmetry at two distinct developmental time points: Developmental Biology, v. 305, p. 577-588.

Chong, J. J., V. Chandrakanthan, M. Xaymardan, N. S. Asli, J. Li, I. Ahmed, C. Heffernan, M. K. Menon, C. J. Scarlett, A. Rashidianfar, C. Biben, H. Zoellner, E. K. Colvin, J. E. Pimanda, A. V. Biankin, B. Zhou, W. T. Pu, O. W. Prall, and R. P. Harvey, 2011, Adult cardiac-resident MSC-like stem cells with a proepicardial origin: Cell Stem Cell, v. 9, p. 527-40.

Christia, P., M. Bujak, C. Gonzalez-Quesada, W. Chen, M. Dobaczewski, A. Reddy, and N. G. Frangogiannis, 2013, Systematic characterization of myocardial inflammation, repair, and remodeling in a mouse model of reperfused myocardial infarction: J Histochem Cytochem, v. 61, p. 555-70.

Chu, W. M., X. M. Song, X. M. Yang, L. Ma, J. Zhu, M. Y. He, Z. L. Wang, and Y. N. Wu, 2014, Neuropilin-1 Promotes Epithelial-to-Mesenchymal Transition by Stimulating Nuclear Factor-Kappa B and Is Associated with Poor Prognosis in Human Oral Squamous Cell Carcinoma: Plos One, v. 9.

Clark, R. A. F., 1988, Wound Repair, *in* R. A. F. Clark, ed., The Molecular and Cellular Biology of Wound Repair: Boston, MA, Springer US, p. 3-50.

Cleutjens, J. P. M., M. J. A. Verluyten, J. F. M. Smits, and M. Daemen, 1995, COLLAGEN REMODELING AFTER MYOCARDIAL-INFARCTION IN THE RAT-HEART: American Journal of Pathology, v. 147, p. 325-338.

Cochain, C., K. M. Channon, and J.-S. Silvestre, 2013, Angiogenesis in the Infarcted Myocardium: Antioxidants & Redox Signaling, v. 18, p. 1100-1113.

Coghill, E. L., A. Hugill, N. Parkinson, C. Davison, P. Glenister, S. Clements, J. Hunter, R. D. Cox, and S. D. Brown, 2002, A gene-driven approach to the identification of ENU mutants in the mouse: Nat Genet, v. 30, p. 255-6.

Cudmore, M. J., P. W. Hewett, S. Ahmad, K. Q. Wang, M. Cai, B. Al-Ani, T. Fujisawa, B. Ma, S. Sissaoui, W. Ramma, M. R. Miller, D. E. Newby, Y. Gu, B. Barleon, H. Weich, and A. Ahmed, 2012, The role of heterodimerization between VEGFR-1 and VEGFR-2 in the regulation of endothelial cell homeostasis: Nat Commun, v. 3, p. 972.

D'Aniello, E., A. B. Rydeen, J. L. Anderson, A. Mandal, and J. S. Waxman, 2013, Depletion of retinoic acid receptors initiates a novel positive feedback mechanism that promotes teratogenic increases in retinoic acid: PLoS Genet, v. 9, p. e1003689.

Darehzereshki, A., N. Rubin, L. Gamba, J. Kim, J. Fraser, Y. Huang, J. Billings, R. Mohammadzadeh, J. Wood, D. Warburton, V. Kaartinen, and C.-L. Lien, 2015, Differential Regenerative Capacity of Neonatal Mouse Hearts after Cryoinjury: Developmental biology, v. 399, p. 91-99.

Davis, A. P., and M. J. Justice, 1998, An Oak Ridge legacy: the specific locus test and its role in mouse mutagenesis: Genetics, v. 148, p. 7-12.

Dawid, I. B., 1987, GENE ACTIVITY IN EARLY DEVELOPMENT, 3RD EDITION - DAVIDSON,EH: Science, v. 235, p. 695-695.

de Pater, E., L. Clijsters, S. R. Marques, Y. F. Lin, Z. V. Garavito-Aguilar, D. Yelon, and J. Bakkers, 2009, Distinct phases of cardiomyocyte differentiation regulate growth of the zebrafish heart: Development, v. 136, p. 1633-41.

de Preux Charles, A.-S., T. Bise, F. Baier, J. Marro, and A. Jaźwińska, 2016a, Distinct effects of inflammation on preconditioning and regeneration of the adult zebrafish heart: Open Biology, v. 6, p. 160102.

de Preux Charles, A.-S., T. Bise, F. Baier, P. Sallin, and A. Jaźwińska, 2016b, Preconditioning boosts regenerative programmes in the adult zebrafish heart: Open Biology, v. 6.

De Smet, F., B. Tembuyser, A. Lenard, F. Claes, J. Zhang, C. Michielsen, A. Van Schepdael, J. M. Herbert, F. Bono, M. Affolter, M. Dewerchin, and P. Carmeliet, 2014, Fibroblast growth factor signaling affects vascular outgrowth and is required for the maintenance of blood vessel integrity: Chem Biol, v. 21, p. 1310-7.

Dejda, A., G. Mawambo, A. Cerani, K. Miloudi, Z. Shao, J. F. Daudelin, S. Boulet, M. Oubaha, F. Beaudoin, N. Akla, S. Henriques, C. Menard, A. Stahl, J. S. Delisle, F. A. Rezende, N. Labrecque, and P. Sapieha, 2014, Neuropilin-1 mediates myeloid cell chemoattraction and influences retinal neuroimmune crosstalk: J Clin Invest, v. 124, p. 4807-22.

Dell, A. L., E. Fried-Cassorla, H. Xu, and J. A. Raper, 2013, cAMP-induced expression of neuropilin1 promotes retinal axon crossing in the zebrafish optic chiasm: J Neurosci, v. 33, p. 11076-88.

Deng, Y., X. Zhang, and M. Simons, 2015, Molecular Controls of Lymphatic VEGFR3 Signaling<span hwp:id="article-title-27" class="sub-article-title">Significance</span&gt: Arteriosclerosis, Thrombosis, and Vascular Biology, v. 35, p. 421.

Derynck, R., and R. J. Akhurst, 2007, Differentiation plasticity regulated by TGF-[beta] family proteins in development and disease: Nat Cell Biol, v. 9, p. 1000-1004.

Dettman, R. W., W. Denetclaw, Jr., C. P. Ordahl, and J. Bristow, 1998, Common epicardial origin of coronary vascular smooth muscle, perivascular fibroblasts, and intermyocardial fibroblasts in the avian heart: Dev Biol, v. 193, p. 169-81.

Deuel, T. F., J. S. Huang, R. T. Proffitt, J. U. Baenziger, D. Chang, and B. B. Kennedy, 1981, Human platelet-derived growth factor. Purification and resolution into two active protein fractions: J Biol Chem, v. 256, p. 8896-9.

Dhar, K., G. Dhar, M. Majumder, I. Haque, S. Mehta, P. J. Van Veldhuizen, S. K. Banerjee, and S. Banerjee, 2010, Tumor cell-derived PDGF-B potentiates mouse mesenchymal stem cells-pericytes transition and recruitment through an interaction with NRP-1: Mol Cancer, v. 9, p. 209.

Dick, A., T. Mayr, H. Bauer, A. Meier, and M. Hammerschmidt, 2000, Cloning and characterization of zebrafish smad2, smad3 and smad4: Gene, v. 246, p. 69-80.

Dimmeler, S., A. M. Zeiher, and M. D. Schneider, 2005, Unchain my heart: the scientific foundations of cardiac repair: J Clin Invest, v. 115, p. 572-83.

Ding, M. M, N. A, B. C, K. JC, C. TR, and B. M, 2015, Neuropilin-2 Identifies Cardiovascular PrecursorCells and is Required for Vascular Differentiation in Murine Embryonic Stem Cells System, J Stem Cell Res Transplant. .

Dixelius, J., T. Makinen, M. Wirzenius, M. J. Karkkainen, C. Wernstedt, K. Alitalo, and L. Claesson-Welsh, 2003, Ligand-induced vascular endothelial growth factor receptor-3 (VEGFR-3) heterodimerization with VEGFR-2 in primary lymphatic endothelial cells regulates tyrosine phosphorylation sites: J Biol Chem, v. 278, p. 40973-9.

Dobaczewski, M., M. Bujak, P. Zymek, G. Ren, M. L. Entman, and N. G. Frangogiannis, 2006, Extracellular matrix remodeling in canine and mouse myocardial infarcts: Cell Tissue Res, v. 324, p. 475-88.

Dobaczewski, M., C. Gonzalez-Quesada, and N. G. Frangogiannis, 2010, The extracellular matrix as a modulator of the inflammatory and reparative response following myocardial infarction: J Mol Cell Cardiol, v. 48, p. 504-11.

Domian, I. J., M. Chiravuri, P. van der Meer, A. W. Feinberg, X. Shi, Y. Shao, S. M. Wu, K. K. Parker, and K. R. Chien, 2009, Generation of functional ventricular heart muscle from mouse ventricular progenitor cells: Science, v. 326, p. 426-9.

Dutta, S., S. Roy, N. S. Polavaram, G. B. Baretton, M. H. Muders, S. Batra, and K. Datta, 2016, NRP2 transcriptionally regulates its downstream effector WDFY1: Scientific Reports, v. 6, p. 23588.

Dyer, L. A., and M. L. Kirby, 2009, Sonic hedgehog maintains proliferation in secondary heart field progenitors and is required for normal arterial pole formation: Dev Biol, v. 330, p. 305-17.

Eisen, J. S., and J. C. Smith, 2008, Controlling morpholino experiments: don't stop making antisense: Development, v. 135, p. 1735-43.

Eisenberg, L. M., and R. R. Markwald, 1995, Molecular Regulation of Atrioventricular Valvuloseptal Morphogenesis: Circulation Research, v. 77, p. 1.

Ellertsdottir, E., A. Lenard, Y. Blum, A. Krudewig, L. Herwig, M. Affolter, and H. G. Belting, 2010, Vascular morphogenesis in the zebrafish embryo: Dev Biol, v. 341, p. 56-65.

Ellison, G. M., C. Vicinanza, A. J. Smith, I. Aquila, A. Leone, C. D. Waring, B. J. Henning, G. G. Stirparo, R. Papait, M. Scarfo, V. Agosti, G. Viglietto, G. Condorelli, C. Indolfi, S. Ottolenghi, D. Torella, and B. Nadal-Ginard, 2013, Adult c-kit(pos) Cardiac Stem Cells Are Necessary and Sufficient for Functional Cardiac Regeneration and Repair: Cell, v. 154, p. 827-842.

Engel, F. B., M. Schebesta, M. T. Duong, G. Lu, S. X. Ren, J. B. Madwed, H. P. Jiang, Y. Wang, and M. T. Keating, 2005, P38 MAP kinase inhibition enables proliferation of adult mammalian cardiomyocytes: Genes & Development, v. 19, p. 1175-1187.

Etoh, T., C. Joffs, A. M. Deschamps, J. Davis, K. Dowdy, J. Hendrick, S. Baicu, R. Mukherjee, M. Manhaini, and F. G. Spinale, 2001, Myocardial and interstitial matrix metalloproteinase activity after acute myocardial infarction in pigs: American Journal of Physiology - Heart and Circulatory Physiology, v. 281, p. H987.

Evans, I. M., M. Yamaji, G. Britton, C. Pellet-Many, C. Lockie, I. C. Zachary, and P. Frankel, 2011, Neuropilin-1 Signaling through p130Cas Tyrosine Phosphorylation Is Essential for Growth Factor-Dependent Migration of Glioma and Endothelial Cells: Molecular and Cellular Biology, v. 31, p. 1174-1185.

Evans, M. A., N. Smart, K. N. Dube, S. Bollini, J. E. Clark, H. G. Evans, L. S. Taams, R. Richardson, M. Levesque, P. Martin, K. Mills, J. Riegler, A. N. Price, M. F. Lythgoe, and P. R. Riley, 2013, Thymosin beta4-sulfoxide attenuates inflammatory cell infiltration and promotes cardiac wound healing: Nat Commun, v. 4, p. 2081.

Fang, Y., V. Gupta, R. Karra, J. E. Holdway, K. Kikuchi, and K. D. Poss, 2013, Translational profiling of cardiomyocytes identifies an early Jak1/Stat3 injury response required for zebrafish heart regeneration: Proc Natl Acad Sci U S A, v. 110, p. 13416-21.

Fantin, A., B. Herzog, M. Mahmoud, M. Yamaji, A. Plein, L. Denti, C. Ruhrberg, and I. Zachary, 2014, Neuropilin 1 (NRP1) hypomorphism combined with defective

VEGF-A binding reveals novel roles for NRP1 in developmental and pathological angiogenesis: Development, v. 141, p. 556-62.

Fantin, A., J. M. Vieira, G. Gestri, L. Denti, Q. Schwarz, S. Prykhozhij, F. Peri, S. W. Wilson, and C. Ruhrberg, 2010, Tissue macrophages act as cellular chaperones for vascular anastomosis downstream of VEGF-mediated endothelial tip cell induction: Blood, v. 116, p. 829-40.

Faxon, D. P., R. J. Gibbons, N. A. Chronos, P. A. Gurbel, and F. Sheehan, 2002, The effect of blockade of the CD11/CD18 integrin receptor on infarct size in patients with acute myocardial infarction treated with direct angioplasty: the results of the HALT-MI study: J Am Coll Cardiol, v. 40, p. 1199-204.

Feldner, J., T. Becker, K. Goishi, J. Schweitzer, P. Lee, M. Schachner, M. Klagsbrun, and C. G. Becker, 2005, Neuropilin-1a is involved in trunk motor axon outgrowth in embryonic zebrafish: Dev Dyn, v. 234, p. 535-49.

Ferrara, N., 2010, Binding to the Extracellular Matrix and Proteolytic Processing: Two Key Mechanisms Regulating Vascular Endothelial Growth Factor Action: Molecular Biology of the Cell, v. 21, p. 687-690.

Fish, J. E., J. D. Wythe, T. Xiao, B. G. Bruneau, D. Y. R. Stainier, D. Srivastava, and S. Woo, 2011, A Slit/miR-218/Robo regulatory loop is required during heart tube formation in zebrafish: Development, v. 138, p. 1409.

Frangogiannis, N. G., 2006, Targeting the inflammatory response in healing myocardial infarcts: Curr Med Chem, v. 13, p. 1877-93.

Frangogiannis, N. G., L. H. Mendoza, G. Ren, S. Akrivakis, P. L. Jackson, L. H. Michael, C. W. Smith, and M. L. Entman, 2003, MCSF expression is induced in healing myocardial infarcts and may regulate monocyte and endothelial cell phenotype: Am J Physiol Heart Circ Physiol, v. 285, p. H483-92.

Frankel, P., C. Pellet-Many, P. Lehtolainen, G. M. D'Abaco, M. L. Tickner, L. Cheng, and I. C. Zachary, 2008, Chondroitin sulphate-modified neuropilin 1 is expressed in human tumour cells and modulates 3D invasion in the U87MG human glioblastoma cell line through a p130Cas-mediated pathway: EMBO Rep, v. 9, p. 983-9.

Frantz, S., J. Bauersachs, and G. Ertl, 2009, Post-infarct remodelling: contribution of wound healing and inflammation: Cardiovasc Res, v. 81, p. 474-81.

Fuh, G., K. C. Garcia, and A. M. de Vos, 2000, The interaction of neuropilin-1 with vascular endothelial growth factor and its receptor flt-1: J Biol Chem, v. 275, p. 26690-5.

Fujisawa, H., T. Ohtsuki, S. Takagi, and T. Tsuji, 1989, An aberrant retinal pathway and visual centers in Xenopus tadpoles share a common cell surface molecule, A5 antigen: Dev Biol, v. 135, p. 231-40.

Fujisawa, H., S. Takagi, and T. Hirata, 1995, Growth-associated expression of a membrane protein, neuropilin, in Xenopus optic nerve fibers: Dev Neurosci, v. 17, p. 343-9.

Gaboriaud, C., L. Gregory-Pauron, F. Teillet, N. M. Thielens, I. Bally, and G. J. Arlaud, 2011, Structure and properties of the Ca(2+)-binding CUB domain, a widespread ligand-recognition unit involved in major biological functions: Biochem J, v. 439, p. 185-93.

Gagnon, M. L., D. R. Bielenberg, Z. Gechtman, H. Q. Miao, S. Takashima, S. Soker, and M. Klagsbrun, 2000, Identification of a natural soluble neuropilin-1 that binds vascular endothelial growth factor: *In vivo* expression and antitumor activity: Proc Natl Acad Sci U S A, v. 97, p. 2573-8.

Garavito-Aguilar, Z. V., H. E. Riley, and D. Yelon, 2010, Hand2 ensures an appropriate environment for cardiac fusion by limiting Fibronectin function: Development, v. 137, p. 3215-3220.

Garbern, Jessica C., and Richard T. Lee, 2013, Cardiac Stem Cell Therapy and the Promise of Heart Regeneration: Cell Stem Cell, v. 12, p. 689-698.

Gassmann, M., F. Casagranda, D. Orioli, H. Simon, C. Lai, R. Klein, and G. Lemke, 1995, Aberrant neural and cardiac development in mice lacking the ErbB4 neuregulin receptor: Nature, v. 378, p. 390-4.

Gaziano, T. A., 2007, Reducing the growing burden of cardiovascular disease in the developing world: Health Aff (Millwood), v. 26, p. 13-24.

Gemmill, R. M., P. Nasarre, J. Nair-Menon, F. Cappuzzo, L. Landi, A. D'Incecco, H. Uramoto, T. Yoshida, E. B. Haura, K. Armeson, and H. A. Drabkin, 2017, The neuropilin 2 isoform NRP2b uniquely supports TGFbeta-mediated progression in lung cancer: Sci Signal, v. 10.

George, E. L., H. S. Baldwin, and R. O. Hynes, 1997, Fibronectins are essential for heart and blood vessel morphogenesis but are dispensable for initial specification of precursor cells: Blood, v. 90, p. 3073-81.

Gerhardt, H., C. Ruhrberg, A. Abramsson, H. Fujisawa, D. Shima, and C. Betsholtz, 2004, Neuropilin-1 is required for endothelial tip cell guidance in the developing central nervous system: Developmental Dynamics, v. 231, p. 503-509.

Giordano, A., P. Cesari, L. Capparuccia, M. Castellucci, and S. Cinti, 2003, Sema3A and neuropilin-1 expression and distribution in rat white adipose tissue: J Neurocytol, v. 32, p. 345-52.

Giraudo, E., L. Primo, E. Audero, H. P. Gerber, P. Koolwijk, S. Soker, M. Klagsbrun, N. Ferrara, and F. Bussolino, 1998, Tumor necrosis factor-alpha regulates expression of vascular endothelial growth factor receptor-2 and of its co-receptor neuropilin-1 in human vascular endothelial cells: J Biol Chem, v. 273, p. 22128-35.

Glinka, Y., and G. J. Prud'homme, 2008, Neuropilin-1 is a receptor for transforming growth factor beta-1, activates its latent form, and promotes regulatory T cell activity: Journal of Leukocyte Biology, v. 84, p. 302-310.

Glinka, Y., S. Stoilova, N. Mohammed, and G. J. Prud'homme, 2011, Neuropilin-1 exerts co-receptor function for TGF-beta-1 on the membrane of cancer cells and enhances responses to both latent and active TGF-beta: Carcinogenesis, v. 32, p. 613-621.

Gluzman-Poltorak, Z., T. Cohen, Y. Herzog, and G. Neufeld, 2000, Neuropilin-2 and Neuropilin-1 Are Receptors for the 165-Amino Acid Form of Vascular Endothelial Growth Factor (VEGF) and of Placenta Growth Factor-2, but Only Neuropilin-2 Functions as a Receptor for the 145-Amino Acid Form of VEGF: Journal of Biological Chemistry, v. 275, p. 18040-18045.

Gluzman-Poltorak, Z., T. Cohen, M. Shibuya, and G. Neufeld, 2001, Vascular endothelial growth factor receptor-1 and neuropilin-2 form complexes: J Biol Chem, v. 276, p. 18688-94.

Gonzalez-Iriarte, M., R. Carmona, J. M. Perez-Pomares, D. Macias, M. Costell, and R. Munoz-Chapuli, 2003, Development of the coronary arteries in a murine model of transposition of great arteries: J Mol Cell Cardiol, v. 35, p. 795-802.

Gonzalez-Rosa, J. M., and N. Mercader, 2012, Cryoinjury as a myocardial infarction model for the study of cardiac regeneration in the zebrafish: Nature Protocols, v. 7, p. 782-788.

Grandclement, C., J. R. Pallandre, S. V. Degano, E. Viel, A. Bouard, J. Balland, J.-P. Remy-Martin, B. Simon, A. Rouleau, W. Boireau, M. Klagsbrun, C. Ferrand, and C. Borg, 2011, Neuropilin-2 Expression Promotes TGF-beta 1-Mediated Epithelial to Mesenchymal Transition in Colorectal Cancer Cells: Plos One, v. 6.

Griffin, K., R. Patient, and N. Holder, 1995, Analysis of FGF function in normal and no tail zebrafish embryos reveals separate mechanisms for formation of the trunk and the tail: Development, v. 121, p. 2983-94.

Grimes, A. C., and M. L. Kirby, 2009, The outflow tract of the heart in fishes: anatomy, genes and evolution: J Fish Biol, v. 74, p. 983-1036.

Gu, C. H., B. J. Limberg, G. B. Whitaker, B. Perman, D. J. Leahy, J. S. Rosenbaum, D. D. Ginty, and A. L. Kolodkin, 2002, Characterization of neuropilin-1 structural features that confer binding to semaphorin 3A and vascular endothelial growth factor 165: Journal of Biological Chemistry, v. 277, p. 18069-18076.

Gu, C. H., E. R. Rodriguez, D. V. Reimert, T. Z. Shu, B. Fritzsch, L. J. Richards, A. L. Kolodkin, and D. D. Ginty, 2003, Neuropilin-1 conveys semaphorin and VEGF signaling during neural and cardiovascular development: Developmental Cell, v. 5, p. 45-57.

Gupta, V., M. Gemberling, R. Karra, G. E. Rosenfeld, T. Evans, and K. D. Poss, 2013, An injury-responsive gata4 program shapes the zebrafish cardiac ventricle: Curr Biol, v. 23, p. 1221-7.

Gupta, V., and K. D. Poss, 2012, Clonally dominant cardiomyocytes direct heart morphogenesis: Nature, v. 484, p. 479-U102.

Guttmann-Raviv, N., N. Shraga-Heled, A. Varshavsky, C. Guimaraes-Sternberg, O. Kessler, and G. Neufeld, 2007, Semaphorin-3A and semaphorin-3F work together to repel endothelial cells and to inhibit their survival by induction of apoptosis: J Biol Chem, v. 282, p. 26294-305.

Haider, H. K., S. A. Akbar, and M. Ashraf, 2009, Angiomyogenesis for Myocardial Repair: Antioxidants & Redox Signaling, v. 11, p. 1929-1944.

Hami, D., A. C. Grimes, H. J. Tsai, and M. L. Kirby, 2011, Zebrafish cardiac development requires a conserved secondary heart field: Development, v. 138, p. 2389-98.

Hao, X., E. A. Silva, A. Mansson-Broberg, K. H. Grinnemo, A. J. Siddiqui, G. Dellgren, E. Wardell, L. A. Brodin, D. J. Mooney, and C. Sylven, 2007, Angiogenic effects of sequential release of VEGF-A165 and PDGF-BB with alginate hydrogels after myocardial infarction: Cardiovasc Res, v. 75, p. 178-85.

Harada, K., M. Friedman, J. J. Lopez, S. Y. Wang, J. Li, P. V. Prasad, J. D. Pearlman, E. R. Edelman, F. W. Sellke, and M. Simons, 1996, Vascular endothelial growth factor administration in chronic myocardial ischemia: Am J Physiol, v. 270, p. H1791-802.

Hardoon, S. L., P. H. Whincup, I. Petersen, S. Capewell, and R. W. Morris, 2011, Trends in longer-term survival following an acute myocardial infarction and prescribing of evidenced-based medications in primary care in the UK from 1991: a longitudinal population-based study: J Epidemiol Community Health, v. 65, p. 770-4.

Harrison, M. R. M., J. Bussmann, Y. Huang, L. Zhao, A. Osorio, C. G. Burns, C. E. Burns, H. M. Sucov, A. F. Siekmann, and C.-L. Lien, 2015, Chemokine guided angiogenesis directs coronary vasculature formation in zebrafish: Developmental cell, v. 33, p. 442-454.

Hassel, D., E. P. Scholz, N. Trano, O. Friedrich, S. Just, B. Meder, D. L. Weiss, E. Zitron, S. Marquart, B. Vogel, C. A. Karle, G. Seemann, M. C. Fishman, H. A. Katus, and W. Rottbauer, 2008, Deficient zebrafish ether-a-go-go-related gene channel gating causes short-QT syndrome in zebrafish reggae mutants: Circulation, v. 117, p. 866-75.

Haubner, B. J., M. Adamowicz-Brice, S. Khadayate, V. Tiefenthaler, B. Metzler, T. Aitman, and J. M. Penninger, 2012, Complete cardiac regeneration in a mouse model of myocardial infarction: Aging, v. 4, p. 966-977.

Haubner, B. J., J. Schneider, U. Schweigmann, T. Schuetz, W. Dichtl, C. Velik-Salchner, J. I. Stein, and J. M. Penninger, 2016, Functional Recovery of a Human Neonatal Heart After Severe Myocardial Infarction: Circ Res, v. 118, p. 216-21.

Haverinen, J., M. Hassinen, and M. Vornanen, 2007, Fish cardiac sodium channels are tetrodotoxin sensitive: Acta Physiol (Oxf), v. 191, p. 197-204.

He, Z., and M. Tessier-Lavigne, 1997, Neuropilin is a receptor for the axonal chemorepellent Semaphorin III: Cell, v. 90, p. 739-51.

Heil, M., and W. Schaper, 2004, Influence of Mechanical, Cellular, and Molecular Factors on Collateral Artery Growth (Arteriogenesis): Circulation Research, v. 95, p. 449.

Henri, O., C. Pouehe, M. Houssari, L. Galas, L. Nicol, F. Edwards-Levy, J. P. Henry, A. Dumesnil, I. Boukhalfa, S. Banquet, D. Schapman, C. Thuillez, V. Richard, P. Mulder, and E. Brakenhielm, 2016, Selective Stimulation of Cardiac Lymphangiogenesis Reduces Myocardial Edema and Fibrosis Leading to Improved Cardiac Function Following Myocardial Infarction: Circulation, v. 133, p. 1484-1497.

Henry, T. D., B. H. Annex, G. R. McKendall, M. A. Azrin, J. J. Lopez, F. J. Giordano, P. K. Shah, J. T. Willerson, R. L. Benza, D. S. Berman, C. M. Gibson, A. Bajamonde, A. C. Rundle, J. Fine, and E. R. McCluskey, 2003, The VIVA trial: Vascular endothelial growth factor in Ischemia for Vascular Angiogenesis: Circulation, v. 107, p. 1359-65.

Hirota, S., T. P. Clements, L. K. Tang, J. E. Morales, H. S. Lee, S. P. Oh, G. M. Rivera, D. S. Wagner, and J. H. McCarty, 2015, Neuropilin 1 balances β8 integrin-activated

TGFβ signaling to control sprouting angiogenesis in the brain: Development, v. 142, p. 4363-4373.

Holmes, D. I., and I. Zachary, 2005, The vascular endothelial growth factor (VEGF) family: angiogenic factors in health and disease: Genome Biol, v. 6, p. 209.

Holtzman, N. G., J. J. Schoenebeck, H. J. Tsai, and D. Yelon, 2007, Endocardium is necessary for cardiomyocyte movement during heart tube assembly: Development, v. 134, p. 2379-86.

Howe, K., M. D. Clark, C. F. Torroja, J. Torrance, C. Berthelot, M. Muffato, J. E. Collins, S. Humphray, K. McLaren, L. Matthews, S. McLaren, I. Sealy, M. Caccamo, C. Churcher, C. Scott, J. C. Barrett, R. Koch, G. J. Rauch, S. White, W. Chow, B. Kilian, L. T. Quintais, J. A. Guerra-Assuncao, Y. Zhou, Y. Gu, J. Yen, J. H. Vogel, T. Eyre, S. Redmond, R. Banerjee, J. X. Chi, B. Y. Fu, E. Langley, S. F. Maguire, G. K. Laird, D. Lloyd, E. Kenyon, S. Donaldson, H. Sehra, J. Almeida-King, J. Loveland, S. Trevanion, M. Jones, M. Quail, D. Willey, A. Hunt, J. Burton, S. Sims, K. McLay, B. Plumb, J. Davis, C. Clee, K. Oliver, R. Clark, C. Riddle, D. Eliott, G. Threadgold, G. Harden, D. Ware, B. Mortimer, G. Kerry, P. Heath, B. Phillimore, A. Tracey, N. Corby, M. Dunn, C. Johnson, J. Wood, S. Clark, S. Pelan, G. Griffiths, M. Smith, R. Glithero, P. Howden, N. Barker, C. Stevens, J. Harley, K. Holt, G. Panagiotidis, J. Lovell, H. Beasley, C. Henderson, D. Gordon, K. Auger, D. Wright, J. Collins, C. Raisen, L. Dyer, K. Leung, L. Robertson, K. Ambridge, D. Leongamornlert, S. McGuire, R. Gilderthorp, C. Griffiths, D. Manthravadi, S. Nichol, G. Barker, S. Whitehead, M. Kay, et al., 2013, The zebrafish reference genome sequence and its relationship to the human genome: Nature, v. 496, p. 498-503.

Hsieh, P. C. H., V. F. M. Segers, M. E. Davis, C. MacGillivray, J. Gannon, J. D. Molkentin, J. Robbins, and R. T. Lee, 2007, Evidence from a genetic fate-mapping study that stem cells refresh adult mammalian cardiomyocytes after injury: Nat Med, v. 13, p. 970-974.

Hu, N., E. B. Clark, and H. J. Yost, 2001, Cardiac morphology and blood pressure in the adult zebrafish: Faseb Journal, v. 15, p. A1231-A1231.

Huang, C. J., C. T. Tu, C. D. Hsiao, F. J. Hsieh, and H. J. Tsai, 2003, Germ-line transmission of a myocardium-specific GFP transgene reveals critical regulatory elements in the cardiac myosin light chain 2 promoter of zebrafish: Developmental Dynamics, v. 228, p. 30-40.

Huang, G. N., J. E. Thatcher, J. McAnally, Y. Kong, X. Qi, W. Tan, J. M. DiMaio, J. F. Amatruda, R. D. Gerard, J. A. Hill, R. Bassel-Duby, and E. N. Olson, 2012, C/EBP Transcription Factors Mediate Epicardial Activation During Heart Development and Injury: Science, v. 338, p. 1599-1603.

Huang, W. C., C. C. Yang, I. H. Chen, Y. M. Liu, S. J. Chang, and Y. J. Chuang, 2013, Treatment of Glucocorticoids Inhibited Early Immune Responses and Impaired Cardiac Repair in Adult Zebrafish: PLoS One, v. 8, p. e66613.

Hubner, G., M. Brauchle, H. Smola, M. Madlener, R. Fassler, and S. Werner, 1996, Differential regulation of pro-inflammatory cytokines during wound healing in normal and glucocorticoid-treated mice: Cytokine, v. 8, p. 548-56.

Huminiecki, L., L. Goldovsky, S. Freilich, A. Moustakas, C. Ouzounis, and C. H. Heldin, 2009, Emergence, development and diversification of the TGF-beta signalling pathway within the animal kingdom: BMC Evol Biol, v. 9, p. 28.

Huse, M., T. W. Muir, L. Xu, Y. G. Chen, J. Kuriyan, and J. Massague, 2001, The TGF beta receptor activation process: an inhibitor- to substrate-binding switch: Mol Cell, v. 8, p. 671-82.

Hwang, W. Y., Y. Fu, D. Reyon, M. L. Maeder, S. Q. Tsai, J. D. Sander, R. T. Peterson, J. R. J. Yeh, and J. K. Joung, 2013, Efficient genome editing in zebrafish using a CRISPR-Cas system: Nature Biotechnology, v. 31, p. 227-229.

Ieda, M., T. Tsuchihashi, K. N. Ivey, R. S. Ross, T.-T. Hong, R. M. Shaw, and D. Srivastava, 2009, Cardiac Fibroblasts Regulate Myocardial Proliferation through β1 Integrin Signaling: Developmental Cell, v. 16, p. 233-244.

Imanaka-Yoshida, K., M. Hiroe, T. Nishikawa, S. Ishiyama, T. Shimojo, Y. Ohta, T. Sakakura, and T. Yoshida, 2001, Tenascin-C modulates adhesion of cardiomyocytes to extracellular matrix during tissue remodeling after myocardial infarction: Lab Invest, v. 81, p. 1015-24.

Ito, N., C. Wernstedt, U. Engstrom, and L. Claesson-Welsh, 1998, Identification of vascular endothelial growth factor receptor-1 tyrosine phosphorylation sites and binding of SH2 domain-containing molecules: J Biol Chem, v. 273, p. 23410-8.

Itou, J., R. Akiyama, S. Pehoski, X. Yu, H. Kawakami, and Y. Kawakami, 2014, Regenerative responses after mild heart injuries for cardiomyocyte proliferation in zebrafish: Developmental dynamics : an official publication of the American Association of Anatomists, v. 243, p. 1477-86.

Itou, J., H. Kawakami, T. Burgoyne, and Y. Kawakami, 2012a, Life-long preservation of the regenerative capacity in the fin and heart in zebrafish: Biology open, v. 1, p. 739-46.

Itou, J., I. Oishi, H. Kawakami, T. J. Glass, J. Richter, A. Johnson, T. C. Lund, and Y. Kawakami, 2012b, Migration of cardiomyocytes is essential for heart regeneration in zebrafish: Development, v. 139, p. 4133-4142.

Jeltsch, M., A. Kaipainen, V. Joukov, X. Meng, M. Lakso, H. Rauvala, M. Swartz, D. Fukumura, R. K. Jain, and K. Alitalo, 1997, Hyperplasia of lymphatic vessels in VEGF-C transgenic mice: Science, v. 276, p. 1423-5.

Jenni, R., J. Rojas, and E. Oechslin, 1999, Isolated noncompaction of the myocardium: N Engl J Med, v. 340, p. 966-7.

Jennings, R. B., C. E. Murray, C. J. Steenbergen, and K. A. Reimer, 1990, DEVELOPMENT OF CELL INJURY IN SUSTAINED ACUTE ISCHEMIA: Circulation, v. 82, p. II2-II12.

Jensen, L. D., M. Nakamura, L. Brautigam, X. Li, Y. Liu, N. J. Samani, and Y. Cao, 2015, VEGF-B-Neuropilin-1 signaling is spatiotemporally indispensable for vascular and neuronal development in zebrafish: Proc Natl Acad Sci U S A, v. 112, p. E5944-53.

Ji, J. D., K. H. Park-Min, and L. B. Ivashkiv, 2009, Expression and function of semaphorin 3A and its receptors in human monocyte-derived macrophages: Hum Immunol, v. 70, p. 211-7.

Johnson, S. L., and J. A. Weston, 1995, Temperature-sensitive mutations that cause stage-specific defects in Zebrafish fin regeneration: Genetics, v. 141, p. 1583-95.

Jopling, C., E. Sleep, M. Raya, M. Marti, A. Raya, and J. C. Izpisua Belmonte, 2010, Zebrafish heart regeneration occurs by cardiomyocyte dedifferentiation and proliferation: Nature, v. 464, p. 606-U168.

Kabir, Z., K. Bennett, E. Shelley, B. Unal, J. A. Critchley, and S. Capewell, 2007, Comparing primary prevention with secondary prevention to explain decreasing Coronary Heart Disease death rates in Ireland, 1985-2000: Bmc Public Health, v. 7.

Kang, Y., C. R. Chen, and J. Massague, 2003, A self-enabling TGFbeta response coupled to stress signaling: Smad engages stress response factor ATF3 for Id1 repression in epithelial cells: Mol Cell, v. 11, p. 915-26.

Karra, R., A. K. Knecht, K. Kikuchi, and K. D. Poss, 2015, Myocardial NF-kappa B activation is essential for zebrafish heart regeneration: Proceedings of the National Academy of Sciences of the United States of America, v. 112, p. 13255-13260.

Katz, T. C., M. K. Singh, K. Degenhardt, J. Rivera-Feliciano, R. L. Johnson, J. A. Epstein, and C. J. Tabin, 2012, Distinct compartments of the proepicardial organ give rise to coronary vascular endothelial cells: Dev Cell, v. 22, p. 639-50.

Kawakami, T., T. Tokunaga, H. Hatanaka, H. Kijima, H. Yamazaki, Y. Abe, Y. Osamura, H. Inoue, Y. Ueyama, and M. Nakamura, 2002, Neuropilin 1 and neuropilin 2 co-expression is significantly correlated with increased vascularity and poor prognosis in nonsmall cell lung carcinoma: Cancer, v. 95, p. 2196-2201.

Kawamura, H., X. Li, K. Goishi, L. A. van Meeteren, L. Jakobsson, S. Cebe-Suarez, A. Shimizu, D. Edholm, K. Ballmer-Hofer, L. Kjellen, M. Klagsbrun, and L. Claesson-Welsh, 2008, Neuropilin-1 in regulation of VEGF-induced activation of p38MAPK and endothelial cell organization: Blood, v. 112, p. 3638-49.

Kawasaki, T., T. Kitsukawa, Y. Bekku, Y. Matsuda, M. Sanbo, T. Yagi, and H. Fujisawa, 1999, A requirement for neuropilin-1 in embryonic vessel formation: Development, v. 126, p. 4895-4902.

Keck, P. J., S. D. Hauser, G. Krivi, K. Sanzo, T. Warren, J. Feder, and D. T. Connolly, 1989, Vascular permeability factor, an endothelial cell mitogen related to PDGF: Science, v. 246, p. 1309.

Keegan, B. R., J. L. Feldman, G. Begemann, P. W. Ingham, and D. Yelon, 2005, Retinoic acid signaling restricts the cardiac progenitor pool: Science, v. 307, p. 247-9.

Kikuchi, K., V. Gupta, J. Wang, J. E. Holdway, A. A. Wills, Y. Fang, and K. D. Poss, 2011a, tcf21(+) epicardial cells adopt non-myocardial fates during zebrafish heart development and regeneration: Development, v. 138, p. 2895-2902.

Kikuchi, K., J. E. Holdway, R. J. Major, N. Blum, R. D. Dahn, G. Begemann, and K. D. Poss, 2011b, Retinoic Acid Production by Endocardium and Epicardium Is an Injury Response Essential for Zebrafish Heart Regeneration: Developmental Cell, v. 20, p. 397-404.

Kikuchi, K., J. E. Holdway, A. A. Werdich, R. M. Anderson, Y. Fang, G. F. Egnaczyk, T. Evans, C. A. MacRae, D. Y. R. Stainier, and K. D. Poss, 2010, Primary contribution to zebrafish heart regeneration by gata4(+) cardiomyocytes: Nature, v. 464, p. 601-U162.

Kikuchi, K., and K. D. Poss, 2012, Cardiac Regenerative Capacity and Mechanisms: Annual Review of Cell and Developmental Biology, Vol 28, v. 28, p. 719-741.

Kim, J., N. Rubin, Y. Huang, T. L. Tuan, and C. L. Lien, 2012, *In vitro* culture of epicardial cells from adult zebrafish heart on a fibrin matrix: Nature Protocols, v. 7, p. 247-255.

Kim, J., Q. Wu, Y. Zhang, K. M. Wiens, Y. Huang, N. Rubin, H. Shimada, R. I. Handin, M. Y. Chao, T.-L. Tuan, V. A. Starnes, and C.-L. Lien, 2010, PDGF signaling is required for epicardial function and blood vessel formation in regenerating zebrafish hearts: Proceedings of the National Academy of Sciences of the United States of America, v. 107, p. 17206-17210.

Kishimoto, Y., K. H. Lee, L. Zon, M. Hammerschmidt, and S. Schulte-Merker, 1997, The molecular nature of zebrafish swirl: BMP2 function is essential during early dorsoventral patterning: Development, v. 124, p. 4457-66.

Kitsukawa, T., M. Shimizu, M. Sanbo, T. Hirata, M. Taniguchi, Y. Bekku, T. Yagi, and H. Fujisawa, 1997, Neuropilin-semaphorin III/D-mediated chemorepulsive signals play a crucial role in peripheral nerve projection in mice: Neuron, v. 19, p. 995-1005.

Kitsukawa, T., A. Shimono, A. Kawakami, H. Kondoh, and H. Fujisawa, 1995, Overexpression of a membrane protein, neuropilin, in chimeric mice causes anomalies in the cardiovascular system, nervous system and limbs: Development, v. 121, p. 4309-4318.

Klinghoffer, R. A., T. G. Hamilton, R. Hoch, and P. Soriano, 2002, An allelic series at the PDGFalphaR locus indicates unequal contributions of distinct signaling pathways during development: Dev Cell, v. 2, p. 103-13.

Klotz, L., S. Norman, J. M. Vieira, M. Masters, M. Rohling, K. N. Dube, S. Bollini, F. Matsuzaki, C. A. Carr, and P. R. Riley, 2015, Cardiac lymphatics are heterogeneous in origin and respond to injury: Nature, v. 522, p. 62-U126.

Knowlton, A. A., C. M. Connelly, G. M. Romo, W. Mamuya, C. S. Apstein, and P. Brecher, 1992, Rapid expression of fibronectin in the rabbit heart after myocardial infarction with and without reperfusion: Journal of Clinical Investigation, v. 89, p. 1060-1068.

Koch, S., Laurens A. van Meeteren, E. Morin, C. Testini, S. Weström, H. Björkelund, S. Le Jan, J. Adler, P. Berger, and L. Claesson-Welsh, 2014, NRP1 Presented in trans to the Endothelium Arrests VEGFR2 Endocytosis, Preventing Angiogenic Signaling and Tumor Initiation: Developmental Cell, v. 28, p. 633-646.

Kok, F. O., M. Shin, C. W. Ni, A. Gupta, A. S. Grosse, A. van Impel, B. C. Kirchmaier, J. Peterson-Maduro, G. Kourkoulis, I. Male, D. F. DeSantis, S. Sheppard-Tindell, L. Ebarasi, C. Betsholtz, S. Schulte-Merker, S. A. Wolfe, and N. D. Lawson, 2015, Reverse genetic screening reveals poor correlation between morpholino-induced and mutant phenotypes in zebrafish: Dev Cell, v. 32, p. 97-108.

Kramer, R., N. Bucay, D. J. Kane, L. E. Martin, J. E. Tarpley, and L. E. Theill, 1996, Neuregulins with an Ig-like domain are essential for mouse myocardial and neuronal development: Proceedings of the National Academy of Sciences, v. 93, p. 4833-4838.

Kumar, S., N. Lockwood, M. C. Ramel, T. Correia, M. Ellis, Y. Alexandrov, N. Andrews, R. Patel, L. Bugeon, M. J. Dallman, S. Brandner, S. Arridge, M. Katan, J. McGinty, P.

Frankel, and P. M. French, 2016, Quantitative *in vivo* optical tomography of cancer progression & vasculature development in adult zebrafish: Oncotarget.
Kupatt, C., and R. Hinkel, 2014, VEGF-B: a more balanced approach toward cardiac neovascularization?: EMBO Molecular Medicine, v. 6, p. 297-298.
Kupperman, E., S. An, N. Osborne, S. Waldron, and D. Y. Stainier, 2000, A sphingosine-1-phosphate receptor regulates cell migration during vertebrate heart development: Nature, v. 406, p. 192-5.
Kyritsis, N., C. Kizil, S. Zocher, V. Kroehne, J. Kaslin, D. Freudenreich, A. Iltzsche, and M. Brand, 2012, Acute inflammation initiates the regenerative response in the adult zebrafish brain: Science, v. 338, p. 1353-6.
Laflamme, M. A., and C. E. Murry, 2011, Heart regeneration: Nature, v. 473, p. 326-335.
Lahteenvuo, J. E., M. T. Lahteenvuo, A. Kivela, C. Rosenlew, A. Falkevall, J. Klar, T. Heikura, T. T. Rissanen, E. Vahakangas, P. Korpisalo, B. Enholm, P. Carmeliet, K. Alitalo, U. Eriksson, and S. Yla-Herttuala, 2009, Vascular endothelial growth factor-B induces myocardium-specific angiogenesis and arteriogenesis via vascular endothelial growth factor receptor-1- and neuropilin receptor-1-dependent mechanisms: Circulation, v. 119, p. 845-56.
Lai, D., X. Liu, A. Forrai, O. Wolstein, J. Michalicek, I. Ahmed, A. N. Garratt, C. Birchmeier, M. Zhou, L. Hartley, L. Robb, M. P. Feneley, D. Fatkin, and R. P. Harvey, 2010, Neuregulin 1 sustains the gene regulatory network in both trabecular and nontrabecular myocardium: Circ Res, v. 107, p. 715-27.
Lambert, J. M., E. F. Lopez, and M. L. Lindsey, 2008, Macrophage Roles Following Myocardial Infarction: International journal of cardiology, v. 130, p. 147-158.
Lanahan, A. A., K. Hermans, F. Claes, J. S. Kerley-Hamilton, Z. W. Zhuang, F. J. Giordano, P. Carmeliet, and M. Simons, 2010, VEGF receptor 2 endocytic trafficking regulates arterial morphogenesis: Developmental cell, v. 18, p. 713-724.
Langenbacher, A. D., Y. Dong, X. Shu, J. Choi, D. A. Nicoll, J. I. Goldhaber, K. D. Philipson, and J. N. Chen, 2005, Mutation in sodium-calcium exchanger 1 (NCX1) causes cardiac fibrillation in zebrafish: Proc Natl Acad Sci U S A, v. 102, p. 17699-704.
Laugwitz, K. L., A. Moretti, J. Lam, P. Gruber, Y. Chen, S. Woodard, L. Z. Lin, C. L. Cai, M. M. Lu, M. Reth, O. Platoshyn, J. X. Yuan, S. Evans, and K. R. Chien, 2005, Postnatal isl1+ cardioblasts enter fully differentiated cardiomyocyte lineages: Nature, v. 433, p. 647-53.
Lavine, K. J., K. Yu, A. C. White, X. Zhang, C. Smith, J. Partanen, and D. M. Ornitz, 2005, Endocardial and epicardial derived FGF signals regulate myocardial proliferation and differentiation *in vivo*: Dev Cell, v. 8, p. 85-95.
Lawson, N. D., and B. M. Weinstein, 2002, *In vivo* imaging of embryonic vascular development using transgenic zebrafish: Dev Biol, v. 248, p. 307-18.
Lazic, S., and I. C. Scott, 2011, Mef2cb regulates late myocardial cell addition from a second heart field-like population of progenitors in zebrafish: Developmental biology, v. 354, p. 123-133.
Leask, A., 2007, TGFbeta, cardiac fibroblasts, and the fibrotic response: Cardiovasc Res, v. 74, p. 207-12.

LeClair, E. E., and J. Topczewski, 2010, Development and regeneration of the zebrafish maxillary barbel: a novel study system for vertebrate tissue growth and repair: PLoS One, v. 5, p. e8737.

Lee, K. F., H. Simon, H. Chen, B. Bates, M. C. Hung, and C. Hauser, 1995, Requirement for neuregulin receptor erbB2 in neural and cardiac development: Nature, v. 378, p. 394-8.

Lee, K. H., Q. Xu, and R. E. Breitbart, 1996, A new tinman-related gene, nkx2.7, anticipates the expression of nkx2.5 and nkx2.3 in zebrafish heart and pharyngeal endoderm: Dev Biol, v. 180, p. 722-31.

Lee, P., K. Goishi, A. J. Davidson, R. Mannix, L. Zon, and M. Klagsbrun, 2002, Neuropilin-1 is required for vascular development and is a mediator of VEGF-dependent angiogenesis in zebrafish: Proceedings of the National Academy of Sciences of the United States of America, v. 99, p. 10470-10475.

Lee, S. H., P. L. Wolf, R. Escudero, R. Deutsch, S. W. Jamieson, and P. A. Thistlethwaite, 2000, Early expression of angiogenesis factors in acute myocardial ischemia and infarction: N Engl J Med, v. 342, p. 626-33.

Leibovich, S. J., P. J. Polverini, H. M. Shepard, D. M. Wiseman, V. Shively, and N. Nuseir, 1987, Macrophage-induced angiogenesis is mediated by tumour necrosis factor-[alpha]: Nature, v. 329, p. 630-632.

Leong, I. U., J. R. Skinner, A. N. Shelling, and D. R. Love, 2010, Zebrafish as a model for long QT syndrome: the evidence and the means of manipulating zebrafish gene expression: Acta Physiol (Oxf), v. 199, p. 257-76.

Lepilina, A., A. N. Coon, K. Kikuchi, J. E. Holdway, R. W. Roberts, C. G. Burns, and K. D. Poss, 2006, A dynamic epicardial injury response supports progenitor cell activity during zebrafish heart regeneration: Cell, v. 127, p. 607-619.

Lerman, R. H., C. S. Apstein, H. M. Kagan, E. L. Osmers, C. O. Chichester, W. M. Vogel, C. M. Connelly, and W. P. Steffee, 1983, Myocardial healing and repair after experimental infarction in the rabbit: Circ Res, v. 53, p. 378-88.

Leung, D. W., G. Cachianes, W. J. Kuang, D. V. Goeddel, and N. Ferrara, 1989, Vascular endothelial growth factor is a secreted angiogenic mitogen: Science, v. 246, p. 1306-9.

Leveen, P., M. Pekny, S. Gebre-Medhin, B. Swolin, E. Larsson, and C. Betsholtz, 1994, Mice deficient for PDGF B show renal, cardiovascular, and hematological abnormalities: Genes Dev, v. 8, p. 1875-87.

Li, F., X. Wang, J. M. Capasso, and A. M. Gerdes, 1996, Rapid transition of cardiac myocytes from hyperplasia to hypertrophy during postnatal development: J Mol Cell Cardiol, v. 28, p. 1737-46.

Li, J. M., R. A. Poolman, and G. Brooks, 1998, Role of G1 phase cyclins and cyclin-dependent kinases during cardiomyocyte hypertrophic growth in rats: American Journal of Physiology - Heart and Circulatory Physiology, v. 275, p. H814-H822.

Lien, C.-L., M. Schebesta, S. Makino, G. J. Weber, and M. T. Keating, 2006, Gene expression analysis of zebrafish heart regeneration: Plos Biology, v. 4, p. 1386-1396.

Lijnen, P., V. Petrov, K. Rumilla, and R. Fagard, 2003, Transforming growth factor-beta 1 promotes contraction of collagen gel by cardiac fibroblasts through their differentiation into myofibroblasts: Methods Find Exp Clin Pharmacol, v. 25, p. 79-86.

Limana, F., C. Bertolami, A. Mangoni, A. Di Carlo, D. Avitabile, D. Mocini, P. Iannelli, R. De Mori, C. Marchetti, O. Pozzoli, C. Gentili, A. Zacheo, A. Germani, and M. C. Capogrossi, 2010, Myocardial infarction induces embryonic reprogramming of epicardial c-kit(+) cells: role of the pericardial fluid: J Mol Cell Cardiol, v. 48, p. 609-18.

Lindblom, P., H. Gerhardt, S. Liebner, A. Abramsson, M. Enge, M. Hellstrom, G. Backstrom, S. Fredriksson, U. Landegren, H. C. Nystrom, G. Bergstrom, E. Dejana, A. Ostman, P. Lindahl, and C. Betsholtz, 2003, Endothelial PDGF-B retention is required for proper investment of pericytes in the microvessel wall: Genes Dev, v. 17, p. 1835-40.

Liu, J., M. Bressan, D. Hassel, J. Huisken, D. Staudt, K. Kikuchi, K. D. Poss, T. Mikawa, and D. Y. Stainier, 2010, A dual role for ErbB2 signaling in cardiac trabeculation: Development, v. 137, p. 3867-75.

Liu, W. B., A. A. Parikh, O. Stoeltzing, F. Fan, M. F. McCarty, J. Wey, D. J. Hicklin, and L. M. Ellis, 2005, Upregulation of neuropilin-1 by basic fibroblast growth factor enhances vascular smooth muscle cell migration in response to VEGF: Cytokine, v. 32, p. 206-212.

Loffredo, F. S., M. L. Steinhauser, J. Gannon, and R. T. Lee, 2011, Bone marrow-derived cell therapy stimulates endogenous cardiomyocyte progenitors and promotes cardiac repair: Cell Stem Cell, v. 8, p. 389-98.

Long, Q., A. Meng, H. Wang, J. R. Jessen, M. J. Farrell, and S. Lin, 1997, GATA-1 expression pattern can be recapitulated in living transgenic zebrafish using GFP reporter gene: Development, v. 124, p. 4105-11.

Losordo, D. W., and S. Dimmeler, 2004, Therapeutic Angiogenesis and Vasculogenesis for Ischemic Disease: Circulation, v. 109, p. 2487.

Lu, F., D. A. Langenbacher, and J.-N. Chen, 2016, Transcriptional Regulation of Heart Development in Zebrafish: Journal of Cardiovascular Development and Disease, v. 3.

Lu, J., T. E. Landerholm, J. S. Wei, X. R. Dong, S. P. Wu, X. Liu, K. Nagata, M. Inagaki, and M. W. Majesky, 2001, Coronary smooth muscle differentiation from proepicardial cells requires rhoA-mediated actin reorganization and p160 rho-kinase activity: Dev Biol, v. 240, p. 404-18.

Lunde, K., S. Solheim, S. Aakhus, H. Arnesen, M. Abdelnoor, T. Egeland, K. Endresen, A. Ilebekk, A. Mangschau, J. G. Fjeld, H. J. Smith, E. Taraldsrud, H. K. Grøgaard, R. Bjørnerheim, M. Brekke, C. Müller, E. Hopp, A. Ragnarsson, J. E. Brinchmann, and K. Forfang, 2006, Intracoronary Injection of Mononuclear Bone Marrow Cells in Acute Myocardial Infarction: New England Journal of Medicine, v. 355, p. 1199-1209.

Luo, Y., D. Raible, and J. A. Raper, 1993, Collapsin: a protein in brain that induces the collapse and paralysis of neuronal growth cones: Cell, v. 75, p. 217-27.

Mahmoud, A. I., F. Kocabas, S. A. Muralidhar, W. Kimura, A. S. Koura, S. Thet, E. R. Porrello, and H. A. Sadek, 2013, Meis1 regulates postnatal cardiomyocyte cell cycle arrest: Nature, v. 497, p. 249-253.

Malliaras, K., Y. Zhang, J. Seinfeld, G. Galang, E. Tseliou, K. Cheng, B. Sun, M. Aminzadeh, and E. Marbán, 2013, Cardiomyocyte proliferation and progenitor cell recruitment underlie therapeutic regeneration after myocardial infarction in the adult mouse heart: EMBO Molecular Medicine, v. 5, p. 191-209.

Manner, J., 1993, Experimental study on the formation of the epicardium in chick embryos: Anat Embryol (Berl), v. 187, p. 281-9.

Mannisi, J. A., H. F. Weisman, D. E. Bush, P. Dudeck, and B. Healy, 1987, Steroid administration after myocardial infarction promotes early infarct expansion. A study in the rat: Journal of Clinical Investigation, v. 79, p. 1431-1439.

Manuel Gonzalez-Rosa, J., V. Martin, M. Peralta, M. Torres, and N. Mercader, 2011, Extensive scar formation and regression during heart regeneration after cryoinjury in zebrafish: Development, v. 138, p. 1663-1674.

Manuel Gonzalez-Rosa, J., M. Peralta, and N. Mercader, 2012, Pan-epicardial lineage tracing reveals that epicardium derived cells give rise to myofibroblasts and perivascular cells during zebrafish heart regeneration: Developmental Biology, v. 370, p. 173-186.

Marin-Juez, R., M. Marass, S. Gauvrit, A. Rossi, S. L. Lai, S. C. Materna, B. L. Black, and D. Y. Stainier, 2016, Fast revascularization of the injured area is essential to support zebrafish heart regeneration: Proc Natl Acad Sci U S A.

Martinez-Estrada, O. M., L. A. Lettice, A. Essafi, J. A. Guadix, J. Slight, V. Velecela, E. Hall, J. Reichmann, P. S. Devenney, P. Hohenstein, N. Hosen, R. E. Hill, R. Munoz-Chapuli, and N. D. Hastie, 2010, Wt1 is required for cardiovascular progenitor cell formation through transcriptional control of Snail and E-cadherin: Nat Genet, v. 42, p. 89-93.

Martyn, U., and S. Schulte-Merker, 2004, Zebrafish neuropilins are differentially expressed and interact with vascular endothelial growth factor during embryonic vascular development: Developmental Dynamics, v. 231, p. 33-42.

Massague, J., 2012, TGF[beta] signalling in context: Nat Rev Mol Cell Biol, v. 13, p. 616-630.

Masters, M., and P. R. Riley, 2014, The epicardium signals the way towards heart regeneration: Stem Cell Research, v. 13, p. 683-692.

Mathew, L. K., S. Sengupta, A. Kawakami, E. A. Andreasen, C. V. Lohr, C. A. Loynes, S. A. Renshaw, R. T. Peterson, and R. L. Tanguay, 2007, Unraveling tissue regeneration pathways using chemical genetics: J Biol Chem, v. 282, p. 35202-10.

McCallum, C. M., L. Comai, E. A. Greene, and S. Henikoff, 2000, Targeted screening for induced mutations: Nat Biotechnol, v. 18, p. 455-7.

Melet, F., B. Motro, D. J. Rossi, L. Zhang, and A. Bernstein, 1996, Generation of a novel Fli-1 protein by gene targeting leads to a defect in thymus development and a delay in Friend virus-induced erythroleukemia: Mol Cell Biol, v. 16, p. 2708-18.

Merki, E., M. Zamora, A. Raya, Y. Kawakami, J. Wang, X. Zhang, J. Burch, S. W. Kubalak, P. Kaliman, J. C. Izpisua Belmonte, K. R. Chien, and P. Ruiz-Lozano, 2005,

Epicardial retinoid X receptor alpha is required for myocardial growth and coronary artery formation: Proc Natl Acad Sci U S A, v. 102, p. 18455-60.

Mikawa, T., and R. G. Gourdie, 1996, Pericardial mesoderm generates a population of coronary smooth muscle cells migrating into the heart along with ingrowth of the epicardial organ: Developmental Biology, v. 174, p. 221-232.

Milan, D. J., A. C. Giokas, F. C. Serluca, R. T. Peterson, and C. A. MacRae, 2006a, Notch1b and neuregulin are required for specification of central cardiac conduction tissue: Development, v. 133, p. 1125-32.

Milan, D. J., I. L. Jones, P. T. Ellinor, and C. A. MacRae, 2006b, *In vivo* recording of adult zebrafish electrocardiogram and assessment of drug-induced QT prolongation: Am J Physiol Heart Circ Physiol, v. 291, p. H269-73.

Mitchell, I. C., T. S. Brown, L. S. Terada, J. F. Amatruda, and F. E. Nwariaku, 2010, Effect of Vascular Cadherin Knockdown on Zebrafish Vasculature during Development: PLOS ONE, v. 5, p. e8807.

Mizutani, M., J. C. Wu, and R. Nusse, 2016, Fibrosis of the Neonatal Mouse Heart After Cryoinjury Is Accompanied by Wnt Signaling Activation and Epicardial-to-Mesenchymal Transition: Journal of the American Heart Association: Cardiovascular and Cerebrovascular Disease, v. 5, p. e002457.

Molina, G., A. Vogt, A. Bakan, W. Dai, P. Queiroz de Oliveira, W. Znosko, T. E. Smithgall, I. Bahar, J. S. Lazo, B. W. Day, and M. Tsang, 2009, Zebrafish chemical screening reveals an inhibitor of Dusp6 that expands cardiac cell lineages: Nat Chem Biol, v. 5, p. 680-7.

Mollova, M., K. Bersell, S. Walsh, J. Savla, L. T. Das, S.-Y. Park, L. E. Silberstein, C. G. dos Remedios, D. Graham, S. Colan, and B. Kuehn, 2013, Cardiomyocyte proliferation contributes to heart growth in young humans: Proceedings of the National Academy of Sciences of the United States of America, v. 110, p. 1446-1451.

Montero, J. A., B. Kilian, J. Chan, P. E. Bayliss, and C. P. Heisenberg, 2003, Phosphoinositide 3-kinase is required for process outgrowth and cell polarization of gastrulating mesendodermal cells: Curr Biol, v. 13, p. 1279-89.

Moustakas, A., and C. H. Heldin, 2009, The regulation of TGFbeta signal transduction: Development, v. 136, p. 3699-714.

Murry, C. E., H. Reinecke, and L. M. Pabon, 2006, Regeneration gaps: observations on stem cells and cardiac repair: J Am Coll Cardiol, v. 47, p. 1777-85.

Naccache, S. N., T. Hasson, and A. Horowitz, 2006, Binding of internalized receptors to the PDZ domain of GIPC/synectin recruits myosin VI to endocytic vesicles: Proc Natl Acad Sci U S A, v. 103, p. 12735-40.

Nag, A. C., 1980, Study of non-muscle cells of the adult mammalian heart: a fine structural analysis and distribution: Cytobios, v. 28, p. 41-61.

Nakamura, F., M. Tanaka, T. Takahashi, R. G. Kalb, and S. M. Strittmatter, 1998, Neuropilin-1 extracellular domains mediate semaphorin D/III-induced growth cone collapse: Neuron, v. 21, p. 1093-100.

Naqvi, N., M. Li, John W. Calvert, T. Tejada, Jonathan P. Lambert, J. Wu, Scott H. Kesteven, Sara R. Holman, T. Matsuda, Joshua D. Lovelock, Wesley W. Howard, Siiri E. Iismaa, Andrea Y. Chan, Brian H. Crawford, Mary B. Wagner, David I. K.

Martin, David J. Lefer, Robert M. Graham, and A. Husain, 2014, A Proliferative Burst during Preadolescence Establishes the Final Cardiomyocyte Number: Cell, v. 157, p. 795-807.

Nasevicius, A., and S. C. Ekker, 2000, Effective targeted gene 'knockdown' in zebrafish: Nat Genet, v. 26, p. 216-20.

Negishi, M., I. Oinuma, and H. Katoh, 2005, Plexins: axon guidance and signal transduction: Cell Mol Life Sci, v. 62, p. 1363-71.

Niederreither, K., V. Subbarayan, P. Dolle, and P. Chambon, 1999, Embryonic retinoic acid synthesis is essential for early mouse post-implantation development: Nat Genet, v. 21, p. 444-8.

Novodvorsky, P., O. Watson, C. Gray, R. N. Wilkinson, S. Reeve, C. Smythe, R. Beniston, K. Plant, R. Maguire, M. K. R. A, S. Elworthy, F. J. van Eeden, and T. J. Chico, 2015, klf2ash317 Mutant Zebrafish Do Not Recapitulate Morpholino-Induced Vascular and Haematopoietic Phenotypes: PLoS One, v. 10, p. e0141611.

Oberpril.Jo, and Oberpril.Jc, 1974, RESPONSE OF ADULT NEWT VENTRICLE TO INJURY: Journal of Experimental Zoology, v. 187, p. 249-259.

Ogryzko, N. V., E. E. Hoggett, S. Solaymani-Kohal, S. Tazzyman, T. J. A. Chico, S. A. Renshaw, and H. L. Wilson, 2014, Zebrafish tissue injury causes upregulation of interleukin-1 and caspase-dependent amplification of the inflammatory response: Disease Models & Mechanisms, v. 7, p. 259-264.

Oh, H., H. Takagi, A. Otani, S. Koyama, S. Kemmochi, A. Uemura, and Y. Honda, 2002, Selective induction of neuropilin-1 by vascular endothelial growth factor (VEGF): A mechanism contributing to VEGF-induced angiogenesis: Proceedings of the National Academy of Sciences, v. 99, p. 383-388.

Oinuma, I., Y. Ishikawa, H. Katoh, and M. Negishi, 2004, The Semaphorin 4D receptor Plexin-B1 is a GTPase activating protein for R-Ras: Science, v. 305, p. 862-5.

Okazaki, T., S. Ebihara, M. Asada, S. Yamanda, Y. Saijo, Y. Shiraishi, T. Ebihara, K. Niu, H. Mei, H. Arai, and T. Yambe, 2007, Macrophage colony-stimulating factor improves cardiac function after ischemic injury by inducing vascular endothelial growth factor production and survival of cardiomyocytes: Am J Pathol, v. 171, p. 1093-103.

Onimaru, M., Y. Yonemitsu, T. Fujii, M. Tanii, T. Nakano, K. Nakagawa, R. Kohno, M. Hasegawa, S. Nishikawa, and K. Sueishi, 2009, VEGF-C regulates lymphangiogenesis and capillary stability by regulation of PDGF-B: Am J Physiol Heart Circ Physiol, v. 297, p. H1685-96.

Oyama, J., C. Blais, Jr., X. Liu, M. Pu, L. Kobzik, R. A. Kelly, and T. Bourcier, 2004, Reduced myocardial ischemia-reperfusion injury in toll-like receptor 4-deficient mice: Circulation, v. 109, p. 784-9.

Pan, Q., Y. Chathery, Y. Wu, N. Rathore, R. K. Tong, F. Peale, A. Bagri, M. Tessier-Lavigne, A. W. Koch, and R. J. Watts, 2007, Neuropilin-1 binds to VEGF121 and regulates endothelial cell migration and sprouting: J Biol Chem, v. 282, p. 24049-56.

Parker, M. W., A. D. Linkugel, H. L. Goel, T. Wu, A. M. Mercurio, and C. W. Vander Kooi, 2015, Structural basis for VEGF-C binding to neuropilin-2 and sequestration by a soluble splice form: Structure, v. 23, p. 677-87.

Pasumarthi, K. B. S., and L. J. Field, 2002, Cardiomyocyte cell cycle regulation: Circulation Research, v. 90, p. 1044-1054.

Pearlman, J. D., M. G. Hibberd, M. L. Chuang, K. Harada, J. J. Lopez, S. R. Gladstone, M. Friedman, F. W. Sellke, and M. Simons, 1995, Magnetic resonance mapping demonstrates benefits of VEGF-induced myocardial angiogenesis: Nat Med, v. 1, p. 1085-1089.

Pellet-Many, C., P. Frankel, I. M. Evans, B. Herzog, M. Junemann-Ramirez, and I. C. Zachary, 2011, Neuropilin-1 mediates PDGF stimulation of vascular smooth muscle cell migration and signalling via p130Cas: Biochemical Journal, v. 435, p. 609-618.

Pellet-Many, C., P. Frankel, H. Jia, and I. Zachary, 2008, Neuropilins: structure, function and role in disease: Biochemical Journal, v. 411, p. 211.

Pellet-Many, C., V. Mehta, L. Fields, M. Mahmoud, V. Lowe, I. Evans, J. Ruivo, and I. Zachary, 2015, Neuropilins 1 and 2 mediate neointimal hyperplasia and re-endothelialization following arterial injury: Cardiovascular Research, v. 108, p. 288-298.

Pennisi, D. J., and T. Mikawa, 2005, Normal patterning of the coronary capillary plexus is dependent on the correct transmural gradient of FGF expression in the myocardium: Developmental biology, v. 279, p. 378-390.

Peralta, M., J. M. Gonzalez-Rosa, I. J. Marques, and N. Mercader, 2014, The Epicardium in the Embryonic and Adult Zebrafish: J Dev Biol, v. 2, p. 101-116.

Peralta, M., E. Steed, S. Harlepp, J. M. Gonzalez-Rosa, F. Monduc, A. Ariza-Cosano, A. Cortes, T. Rayon, J. L. Gomez-Skarmeta, A. Zapata, J. Vermot, and N. Mercader, 2013, Heartbeat-driven pericardiac fluid forces contribute to epicardium morphogenesis: Curr Biol, v. 23, p. 1726-35.

Perez-Pomares, J. M., R. Carmona, M. Gonzalez-Iriarte, G. Atencia, A. Wessels, and R. Munoz-Chapuli, 2002, Origin of coronary endothelial cells from epicardial mesothelium in avian embryos: Int J Dev Biol, v. 46, p. 1005-13.

Perner, B., C. Englert, and F. Bollig, 2007, The Wilms tumor genes wt1a and wt1b control different steps during formation of the zebrafish pronephros: Developmental Biology, v. 309, p. 87-96.

Peshkovsky, C., R. Totong, and D. Yelon, 2011, Dependence of cardiac trabeculation on neuregulin signaling and blood flow in zebrafish: Dev Dyn, v. 240, p. 446-56.

Pfeffer, M. A., and E. Braunwald, 1990, Ventricular remodeling after myocardial infarction. Experimental observations and clinical implications: Circulation, v. 81, p. 1161-72.

Phillips, R. B., A. Amores, M. R. Morasch, C. Wilson, and J. H. Postlethwait, 2006, Assignment of zebrafish genetic linkage groups to chromosomes: Cytogenet Genome Res, v. 114, p. 155-62.

Pierce, G. F., T. A. Mustoe, B. W. Altrock, T. F. Deuel, and A. Thomason, 1991, Role of platelet-derived growth factor in wound healing: J Cell Biochem, v. 45, p. 319-26.

Plavicki, J. S., P. Hofsteen, M. S. Yue, K. A. Lanham, R. E. Peterson, and W. Heideman, 2014, Multiple modes of proepicardial cell migration require heartbeat: BMC Dev Biol, v. 14, p. 18.

Plein, A., A. Calmont, A. Fantin, L. Denti, N. A. Anderson, P. J. Scambler, and C. Ruhrberg, 2015, Neural crest–derived SEMA3C activates endothelial NRP1 for cardiac outflow tract septation: The Journal of Clinical Investigation, v. 125, p. 2661-2676.

Poelmann, R. E., H. Lie-Venema, and A. C. Gittenberger-de Groot, 2002, The Role of the Epicardium and Neural Crest: as Extracardiac Contributors to Coronary Vascular Development: Texas Heart Institute Journal, v. 29, p. 255-261.

Pogoda, H.-M., and D. Meyer, 2002, Zebrafish smad7 is regulated by Smad3 and BMP signals: Developmental Dynamics, v. 224, p. 334-349.

Polizzotti, B. D., B. Ganapathy, B. J. Haubner, J. M. Penninger, and B. Kuhn, 2016, A cryoinjury model in neonatal mice for cardiac translational and regeneration research: Nat. Protocols, v. 11, p. 542-552.

Poon, K. L., and T. Brand, 2013, The zebrafish model system in cardiovascular research: A tiny fish with mighty prospects: Global Cardiology Science & Practice, v. 2013, p. 9-28.

Porrello, E. R., B. A. Johnson, A. B. Aurora, E. Simpson, Y.-J. Nam, S. J. Matkovich, G. W. Dorn, II, E. van Rooij, and E. N. Olson, 2011a, miR-15 Family Regulates Postnatal Mitotic Arrest of Cardiomyocytes: Circulation Research, v. 109, p. 670-U208.

Porrello, E. R., A. I. Mahmoud, E. Simpson, J. A. Hill, J. A. Richardson, E. N. Olson, and H. A. Sadek, 2011b, Transient Regenerative Potential of the Neonatal Mouse Heart: Science, v. 331, p. 1078-1080.

Porrello, E. R., and E. N. Olson, 2014, A neonatal blueprint for cardiac regeneration: Stem Cell Research, v. 13, p. 556-570.

Poss, K. D., L. G. Wilson, and M. T. Keating, 2002, Heart regeneration in zebrafish: Science, v. 298, p. 2188-2190.

Postlethwait, J. H., Y. L. Yan, M. A. Gates, S. Horne, A. Amores, A. Brownlie, A. Donovan, E. S. Egan, A. Force, Z. Y. Gong, C. Goutel, A. Fritz, R. Kelsh, E. Knapik, E. Liao, B. Paw, D. Ransom, A. Singer, M. Thomson, T. S. Abduljabbar, P. Yelick, D. Beier, J. S. Joly, D. Larhammar, F. Rosa, M. Westerfield, L. I. Zon, S. L. Johnson, and W. S. Talbot, 1998, Vertebrate genome evolution and the zebrafish gene map: Nature Genetics, v. 18, p. 345-349.

Prahst, C., M. Heroult, A. A. Lanahan, N. Uziel, O. Kessler, N. Shraga-Heled, M. Simons, G. Neufeld, and H. G. Augustin, 2008, Neuropilin-1-VEGFR-2 complexing requires the PDZ-binding domain of neuropilin-1: J Biol Chem, v. 283, p. 25110-4.

Presta, M., P. Dell'Era, S. Mitola, E. Moroni, R. Ronca, and M. Rusnati, 2005, Fibroblast growth factor/fibroblast growth factor receptor system in angiogenesis: Cytokine Growth Factor Rev, v. 16, p. 159-78.

Red-Horse, K., H. Ueno, I. L. Weissman, and M. A. Krasnow, 2010, Coronary arteries form by developmental reprogramming of venous cells: Nature, v. 464, p. 549-53.

Reifers, F., E. C. Walsh, S. Leger, D. Y. Stainier, and M. Brand, 2000, Induction and differentiation of the zebrafish heart requires fibroblast growth factor 8 (fgf8/acerebellar): Development, v. 127, p. 225-35.

Reiter, J. F., J. Alexander, A. Rodaway, D. Yelon, R. Patient, N. Holder, and D. Y. Stainier, 1999, Gata5 is required for the development of the heart and endoderm in zebrafish: Genes Dev, v. 13, p. 2983-95.

Ren, G., L. H. Michael, M. L. Entman, and N. G. Frangogiannis, 2002, Morphological characteristics of the microvasculature in healing myocardial infarcts: J Histochem Cytochem, v. 50, p. 71-9.

Rohm, B., A. Ottemeyer, M. Lohrum, and A. W. Puschel, 2000, Plexin/neuropilin complexes mediate repulsion by the axonal guidance signal semaphorin 3A: Mech Dev, v. 93, p. 95-104.

Rohr, S., C. Otten, and S. Abdelilah-Seyfried, 2008, Asymmetric involution of the myocardial field drives heart tube formation in zebrafish: Circ Res, v. 102, p. e12-9.

Roman, B. L., V. N. Pham, N. D. Lawson, M. Kulik, S. Childs, A. C. Lekven, D. M. Garrity, R. T. Moon, M. C. Fishman, R. J. Lechleider, and B. M. Weinstein, 2002, Disruption of acvrl1 increases endothelial cell number in zebrafish cranial vessels: Development, v. 129, p. 3009-19.

Rosenkranz, S., 2004, TGF-beta1 and angiotensin networking in cardiac remodeling: Cardiovasc Res, v. 63, p. 423-32.

Rossi, A., Z. Kontarakis, C. Gerri, H. Nolte, S. Holper, M. Kruger, and D. Y. R. Stainier, 2015, Genetic compensation induced by deleterious mutations but not gene knockdowns: Nature, v. 524, p. 230-233.

Rossignol, M., M. L. Gagnon, and M. Klagsbrun, 2000, Genomic organization of human neuropilin-1 and neuropilin-2 genes: Identification and distribution of splice variants and soluble isoforms: Genomics, v. 70, p. 211-222.

Roth, L., C. Prahst, T. Ruckdeschel, S. Savant, S. Westrom, A. Fantin, M. Riedel, M. Heroult, C. Ruhrberg, and H. G. Augustin, 2016, Neuropilin-1 mediates vascular permeability independently of vascular endothelial growth factor receptor-2 activation: Sci Signal, v. 9, p. ra42.

Rottbauer, W., K. Baker, Z. G. Wo, M. A. Mohideen, H. F. Cantiello, and M. C. Fishman, 2001, Growth and function of the embryonic heart depend upon the cardiac-specific L-type calcium channel alpha1 subunit: Dev Cell, v. 1, p. 265-75.

Rumyantsev, P. P., 1977, Interrelations of the proliferation and differentiation processes during cardiact myogenesis and regeneration: International review of cytology, v. 51, p. 186-273.

Samsa, L. A., B. Yang, and J. Liu, 2013, Embryonic Cardiac Chamber Maturation: Trabeculation, Conduction and Cardiomyocyte Proliferation: American journal of medical genetics. Part C, Seminars in medical genetics, v. 163, p. 157-168.

Sander, J. D., and J. K. Joung, 2014, CRISPR-Cas systems for editing, regulating and targeting genomes: Nat Biotechnol, v. 32, p. 347-55.

Sander, V., G. Sune, C. Jopling, C. Morera, and J. C. Izpisua Belmonte, 2013, Isolation and *in vitro* culture of primary cardiomyocytes from adult zebrafish hearts: Nature Protocols, v. 8, p. 800-809.

Sanger, F., S. Nicklen, and A. R. Coulson, 1977, DNA sequencing with chain-terminating inhibitors: Proc Natl Acad Sci U S A, v. 74, p. 5463-7.

Schachinger, V., S. Erbs, A. Elsasser, W. Haberbosch, R. Hambrecht, H. Holschermann, J. Yu, R. Corti, D. G. Mathey, C. W. Hamm, T. Suselbeck, B. Assmus, T. Tonn, S. Dimmeler, and A. M. Zeiher, 2006, Intracoronary bone marrow-derived progenitor cells in acute myocardial infarction: N Engl J Med, v. 355, p. 1210-21.

Scherz, P. J., J. Huisken, P. Sahai-Hernandez, and D. Y. Stainier, 2008, High-speed imaging of developing heart valves reveals interplay of morphogenesis and function: Development, v. 135, p. 1179-87.

Schimpf, R., C. Wolpert, F. Gaita, C. Giustetto, and M. Borggrefe, 2005, Short QT syndrome: Cardiovasc Res, v. 67, p. 357-66.

Schnabel, K., C. C. Wu, T. Kurth, and G. Weidinger, 2011, Regeneration of Cryoinjury Induced Necrotic Heart Lesions in Zebrafish Is Associated with Epicardial Activation and Cardiomyocyte Proliferation: Plos One, v. 6.

Schneider, C. A., W. S. Rasband, and K. W. Eliceiri, 2012, NIH Image to ImageJ: 25 years of image analysis: Nat Meth, v. 9, p. 671-675.

Schoenebeck, J. J., B. R. Keegan, and D. Yelon, 2007, Vessel and blood specification override cardiac potential in anterior mesoderm: Dev Cell, v. 13, p. 254-67.

Schulte-Merker, S., and D. Y. R. Stainier, 2014, Out with the old, in with the new: reassessing morpholino knockdowns in light of genome editing technology: Development, v. 141, p. 3103.

Schwarz, E. R., M. T. Speakman, M. Patterson, S. S. Hale, J. M. Isner, L. H. Kedes, and R. A. Kloner, 2000, Evaluation of the effects of intramyocardial injection of DNA expressing vascular endothelial growth factor (VEGF) in a myocardial infarction model in the rat--angiogenesis and angioma formation: J Am Coll Cardiol, v. 35, p. 1323-30.

Sedmera, D., T. Pexieder, M. Vuillemin, R. P. Thompson, and R. H. Anderson, 2000, Developmental patterning of the myocardium: Anat Rec, v. 258, p. 319-37.

Sedmera, D., M. Reckova, A. deAlmeida, M. Sedmerova, M. Biermann, J. Volejnik, A. Sarre, E. Raddatz, R. A. McCarthy, R. G. Gourdie, and R. P. Thompson, 2003, Functional and morphological evidence for a ventricular conduction system in zebrafish and Xenopus hearts: Am J Physiol Heart Circ Physiol, v. 284, p. H1152-60.

Seerapu, H. R., S. Borthakur, N. Kong, S. Agrawal, J. Drazba, A. Vasanji, A. Fantin, C. Ruhrberg, M. Buck, and A. Horowitz, 2013, The cytoplasmic domain of neuropilin-1 regulates focal adhesion turnover: FEBS letters, v. 587, p. 10.1016/j.febslet.2013.08.040.

Seetharam, L., N. Gotoh, Y. Maru, G. Neufeld, S. Yamaguchi, and M. Shibuya, 1995, A unique signal transduction from FLT tyrosine kinase, a receptor for vascular endothelial growth factor VEGF: Oncogene, v. 10, p. 135-47.

Senior, R. M., G. L. Griffin, and R. P. Mecham, 1980, Chemotactic activity of elastin-derived peptides: Journal of Clinical Investigation, v. 66, p. 859-862.

Senyo, S. E., M. L. Steinhauser, C. L. Pizzimenti, V. K. Yang, L. Cai, M. Wang, T.-D. Wu, J.-L. Guerquin-Kern, C. P. Lechene, and R. T. Lee, 2013, Mammalian heart renewal by pre-existing cardiomyocytes: Nature, v. 493, p. 433-U186.

Serini, G., M. L. Bochaton-Piallat, P. Ropraz, A. Geinoz, L. Borsi, L. Zardi, and G. Gabbiani, 1998, The fibronectin domain ED-A is crucial for myofibroblastic phenotype induction by transforming growth factor-beta1: J Cell Biol, v. 142, p. 873-81.

Serluca, F. C., 2008, Development of the proepicardial organ in the zebrafish: Dev Biol, v. 315, p. 18-27.

Shimizu, I., Y. Yoshida, J. Moriya, A. Nojima, A. Uemura, Y. Kobayashi, and T. Minamino, 2013, Semaphorin3E-Induced Inflammation Contributes to Insulin Resistance in Dietary Obesity: Cell Metabolism, v. 18, p. 491-504.

Shintani, Y., S. Takashima, Y. Asano, H. Kato, Y. Liao, S. Yamazaki, O. Tsukamoto, O. Seguchi, H. Yamamoto, T. Fukushima, K. Sugahara, M. Kitakaze, and M. Hori, 2006, Glycosaminoglycan modification of neuropilin-1 modulates VEGFR2 signaling: Embo j, v. 25, p. 3045-55.

Shoji, W., S. Isogai, M. Sato-Maeda, M. Obinata, and J. Y. Kuwada, 2003, Semaphorin3a1 regulates angioblast migration and vascular development in zebrafish embryos: Development, v. 130, p. 3227-36.

Sidney, S., W. D. Rosamond, V. J. Howard, R. V. Luepker, and P. National Forum for Heart Disease and Stroke, 2013, The "heart disease and stroke statistics--2013 update" and the need for a national cardiovascular surveillance system, Circulation, v. 127: United States, p. 21-3.

Smart, N., S. Bollini, K. N. Dube, J. M. Vieira, B. Zhou, S. Davidson, D. Yellon, J. Riegler, A. N. Price, M. F. Lythgoe, W. T. Pu, and P. R. Riley, 2011, De novo cardiomyocytes from within the activated adult heart after injury: Nature, v. 474, p. 640-4.

Smart, N., C. A. Risebro, A. A. D. Melville, K. Moses, R. J. Schwartz, K. R. Chien, and P. R. Riley, 2007, Thymosin [bgr]4 induces adult epicardial progenitor mobilization and neovascularization: Nature, v. 445, p. 177-182.

Smith, L. M., J. Z. Sanders, R. J. Kaiser, P. Hughes, C. Dodd, C. R. Connell, C. Heiner, S. B. Kent, and L. E. Hood, 1986, Fluorescence detection in automated DNA sequence analysis: Nature, v. 321, p. 674-9.

Smits, M. A., and R. P. Riley, 2014, Epicardium-Derived Heart Repair: Journal of Developmental Biology, v. 2.

Soker, S., S. Takashima, H. Q. Miao, G. Neufeld, and M. Klagsbrun, 1998, Neuropilin-1 is expressed by endothelial and tumor cells as an isoform-specific receptor for vascular endothelial growth factor: Cell, v. 92, p. 735-745.

Sorrell, M. R., and J. S. Waxman, 2011, Restraint of Fgf8 signaling by retinoic acid signaling is required for proper heart and forelimb formation: Dev Biol, v. 358, p. 44-55.

Stainier, D. Y., 2001, Zebrafish genetics and vertebrate heart formation: Nat Rev Genet, v. 2, p. 39-48.

Stainier, D. Y., R. K. Lee, and M. C. Fishman, 1993, Cardiovascular development in the zebrafish. I. Myocardial fate map and heart tube formation: Development, v. 119, p. 31-40.

Stainier, D. Y., B. M. Weinstein, H. W. Detrich, 3rd, L. I. Zon, and M. C. Fishman, 1995, Cloche, an early acting zebrafish gene, is required by both the endothelial and hematopoietic lineages: Development, v. 121, p. 3141-50.

Stankunas, K., C. T. Hang, Z. Y. Tsun, H. Chen, N. V. Lee, J. I. Wu, C. Shang, J. H. Bayle, W. Shou, M. L. Iruela-Arispe, and C. P. Chang, 2008, Endocardial Brg1 represses ADAMTS1 to maintain the microenvironment for myocardial morphogenesis: Dev Cell, v. 14, p. 298-311.

Stanton, M. J., S. Dutta, H. Zhang, N. S. Polavaram, A. A. Leontovich, P. Honscheid, F. A. Sinicrope, D. J. Tindall, M. H. Muders, and K. Datta, 2013, Autophagy control by the VEGF-C/NRP-2 axis in cancer and its implication for treatment resistance: Cancer Res, v. 73, p. 160-71.

Staudt, D. W., J. Liu, K. S. Thorn, N. Stuurman, M. Liebling, and D. Y. Stainier, 2014, High-resolution imaging of cardiomyocyte behavior reveals two distinct steps in ventricular trabeculation: Development, v. 141, p. 585-93.

Stein, C., M. Caccamo, G. Laird, and M. Leptin, 2007, Conservation and divergence of gene families encoding components of innate immune response systems in zebrafish: Genome Biol, v. 8, p. R251.

Stepanova, O. I., A. V. Krylov, V. I. Lioudyno, and E. P. Kisseleva, 2007, Gene expression for VEGF-A, VEGF-C, and their receptors in murine lymphocytes and macrophages: Biochemistry (Mosc), v. 72, p. 1194-8.

Sternberg, P. W., and J. Alberola-Ila, 1998, Conspiracy Theory: RAS and RAF Do Not Act Alone: Cell, v. 95, p. 447-450.

Strungs, E. G., E. L. Ongstad, M. P. O'Quinn, J. A. Palatinus, L. J. Jourdan, and R. G. Gourdie, 2013, Cryoinjury Models of the Adult and Neonatal Mouse Heart for Studies of Scarring and Regeneration, *in* R. G. Gourdie, and T. A. Myers, eds., Wound Regeneration and Repair: Methods and Protocols: Totowa, NJ, Humana Press, p. 343-353.

Sucov, H. M., E. Dyson, C. L. Gumeringer, J. Price, K. R. Chien, and R. M. Evans, 1994, RXR alpha mutant mice establish a genetic basis for vitamin A signaling in heart morphogenesis: Genes Dev, v. 8, p. 1007-18.

Sulpice, E., J. Plouët, M. Bergé, D. Allanic, G. Tobelem, and T. Merkulova-Rainon, 2008, Neuropilin-1 and neuropilin-2 act as coreceptors, potentiating proangiogenic activity: Blood, v. 111, p. 2036.

Sun, J., S. H. Li, S. M. Liu, J. Wu, R. D. Weisel, Y. F. Zhuo, T. M. Yau, R. K. Li, and S. S. Fazel, 2009a, Improvement in cardiac function after bone marrow cell thearpy is associated with an increase in myocardial inflammation: Am J Physiol Heart Circ Physiol, v. 296, p. H43-50.

Sun, P., Y. Zhang, F. Yu, E. Parks, A. Lyman, Q. Wu, L. Ai, C. H. Hu, Q. Zhou, K. Shung, C. L. Lien, and T. K. Hsiai, 2009b, Micro-electrocardiograms to study post-ventricular amputation of zebrafish heart: Ann Biomed Eng, v. 37, p. 890-901.

Sun, Z., P. Jin, T. Tian, Y. Gu, Y.-G. Chen, and A. Meng, 2006, Activation and roles of ALK4/ALK7-mediated maternal TGFβ signals in zebrafish embryo: Biochemical and Biophysical Research Communications, v. 345, p. 694-703.

Suri, C., P. F. Jones, S. Patan, S. Bartunkova, P. C. Maisonpierre, S. Davis, T. N. Sato, and G. D. Yancopoulos, 1996, Requisite role of angiopoietin-1, a ligand for the TIE2 receptor, during embryonic angiogenesis: Cell, v. 87, p. 1171-80.

Suzuki, K., A. Kumanogoh, and H. Kikutani, 2008, Semaphorins and their receptors in immune cell interactions: Nat Immunol, v. 9, p. 17-23.

Taichman, N. S., S. Young, A. T. Cruchley, P. Taylor, and E. Paleolog, 1997, Human neutrophils secrete vascular endothelial growth factor: J Leukoc Biol, v. 62, p. 397-400.

Takagi, S., T. Hirata, K. Agata, M. Mochii, G. Eguchi, and H. Fujisawa, 1991, The A5-Antigen, A Candidate For The Neuronal Recognition Molecule Has Homologies To Complement Components And Coagulation-Factors: Neuron, v. 7, p. 295-307.

Takagi, S., T. Tsuji, T. Amagai, T. Takamatsu, and H. Fujisawa, 1987, Specific cell surface labels in the visual centers of Xenopus laevis tadpole identified using monoclonal antibodies: Dev Biol, v. 122, p. 90-100.

Takahashi, T., A. Fournier, F. Nakamura, L. H. Wang, Y. Murakami, R. G. Kalb, H. Fujisawa, and S. M. Strittmatter, 1999, Plexin-neuropilin-1 complexes form functional semaphorin-3A receptors: Cell, v. 99, p. 59-69.

Takahashi, T., F. Nakamura, and S. M. Strittmatter, 1997, Neuronal and non-neuronal collapsin-1 binding sites in developing chick are distinct from other semaphorin binding sites: Journal of Neuroscience, v. 17, p. 9183-9193.

Takashima, S., M. Kitakaze, M. Asakura, H. Asanuma, S. Sanada, F. Tashiro, H. Niwa, J. Miyazaki, S. Hirota, Y. Kitamura, T. Kitsukawa, H. Fujisawa, M. Klagsbrun, and M. Hori, 2002, Targeting of both mouse neuropilin-1 and neuropilin-2 genes severely impairs developmental yolk sac and embryonic angiogenesis: Proceedings of the National Academy of Sciences of the United States of America, v. 99, p. 3657-3662.

Takeichi, M., K. Nimura, M. Mori, H. Nakagami, and Y. Kaneda, 2013, The Transcription Factors Tbx18 and Wt1 Control the Epicardial Epithelial-Mesenchymal Transition through Bi-Directional Regulation of Slug in Murine Primary Epicardial Cells: Plos One, v. 8.

Tamagnone, L., S. Artigiani, H. Chen, Z. He, G. I. Ming, H. Song, A. Chedotal, M. L. Winberg, C. S. Goodman, M. Poo, M. Tessier-Lavigne, and P. M. Comoglio, 1999, Plexins are a large family of receptors for transmembrane, secreted, and GPI-anchored semaphorins in vertebrates: Cell, v. 99, p. 71-80.

Tang, Y., J. R. Nyengaard, J. B. Andersen, U. Baandrup, and H. J. Gundersen, 2009, The application of stereological methods for estimating structural parameters in the human heart: Anat Rec (Hoboken), v. 292, p. 1630-47.

Tao, J., Y. Doughman, K. Yang, D. Ramirez-Bergeron, and M. Watanabe, 2013, Epicardial HIF signaling regulates vascular precursor cell invasion into the myocardium: Developmental biology, v. 376, p. 136-149.

Tao, Q., S. C. Spring, and B. I. Terman, 2003, Characterization of a new alternatively spliced neuropilin-1 isoform: Angiogenesis, v. 6, p. 39-45.

Tessadori, F., J. H. van Weerd, S. B. Burkhard, A. O. Verkerk, E. de Pater, B. J. Boukens, A. Vink, V. M. Christoffels, and J. Bakkers, 2012, Identification and functional characterization of cardiac pacemaker cells in zebrafish: PLoS One, v. 7, p. e47644.

Tevosian, S. G., A. E. Deconinck, M. Tanaka, M. Schinke, S. H. Litovsky, S. Izumo, Y. Fujiwara, and S. H. Orkin, 2000, FOG-2, a cofactor for GATA transcription factors, is essential for heart morphogenesis and development of coronary vessels from epicardium: Cell, v. 101, p. 729-39.

Thisse, B., and C. Thisse, 2005, Functions and regulations of fibroblast growth factor signaling during embryonic development: Developmental Biology, v. 287, p. 390-402.

Thompson, M. A., D. G. Ransom, S. J. Pratt, H. MacLennan, M. W. Kieran, H. W. Detrich, 3rd, B. Vail, T. L. Huber, B. Paw, A. J. Brownlie, A. C. Oates, A. Fritz, M. A. Gates, A. Amores, N. Bahary, W. S. Talbot, H. Her, D. R. Beier, J. H. Postlethwait, and L. I. Zon, 1998, The cloche and spadetail genes differentially affect hematopoiesis and vasculogenesis: Dev Biol, v. 197, p. 248-69.

Tian, X., T. Hu, H. Zhang, L. He, X. Huang, Q. Liu, W. Yu, Z. Yang, Z. Zhang, T. P. Zhong, X. Yang, Y. Yan, A. Baldini, Y. Sun, J. Lu, R. J. Schwartz, S. M. Evans, A. C. Gittenberger-de Groot, K. Red-Horse, and B. Zhou, 2013, Subepicardial endothelial cells invade the embryonic ventricle wall to form coronary arteries: Cell Res, v. 23, p. 1075-90.

Timmers, L., G. Pasterkamp, V. C. de Hoog, F. Arslan, Y. Appelman, and D. P. de Kleijn, 2012, The innate immune response in reperfused myocardium: Cardiovasc Res, v. 94, p. 276-83.

Timmers, L., J. P. Sluijter, J. K. van Keulen, I. E. Hoefer, M. G. Nederhoff, M. J. Goumans, P. A. Doevendans, C. J. van Echteld, J. A. Joles, P. H. Quax, J. J. Piek, G. Pasterkamp, and D. P. de Kleijn, 2008, Toll-like receptor 4 mediates maladaptive left ventricular remodeling and impairs cardiac function after myocardial infarction: Circ Res, v. 102, p. 257-64.

Tomanek, R. J., Y. Ishii, J. S. Holifield, C. L. Sjogren, H. K. Hansen, and T. Mikawa, 2006, VEGF Family Members Regulate Myocardial Tubulogenesis and Coronary Artery Formation in the Embryo: Circulation Research, v. 98, p. 947.

Tordjman, R., Y. Lepelletier, V. Lemarchandel, M. Cambot, P. Gaulard, O. Hermine, and P. H. Romeo, 2002, A neuronal receptor, neuropilin-1, is essential for the initiation of the primary immune response: Nat Immunol, v. 3, p. 477-82.

Trinh, L. A., and D. Y. Stainier, 2004, Fibronectin regulates epithelial organization during myocardial migration in zebrafish: Dev Cell, v. 6, p. 371-82.

Tsai, C. T., C. K. Wu, F. T. Chiang, C. D. Tseng, J. K. Lee, C. C. Yu, Y. C. Wang, L. P. Lai, J. L. Lin, and J. J. Hwang, 2011, In-vitro recording of adult zebrafish heart electrocardiogram - a platform for pharmacological testing: Clin Chim Acta, v. 412, p. 1963-7.

Ulrich, M. M., A. M. Janssen, M. J. Daemen, L. Rappaport, J. L. Samuel, F. Contard, J. F. Smits, and J. P. Cleutjens, 1997, Increased expression of fibronectin isoforms after myocardial infarction in rats: J Mol Cell Cardiol, v. 29, p. 2533-43.

Unal, B., J. A. Critchley, and S. Capewell, 2005, Modelling the decline in coronary heart disease deaths in England and Wales, 1981-2000: comparing contributions from primary prevention and secondary prevention: British Medical Journal, v. 331, p. 614-617.

van Amerongen, M. J., M. C. Harmsen, N. van Rooijen, A. H. Petersen, and M. J. van Luyn, 2007, Macrophage depletion impairs wound healing and increases left ventricular remodeling after myocardial injury in mice: Am J Pathol, v. 170, p. 818-29.

van Berlo, J. H., O. Kanisicak, M. Maillet, R. J. Vagnozzi, J. Karch, S.-C. J. Lin, R. C. Middleton, E. Marban, and J. D. Molkentin, 2014, c-kit+ cells minimally contribute cardiomyocytes to the heart: Nature, v. 509, p. 337-341.

van Impel, A., Z. Zhao, D. M. Hermkens, M. G. Roukens, J. C. Fischer, J. Peterson-Maduro, H. Duckers, E. A. Ober, P. W. Ingham, and S. Schulte-Merker, 2014, Divergence of zebrafish and mouse lymphatic cell fate specification pathways: Development, v. 141, p. 1228-38.

van Wijk, B., Q. D. Gunst, A. F. M. Moorman, and M. J. B. van den Hoff, 2012, Cardiac Regeneration from Activated Epicardium: Plos One, v. 7.

van Wijk, B., G. van den Berg, R. Abu-Issa, P. Barnett, S. van der Velden, M. Schmidt, J. M. Ruijter, M. L. Kirby, A. F. M. Moorman, and M. J. B. van den Hoff, 2009, Epicardium and Myocardium Separate From a Common Precursor Pool by Crosstalk Between Bone Morphogenetic Protein– and Fibroblast Growth Factor–Signaling Pathways: Circulation research, v. 105, p. 431-441.

Vega-Hernandez, M., A. Kovacs, S. De Langhe, and D. M. Ornitz, 2011, FGF10/FGFR2b signaling is essential for cardiac fibroblast development and growth of the myocardium: Development, v. 138, p. 3331-40.

Vihtelic, T. S., and D. R. Hyde, 2000, Light-induced rod and cone cell death and regeneration in the adult albino zebrafish (Danio rerio) retina: J Neurobiol, v. 44, p. 289-307.

Virag, J. A. I., M. L. Rolle, J. Reece, S. Hardouin, E. O. Feigl, and C. E. Murry, 2007, Fibroblast growth factor-2 regulates myocardial infarct repair - Effects on cell proliferation, scar contraction, and ventricular function: American Journal of Pathology, v. 171, p. 1431-1440.

Viragh, S., and C. E. Challice, 1981, The origin of the epicardium and the embryonic myocardial circulation in the mouse: Anat Rec, v. 201, p. 157-68.

Volders, P. G. A., 2010, Novel insights into the role of the sympathetic nervous system in cardiac arrhythmogenesis: Heart Rhythm, v. 7, p. 1900-1906.

von Gise, A., B. Zhou, L. B. Honor, Q. Ma, A. Petryk, and W. T. Pu, 2011, WT1 regulates epicardial epithelial to mesenchymal transition through beta-catenin and retinoic acid signaling pathways: Developmental Biology, v. 356, p. 421-431.

Wada, A. M., T. K. Smith, M. E. Osler, D. E. Reese, and D. M. Bader, 2003, Epicardial/mesothelial cell line retains vasculogenic potential of embryonic epicardium: Circulation Research, v. 92, p. 525-531.

Waldo, K. L., D. H. Kumiski, K. T. Wallis, H. A. Stadt, M. R. Hutson, D. H. Platt, and M. L. Kirby, 2001, Conotruncal myocardium arises from a secondary heart field: Development, v. 128, p. 3179-88.

Walsh, S., A. Ponten, B. K. Fleischmann, and S. Jovinge, 2010, Cardiomyocyte cell cycle control and growth estimation *in vivo*--an analysis based on cardiomyocyte nuclei: Cardiovasc Res, v. 86, p. 365-73.

Waltenberger, J., L. Claesson-Welsh, A. Siegbahn, M. Shibuya, and C. H. Heldin, 1994, Different signal transduction properties of KDR and Flt1, two receptors for vascular endothelial growth factor: J Biol Chem, v. 269, p. 26988-95.

Wang, J., J. Cao, A. L. Dickson, and K. D. Poss, 2015, Epicardial regeneration is guided by cardiac outflow tract and Hedgehog signalling: Nature, v. 522, p. 226-230.

Wang, J., R. Karra, A. L. Dickson, and K. D. Poss, 2013a, Fibronectin is deposited by injury-activated epicardial cells and is necessary for zebrafish heart regeneration: Developmental Biology, v. 382, p. 427-435.

Wang, J., R. Karra, A. L. Dickson, and K. D. Poss, 2013b, Fibronectin is deposited by injury-activated epicardial cells and is necessary for zebrafish heart regeneration: Dev Biol, v. 382, p. 427-35.

Wang, J., D. Panakova, K. Kikuchi, J. E. Holdway, M. Gemberling, J. S. Burris, S. P. Singh, A. L. Dickson, Y.-F. Lin, M. K. Sabeh, A. A. Werdich, D. Yelon, C. A. MacRae, and K. D. Poss, 2011, The regenerative capacity of zebrafish reverses cardiac failure caused by genetic cardiomyocyte depletion: Development, v. 138, p. 3421-3430.

Wang, L., H. Zeng, P. Wang, S. Soker, and D. Mukhopadhyay, 2003, Neuropilin-1-mediated vascular permeability factor/vascular endothelial growth factor-dependent endothelial cell migration: J Biol Chem, v. 278, p. 48848-60.

Waxman, J. S., B. R. Keegan, R. W. Roberts, K. D. Poss, and D. Yelon, 2008, Hoxb5b acts downstream of retinoic acid signaling in the forelimb field to restrict heart field potential in zebrafish: Dev Cell, v. 15, p. 923-34.

Weathington, N. M., A. H. van Houwelingen, B. D. Noerager, P. L. Jackson, A. D. Kraneveld, F. S. Galin, G. Folkerts, F. P. Nijkamp, and J. E. Blalock, 2006, A novel peptide CXCR ligand derived from extracellular matrix degradation during airway inflammation: Nat Med, v. 12, p. 317-23.

West, D. C., C. G. Rees, L. Duchesne, S. J. Patey, C. J. Terry, J. E. Turnbull, M. Delehedde, C. W. Heegaard, F. Allain, C. Vanpouille, D. Ron, and D. G. Fernig, 2005, Interactions of multiple heparin binding growth factors with neuropilin-1 and potentiation of the activity of fibroblast growth factor-2: Journal of Biological Chemistry, v. 280, p. 13457-13464.

Wienholds, E., S. Schulte-Merker, B. Walderich, and R. H. Plasterk, 2002, Target-selected inactivation of the zebrafish rag1 gene: Science, v. 297, p. 99-102.

Wienholds, E., F. van Eeden, M. Kosters, J. Mudde, R. H. A. Plasterk, and E. Cuppen, 2003, Efficient Target-Selected Mutagenesis in Zebrafish: Genome Research, v. 13, p. 2700-2707.

Wiens, K. M., H. L. Lee, H. Shimada, A. E. Metcalf, M. Y. Chao, and C. L. Lien, 2010, Platelet-derived growth factor receptor beta is critical for zebrafish intersegmental vessel formation: PLoS One, v. 5, p. e11324.

Willems, I. E., J. W. Arends, and M. J. Daemen, 1996, Tenascin and fibronectin expression in healing human myocardial scars: J Pathol, v. 179, p. 321-5.

Wills, A. A., J. E. Holdway, R. J. Major, and K. D. Poss, 2008, Regulated addition of new myocardial and epicardial cells fosters homeostatic cardiac growth and maintenance in adult zebrafish: Development, v. 135, p. 183-192.

Witzenbichler, B., T. Asahara, T. Murohara, M. Silver, I. Spyridopoulos, M. Magner, N. Principe, M. Kearney, J. S. Hu, and J. M. Isner, 1998, Vascular endothelial growth factor-C (VEGF-C/VEGF-2) promotes angiogenesis in the setting of tissue ischemia: Am J Pathol, v. 153, p. 381-94.

Wolman, M. A., Y. Liu, H. Tawarayama, W. Shoji, and M. C. Halloran, 2004, Repulsion and attraction of axons by Semaphorin3D are mediated by different neuropilins *in vivo*: Journal of Neuroscience, v. 24, p. 8428-8435.

Worzfeld, T., and S. Offermanns, 2014, Semaphorins and plexins as therapeutic targets: Nat Rev Drug Discov, v. 13, p. 603-621.

Wrana, J. L., L. Attisano, R. Wieser, F. Ventura, and J. Massague, 1994, Mechanism of activation of the TGF-beta receptor: Nature, v. 370, p. 341-7.

Wu, B., Z. Zhang, W. Lui, X. Chen, Y. Wang, A. A. Chamberlain, R. A. Moreno-Rodriguez, R. R. Markwald, B. P. O'Rourke, D. J. Sharp, D. Zheng, J. Lenz, H. S. Baldwin, C.-P. Chang, and B. Zhou, 2012, Endocardial Cells Form the Coronary Arteries by Angiogenesis through Myocardial-Endocardial VEGF Signaling: Cell, v. 151, p. 1083-1096.

Wu, M. Y., and C. S. Hill, 2009, TGF-β Superfamily Signaling in Embryonic Development and Homeostasis: Developmental Cell, v. 16, p. 329-343.

Xu, H., M. Morishima, J. N. Wylie, R. J. Schwartz, B. G. Bruneau, E. A. Lindsay, and A. Baldini, 2004, Tbx1 has a dual role in the morphogenesis of the cardiac outflow tract: Development, v. 131, p. 3217-27.

Xu, J., S. Lamouille, and R. Derynck, 2009, TGF-beta-induced epithelial to mesenchymal transition: Cell Res, v. 19, p. 156-72.

Xu, X., S. E. Meiler, T. P. Zhong, M. Mohideen, D. A. Crossley, W. W. Burggren, and M. C. Fishman, 2002, Cardiomyopathy in zebrafish due to mutation in an alternatively spliced exon of titin: Nat Genet, v. 30, p. 205-209.

Xu, Y., L. Yuan, J. Mak, L. Pardanaud, M. Caunt, I. Kasman, B. Larrivee, R. del Toro, S. Suchting, A. Medvinsky, J. Silva, J. Yang, J.-L. Thomas, A. W. Koch, K. Alitalo, A. Eichmann, and A. Bagri, 2010, Neuropilin-2 mediates VEGF-C-induced lymphatic sprouting together with VEGFR3: Journal of Cell Biology, v. 188, p. 115-130.

Yamada, Y., N. Takakura, H. Yasue, H. Ogawa, H. Fujisawa, and T. Suda, 2001, Exogenous clustered neuropilin 1 enhances vasculogenesis and angiogenesis: Blood, v. 97, p. 1671-8.

Yanagisawa-Miwa, A., Y. Uchida, F. Nakamura, T. Tomaru, H. Kido, T. Kamijo, T. Sugimoto, K. Kaji, M. Utsuyama, C. Kurashima, and et al., 1992, Salvage of infarcted myocardium by angiogenic action of basic fibroblast growth factor: Science, v. 257, p. 1401-3.

Yano, T., T. Miura, Y. Ikeda, E. Matsuda, K. Saito, T. Miki, H. Kobayashi, Y. Nishino, S. Ohtani, and K. Shimamoto, 2005, Intracardiac fibroblasts, but not bone marrow derived cells, are the origin of myofibroblasts in myocardial infarct repair: Cardiovasc Pathol, v. 14, p. 241-6.

Yelland, T., and S. Djordjevic, 2016, Crystal Structure of the Neuropilin-1 MAM Domain: Completing the Neuropilin-1 Ectodomain Picture: Structure(London, England:1993), v. 24, p. 2008-2015.

Yelon, D., S. A. Horne, and D. Y. R. Stainier, 1999, Restricted expression of cardiac myosin genes reveals regulated aspects of heart tube assembly in zebrafish: Developmental Biology, v. 214, p. 23-37.

Yoshida, S., M. Ono, T. Shono, H. Izumi, T. Ishibashi, H. Suzuki, and M. Kuwano, 1997, Involvement of interleukin-8, vascular endothelial growth factor, and basic fibroblast growth factor in tumor necrosis factor alpha-dependent angiogenesis: Mol Cell Biol, v. 17, p. 4015-23.

Yu, H.-H., C. Houart, and C. B. Moens, 2004, Cloning and embryonic expression of zebrafish neuropilin genes: Gene Expression Patterns, v. 4, p. 371-378.

Zachary, I., and R. D. Morgan, 2011, Therapeutic angiogenesis for cardiovascular disease: biological context, challenges, prospects: Heart, v. 97, p. 181-9.

Zhao, L., A. L. Borikova, R. Ben-Yair, B. Guner-Ataman, C. A. MacRae, R. T. Lee, C. G. Burns, and C. E. Burns, 2014, Notch signaling regulates cardiomyocyte proliferation during zebrafish heart regeneration: Proceedings of the National Academy of Sciences, v. 111, p. 1403-1408.

Zhao, T., W. Zhao, Y. Chen, R. A. Ahokas, and Y. Sun, 2011, Acidic and basic fibroblast growth factors involved in cardiac angiogenesis following infarction: Int J Cardiol, v. 152, p. 307-13.

Zhou, B., L. B. Honor, H. He, Q. Ma, J.-H. Oh, C. Butterfield, R.-Z. Lin, J. M. Melero-Martin, E. Dolmatova, H. S. Duffy, A. von Gise, P. Zhou, Y. W. Hu, G. Wang, B. Zhang, L. Wang, J. L. Hall, M. A. Moses, F. X. McGowan, and W. T. Pu, 2011a, Adult mouse epicardium modulates myocardial injury by secreting paracrine factors: Journal of Clinical Investigation, v. 121, p. 1894-1904.

Zhou, B., Q. Ma, S. Rajagopal, S. M. Wu, I. Domian, J. Rivera-Feliciano, D. Jiang, A. von Gise, S. Ikeda, K. R. Chien, and W. T. Pu, 2008, Epicardial progenitors contribute to the cardiomyocyte lineage in the developing heart: Nature, v. 454, p. 109-U5.

Zhou, B., and W. T. Pu, 2011, Epicardial epithelial-to-mesenchymal transition in injured heart: Journal of Cellular and Molecular Medicine, v. 15, p. 2781-2783.

Zhou, Y., T. J. Cashman, K. R. Nevis, P. Obregon, S. A. Carney, Y. Liu, A. Gu, C. Mosimann, S. Sondalle, R. E. Peterson, W. Heideman, C. E. Burns, and C. G. Burns, 2011b, Latent TGF-beta binding protein 3 identifies a second heart field in zebrafish: Nature, v. 474, p. 645-8.

Zipes, D. P., 2008, Heart-brain interactions in cardiac arrhythmias: role of the autonomic nervous system: Cleveland Clinic journal of medicine, v. 75 Suppl 2, p. S94-6.

Zogbi, C., A. E. T. Saturi de Carvalho, J. S. Nakamuta, V. d. M. Caceres, S. Prando, M. C. P. Giorgi, C. E. Rochitte, J. C. Meneghetti, and J. E. Krieger, 2014, Early postnatal rat ventricle resection leads to long-term preserved cardiac function despite tissue hypoperfusion: Physiological Reports, v. 2, p. e12115.